Reviews of Geophysics

Key Points:
- Recent soil moisture measurement and monitoring techniques and estimation models from the point to the global scales and their limitations are presented
- The importance and application of soil moisture information for various Earth and environmental sciences disciplines such as forecasting weather and climate variability, modeling hydrological processes, and predicting and monitoring extreme events and their impacts on the environment and human society are presented

Correspondence to:
M. Tuller,
mtuller@email.arizona.edu

Ground, Proximal, and Satellite Remote Sensing of Soil Moisture

Ebrahim Babaeian[1] , Morteza Sadeghi[2] , Scott B. Jones[2] , Carsten Montzka[3] , Harry Vereecken[3] , and Markus Tuller[1]

[1]Department of Soil, Water and Environmental Science, The University of Arizona, Tucson, AZ, USA, [2]Department of Plants, Soils and Climate, Utah State University, Logan, UT, USA, [3]Forschungszentrum Jülich GmbH, Institute of Bio- and Geosciences: Agrosphere (IBG-3), Jülich, Germany

Abstract Soil moisture (SM) is a key hydrologic state variable that is of significant importance for numerous Earth and environmental science applications that directly impact the global environment and human society. Potential applications include, but are not limited to, forecasting of weather and climate variability; prediction and monitoring of drought conditions; management and allocation of water resources; agricultural plant production and alleviation of famine; prevention of natural disasters such as wild fires, landslides, floods, and dust storms; or monitoring of ecosystem response to climate change. Because of the importance and wide-ranging applicability of highly variable spatial and temporal SM information that links the water, energy, and carbon cycles, significant efforts and resources have been devoted in recent years to advance SM measurement and monitoring capabilities from the point to the global scales. This review encompasses recent advances and the state-of-the-art of ground, proximal, and novel SM remote sensing techniques at various spatial and temporal scales and identifies critical future research needs and directions to further advance and optimize technology, analysis and retrieval methods, and the application of SM information to improve the understanding of critical zone moisture dynamics. Despite the impressive progress over the last decade, there are still many opportunities and needs to, for example, improve SM retrieval from remotely sensed optical, thermal, and microwave data and opportunities for novel applications of SM information for water resources management, sustainable environmental development, and food security.

1. Introduction

Soil moisture (SM) is a key hydrologic state variable that links land surface and atmospheric processes (Robinson et al., 2008). Detailed knowledge about the state of SM and its spatial and temporal dynamics is of crucial importance for numerous meteorological, climatologic, and hydrologic applications and to improve our understanding of the water, energy and carbon cycles, as well as for forecasting of extreme climate events (Li et al., 2007; Robock & Li, 2006; Seneviratne et al., 2010; Vereecken et al., 2014). In general, in situ gravimetric measurements and electromagnetic (EM) sensor networks are considered as the most reliable means for direct and accurate determination of moisture within the soil profile. However, in situ measurements may be prone to uncertainties due to, for example, high salinity levels, loss of intimate contact between sensors and the surrounding soil because of shrinkage or biological activity, or lack of calibration, especially for soils with high specific surface areas. In addition, implementation of such methods is destructive, expensive, and laborious (Rahimzadeh-Bajgiran et al., 2013; Zhang et al., 2014) and they only provide localized information about SM dynamics and are not always representative of the larger surrounding area (Petropoulos et al., 2013). Because of the high spatial and temporal SM variability due to spatiotemporal variations of associated meteorological (precipitation, temperature, solar radiation, wind speed, and humidity) and biogeophysical (soil properties, topographic features, and vegetation characteristics) parameters, measurement, and monitoring of large-scale SM dynamics is challenging.

During the last decade numerous noninvasive techniques have been developed and employed to analyze SM patterns and dynamics across various spatial and temporal scales. For example, at the field and catchment scales, noninvasive proximal sensing techniques have been successfully applied to measure profile SM dynamics (Huisman et al., 2003; Kiseleva et al., 2014; Loijens, 1980; Moghadas et al., 2010).

Today, ground-based and airborne and spaceborne remote sensing (RS) techniques provide an exceedingly powerful means for characterization and monitoring of large-scale near-surface soil properties and processes at reasonable temporal and spatial resolutions. Numerous studies have provided surface and near-surface SM estimates based on reflectance and/or emission of EM radiation within the optical (Sadeghi et al., 2015; Schnur et al., 2010; Zhang et al., 2014), thermal (Lei et al., 2014; Rahimzadeh-Bajgiran et al., 2013; Verstraeten et al., 2006), active (Bartalis et al., 2018; Ulaby et al., 1982; Vinnikov et al., 1999; Wagner et al., 2012), and passive (Chen et al., 2018; Jackson et al., 2010; Kerr et al., 2016; Koike et al., 2004; Njoku & Entekhabi, 1996) microwave frequency ranges at various spatial scales that include the field scale (Jonard et al., 2011; Wigneron et al., 2007), the catchment scale (Baatz et al., 2014; Rosenbaum et al., 2012; Western et al., 2004), the regional scale (Louvet et al., 2015; Romshoo, 2004; Zhao et al., 2013), and the continental/global scale (Entin et al., 2000; Li & Rodell, 2013; Renzullo et al., 2014). Because of the limited measurement depth of microwaves, novel data assimilation techniques have been developed and implemented in hydrological models to establish links between remotely sensed near-surface and root-zone SM (Das et al., 2008; Draper et al., 2012; Dumedah et al., 2015; Montzka et al., 2011).

Accurate monitoring of large-scale SM status is essential for the management of agricultural water resources to not only improve knowledge of plant water availability, water use efficiency, and water productivity but also to reduce the risks of detrimental anthropogenic environmental impacts. SM is an effective indicator for drought conditions and flood risks, two major meteorological hazards, and thus plays a unique role in their prediction (e.g., under drought conditions the SM anomaly typically proceeds the anomaly of the vegetation indices). Saturated soils are not able to absorb additional water, which leads to an increase in surface runoff and subsequently to flooding. Detailed information about the soil water status aids in improving flood prediction accuracy and provides means for near-real-time (NRT) flood forecasting. Continuously monitoring the root-zone SM status of agricultural crops aids in detection of plant water stress and the onset of drought conditions as well as provides the basis for precision irrigation management for provision of a water stress-free rhizosphere environment, while preventing leaching of agrochemicals and potential groundwater contamination. SM also influences precipitation patterns by controlling evapotranspiration, which affects the development of the daytime atmospheric boundary layer and thereby the initiation and intensity of convective rainfall events. Feedbacks between SM and precipitation are of significant importance for weather forecasting (Koster et al., 2004) and the regional hydroclimatic variability (Ines & Mohanty, 2008a; Mahmood & Hubbard, 2007).

Because of the significance and wide-ranging applicability of SM information, related research and technological advances have gained substantial scientific and public attention in recent years. Of late, SM has been included in the list of the 50 most essential climate variables (Dorigo et al., 2015) in order to support international organizations with the assessment of climate change impacts. In 2010, the Global Climate Observing System initiative has defined SM as a fundamental climate variable (Global Climate Observing System, 2010). This has prompted the European Space Agency (ESA) to incorporate SM in the climate change initiative (CCI; Hollmann et al., 2013). During the past decade, several instruments such as the Japan Aerospace Exploration Agency (JAXA) Advanced Microwave Scanning Radiometer (AMSR-E on the National Aeronautics and Space Administration's [NASA] Aqua satellite and Advanced Microwave Scanning Radiometer 2 [AMSR-2] on the Global Change Observation Mission-Water [GCOM-W1] satellite), the European Organization for the Exploitation of Meteorological Satellites (EUMETSAT) Advanced SCATterometer (ASCAT), the ESA Soil Moisture and Ocean Salinity (SMOS), the NASA Aquarius, the NASA Soil Moisture Active Passive (SMAP), and the ESA Sentinel-1 that operate in the microwave frequency range are dedicated to the measurement of land surface SM (Entekhabi et al., 2010; Kerr et al., 2001; Njoku et al., 2003; Paloscia et al., 2013; Wagner et al., 2013). Seneviratne et al. (2010) have discussed the role of SM in climate and atmospheric processes with focus on SM-temperature and SM-precipitation feedbacks. Dobriyal et al. (2012) have provided an overview of landscape-scale SM estimation methods with emphasis on water resources sustainability and management. Vereecken et al. (2014) have discussed the state of the art of characterizing spatiotemporal field-scale SM dynamics and provided an overview of advanced measurement techniques. Petropoulos et al. (2015) have provided a comprehensive overview of efforts invested over the last 20 years in surface SM retrieval from microwave sensors. Noninvasive techniques for characterization of SM dynamics at the field to basin scales have been presented in Bogena et al. (2015).

This review is aimed at (1) an inclusive presentation and discussion of recent advances in ground, proximal, and airborne and spaceborne RS techniques that provide novel means for characterization and continuous monitoring of SM dynamics across various spatial scales and (2) summarizing the available SM data resources and rapidly expanding repositories to promote and stimulate future research about novel applications of SM information. The review is organized in 10 sections. After introducing the importance and wide-ranging impact of SM information, section 2 provides a definition of SM and its relationship to various spatial scales. Section 3 presents ground-based point measurement techniques and SM sensor networks. Section 4 is devoted to proximal sensing techniques for SM retrieval. In section 5, an overview of RS techniques for SM retrieval from optical, thermal, and microwave RS information is provided. Section 6 describes available data and monitoring resources such as global sensor networks and microwave satellite and airborne RS missions and provides an evaluation of microwave satellite retrievals. After a discussion of the basic principles of analytical and numerical root-zone SM derivations from remotely sensed SM information and data assimilation in section 7, spatial and temporal variability inherent to RS of SM applications is presented in section 8. In section 9, potential applications of SM information are presented and an outlook for future research opportunities is provided. Finally, a summary and conclusions are provided in section 10.

2. Definition of SM

The SM or soil water content, which may be expressed on a gravimetric, θ_m, or volumetric, θ_v, basis represents the amount of water present in the soil at a given matric potential (Tuller & Or, 2005a). The matric potential, Ψ_m (or matric head, h), is synonymous with the combined capillary and adsorptive surface forces that hold water within the solid soil matrix and are uniquely related to SM under hydrostatic conditions. The highly nonlinear relationship between SM and Ψ_m is termed the soil water characteristic and exhibits a very distinctive shape for each individual soil texture (Figure 1). A comprehensive discussion about the origin of, Ψ_m, and the measurement and modeling of the soil water characteristic are provided in Tuller and Or (2005a) and Tuller et al. (1999).

The gravimetric SM, θ_m (g/g), which can be directly determined by oven drying a wet bulk soil sample at 105 °C, is defined as the ratio of the mass of water within the soil sample and the mass of the oven-dry solid material. The volumetric SM, θ_v (cm^3/cm^3), defined as the volume of water within a given soil volume may be expressed in terms of θ_m as (Robinson, Campbell, et al., 2008)

$$\theta_v = \theta_m \left(\frac{\rho_b}{\rho_w} \right) \tag{1}$$

where ρ_b is the dry bulk density (g/cm^3) of the soil and ρ_w is the density of water (g/cm^3). When all pores are filled with water, θ_v is termed saturated water content, θ_s. In some instances, it is advantageous to express SM in terms of relative saturation, $S_e = \theta_v/\theta_s$, which is the volumetric SM content normalized to θ_s (i.e., pore volume; Wagner et al., 2013). In theory, S_e ranges from zero, when the soil is completely dry, to 1, when all soil pores are completely filled with water. In practice, however, it is not possible to attain complete dry or saturated conditions. There is always a residual moisture content, θ_r, present under dry conditions, and it is virtually impossible to completely de-air soil as air bubbles remain entrapped in dead-end pores and cavitation nuclei are held tightly in crevices of rough particle surfaces (Sadeghi et al., 2018). To account for residual moisture, relative saturation is commonly defined as

$$S_e = \frac{\theta_v - \theta_r}{\theta_s - \theta_r} \tag{2}$$

Under wet conditions, due to air entrapment in the soil pores, the maximum attainable S_e ranges from about 0.94 to 0.97 (−) for fine-textured (i.e., clay) and coarse-textured (i.e., sand) soils, respectively.

For agricultural applications, a plant available (or extractable) soil water content, θ_{PAW}, is often defined as the difference between the water content at field capacity, θ_{FC}, and the water content at the permanent wilting point, θ_{PWP} (see Figure 1; Kabat & Beekma, 1994). The θ_{FC} is defined as the water content after internal redistribution of water within the soil matrix due to gravity (free drainage) and for practical purposes is often assumed to coincide with a matric potential of −330 cm. This definition is not entirely correct as θ_{FC} is
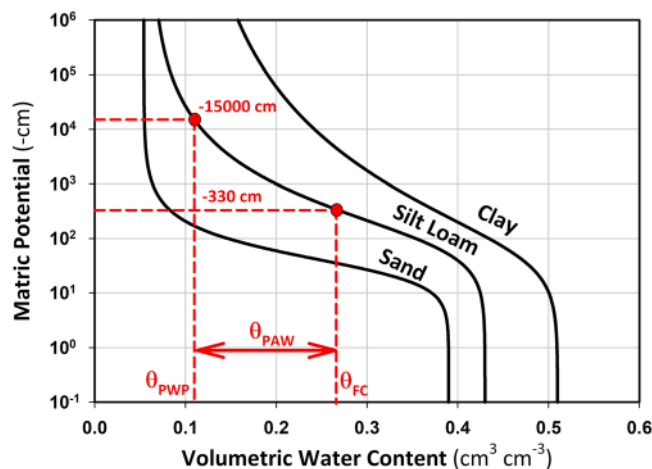
Figure 1. Soil water characteristics for different soil textures.

dependent on the soil texture. For example, θ_{FC} for a sandy soil more likely coincides with $\Psi_m = -100$ cm. Below the permanent wilting point that is defined as the water content at $-15,000$ cm matric potential, water is so tightly bound within the soil matrix that plants are no longer able to recover their turgidity and irreversibly wilt. Again, this is only an approximation, as the permanent wilting point is dependent on plant physiology. Desert plants, for example, can withstand significantly lower matric potentials (drier conditions; Hupet et al., 2005). For water balance calculations it is convenient to express SM in length units to be consistent with other variables such as precipitation or evapotranspiration. This so-called equivalent depth of wetting is obtained by multiplying θ_v with the depth of the soil layer of interest.

2.1. SM and Measurement Depth of EM Radiation

Dependent on the penetration depth of EM radiation as well as within the context of land surface modeling, the SM content is commonly referred to as (1) skin or surface SM, (2) near-surface SM, (3) root-zone SM, or (4) vadose zone SM. Skin or surface SM is commonly used within the context of optical and thermal RS and describes the water content in the uppermost, very thin soil layer ($\sim z \leq 1$ mm) at the interface between the land and the atmosphere. The term near-surface SM is usually related to the maximum measurement depth of microwave remote sensors (i.e., X-band, C-band, and L-band) and is defined as the average water content within the top few centimeters ($\sim 1 < z \leq 10$ cm) of surface soil. Root-zone SM (RZSM) defines the amount of water stored within the plant root-zone and is available for transpiration and biomass production (i.e., photosynthesis). While from a terrestrial hydrology point of view, the RZSM is highly variable in space and time, it is commonly assumed as the water content of the top 1-m soil layer. It can be directly measured with weighing lysimeters or determined with P-band microwave remote sensors, cosmic ray sensors (section 3.4), profiling EM sensors (section 4), or via modeling approaches (section 7). The vadose or unsaturated zone is defined as the soil compartment that extends from the land surface to the depth of the unconfined groundwater table. Vadose zone SM can be measured with deep penetrating EM radiation such as applied in airborne EM surveys (section 6.3.1).

The measurement depth of EM radiation is dependent on its frequency (wavelength). Optical RS techniques measure changes in surface reflectance that are associated with a change in soil color (i.e., moist soil appears darker than a dry soil). The spectral soil surface reflectance within the visible (Vis, 400–700 nm), near-infrared (NIR, 700–1,400 nm), and shortwave infrared (SWIR, 1,400–2,500 nm) EM range decreases with increasing SM content (Sadeghi et al., 2015). Thermal infrared techniques monitor changes in skin soil temperature that is intimately related to SM. In contrast to optical and thermal methods, microwave RS measures bulk dielectric soil properties (i.e., bulk dielectric permittivity) that are governed by SM content (section 3.2).

Table 1 summarizes the measurement depths of microwave bands (C-band, L-band, and P-band) for various land surface covers. While short wavelengths (C-band) are applicable for SM retrieval for bare soils or sparse vegetation cover (Baghdadi et al., 2012; Prigent et al., 2005), longer wavelengths (L-band and P-band) are less (partially) attenuated by vegetation canopies and are amenable for near-surface and RZSM determination (Jackson & Schmugge, 1995; Jonard et al., 2011; Moghaddam et al., 2000). Jackson and Schmugge (1995) pointed out that the depth of the soil layer that contributes to the measured microwave signals (e.g., brightness temperature) increases with wavelength. They also discussed that for vegetated surfaces the attenuation of the microwave signal increases, affecting the soil layer depth contributing to SM retrieval.

2.2. Spatial Scales of SM

SM can be defined for different spatial scales that range from point measurements (Miralles et al., 2010; Teuling et al., 2006) all the way to the global scale (Kerr et al., 2001; Naeimi et al., 2009). Point observations are commonly directly obtained with in situ techniques such as simple gravimetric sampling, various EM sensors (time domain reflectometry [TDR], amplitude domain reflectometry [ADR], and frequency domain reflectometry [FDR]; see section 3.2) or application of neutron radiation (Famiglietti et al., 1999; Fares et al.,

Table 1
Approximate Microwave Measurement Depths for Bare Soil and Different Land Surface Covers

Land surface cover	X-band (2.5–3.75 cm) (8–12 GHz)	C-band (3.75–7.5 cm) (4–8 GHz)	L-band (15–30 cm) (1–2 GHz)	P-band (30–100 cm) (0.3–1 GHz)
Bare soil	~1.25–1.87 cm	~1.87–3.75 cm	~7.5–15 cm	~15–50 cm
Agriculture and rangeland	~0.5–0.75 cm	~0.75–1.5 cm	~3–6 cm	~6–20 cm
Forest	~0.25–0.37 cm	~0.37–0.75 cm	~1.5–3 cm	~3–10 cm

Note. The measurement depth ranges for each microwave band were calculated based on one tenth ($\lambda/10$), one fifth ($\lambda/5$), and one half ($\lambda/2$) of the wavelength ranges (Karthikeyan et al., 2017a; Wilheit, 1978) assumed for bare soil and sparsely and fully vegetated surfaces, respectively. It should be noted that soil moisture content, soil texture, and surface roughness also affect the measurement depth of microwave signals.

2016; Grayson & Western, 1998; Wang et al., 2016) with sensing volumes ranging from about 2 to 40 cm. The significant spatial variability of SM, even over a distance of only a few meters (Vereecken et al., 2014), creates challenges for accurate determination of larger-scale SM with point measurement techniques, unless a large number of sensors are deployed. This in many cases is prohibitively expensive and laborious. If spatially averaged large-scale SM is of interest, airborne or spaceborne microwave RS sensors with spatial resolutions on the order of tens of meters to tens of kilometers are applied. To bridge the gap between point and satellite observations, proximal sensing techniques can be applied. Figure 2 shows a classification of the SM retrieval techniques presented in this review.

A unique definition of the spatial scales of SM measurements has been provided by Western and Bloschl (1999). They proposed a scale definition based on spacing, extent, and support that applies to both SM measurements and models. The term "spacing" refers to the distance between measurement points or model elements, the term "extent" to the overall coverage, and "support" refers to the measurement or model integration volume or area. As an example, for a network of TDR SM sensors deployed in a field, the scale may be defined based on 10^1-m spacing (distance between sensors), 10^2-m^2 extent (area of the field), and 10^3-cm^3 support (volume of the soil sampled with a TDR sensor). Similarly, for a satellite image (e.g., Landsat-8) the scale would be defined based on 30-m spacing (distance between the centers of two
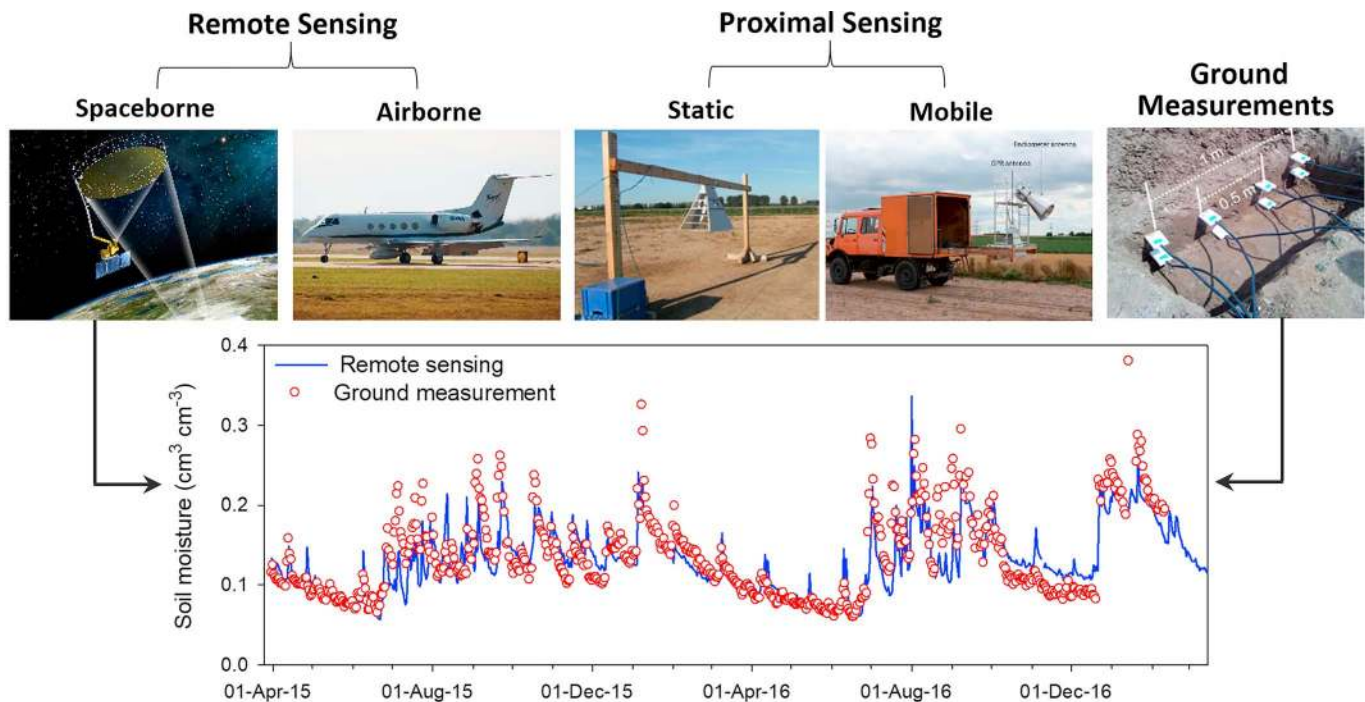

Figure 2. Classification of soil moisture (SM) measurement methods: spaceborne and airborne remote sensing techniques (top left), static and mobile proximal sensing methods (top middle), and in situ/ground sensor measurements (top right) for continuous monitoring of SM dynamics (bottom scatterplot, illustrating an example of Soil Moisture Active Passive (SMAP) surface SM vs. in situ data for the Arizona Walnut Gulch site).
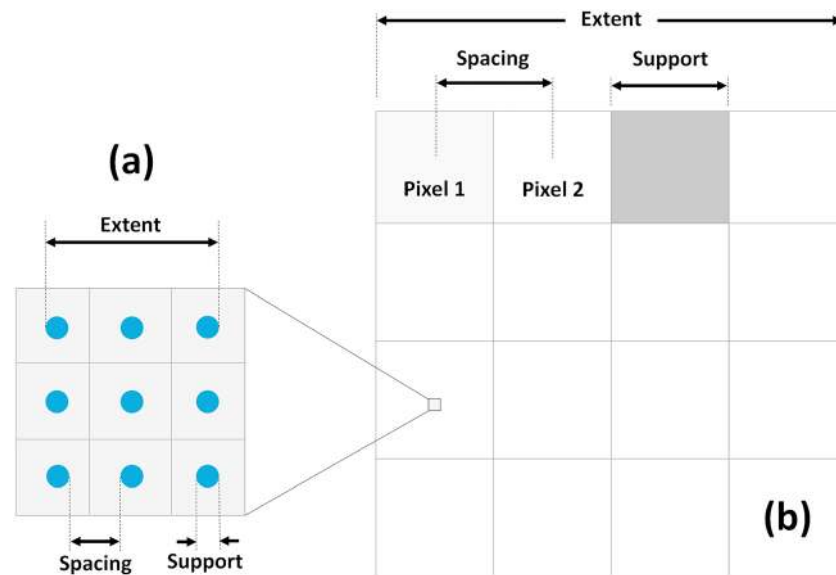
Figure 3. Definition of spatial scales based on "support," "spacing," and "extent" as related to (a) in situ sensor networks and (b) satellite remote sensing observations.

neighboring pixels), 170 km × 185 km extent (the footprint area), and 30^2-m^2 support (the pixel size for bands 1 to 9; Figure 3). The major application of such spatial terms is to study spatial variability of SM with respect to the effect of geophysical and climate parameters. An overview of spatial scale in terms of support and extent of existing SM measurement instruments and networks is provided in Table 2.

3. Ground-Based Point Measurements and Sensor Networks

This section is devoted to novel and evolving SM measurement techniques ranging from neutron scattering, EM, and heat pulse probe (HPP) point-scale methods to larger-scale cosmic ray neutron and other EM-based methods. In addition, other recent technologies such as (wireless) SM networks (WSMN) are introduced and their potential to improve our understanding of hydrologic processes is evaluated.

3.1. Neutron Scattering

The neutron scattering technology was first introduced by Brummer and Mardock (1945) for laboratory applications. Underwood et al. (1954) and Holmes (1955) were the first to develop and deploy portable neutron probes (NP) for in situ SM measurements for agricultural applications. The theory at the core of the

Table 2
Overview of Spatial Scales (Support and Extent) of Existing SM Instruments and Networks

Instrument/network	Support[a]	Extent
Neutron probe	Sphere (radius 15–40 cm)	1–20 m
TDR sensor array	~3-cm radius around waveguide	1–20 m
Mobile invasive TDR	3-cm radius around waveguide	10 m to 1 km
EMI	0.5–2 m^3	10 m to 10 km
GPR	0.5–2 m^3	10 m to 10 km
Cosmic ray neutron	40–400 m^3	500–3,000 km^2
GNSS reflectometry	The radius area varies from 50 m (for antenna with 1-m height) to 330 m (for antenna with 20-m height)	5,000–12,000 km^2
Gamma ray	12–15 m^3 (for a radius 100 m and bulk density 1.6 g/cm^3)	5,000–12,000 km^2
Sensor network	~3- to 10-cm radius around sensors	10 m to 10 km
Airborne remote sensing	1–100 m	50 m to 100 km
Satellite remote sensing	10–40 km	1–1,000 km

Note. SM = soil moisture; TDR = time domain reflectometry; EMI = electromagnetic induction; GPR = ground penetrating radar; GNSS = Global Navigation Satellite Systems.
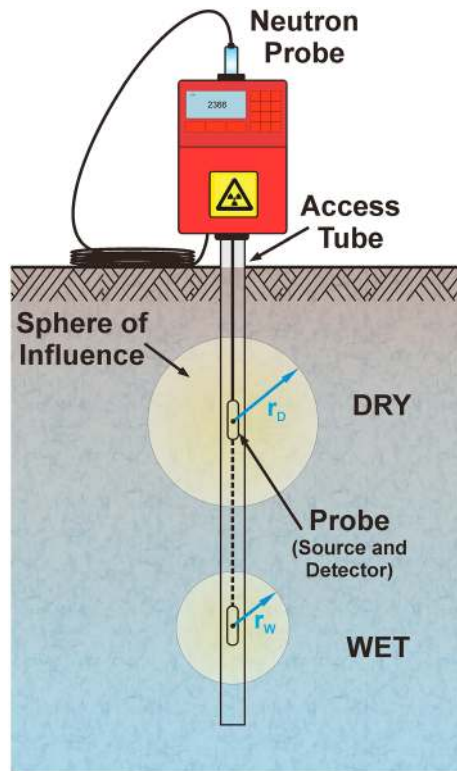[a]The effective support strongly depends on SM content.

Figure 4. Schematic of a portable neutron probe.

neutron scattering technique is based on the tendency for hydrogen nuclei to slow (thermalize) high-energy (2–4 MeV) neutrons to approach the characteristic speed of particles at ambient temperature with corresponding energies of about 0.03 eV. A typical NP consists of a radioactive neutron source (americium-241 and beryllium) and a detector to determine the flux of thermalized neutrons that form a cloud of nearly constant density near the probe. Neutrons lose different amounts of energy when colliding with various atomic nuclei. The greatest energy loss is due to collisions with particles of similar mass, such as hydrogen. The quantity of hydrogen in the soil is largely dependent on the amount of water and to a lesser extent on the amount of organic matter and clay minerals. Therefore, a calibration function that relates the number of detected slow neutrons to soil water content can be developed. The sphere of influence (measurement volume) of a NP depends on the SM content and chemical composition and on the strength of the radioactive source (Figure 4). Note that reliable measurements cannot be obtained close to the soil surface (i.e., top 20 cm) as neutrons escape into the atmosphere. Ideally, the NP should be calibrated for each soil type (soil-specific calibration) and access tube material (Vachaud et al., 1977). Prior to the terrorist attacks on 9/11, NPs utilizing a radioactive source and detector were widely used for SM profile assessment as part of irrigation management owing to the ability to monitor water content in bore holes. The subsequent increase in regulations and paperwork related to radioactive devices has made NPs impractical for most users. Additional information about the practical and theoretical aspects of neutron scattering for SM measurements are provided in Sadeghi, Babaeian, et al. (2018).

The cosmic ray neutron probe (CRNP) for recording the neutrons that are generated by cosmic rays within air and soil and other materials is a newer method for noninvasively measuring area-averaged (effective) SM within the top soil (Zreda et al., 2008). Similar to the NP method, a calibration function is commonly developed to relate the change in low-energy neutrons to the change in hydrogen content for SM determination. For instance, a common theoretical function has been developed by Desilets et al. (2010) relating SM to relative neutron counts

$$\theta_v(N) = \frac{0.0808}{\left(\frac{N}{N_0}\right) - 0.372} - 0.115 \tag{3}$$

where N is the neutron count rate (count per hour) normalized to a reference atmospheric pressure and solar activity level and N_0 is the counting rate (count per hour) over dry soil under the same reference conditions. A detailed description of the cosmic ray technique can be found in Zreda et al. (2012).

Due to the higher propagation of cosmic rays in thin air, the lateral footprint extent is inversely proportional to the atmospheric (vapor) pressure and is up to 300 m in diameter, while the penetration depth strongly depends on the SM content (Franz et al., 2012; Zreda et al., 2008) and ranges from 15 cm in wet soils to approximately 70 cm in dry soils (Figure 5) which decreases exponentially with distance to the sensor (Kohli et al., 2015). The exact CRNP footprint and sensitivity are still an active area of research. At present, most research is being conducted to interpret the measured signals, as the sensors measure not only SM but also the presence of water in vegetation, subsurface biomass and organic matter, surface water, atmospheric vapor, and clay lattices water (Baatz et al., 2015) as well as to determine the radius of influence (Kohli et al., 2015).

SM derived from CRNP is frequently validated using local-scale wireless SM networks (Franz et al., 2012). Comparison of CRNP measurements with TDR SM data at 10 test sites in Germany (catchment of the river Rur) demonstrated reliable measurements of SM with root-mean-square error (RMSE) of 0.032 cm³/cm³ (Baatz et al., 2014). Baatz et al. (2014) installed a catchment-wide network consisting of 10 cosmic ray sensor systems at the Terrestrial Environmental Observatories (TERENO) Rur site in Germany in order to compare
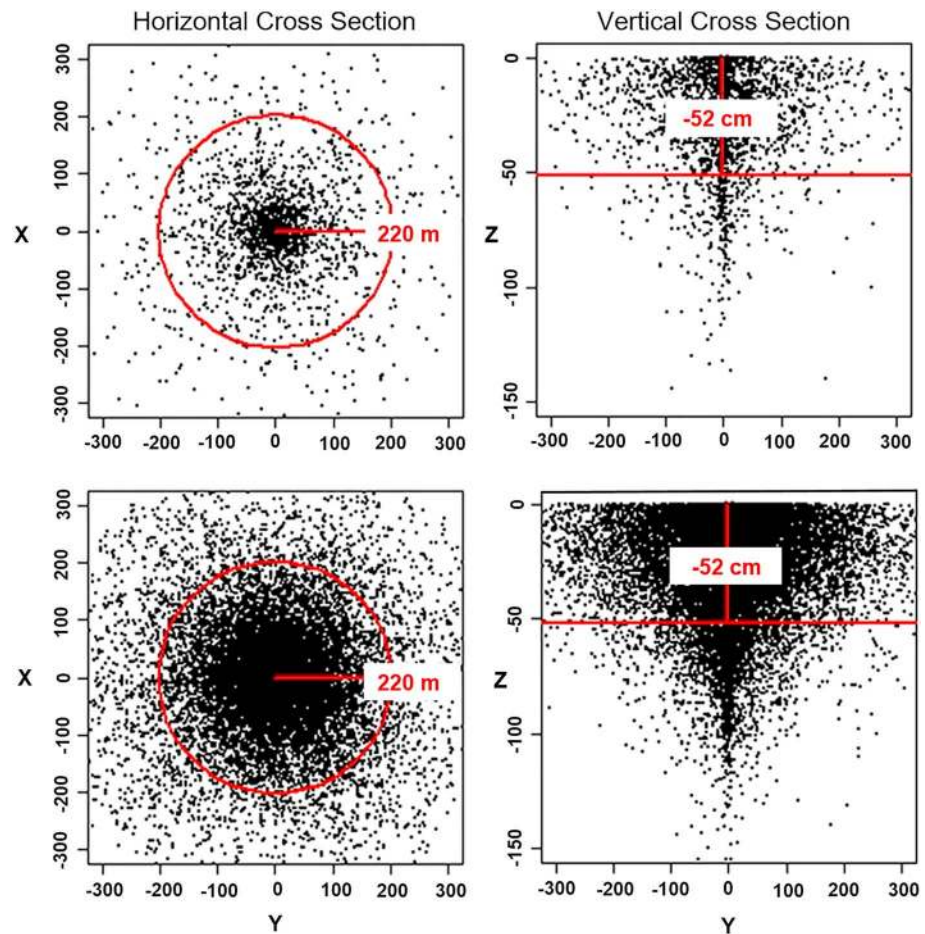
Figure 5. Interactions of cosmic ray neutrons (black dots) with the soil in directions *XY* (left) and *YZ* (right), prior to detection with a central sensor. The footprint (red circle) is denoted as distance ($X = 220$ m, $Y = 220$ m) or depth ($Z = 0.52$ m) within which about 86% of the detected neutrons are characterized.

three different parameterization methods: (1) the N-O method, (2) the hydrogen molar fraction method (hmf method), and (3) the Cosmic method. All three methods were found to perform well after calibration. The hmf and Cosmic methods showed more similar calibration curves than the N-O method.

First attempts are now being undertaken to establish networks of CRNP at larger scales. The COsmic ray Soil Moisture Observing System (COSMOS) network (Zreda et al., 2012) is presently being installed in the United States with the aim to install 500 cosmic ray sensors (see section 6.1). Currently, there are approximately 194 permanent CRNP stations worldwide (Andreasen et al., 2017) including 109 COSMOS stations in the United States (Zreda et al., 2012), 20 TERENO stations in Germany (Baatz et al., 2015), 13 CosmOz stations in Australia (Hawdon et al., 2014), and 32 COSMOS-UK stations in the United Kingdom (Evan et al., 2016). Also, mobile CRNP rover systems have been developed (Dong et al., 2014). Due to its large footprint, the CRNP could potentially fill the spatial gap between SM ground point data and satellite estimates; hence, it can serve as a reference for the validation of satellite SM products. The CRNP SM has been recently used for validation of spaceborne SM products such as SMAP, SMOS, and ASCAT in the United States, Australia, Europe and Africa (Akbar & Moghaddam, 2015; Babaeian et al., 2018; Fascetti et al., 2016; Montzka et al., 2017; Van der Schalie et al., 2016).

One important limitation of the CRNP in humid climates and wooded regions is that it is significantly influenced by various sources of hydrogen in environment (e.g., water vapor in the atmosphere, litter water, organic matter, and root biomass), which in some cases yield volumetric SM contents that exceed soil porosity. Thus, CRNP data need some additional adjustments to remove the effect of additional hydrogen contained in these pools. Adjustment methods have been presented in Franz, Zreda, Ferre, et al. (2012) and
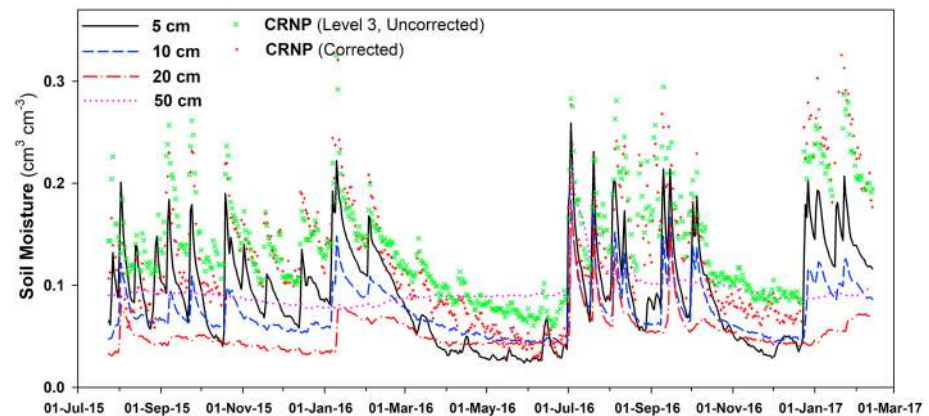
Figure 6. Correction of CRNP soil moisture data for the Walnut Gulch site in Arizona. Uncorrected and corrected data after removing the effects of additional hydrogen pools (water vapor, organic matter water content, and lattice water) are shown. The colored lines represent Soil Climate Analysis Network (SCAN) soil moisture data at different depths. CRNP = Cosmic Ray Neutron Probe.

Bogena et al. (2013). Figure 6 shows an example of CRNP data adjustment for the Arizona Walnut Gulch site after subtracting the contribution of additional hydrogen pools during converting neutron counts into SM content. It is obvious that corrected CRNP data better capture in situ SM data from the Soil Climate Analysis Network (SCAN).

3.2. EM SM Sensors

Topp et al. (1980) revolutionized soil water content sensing with the introduction of TDR. At that time, the first TDR instruments were very expensive and only deployable for laboratory measurements. Since then, the costs of TDR devices have decreased by several orders of magnitude, while other EM sensors based on capacitance or impedance circuits have also been developed. As a result, over the last decade, numerous companies have developed a variety of sensors based on EM measurements of soil permittivity (Bogena et al., 2007; Jones et al., 2005; Seyfried & Murdock, 2004; Vaz et al., 2013). Permittivity, also called dielectric constant, is a measure of the electrical potential energy of a substance under the influence of an EM field. The EM sensor electric field is generally directed into the soil along 2-, 3-, or 4-parallel electrodes or an adjacent pair of rings. For example, the Hydra Probe (Stevens Water Monitoring Systems Inc.) uses one central and three outer electrodes based on an impedance circuit operating at 50 MHz. The Hydra Probe is the only EM water content sensor offering both real and imaginary permittivity output (Figure 7a). While there is potential to extract additional information from complex permittivity, few have attempted to fully utilize these measurements (Kelleners et al., 2005; Peplinski et al., 1995). The Hydra Probe is widely used by the U.S. federal agencies in weather and snow monitoring stations (e.g., SCAN; SNOwpack TELemetry, and SNOTEL). The measurement of permittivity provides a highly accurate determination of water content in soil because the permittivity of water is about 80, while permittivities of solids and air are around 4 and 1, respectively. Interestingly, the most accurate water content determination method remains the original TDR method operating at around 1-GHz frequency, despite a larger number of low-cost low-frequency (<100 MHz) water content sensors being marketed today (Blonquist et al., 2005; Vaz et al., 2013). In general, TDR does not require soil-specific calibration and is less susceptible to secondary effects such as electrical conductivity, temperature and relaxation (from high clay or organic matter content) than lower-frequency EM sensors. This immunity to secondary effects comes in part because of the higher measurement frequency (~1 GHz) and the use of travel time as the measurement method. The travel time, t, of the EM signal is proportional to the relative permittivity, K_r, of the substance through which it travels according to

$$t = \frac{2l\sqrt{K_r}}{c} \qquad (4)$$

where l is the length of the TDR electrodes and c is the speed of light (3×10^8 m/s) (Robinson et al., 2003). Once K_r is measured, the relationship between the volumetric moisture content (θ) of the substance and K_r is given from a general mixing model (Dobson et al., 1985; Jones et al., 2002), written as
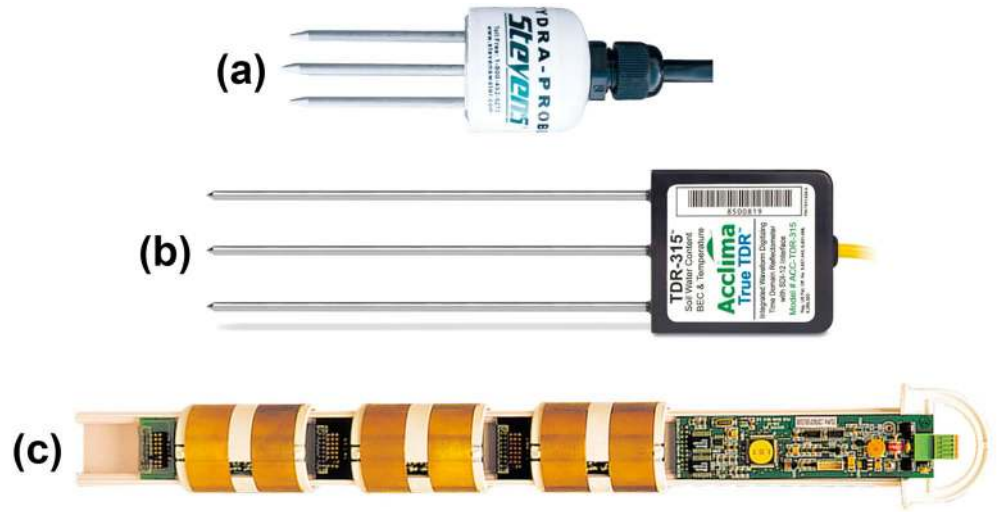
Figure 7. Examples of electromagnetic water content sensors are (a) the Stevens Water impedance-based Hydra Probe measuring at 50 MHz, (b) the Acclima True TDR measuring in the range of 1000 MHz, and (c) the Sentek capacitance-based EnviroSCAN sensor, which employs frequency domain resonance, that is, the water content determines the resonant frequency in the range from 100 to 150 MHz. (Please note that sensor manufacturers are only named for the convenience of readers, which does not imply an endorsement of specific sensors by the authors).

$$\theta = \frac{K_r^\beta - (1-n)K_s^\beta - nK_a^\beta}{K_w^\beta - K_a^\beta} \tag{5}$$

where n is the soil porosity and subscripts s, a, and w refer to permittivities of constituent solids (minerals), air, and water, respectively. The exponent β summarizes the geometry of the substance and has a range $-1 < \beta < 1$, with $\beta = 0.5$ representing an isotropic mixed medium. Recently, gigahertz frequency TDR (Figure 7b) has been developed and reduced in size using low-cost cellular phone components, facilitating production of TDR sensors that are competitively priced with more common lower-frequency sensors. Limitations of the TDR method include restricted applicability under highly saline conditions due to signal attenuation and the requirement of soil-specific calibration for soils with high clay or organic matter (OM) contents. Severe attenuation of TDR waveforms in the presence of high salinity and/or some clays having high surface area and surface charge may interfere with, or even preclude, water content measurements. In soils with an abundance of 2:1 clay minerals that commonly exhibit large specific surface areas, the bulk dielectric permittivity is more susceptible to temperature fluctuations due to the release of bound water under very dry conditions (Escorihuela et al., 2007; Wraith & Or, 1999). In organic matter rich soils, the amount of bound water is commonly higher due to the large specific surface are and associated higher adsorptive surface forces, which is manifested in lower bulk permittivity values when compared to soils with low OM contents (Bircher et al., 2016). Further limitations include the inability to measure the frozen water content due to the similarity of the permittivities of ice and the mineral soil constituents (Jagdhuber et al., 2014) and restricted applicability in highly structured soils with an abundance of large pores that prevent a close contact between the sensor electrodes and the soil matrix.

In recent years, several EM-based borehole or downhole solutions, most employing parallel rings and capacitance circuitry to estimate water content in the vicinity of the cylindrical sensor (Figure 7c), have been developed. A growing trend for environmental sensors in general is to employ SDI-12 communication, which uses addressing to facilitate multiple sensors connected to a single digital port of a data logger. With options for addressing with single digit numbers and both uppercase and lowercase letters, more than 60 sensors can be connected to each available port on a data logging device. Given these advances, deployment of water content sensors for RS calibration has become more user friendly with lower costs.
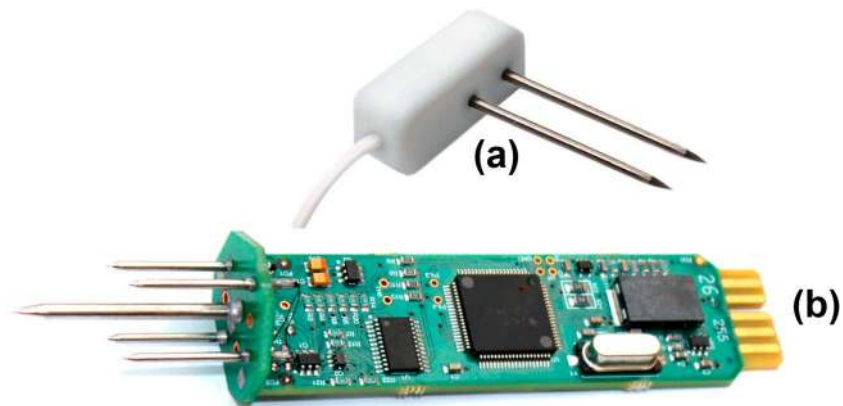
Figure 8. Heat pulse probes used for thermal property assessment: (a) a commercial dual-needle probe for heat capacity determination (METER Group Inc., Pullman, WA, USA) and (b) the Utah State University-developed penta-needle heat pulse probe yielding thermal conductivity and diffusivity in addition to heat (and water) velocity in two directions. (Please note that sensor manufacturers are only named for the convenience of readers, which does not imply an endorsement of specific sensors by the authors).

In general, EM-sensors are well suited for monitoring SM profiles, but seemingly few if any were developed specifically for near-surface moisture monitoring. In order to calibrate optical RS measurements from satellites or drones, the soil "skin" moisture content is needed, but common practice has the closest sensor to the surface at just 5 cm below the surface. This leads to a great deal of uncertainty since the soil typically wets and dries from the surface downward. There are certainly times when the surface has been wetted by rainfall, but the wetting did not penetrate to the sensor, and similarly, when the surface has air dried while the soil 5 cm below the surface is still quite moist. For these scenarios and others, novel and improved EM-based sensors are desired to address the growing need for accurately calibrating soil surface RS data using ground measurements more focused on the soil skin. Recently, a novel sensing instrument has been developed for more accurate measuring surface and near-surface SM content. Sheng et al. (2017) designed and tested a TDR array sensor that provides centimeter-resolution measurements of near-surface SM (0–8 cm) with high accuracy (± 1 permittivity unit).

3.3. HPPs

The use of heat as a tracer for thermal property determination in soil was pioneered several decades ago, but technological limitations hindered application of this method (Al Nakshabandi & Kohnke, 1965; De Vries, 1958). HPP were miniaturized, and their measurements automated in the early 1990's (Bristow et al., 1993; Campbell et al., 1991), and a growing body of literature attests to the many applications for which they are well suited owing to the water content dependence of soil thermal properties (Hopmans et al., 2002; Kamai et al., 2008; Y. Lu et al., 2014, Lu et al., 2016; Ochsner et al., 2003; Ren et al., 2000; Yang et al., 2013). Probes generally consist of one heater needle (typically 18 Ga or 1.27-mm diameter) and one to five thermistor needles spaced approximately 6 mm from the heater needle, which makes them ideally suited to small sample interrogation (Figure 8). Various algorithms have been developed and applied to infer thermal conductivity (λ, W·m^{-1}·K^{-1}), thermal diffusivity (k, m^2/s), or heat capacity (C, J·m^{-3}·K^{-1}) from HPP temperature rise measurements. The interrelationship between these three thermal properties means that only two of the three parameters must be determined for calculation of the third. The heat capacity can be computed from

$$C = \lambda/k \tag{6}$$

A heat pulse of 8 s is generally applied resulting in a temperature rise of about 1 °C at the sensing needles. This translates to 5% precision in heat capacity estimation if temperature measurements are on the order of 0.05 °C accuracy (Kluitenberg et al., 1993). These measured temperature rise data are used to fit one or more thermal properties as functions of analytical or numerical solutions. One estimate of k is given as (Bristow et al., 1994)

$$k = \frac{r^2}{4} \left[\frac{\frac{1}{t_m - t_0} - \frac{1}{t_m}}{\ln\left(\frac{t_m}{t_m - t_0}\right)} \right] \qquad (7)$$

where r is the mean heater needle to thermistor needle spacing, t_m is the time from the initiation of heating to the occurrence of the maximum temperature, $T_{\max}$, and t_0 is the heating duration (8 s). To estimate λ, an expression for C from Knight and Kluitenberg (2004) is multiplied with the thermal diffusivity

$$\lambda = kC = \frac{kq't_0}{e\pi r^2 T_{\max}} \left(1 - \frac{\varepsilon^2}{8} \left\{ \frac{1}{3} + \varepsilon \left[\frac{1}{3} + \frac{\varepsilon}{8} \left(\frac{5}{2} + \frac{7\varepsilon}{3} \right) \right] \right\} \right) \qquad (8)$$

where e is the Naperian constant (≈ 2.718) and $\varepsilon = t_0/t_m$. The soil volumetric heat capacity is an important link between thermal properties and volumetric moisture content of soil (θ). The soil heat capacity describes the amount of heat stored in the soil, which can be summed as the heat capacities of individual constituents according to (De Vries, 1963)

$$C = (\rho c)_s (1 - \varphi) + (\rho c)_w \theta + (\rho c)_a (\varphi - \theta) \qquad (9)$$

where ρ is constituent density (kg/m^3), c is constituent specific heat (J·kg^{-1}·K^{-1}), ϕ is total porosity, and subscripts s, w, and a indicate the soil's solid, water, and air phases, respectively. If the air phase is neglected and the solid phase is assumed to exhibit typical soil mineral density and heat capacity, we can substitute $C_w = (\rho c)_w$ and $C_s = (\rho c)_s$ resulting in a simplified relationship written as (Campbell, 1985)

$$C = C_s(1 - \varphi) + C_w \theta \qquad (10)$$

Estimates of C can ultimately be used to estimate the soil volumetric water content, θ, using the expression

$$\theta = \frac{C - \rho_b c_s}{C_w} \qquad (11)$$

where ρ_b is soil bulk density (kg/m^3) and c_s is the specific heat capacity of the soil solids (J·kg^{-1}·°C^{-1}).

Heat pulse sensor needles are generally short, and needle spacing is several millimeters apart because of the interest in minimizing energy input to the soil while maximizing the signal to noise ratio. This makes heat pulse measurements well suited for near-surface determination of soil properties including SM content (Mori et al., 2003).

3.4. Other SM Sensors

A potential new source of information about continental-scale SM is observations of temporal changes in gamma radiation. It has long been recognized that airborne gamma radiation surveys with low-flying planes can be used to determine SM content (Carroll, 1981) and snow water equivalent (SWE) for flood forecasting applications (Peck et al., 1971). The GAMMA instrument on the NOAA AC690A Turbo Commander aircraft has been used operationally by NOAA's National Weather Service since 1979 to measure the mean areal SWE and SM along the flight path (Peck et al., 1980). Attenuation of natural terrestrial gamma radiation by water in air, snow, soil, and vegetation between the ground and the aircraft is the basis of SWE and SM measurements. After the nuclear reactor accident in Chernobyl in 1986, most countries of the European Union established in situ monitoring networks measuring outdoor gamma radiation for early warning. The data are composite gamma radiation measurements over a broad energy spectrum, and the sources of gamma radiation can be separated into terrestrial, cosmic, and artificial origin. These gamma radiation measurements are published in near-real time and archived by the EUropean Radiological Data Exchange Platform. As a result of this network of networks, measurements of more than 4,600 monitoring stations are made accessible to the public at least once a day. The footprint of a typical EUropean Radiological Data Exchange Platform gamma ray monitoring station has a radius of about 7 m and 90% of the sensor response originates from the top 12 to 25 cm of the soil (Bogena et al., 2015; Mao et al., 2015). The gamma ray intensity measured near the soil surface has been shown to be related to soil water content (Mao et al., 2015), but it is also known to depend on cosmic rays that enter and interact with the atmosphere, anthropogenic Cs^{137} from nuclear tests and accidents, and atmospheric Rn^{222}. For accurate SM estimation from gamma radiation measurements, all interfering time variable, anthropogenic, and nonterrestrial
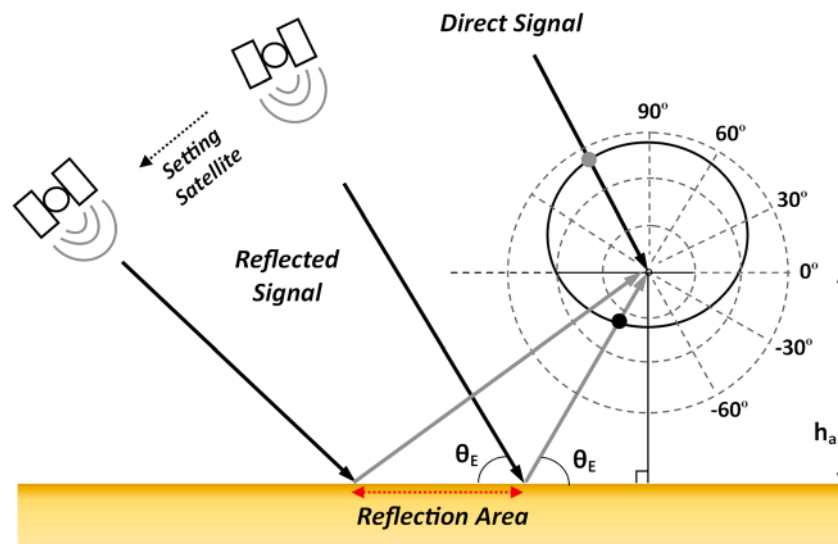
Figure 9. Sketch illustrating the geometry of a multipath signal for antenna height h_a and satellite elevation angle θ_E. Black and gray arrows represent the Global Positioning System signal transmitted from the satellite and the reflected signal from the ground, respectively. The solid circle represents the gain pattern of the antenna, and the dashed circles indicate power levels of the receiving antenna gain pattern. When the satellite is approaching the horizon, the reflected signal is associated to a larger distance to the Global Positioning System antenna.

signals have to be removed from the data (Bogena et al., 2015). If this can be achieved, SM of the top 25 cm of the soil can be determined with an expected accuracy of 0.025 g/g (Loijens, 1980). Recently, the potential of gamma ray sensors for measuring SM has gained popularity, especially in Europe where these sensors have been deployed in the aftermath of the Chernobyl nuclear accident to monitor the spread and fate of radionuclides. A comprehensive review of these methods is provided in Bogena et al. (2015).

Another promising technology for SM determination at larger scales is the utilization and analysis of signals that are recorded on the ground through Global Navigation Satellite Systems (GNSS) such as Global Positioning System (GPS) receivers (Katzberg et al., 2006; Larson et al., 2008; Rodriguez-Alvarez et al., 2009) that have initially been established for geodynamic (navigation and positioning) applications. In this technique, also called GPS interferometric reflectometry (GPS-IR or GNSS-IR), SM retrieval is based on the analysis of power variations of the GNSS signals, where the direct signal from the GNSS satellite and the signal reflected by the land surface are simultaneously received by the antenna (Figure 9). Considering their phase difference due to the motion of the GNSS satellites, the simultaneously received direct and coherently reflected signals cause an interference pattern in the signal power. This interference pattern is dependent on the height differences between the GNSS antenna and the reflection level (Vey et al., 2016). The interference between the direct and reflected signals produces a modulation that can be observed in temporal variations of the signal-to-noise ratio (SNR) recorded by the GPS receiver. A change in the soil permittivity (due to change in moisture content) affects all three GPS interferogram parameters, including the effective reflector height, amplitude, and phase (Larson et al., 2008), where the phase of the SNR is the most sensitive parameter for SM determination. If the soil is wet, the active L-band microwave GNSS signal (~1.2 and 1.5 GHz) is reflected from a layer just below the land surface, while for dry soil the signal penetrates deeper into the soil and is reflected within a surface layer of up to 7-cm thickness (Bogena et al., 2015). It has been shown that the changes in SNR are highly correlated with near-surface SM in the top 5 cm of soil (Larson et al., 2010; Rodriguez-Alvarez et al., 2009, 2010). It has been also demonstrated that GPS-based SM estimates are independent of the soil type (Chew et al., 2014).

The GNSS-IR has been shown to have great potential for SM estimation using ground-based receivers (Chew et al., 2014; Zhang et al., 2018). However, variables such as snow depth and vegetation water over land may affect SM retrieval accuracy (Larson et al., 2008; Zhang et al., 2017). The GNSS-IR footprint can cover up to thousands of square meters, depending on antenna height and satellite elevation angle (Larson et al., 2010).
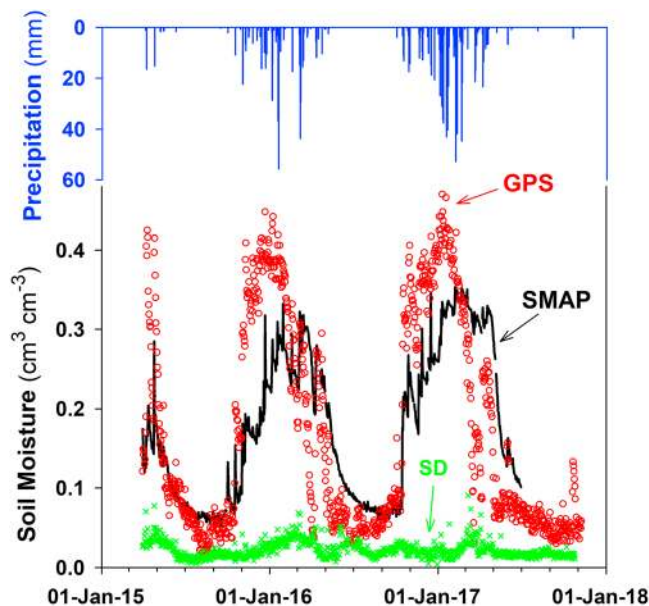
Figure 10. Soil moisture content inferred with GPS-IR (circles) compared to SMAP L4 surface soil moisture (black line) over California (Calaveras GPS site with Savanna vegetation cover) and daily precipitation (blue bars) from April 2015 to October 2017. The green symbols represent standard deviation (SD). GPS = Global Positioning System; SMAP = Soil Moisture Active Passive.

For a GPS antenna installed at heights of 1 and 50 m, the footprint area radius varies from 50 to 330 m (Bogena et al., 2015). In this technique, the current temporal resolution of SM retrievals is daily because each GPS satellite has a 1-day revisit time at any antenna location.

Numerous studies have been conducted in different regions of the World indicating the good accuracy of SM retrievals from GNSS data (Chew et al., 2018; Rodriguez-Alvarez et al., 2009; Sanchez et al., 2015). Recently, Zhang et al. (2018) analyzed GNSS-IR data over a dense grassland site in southwestern France and compared the GNSS SM retrievals to in situ observations at 5-cm depth and reported RMSE values of 0.035 cm^3/cm^3 (for grass covered surfaces) and 0.018 cm^3/cm^3 (after grass has been cut). We also compared the GPS SM inferred over a Savana site in California to the SMAP L4 surface SM values and obtained a very similar pattern with R^2 and RMSE values of 0.52 and 0.09 cm^3/cm^3, respectively (Figure 10).

The NASA Cyclone Global Navigation Satellite System (CyGNSS) that has been designed for tropical ocean surface wind sensing is also capable to record GNSS reflections over land and thus has potential for large-scale SM estimations. In a study by Kim and Lakshmi (2018), they used the CyGNSS in conjunction with SMAP SM and provided improved SM estimates with higher temporal resolution (five times per day). Chew and Small (2018) related L-band CyGNSS signals to SMAP SM and found a strong positive linear correlation between the change in CyGNSS reflectivity and the change in SMAP SM with a daily averaged RMSE of 0.045 cm^3/cm^3. Yet direct applications of this technology to improve our understanding of hydrological processes need to be documented in literature. The value of these larger-scale networks resides less in their potential to directly study hydrological processes but rather in their ability to provide spatially averaged data for the calibration and validation of remotely sensed data and their use in data assimilation methods to improve predictions of hydrological fluxes and states. The GPS SM data are available publicly through the National Science Foundation Plant Boundary Observatory (NSF'Topps Plant Boundary Observatory) at *http://xenon. colorado. edu/portal/*.

3.5. Wireless Network Technology
3.5.1. Network Structure

The development of WSMNs has gained a strong momentum in the last few years due to the development of low-cost SM sensors and transmitting technologies, offering the potential to determine spatiotemporal SM dynamics at the field to catchment scales (Bogena et al., 2015; Vereecken et al., 2014) and permitting real-time data access to distributed SM sensors through a centralized communication architecture.

Most WSMNs consist of five basic elements, including (1) a series of SM probe/sensor nodes, (2) a series of infrastructure nodes or routers, (3) an end node (gateway or coordinator) for data gathering and transfer, (4) a datalogger or PC, and (5) an internet server with a web interface.

SM probes which are installed below the soil surface should be low cost, reliable, low power, and easy to install (Robinson, Campbell, et al., 2008). The most promising sensors are those that measure soil electrical permittivity, as described above in section 3.2. The routers are commonly installed above the ground. They receive data from SM probe nodes and other infrastructure nodes and transfer to the coordinator. Each network has only a single coordinator which controls and keeps the network running and streams information from the sensor network to the user and vice versa. ZigBee Alliance (ZigBee Alliance, 2010) is a low-cost mesh networking property standard that has been widely used for communication in wireless control and monitoring applications (Bogena et al., 2010; Kuorilehto et al., 2008; Valente et al., 2006).

Two main topologies for wireless sensor networks have been proposed: (i) underground topology and (ii) hybrid topology (Akyildiz & Stuntebeck, 2006). In underground topology all sensor units are deployed below the soil surface except for the coordinator unit (Ritsema et al., 2009). Whereas in hybrid topology a
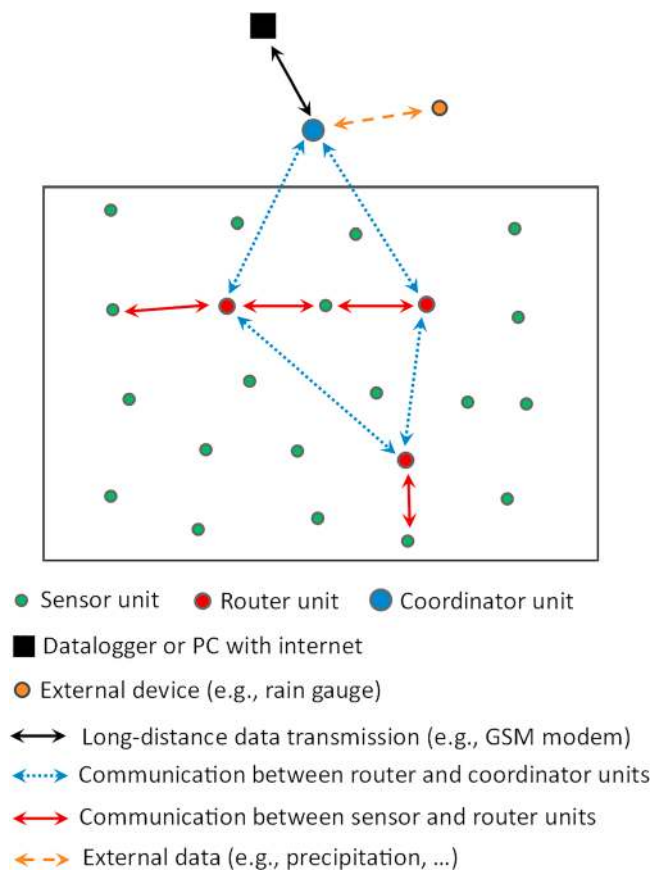
Figure 11. An example for a hybrid topology wireless soil moisture network (adapted from Bogena et al., 2010).

combination of underground and aboveground devices is considered. It has been pointed out that a hybrid topology, which is composed of a mixture of underground sensors and aboveground router devices, is preferable to achieve longer transmission ranges (Bogena et al., 2009). The basic structure of hybrid topology is illustrated in Figure 11.

Since WSMNs mainly operate on battery power, overall power consumption becomes a critical constraint. Thus, it is important to design WSMNs that minimize retransmissions. Underground topologies require considerable power to overcome soil attenuation. Hybrid topologies on the other hand allow data to be routed from the underground in a few steps, thus reducing underground travel distance to conserve power (Bogena et al., 2010).

3.5.2. WSMN Applications

Many WSMNs have been used to study spatiotemporal dynamics of SM at the field (Vereecken et al., 2014), catchment (Graf et al., 2014; Schröter et al., 2015) and landscape (Qu et al., 2015) scales. Earlier work has focused on the identification of SM patterns and their temporal stability (Brocca, Tullo, et al., 2012; Mittelbach & Seneviratne, 2012; Western et al., 1999). The seminal work of Western et al. (1999) about the Tarrawarra catchment where they deployed an array of SM sensors showed that SM in catchments exhibits dry and wet states that switch in function due to the interplay between local and nonlocal hydrological controls. This finding has been further corroborated in other catchment studies such as at the TERENO Wüstebach site in Germany (Graf et al., 2014). Brocca et al. (2014) used data from six SM networks around the Earth to study absolute versus temporal anomaly and percentage of global SM saturation. One major application of WSMNs is the validation of SM products from microwave RS missions.

Recently, Wiekenkamp et al. (2016) used wireless SM networks to identify the occurrence and controls of preferential flow in a forested catchment. Their approach is based on the work of Graham and Lin (2011), who based on the changes in SM observed at different depths after rainfall events identified three major flow regimes: preferential flow, sequential flow, and nondetectable flow. Preferential flow refers to out of sequence SM changes where deeper locations respond earlier to an increase in soil water than locations closer to the surface. The SM measurements indicated that preferential flow occurred throughout the catchment. No clear controls triggering the spatial occurrence of preferential flow could be identified. Wiekenkamp et al. (2016) used the WSMN at the Wüstebach site to analyze catchment-wide controls of preferential flow. Based on the sensor response times, they identified four different flow regimes: (1) nonsequential preferential flow, (2) velocity-based preferential flow, (3) sequential flow, and (4) no response. Different potential factors that may control preferential flow and its spatial occurrence were analyzed: hydrological, topographical, and soil physical and chemical parameters as well as temporal factors such as precipitation events and antecedent SM status were studied. None of these factors were found to control preferential flow. Apparently, occurrence of preferential flow was governed by small-scale soil and biological processes. During storm events, the preferential flow occurred across the whole catchment. Blume et al. (2009) used a combination of sparse SM measurements in space, but with high temporal resolution, and rainfall simulation experiments and dye tracing to study the controls of preferential flow. They found that hydrophobicity in combination with small-scale variability in rainfall and strong heterogeneity in hydraulic conductivity were the main drivers controlling preferential flow. Stockinger et al. (2014) used the WSMN in combination with stable δO^{18} isotope measurements in water to study travel time distributions in the Wüstebach catchment. They showed that the presence of wet and dry states is reflected in the stream flow discharge pattern. Under the dry state, the uphill regions of the headwater catchment are disconnected from the river system and were found not to contribute to discharge. Only the riparian part of the catchment is contributing to river discharge under this state. Under the wet state both the uphill and riparian part of the catchment supply water for river discharge. The change

from wet to dry state was found to occur at a mean water content of 0.35 cm^3/cm^3, which corresponds to the maximum spatial variation of soil water.

SM data obtained from wireless sensor networks can be coalesced to produce the mean water content (σ_θ) function (i.e., the relationship between the spatial mean of SM and its standard deviation) for the observation area. The interpretation and analysis of this function has been the focus of various studies (Qu et al., 2014; Rosenbaum et al., 2012). Vereecken et al. (2007) was the first to use a closed form analytical expression based on stochastic perturbation theory to predict this function. Rosenbaum et al. (2012) observed the presence of hysteretic behavior in the σ_θ with drying events leading to a decrease in the spatial variability and wetting events to an increase for identical mean water content values. Qu et al. (2014) applied inverse optimization of the observed SM content values using the Hydrus-1D model at 102 points at the German TERENO Rollesbroich site to link temporal stability of measured locations with key soil hydraulic properties (SHPs). Qu et al. (2015) expanded the work of Vereecken (2007) by deriving a closed form expression for the van Genuchten (1980) equation. Using pedotransfer functions (PTFs) to generate the input parameters for the closed form expression, they were able to predict the σ_θ function for different sites. This approach has been applied at the global scale by Montzka et al. (2017).

4. Proximal Sensing Methods

Because of high costs and laborious installation of point-scale SM sensors, they are not well suited to provide spatially continuous profile SM distributions at larger scales. In recent years, several geophysical proximal sensing methods such as ground penetrating radar (GPR), ground-based radiometer and radar systems, electromagnetic induction (EMI), and magnetic resonance imaging (MRI) techniques have been developed for field-scale SM determination (Robinson et al., 2008; Robinson, Campbell, et al., 2008). It should be noted that CRNP and GPS methods (section 3.4) may be considered as proximal sensing techniques. However, here we classify them as ground-based techniques as they provide temporally continuous SM measurements and have been used in SM networks for calibration and validation of remotely sensed SM estimates. This section provides an overview of the basic principles and recent advances of proximal sensing techniques.

4.1. GPR

GPR, also known as georadar, subsurface radar, and ground probing radar, is a promising proximal soil sensing technique that has proven to be applicable for high-resolution profile SM mapping in two or three dimensions at the field scale. The GPR technique can be used to bridge the present scale gap between small-scale invasive sensors (e.g., TDR sensors) and large-scale airborne or satellite RS observations. GPRs transmit high-frequency (1 MHz to 1 GHz) EM signals into the subsurface in a noninvasive manner. The travel time associated with an EM signal traveling between a radar transmitter and receiver is measured and used to estimate the dielectric permittivity of the soil (Huisman et al., 2002, 2003). GPR-derived dielectric bulk permittivity is then transformed to volumetric SM content using, for example, Topp's empirical relationship (Topp et al., 1980) or other dielectric mixing models (Sihvola, 1999). Three GPR types including cross-borehole, airborne or off-ground, and surface-based or on-ground systems are commonly deployed for SM determination (Huisman, Hubbard, et al., 2003). Cross-borehole systems are used to monitor SM dynamics in the vadose zone. The transmitting and receiving antennas are located in two parallel boreholes and generate a two-dimensional velocity image between the boreholes, which can then be converted to dielectric permittivity and consequently to SM (Binley et al., 2002; Looms et al., 2008). The borehole GPR has been successfully applied to reconstruct two-dimensional images (tomographs) of SM distributions between borehole locations (Binley et al., 2001; Looms et al., 2008), but it remains limited to smaller-scale (a few meters) applications, as it requires the installation of vertical boreholes for transmitter and receiver deployment. Although borehole GPR performs well (van der Kruk, 2006), the systems are time consuming to operate, effectively limiting their suitability for larger-scale spatial investigations.

Alternatively, off-ground and on-ground GPR systems have been deployed to map SM variability at the field scale (Ardekani, 2013; Jonard et al., 2011; Minet et al., 2012; Serbin & Or, 2003). Off-ground GPR configurations are installed at distinct heights above the soil surface and in many cases mounted on mobile platforms to rapidly move over the soil surface. Such systems are also used for airborne and spaceborne applications (Ulaby et al., 1986). Using full-waveform GPR signal modeling, field-scale SM mapping is feasible (Lambot et al., 2004; Minet et al., 2012; Weihermüller et al., 2007). Combined with a vector network
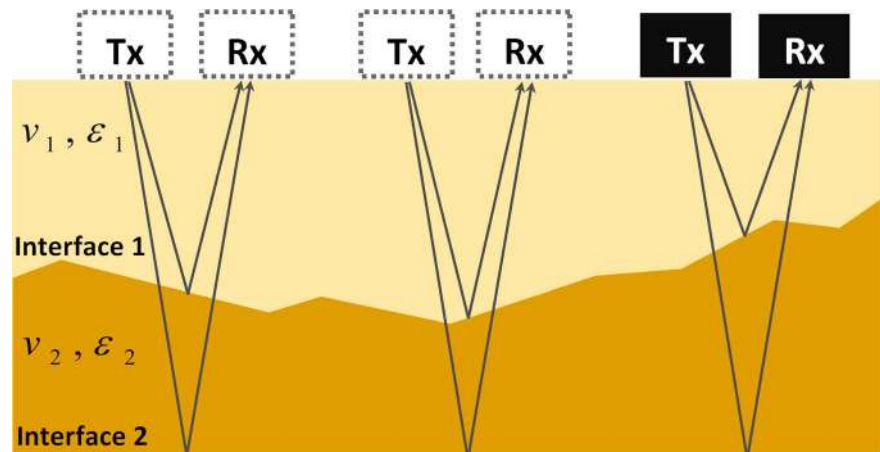
Figure 12. Sketch illustrating the on-ground Ground Penetrating Radar (GPR) basic principle and reflection profiling, where Tx is the transmitting and Rx is receiving antenna. Reflections at interfaces arise from changes in subsurface velocity (v) and dielectric constant (ε).

analyzer, off-ground systems commonly use the surface reflection coefficient for soil characterization and SM estimation (Jonard et al., 2011; Serbin & Or, 2003). The main challenge for off-ground GPR is its sensitivity to surface roughness (Lambot et al., 2006; Van der Kruk et al., 2010) and the shallow measurement depth of the signal as compared to on-ground GPR techniques (Vereecken et al., 2014). However, the effect of surface roughness may be alleviated by operating at low frequencies (0.2–0.8 GHz; Jonard et al., 2011). The off-ground GPR may be used for validation of microwave RS SM products (Koyama et al., 2017).

On-ground GPR systems represent a perfect alternative for mapping of profile SM because of their ability to measure direct ground wave propagation velocity (Grote et al., 2003; Huisman et al., 2002, 2001), which allows for deeper signal penetration when compared to the off-ground systems due to ground coupling. On-ground GPR measurements are performed with a fixed separation distance between transmitting and receiving antennas (Figure 12). The combination of GPR signals with other sensors/data such as EMI (Moghadas et al., 2010) and seismic (Ghose & Slob, 2006) has become more common for providing better estimates of SM. However, GPR has limitations such as poor performance in clay or electrically conductive soils, contact issues in dense shrubs, and soils with rock fragments (i.e., on-ground GPR), as well as requiring more sophisticated data interpretation (Robinson et al., 2012). A detailed review about the application of GPR for measuring SM is provided in Klotzsche et al. (2018).

4.2. EM Induction

SM determination with EMI sensors relies on the strong correlation between soil water content and the EMI measured apparent soil electrical conductivity (EC_a; Moghadas et al., 2010). Applications of EMI for SM variability mapping and monitoring at intermediate (hillslope to catchment) scales are discussed in, for example, Sheets and Hendrickx (1995), Allred et al. (2005), and Huth and Poulton (2007), Tromp-van Meerveld and McDonnell (2009), and Shanahan et al. (2015).

EMI sensors apply current to the soil through EMI; hence, no direct contact with the soil surface is required (Corwin & Lesch, 2003). Common instruments consist of a transmitter coil that, when energized with alternating current (AC) at audio frequency, produces an EM field (Figure 13). The time-varying EM field emitted from the transmitter coil induces weak circular eddy current loops in the conducting soil, which in turn generate a secondary EM field that differs in amplitude and phase from the primary field (McNeill, 1980). The magnitude of amplitude and phase differences between primary and secondary fields primarily depends on soil properties including moisture content, type, and concentration of ions in the soil solution, the amount, and type of clay minerals in the soil matrix, the temperature, and the phase of soil water (Brevik & Fenton, 2002; Carroll & Oliver, 2005; Kachanoski et al., 1990; Reedy & Scanlon, 2003) as well as spacing between the transmitter and receiver coil, the distance between coils and soil surface, and coil orientation (parallel or perpendicular to the soil surface). The effect of magnetic permeability of the
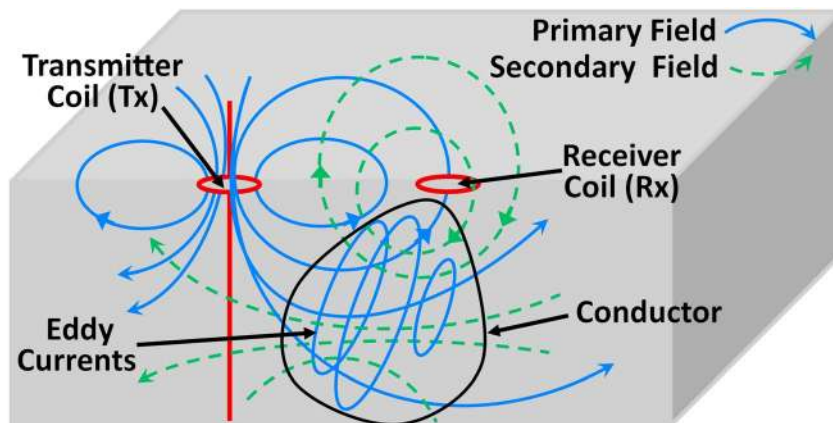
Figure 13. Sketch illustrating the propagation of electromagnetic fields in soil for an electromagnetic induction (EMI) sensor.

soil seems to be negligible according to De Jong et al. (1979). The primary and secondary fields are sensed as apparent conductivity at the receiver coil in Siemens per meter (S/m; McNeill, 1980). A detailed description of the theoretical background of EMI is provided in Tuller and Islam (2005).

EMI sensors commonly used for soil investigations include monofrequency (e.g., DUALEM-1, DUALEM-2, EM31, EM38, EM38-DD, EM38-MK2, and EMP-400) and multifrequency (e.g., GEM-300) sensors. EMI has been also thoroughly tested for estimating soil salinity (Williams et al., 2006), soil texture (White et al., 2012), clay content (Harvey & Morgan, 2009), cation exchange capacity (Triantafilis et al., 2009), soil compaction (Sudduth et al., 2010), soil pH (Van Meirvenne et al., 2013), soil organic carbon (Martinez et al., 2009), leaching rates of solutes (Slavich & Yang, 1990), herbicide partition coefficients (Jaynes et al., 1994), groundwater recharge (Williams et al., 2006), and for estimation of the leaf area index (Rudolph et al., 2015). An excellent review by Doolittle and Brevik (2014) details EMI applications for soil studies.

Monofrequency instruments have been recurrently used to estimate SM, yielding R^2 values ranging from 0.11 to 0.99 (Robinson, Binley, et al., 2008; Tromp-van Meerveld & McDonnell, 2009). Recently, several studies have shown that multifrequency EMI sensors can be effectively used for measurement of SM distributions within soil profiles (Tromp-van Meerveld & McDonnell, 2009). For example, Calamita et al. (2015) used a multifrequency sensor with eight frequencies between 7 and 2 KHz for the retrieval of shallow SM at four sites in Italy and indicated a linear relationship between SM and EC_a with R^2 between 0.46 and 0.69 and RMSE between 0.064 and 0.077 cm^3/cm^3. Tromp-van Meerveld and McDonnell (2009) tested a multifrequency sensor with four frequencies (7–14 KHz) to monitor SM for a 9-month period over an upland forested hillslope and found a better relationship between EC_a and SM at depths ~>30 cm (R^2~0.84–0.87) than at a depth <15 cm (R^2~0.78-0.83).

Combining GPR and EMI data in an integrated inverse modeling scheme that increases the information extracted from geophysical data has become more common. Moghadas et al. (2010) investigated the joint analysis of GPR and EMI synthetic data to reconstruct the electrical properties of a two-layer medium and reported that the GPR-EMI inversion approach can accurately estimate the soil electrical parameters when the values of conductivity and permittivity of the first layer are low.

4.3. Nuclear Magnetic Resonance

Nuclear magnetic resonance imaging (NMRI; also called magnetic resonance imaging, MRI) is another proximal sensing technique for noninvasive SM determination. It is based on the sensitivity of the MRI signal intensity (echo) to SM content. Paetzold et al. (1985) first applied this concept to monitor SM. Guillot et al. (1989) then recorded the first images of a porous medium during moisture depletion.

The most fundamental MRI principle for SM is spin-echo imaging (Merz et al., 2016), in which an echo is created by a 180° radiofrequency pulse following an initial 90° radio frequency pulse. The echo intensity depends on the proton density, which is proportional to the water content of the medium and the
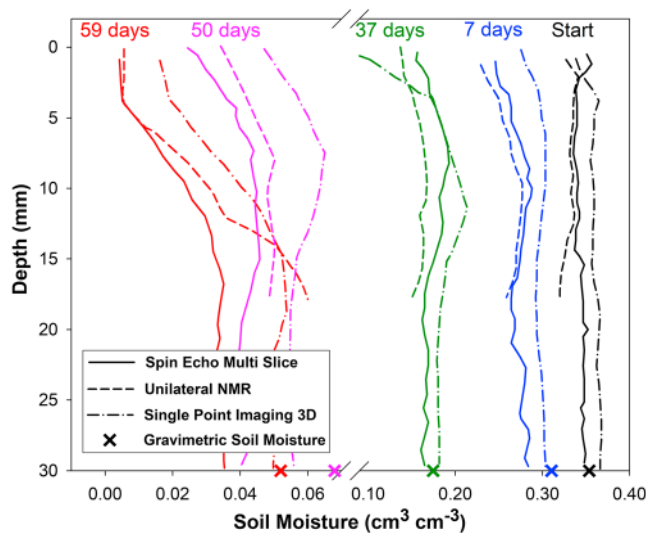
Figure 14. Temporal near-surface soil moisture profile evolution measured by Spin Echo Multi Slice (SEMS), Single Point Imaging 3D (SPI3D), and unilateral Nuclear Magnetic Resonance (NMR) Magnetic Resonance Imaging (MRI) techniques. The crosses at the abscissa represent the gravimetric water content (Merz et al., 2014).

relaxation times. Since relaxation times also change with water content, the echo intensity is not necessarily proportional to the water content (Barrie, 2000). Because echo intensity itself is also affected by experimental parameters like echo time and repetition time, it is preferable to record an entire series of echoes and extrapolate to zero to obtain a quantity that is proportional to the water content if the relaxation time is sufficiently long (Edzes et al., 1998). In most natural porous media that include high content of silt or clay, the relaxation time might be quite short. In this case the so-called single point imaging (SPI) technique, originally developed to monitor water in saturated rocks, may provide more reliable estimates (Balcom et al., 2003). Merz et al. (2014) tested three MRI methods (unilateral NMR, spin echo multiscale (SEMS), and SPI3D) for estimating near-surface moisture based on equation (12)

$$\theta_{MR} = (\theta_{a,MR} - \theta_{r,MR})/(1 - \theta_{r,MR}) \qquad (12)$$

with $\theta_{\alpha,MR} = M(0,r)/M(0,r)_{saturated}$ in which $M(0,r)$ and $M(0,r)_{saturated}$ denote the signal amplitude at partial and initial saturation, respectively, $\theta_{r,MR}$ is the relative magnetic resonance (MR) signal at dry (residual) soil condition. The assumption of this model is the linear relationship between MR signals and the moisture content. Figure 14 depicts high-resolution near-surface moisture profiles of medium sand monitored over time with the three MRI methods.

4.4. ELBARA/JULBARA and ComRAD Ground-Based Radiometer and Radar Systems

The Eidgenössische Technische Hochschule (ETH) Zürich L-Band Radiometer (ELBARA) is a passive system operating at a frequency of 1.4–1.427 GHz. It was constructed by the University of Bern in collaboration with ETH to infer SHPs from the SM dynamics of top soil. The radiometer consists of a dual-mode conical horn antenna mounted on a back of a truck (mobile) or a tower (fixed) with 4–17 m elevation at zenith angle between 30 and 330°. It measures the brightness temperature at the soil surface for SM retrieval. The radiometer is equipped with internal cold (273°K) and hot (338°K) loads for measurement calibration (Jonard et al., 2011). The ELBARA II system has been designed by ESA as part of SMOS, and it is used for ground-based campaigns in Europe for calibration of SMOS and SMAP SM algorithms and for validation of SM retrievals (Miernecki et al., 2014; Schwank et al., 2010; Wigneron et al., 2012). Miernecki et al. (2014) used ELBARA II SM estimates for evaluation of SMAP and SMOS SM retrieval algorithms and demonstrated that SMAP single channel (Single Channel Algorithm [SCA]-H and SCA-V) and dual channel (DCA) algorithms and the SMOS land parameter retrieval model (LPRM) provide results very close (RMSEs 0.035–0.056 cm³/cm³) to those obtained from L-band Microwave Emission of the Biosphere (L-MEB) model-based multi-angular ELBARA II measurements. The JULBARA system at the Forschungszentrum Jülich in Germany is a Dick-type L-band (1.414 GHz) radiometer that has been used for SM retrieval at the field scale with RMSEs of 0.062 (horizontal polarization) and 0.054 cm³/cm³ (vertical polarization) (Jonard et al., 2011).

The Combined Radar and Radiometer (ComRAD) ground-based L-band simulator (O'Neill et al., 2007) developed jointly by NASA/GSFC and George Washington University has been used to refine SMAP SM retrieval algorithms under controlled conditions (Srivastava et al., 2015) and to develop new radiative transfer based SM retrieval models for vegetated terrain and small tree canopies (Kurum et al., 2011). It consists of a quad-polarized radar (1.25 GHz) and a dual-polarized radiometer (1.4 GHz) sharing the same 1.22-m parabolic dish antenna with 12° field of view and mounted on a 19-m hydraulic boom truck for field deployment. Before field measurements, the radiometer is calibrated with cold sky and ambient microwave absorber targets. In a study by Srivastava, et al. (2015), ComRAD data were used for evaluation of the SCA-H algorithm integrated with Mironov/Dobson dielectric mixing models for SM retrieval at a USDA field site covered with corn and soybeans. Results indicated that SCA-H is promising for L-band SM retrieval with a RMSE of 0.04 cm³/cm³.

Table 3
Overview of Remote Sensing Methods for SM Measurement and Monitoring

Group	Advantages	Constraints	References
Optical (Vis-NIR-SWIR)	Wide spatial coverage High spatial resolution Potential for real-time applications (e.g., Drone) Promising multi spectral and hyperspectral sensor results	Limited surface measurement depth (a few millimeters) High signal perturbation by clouds and vegetation Attenuated by Earth's atmosphere Low temporal resolution	Lesaignoux et al. (2013), Oltra-Carrio et al. (2015), Sadeghi et al. (2015), and Zhang et al. (2013)
Thermal	Wide spatial coverage High spatial resolution Potential for real-time applications (e.g., Drone) Strong correlation between surface SM and temperature	Limited surface measurement depth (a few millimeters) High signal perturbation by clouds and vegetation Attenuated by Earth's atmosphere Perturbed by vegetation biomass	Sugathan et al. (2014) and Verstraeten et al. (2006)
Active microwave	Sensitive to soil-water dielectric constant/permittivity Wide spatial coverage (global) Surface measurement depth (up to 5 cm) High spatial resolution Strong correlation between SM and backscattered power Backscatter not perturbed by clouds and atmospheric constituents Backscatter is independent of solar illumination	Low temporal resolution Perturbation of signals by surface roughness and vegetation biomass	Crapolicchio and Lecomte (2004) and Wagner et al. (2007, 2013)
Passive microwave	Sensitive to soil-water dielectric constant/permittivity Wide spatial coverage Surface measurement depth (up to 5 cm) High temporal resolution Brightness temperature not perturbed by atmospheric constituents and clouds	Low spatial resolution Perturbation of signals by surface roughness and vegetation biomass	Chan et al. (2016), Entekhabi et al. (2010), and Kerr (2007), and Njoku et al. (2003)

Note. SM = soil moisture; NIR = near infrared; SWIR = shortwave infrared.

5. RS Methods for SM Retrieval

RS approaches for SM estimation have been applied since the 1970s. These promising methods produce spatially explicit measurements of SM. This section provides an overview of progress and constraints of optical, thermal, and microwave RS techniques for skin and near-surface SM measurements and monitoring. A brief overview of these RS techniques for SM retrieval and associated pros and cons is provided in Table 3.

5.1. Optical RS

In optical RS, the Vis, NIR, and SWIR EM radiation bands with wavelengths ranging from 350 to 2,500 nm are used to provide SM estimates from spectral surface reflectance information. Optical RS systems are classified into multispectral and hyperspectral imaging systems, depending on the number of spectral bands used in the imaging process. In this section, we discuss optical imagery and reflectance spectroscopy techniques that are deployed for SM retrieval at large and small (laboratory) scales.

5.1.1. Optical Imagery

Optical RS methods have been proposed to quantify skin SM from broadband and narrowband optical satellite and airborne remote sensors such as Landsat (Profeti & Macintosh, 1997; Vincente-Serrano et al., 2004), MODIS (Zhang & Wegehenkel, 2006), Hyperion (Song, Ma, et al., 2014), HyMap (Haubrock et al., 2008) and simulated satellite bands (Castaldi et al., 2015; Muller & Decamps, 2000). Despite the numerous optical remote sensors currently in orbit, a limited body of literature exists on the exploitation of optical observations for skin SM estimation. This seems to be partly due to the inability of optical signals to penetrate clouds and vegetation covers (Zhao & Li, 2013) and the lack of an agreed physically based model for accurate estimation of SM from optical data (Sadeghi et al., 2017). In addition, some optical and hyperspectral data from

satellite sensors exhibit low temporal resolution, which limits their applicability for monitoring state variables such as SM.

Because of the wider spectral resolution of satellite/airborne sensors when compared to laboratory instruments that operate within the 1- to 8-nm spectral range and natural heterogeneities at larger scales, it is challenging to directly apply laboratory-developed SM retrieval methods to RS measurements. Besides SM, other soil properties (e.g., organic matter, color, salinity, texture, vegetation, roughness, and crust) affect surface reflectance; hence, RS spectral measurements are highly variable in space (Ben-Dor et al., 2002). This affects the accuracy of large-scale applications. Despite these limitations there is significant interest in SM estimation from optical RS data, because the high spatial resolution SM products are useful for agricultural applications.

Recently, Hassan-Esfahani et al. (2015) developed a neural network method that translates high spatial resolution unmanned aireal system (i.e., AggieAir) imagery to reasonably accurate SM estimates (RMSE less than 0.03 cm^3/cm^3) for a large center pivot irrigated field in Scipio, Utah. Although the application of hyperspectral imaging has generally provided promising results for surface SM (Anne et al., 2014; Peng et al., 2013; Wang et al., 2011), the usefulness of this technique needs to be further explored in future research. Hyperspectral sensors with finer spatial resolution and narrow spectral bands may offer an alternative to traditional multispectral analysis of SM, in particular for landscapes with high spatial heterogeneity. New missions such as Hyperspectral Precursor and Application Mission (Galeazzi et al., 2008), the Environmental Mapping and Analysis Program, that will be launched in 2020 (Stuffler et al., 2006), or the HYPerspectral IMager, scheduled to launch prior to 2020 (Michel et al., 2010), are able to fully cover the solar domain (400 to 2,500 nm) with high spectral resolution (average of 10 nm) and offer new opportunities for estimating surface moisture from hyperspectral imagery.

5.1.2. Reflectance Spectroscopy

Reflectance spectroscopy (diffuse optical spectroscopy) has been applied as a powerful means for large-scale SM estimation or for skin SM measurements at smaller scales. This spectroscopic technique exploits the fact that the EM spectrum exhibits several distinct water absorption bands within the NIR (~1,414 nm) and SWIR (~1,915 and 2,210 nm) frequency ranges (Clark, 1999; Viscarra Rossel et al., 2006). Reflectance spectroscopy can be also classified as a proximal sensing techniques. Diffuse reflectance relies on a focused projection of the spectrometer beam onto a sample of interest, where it is reflected, scattered, and transmitted through the sample material. Spectrometers that operate within the Vis, NIR, and SWIR (400–2,500 nm) range are applied for both laboratory and field measurements.

The relationship between skin SM and spectral reflectance has been extensively studied and is well documented in literature (Ben-Dor & Banin, 1995; Bogrekci, & Lee, W. S., 2006; Chang et al., 2001; Hummel et al., 2001). Numerous studies have been conducted, mainly at the laboratory scale, to explore the relationships between spectral reflectance and skin SM for a wide range of soil types (Gao et al., 2013; Lobell & Asner, 2002; Philpot, 2010; Tian & Philpot, 2015). Findings from these studies indicate that reflectance decreases relative to an increase of SM with the effect being more pronounced in the SWIR range (Angstrom, 1925; Liu et al., 2002; Sadeghi et al., 2015; Weidong et al., 2002). Exceptions to this trend have been observed, particularly when approaching saturation (Liu et al., 2002; Neema et al., 1987) and when models that consider Fresnel reflectance were applied (Sadeghi et al., 2015).

In general, empirical and physical approaches can be discerned for estimating SM from spectral reflectance data. Most studies that capitalized on the full hyperspectral signature of soils have focused on empirical regression models such as partial least squares regression (Bogrekci, & Lee, W. S., 2006; Castaldi et al., 2015), principal component regression (Chang et al., 2001), and multiple linear regression (Ben-Dor & Banin, 1995; Liu et al., 2002; Lobell & Asner, 2002) to estimate SM. Hyperspectral signatures measured in the laboratory are very repetitive and highly oversampled with a high degree of intercorrelation between neighboring bands. For such cases, band aggregation can be applied as a simple method to reduce and downsample spectral data, which in turn is helpful to obtain accurate calibrations (Lopez et al., 2013). Several empirical indices have been defined to estimate skin SM from measured surface reflectance. The most reliable results have been obtained with the Water Index SOIL (Bryant et al., 2003), the Normalized SM Index (Haubrock et al., 2008), and the Shortwave Angle Slope Index (Khanna et al., 2007). The main drawback of such indices is the use of bands located within the water absorption features, making them very sensitive to
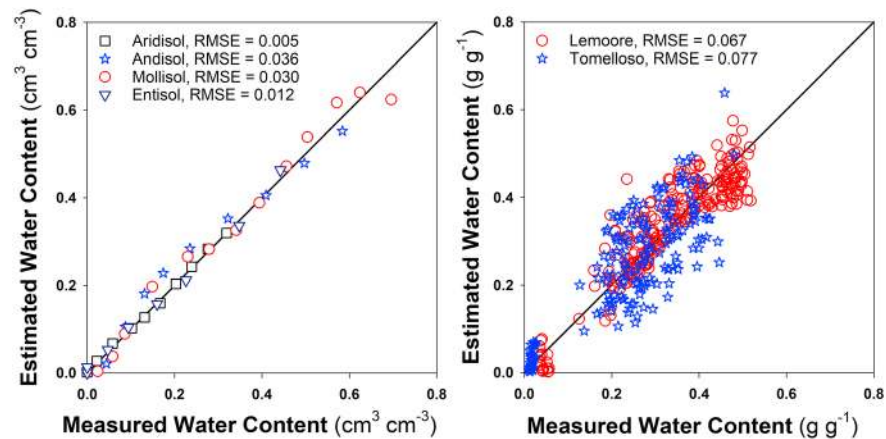
Figure 15. Comparison of the Sadeghi et al. (2015) model estimates with directly measured skin soil moisture for single samples representing four different soil orders (left) and multiple samples of two different watersheds (right). RMSE = root-mean-square error.

effects of atmospheric water vapor. Although empirical methods seem to work reasonably well for the distinct conditions they were developed for, they cannot be universally applied as spatially significantly varying soil composition (i.e., SM, organic matter content, minerals, and salts) strongly affects spectral reflectance (Huan-Jun et al., 2009).

Physical approaches for SM estimation from optical reflectance are mainly based on radiative transfer theory (Philpot, 2010; Twomey et al., 1986). Sadeghi et al. (2015) proposed a promising physically based method to determine skin SM from transformed reflectance of bare and sparsely vegetated soils based on the Kubelka-Munk (Kubelka & Munk, 1931) two-flux radiative transfer theory, which describes diffuse reflectance from a uniform, optically thick, absorbing, and scattering medium. This approach yielded reasonable results with a RMSE of less than 0.07 cm^3/cm^3 when compared to directly laboratory-measured water contents for various soils (Figure 15). The potential applicability for large-scale skin SM measurements and associated challenges is yet to be assessed. While diffuse spectroscopy has been proven to yield good skin SM results, a few studies also documented its potential for accurate predictions of more complex properties such as water retention and hydraulic properties (Babaeian et al., 2015; Santra et al., 2009).

It is apparent that while the application of diffuse spectroscopy under laboratory conditions in most cases provides reasonable results, field measurements exhibit higher uncertainty due to natural heterogeneity of soil properties, topography, and vegetation effects. This points to the need for further investigations of spatial heterogeneity effects on the relationships between reflectance and skin SM. A more detailed analysis of reflectance spectra and comparison to laboratory spectral resolutions are required to overcome this limitation (Haubrock, Chabrillat, Lemmnitz, & Kaufmann, 2008).

5.2. Thermal Infrared RS

Thermal infrared RS exploits the EM wave band between 3,500 and 14,000 nm for SM retrieval from land surface temperature (LST) determined with the thermal inertia method (Jackson, 1982; Price, 1980; Schieldge et al., 1982; Verstraeten et al., 2006) or in conjunction with vegetation indices (VI; Claps & Laguardia, 2004). Over the past three decades, the LST-VI concept has been widely applied for the estimation of SM (Gillies et al., 1997; Mallick et al., 2009) and evapotranspiration (Heilman et al., 1976; Stisen et al., 2008). Several studies have documented the LST-VI/fractional vegetation cover (FVC) relationship within a triangular (Carlson, 2007) or trapezoidal space (Moran et al., 1994). The FVC ranges between 0 for bare soil and 1 for full vegetation cover. The so-called "universal triangle" concept was first proposed by Price (1990) for prediction of evapotranspiration and later adapted for surface SM retrieval (Carlson et al., 1994; Gillies et al., 1997).

A central assumption of the triangle method is that when a large number of pixels capturing the full range of soil surface moisture and FVC are considered, sharp boundaries in the LST-VI scatter plot reflect real
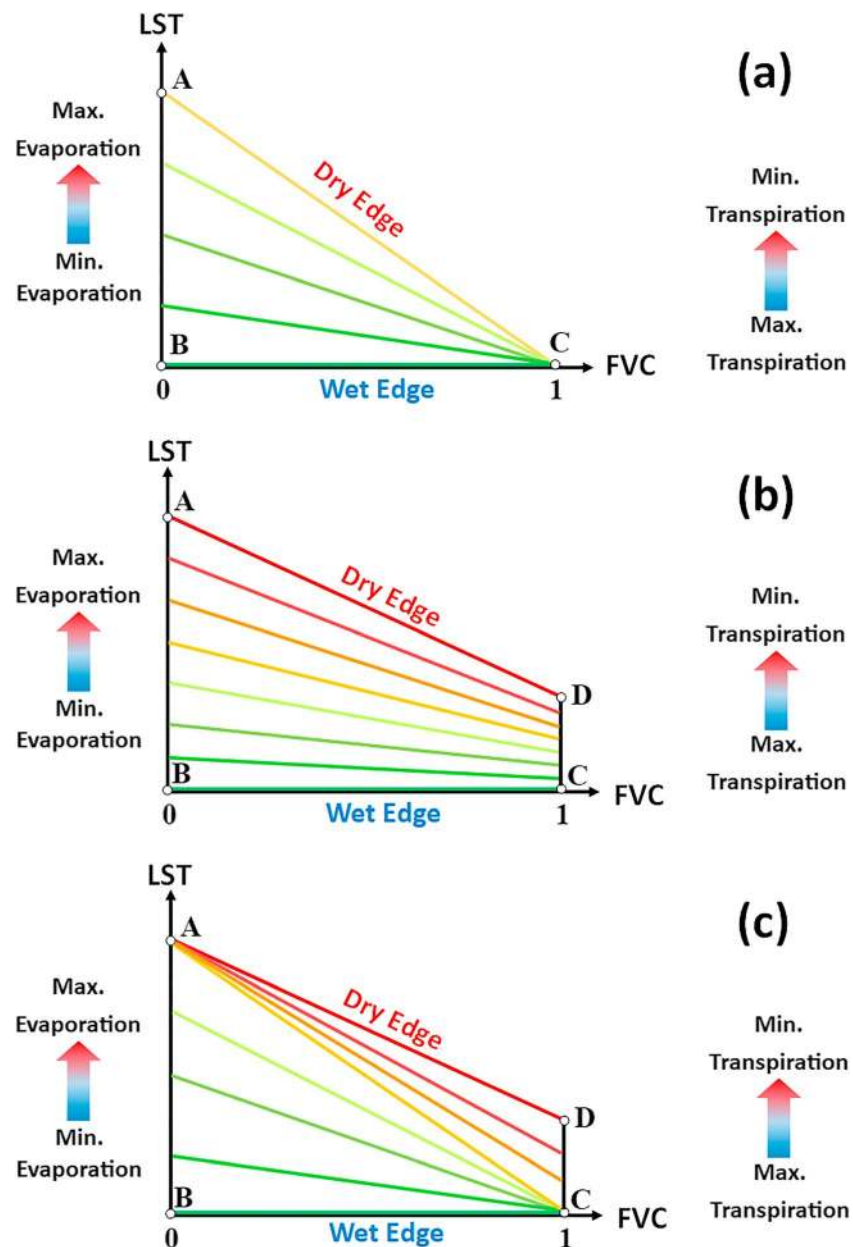
Figure 16. Triangular LST-FVC space (a), conventional trapezoidal LST-FVC space (b), and two-stage trapezoidal LST-FVC space (c) reproduced from Sun (2016). LST = land surface temperature; FVC = fractional vegetation cover.

physical limits that include bare soil, full-cover vegetation, and lower and upper limits for surface SM (e.g., completely dry points A and C and saturated points B and C in Figure 16a). The dry and wet edges intersect at point C for full vegetation cover. The relative value of surface SM and the surface energy fluxes for each pixel can be defined in terms of its position within the triangle (Wang et al., 2011). A detailed description of the universal triangle method is provided in Carlson (2007). While an advantage of the triangle method is its independence of ancillary data (atmospheric and surface data), it is challenging to define the triangular space for locations with narrow VI range or for regions with rainy/dry seasons, which results in narrow scattering of the LST-VI points. The establishment of the LST-VI relationship is more complicated for large scales due to the spatial heterogeneity of surface properties that may affect the shape of LST-VI space and thereby interfere with the precise determination of the dry and wet edges (Wang et al., 2011).

Numerous studies have been devoted to estimation of surface SM from the LST-VI space. For example, Sandholt et al. (2002) proposed a dryness index for estimation of SM via linking the surface temperature Ts-Normalized Difference Vegetation Index (NDVI) scatter plot with a temperature-vegetation dryness index and found similar spatial patterns ($R^2 = 0.70$) between TDVI and SM simulated with a hydrological model. Wang et al. (2001) proposed a Vegetation Temperature Condition Index for monitoring drought occurrence and its spatial distribution at the regional scale in China. Rahimzadeh-Bajgiran et al. (2013) developed a new method to estimate SM from the surface evaporative fraction retrieved from the LST-FVC space. Some studies used multiple regression analysis for estimation of SM. For example, Sobrino et al. (2012) applied high-resolution thermal images acquired with the Airborne Hyperspectral Scanner to estimate SM at field scale from emissivity, NDVI, and LST data and obtained a RMSE value of 0.05 cm^3/cm^3.

Based on the triangular LST-FVC feature space method, Zhang et al. (2015) proposed a simple method to estimate SM for the North China Plain with a second-order polynomial interpolation function. This method requires a number of atmospheric input parameters to establish the edges of the triangular LST-FVC space from energy balance considerations, which allows comparison of the directly derived SM for a wide range of atmospheric forcing conditions. Validation experiments with ground data for 10- and 20-cm depths yielded RMSEs from 0.04 and 0.10 m^3/m^3, respectively.

The universal triangle method has been previously employed to predict SM at the regional/global scales from low spatial resolution but high revisit frequency satellite imagery such as provided by MODIS and Advanced Very High Resolution Radiometer for a wide range of land surface covers (Sandholt et al., 2002; Wan et al., 2004). NASA's Landsat-8 satellite that was launched in February 2013 provides thermal data (bands 10 and 11) at a moderate resolution of 100 m that has been applied for thermal SM RS (Amani et al., 2016; Shafian & Maas, 2015).

The trapezoid method first proposed by Moran et al. (1994) describes the relationship between the surface soil and air temperature difference (Ts-Ta) and the FVC. This method has been applied to estimate evapotranspiration rates for both fully covered and partially vegetated land surfaces via the Water Deficit Index (WDI). While the universal triangle method establishes the dry and wet edges empirically, the trapezoid method is based on physical processes (Yang et al., 2015); hence, derived WDI values are comparable for different times. In addition, the trapezoid method is applicable for finer scales and regions with a narrow SM and vegetation cover range (Wang et al., 2011). Although the idea of a trapezoidal (Ts-Ta)-FVC space is widely accepted, only a few applications for SM estimation are documented in literature. This is partly due to challenges associated with the calculation of the soil surface and air temperature difference (Ts-Ta) and partly due to the lack of atmospheric data (i.e., air temperature, wind speed, and relative humidity). These limitations motivated Wang et al. (2011) to apply the Ts-VI space. They proposed an iterative procedure for quantifying the Ts-VI trapezoid and calculated the WDI from MODIS surface temperature and an Enhanced Vegetation Index. SM validation experiments in the Walnut Gulch Experimental Watershed in Arizona revealed that while temporal variations of SM can be captured reasonably well, the quantification of spatial variations is limited, at least for semiarid climatic conditions. This might be due to the often erroneous assumption of a linear relationship between SM and soil temperature. Although this assumption yielded reasonable SM estimates in the past, it is not supported by laboratory and field measurements. A simple evaporation experiment conducted in our laboratories revealed a nonlinear (L-shaped) relationship between soil surface temperature and surface SM that is also confirmed by field observations at a SCAN site within the Little River Watershed in Georgia (Figure 17). These observations point to the need to quantify and apply the actual soil temperature-SM relationship that is mainly influenced by atmospheric forcing (i.e., air temperature, humidity, and wind) to improve SM predictions.

Recent attempts to modify the trapezoid method have mainly focused on a more accurate definition of space edges based on the actual response of soil and vegetation to SM dynamics. For example, a two-stage trapezoid method (i.e., two merged triangular spaces) proposed by Sun (2016) proved to be more efficient than the conventional trapezoid method as it resolves some of the challenges discussed above (Figures 16b and 16c). The central assumption of the two-stage trapezoid is that Ts is governed by surface SM within the LST-FVC space, while vegetation temperature (Tv) is governed by RZSM (Carlson, 2013). In fact, when moisture within a vegetated soil profile varies from its wettest to its driest value, the surface moisture
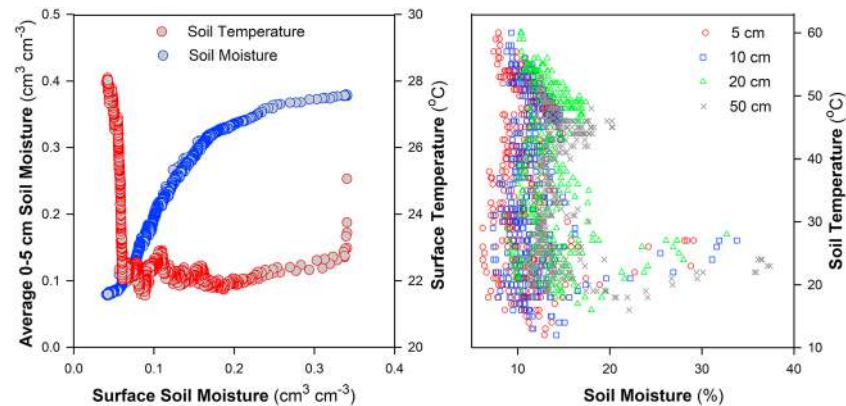
Figure 17. Nonlinear relationship between laboratory measured surface/skin SM (soil moisture) and average (0–5 cm) SM (blue circles) and surface temperature (red circles) during evaporative drying of a sand column (left). Field-measured SM and temperature at different depths at a Soil Climate Analysis Network site in 2013 within the Little River Watershed in Georgia (right).

approaches its lowest value before the RZSM does. This indicates a difference in variation rates for Tv and Ts, where Tv is lagging Ts because vegetation absorbs RZSM for photosynthesis and transpiration.

Sun (2016) simulated the LST-FVC space with the "SimSphere" model and demonstrated that the new trapezoid is more consistent with the simulated LST-FVC space and can evolve the LST-FVC space from the triangular to the trapezoidal form (Figure 16c). Additionally, they compared both the two-stage trapezoid and the conventional trapezoid to estimate the evaporative fraction based on 110 MODIS LST and VI products. Comparisons have indicated that the two-stage trapezoid is more effective than the classical trapezoid for evaporative fraction estimation. The uncertainty analysis has also revealed that this method is better suited for areas and periods exhibiting low SM levels.

Recently, Sadeghi, Babaeian, et al. (2017) and Babaeian et al. (2018) proposed a novel optical trapezoid model named OPTRAM as an alternative to the conventional triangle/trapezoid methods for estimating SM from transformed reflectance (SWIR transformed reflectance, STR) data of Sentinel-2, Landsat-8, and MODIS in the SWIR band. The trapezoid is formed by distribution of NDVI as a measure of vegetation fraction versus STR as a measure of SM (Figure 18, left). The latter is based on a simple two-flux radiative transfer model indicating a linear relationship between surface SM and STR within SWIR bands, which proved to be valid for a broad range of soils (Sadeghi et al., 2015; Sadeghi et al., 2018).

$$\frac{\theta}{\theta_s} = \frac{r - r_d}{r_s - r_d} \tag{13}$$

where θ_s is the saturated water content, r is transformed reflectance, and r_s and r_d are the transformed reflectance of saturated and dry soils, respectively. This novel approach was evaluated based on in situ measurements of SM in different watersheds in the United States and showed reasonably good performance for SM retrieval (see Figure 18, right). The OPTRAM model has also performed equally well or, in some cases, better than the traditional trapezoid models. The main advantage of OPTRAM is its applicability to new higher spatial resolution optical satellites with no thermal band (e.g., Sentinel-2).

5.3. Microwave RS

As with EM in situ SM sensors, the vast disparity in dielectric permittivity of water, air, and solids is also exploited for microwave RS (Ulaby et al., 1982). The dielectric properties of the soil phases (i.e., water, air, and solids) affect the emissivity and backscattering of microwaves at the soil surface. SM is routinely retrieved from low-frequency microwave data, including the P-band, L-band, C-band, and X-band. Several dielectric mixing and empirical models have been proposed to infer bulk soil permittivity that can be related to SM content (Dobson et al., 1985; Mironov et al., 2009; Roth et al., 1990; Topp et al., 1980; Wang and Schmugge, 1980). Passive and active microwave RS of SM are currently the most promising techniques for
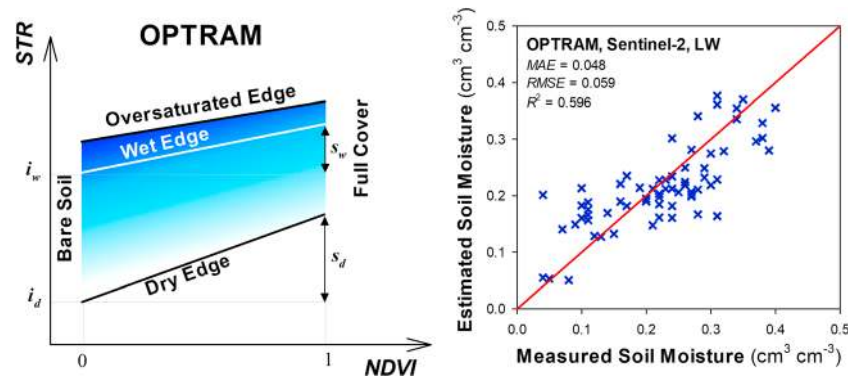
Figure 18. Sketch illustrating OPTRAM trapezoid (left), and the evaluation results of the optical trapezoid using Sentinel-2 data in the Little Washita watershed in Oklahoma (right) (Sadeghi, Babaeian, et al., 2017). STR = SWIR transformed reflectance; NDVI = Normalized Difference Vegetation Index; MAE = mean absolute error; RMSE = root-mean-square error LW = Little Washita watershed.

global-scale monitoring. Microwave-based SM products are the only ones routinely supplied various satellite missions. In terms of continues availability of large-scale data products, microwave-based techniques are substantially more advanced than optical- and thermal infrared-based SM products. For example, some agencies (e.g., EUMSETAT and JAXA) have made operational commitments to their microwave SM products (i.e., ASCAT and AMSR-2) by launching a new mission to ensure product continuity in the event of a satellite/sensor failure.

5.3.1. Passive Microwave RS

Passive microwave sensors (radiometers) record the natural microwave emission (brightness temperature, T_b) that is dependent on emissivity and physical temperature of the emitting body. For passive SM retrieval, knowledge of the physical temperature of the land surface is required. The Fresnel reflection equations describe the emissivity of a smooth bare soil surface based on the incidence angle of the sensor and the complex dielectric constant of the soil. Typically, soils have a rough surface, which decreases reflectivity and thus increases emissivity. Vegetation cover also alters microwave emissions and adds a separate contribution to the land surface emission signal. To simulate these effects, Mo et al. (1982) developed the τ-ω model that requires the optical depth (τ) and the single-scattering albedo of the vegetation (ω) as input parameters. The τ-ω model is the basis for virtually all passive microwave SM retrieval models that include the SCA, the L-MEB Model, the Community Microwave Emission Model, and the LPRM as presented in Mladenova et al. (2014), Wigneron et al. (2007), and Drusch et al. (2009). Where vegetation opacity governs the attenuation effects, the single scattering albedo describes the scattering effects within the canopy (Brunfeldt & Ulaby, 1984). Because the optical depth is typically not directly available, it can be derived from vegetation water content (VWC; Njoku & Entekhabi, 1996) or vegetation indices (Hasan et al., 2014). A more detailed discription of current passive microwave instruments is presented in section 6.2.

5.3.2. Active Microwave RS

While radiometers capture weak natural microwave emissions from the land surface, radars actively transmit a microwave signal and record the normalized backscattered fraction, which after SAR (Synthetic Aperture Radar) proccessing provides higher spatial resolutions than obtained with passive systems. The microwave energy backscattered from land surfaces is determined by soil properties as well as vegetation cover. As the roughness of the surface increases, the specular reflection decreases and surface scattering increases, which in turn increases the backscatter returned to the sensor (Ulaby et al., 1982). Because of these interactions, SM retrieval is highly dependant on accurate characterization of soil surface roughness (Verhoest et al., 2008). The effect of soil surface roughness on SM estimates can be removed by means of multiincidence angle or multipolarimetric observations, which eliminates the need for independent roughness measurements (Jagdhuber et al., 2013; Kweon & Oh, 2014; Oh, 2006; Rahman et al., 2008; Srivastava et al., 2003). Existing SM retrieval methods from active microwave measurements can be classified as empirical (Le Hégarat-Mascle et al., 2002), semiempirical (Oh et al., 2002), or physically based (Elfouhaily & Guérin, 2004). In the presence of vegetation cover, the scattering process is more complex as it is affected by plant geometry and plant moisture content. The plant contribution to backscattering depends on the specific vegetation

structure that is determined by occurrence, orientation, water content, and optical depth of stalks, branches, and trunks. Vegetation effects are commonly taken into consideration by means of multiangular observations (Gherboudj et al., 2011; Grant et al., 2010; Magagi and Kerr, 1997), multilayer canopy representation (Toure et al., 1994), or polarimetric decomposition of vegetation and soil contributions (Jagdhuber et al., 2013, 2015). More details regarding radar microwave instruments are given in section 6.2.

5.3.3. Downscaling Coarse (Passive) Microwave RS Data

Because of its coarse spatial resolution, passive microwave-based SM is not suitable for small-scale (e.g., field scale and catchment scale) applications, where SM commonly exhibits significant horizontal spatial variability. Recently, some progress has been made toward improvement of spatial SM representation via downscaling of radiometer data. The general idea behind combining active and passive microwave observations for SM retrieval from SMAP was driven by the fact that passive (radiometer) observations are typically more accurate but exhibit low spatial resolution, whereas active (radar) observations are more susceptible to surface roughness conditions but exhibit higher spatial resolution (Das, Entekhabi, Dunbar et al., 2018). Combining both observations may provide lower accuracy but higher spatial resolution. Das, Entekhabi, Dunbar et al. (2018), Das, Entekhabi, Kim et al. (2018) applied the SMAP active-passive algorithm and combined 3-km L-band radar and 36-km radiometer observations as an effective approach to high spatial resolution (3 and 9 km) and accurate SM estimation (ubRMSE of 0.039 cm^3/cm^3). Several other published approaches for active/passive microwave data fusion include the temporal change detection method (Piles et al., 2009, 2014), a Bayesian merging approach (Zhan et al., 2006), and the fusion of two single-source SM products from radar and radiometer (Montzka et al., 2016). Akbar and Moghaddam (2015) developed a combined active-passive SM retrieval algorithm, which is based on Monte Carlo simulations and optimization. Their approach yields reasonable results for a wide range of SM (0.04 to 0.40 cm^3/cm^3) and vegetation (VWC, between 0 and 5 kg/m^2) conditions. They concluded that the application of the combined active-passive algorithm for corn surface cover (with VWC 5 kg/m^2) reduced the SM retrieval error from 0.050 cm^3/cm^3 (active only) and 0.045 cm^3/cm^3 (passive only) to 0.035 cm^3/cm^3. The performance of active-passive microwave observations and various retrieval and fusion methods have been evaluated for several regions of the World; for example, North America (Bindlish et al., 2009; Colliander et al., 2012; Magagi et al., 2013; Narayan et al., 2006; Njoku et al., 2002), Australia (Panciera et al., 2014), and Europe (Montzka et al., 2016).

The combined application of active and passive microwave observations is exploited not only to improve the spatial resolution but also to improve the parameterization of retrieval models. The combined application dates back to Ulaby et al. (1983). Recently, Rötzer et al. (2017) estimated the relationship between radar backscatter and vegetation opacity for radiometer brightness temperature inversion for SM estimation from Aquarius data. Dente et al. (2014) applied a discrete scattering model to forward simulate both emission and backscatter and used C-band AMSR-E and ASCAT observations for calibration. The application of active and passive microwave observations in conjunction with optical NDVI data in an artificial neural network simulation scheme improved SM retrieval accuracy (Santi et al., 2016). The potential of SMAP combined L-band radar-radiometer for high spatial resolution (3 and 9 km) and accurate global SM has been demonstrated in Das et al. (2018a).

Additional downscaling methods are based on optical/thermal high-resolution remote sensors, mainly relying on MODIS LST/NDVI products (Merlin et al., 2012, 2013; Piles et al., 2011, 2014; Srivastava et al., 2013), cumulative distribution function (CDF) matching (Kornelsen & Coulibaly, 2014), and MODIS soil evaporative efficiency (Djamai et al., 2015; Merlin et al., 2008) and provide SM estimates at finer resolutions ranging from 100-m to 1-km pixel size. In the course of the Southern Great Plains (SGP-97) experiment, Chauhan et al. (2003) inverted the brightness temperature from the Special Sensor Microwave Imager (SSM/I) to SM and then linked the SSM/I-derived low-resolution SM to Advanced Very High Resolution Radiometer-derived parameters NDVI, surface albedo, and LST, to obtain higher resolution SM estimates. Similarly, Merlin et al. (2013) downscaled ~40-km SMOS SM data with 1-km soil evaporative efficiency data from MODIS. Fang et al. (2018) improved a passive microwave SM downscaling algorithm based on thermal inertia for the use with SMAP. Pellenq et al. (2003) coupled a radiative transfer model with a hydrological model to consider topography and soil texture patterns for SM downscaling. Montzka et al. (2018) used soil textural information to estimate the subgrid SM heterogeneity to account for during downscaling. A good review of the existing methods for spatial downscaling of coarse-scale SM products is provided by Peng et al. (2016).

6. Data Resources

This section provides an overview of ground and RS data resources available for long-term monitoring of SM. First, an overview of SM monitoring networks used for RS measurement validation is provided. Then newly developed active and passive microwave satellite instruments and microwave airborne remote sensors for near-surface and root-zone SM retrieval are described.

6.1. SM Monitoring Networks

Due to the importance of measurements in identifying SM patterns and key hydrological processes, field to catchment-scale SM data have been integrated in global or continental networks. These data have found use both for evaluating models and for validating remotely sensed SM estimates. The International SM Network, ISMN, (Dorigo et al., 2011) combines and hosts in situ SM data from various networks including the U.S. Climate Reference Network, USCRN (Coopersmith et al., 2015) and the SCAN (Schaefer et al., 2007) for vadose zone research applications (Wang & Franz, 2015). Robock et al. (2000) were the first to initiate a global SM data bank including about 600 stations in five regions. The ISMN has been initiated in 2009 by ESA for the SMOS project and made possible through the voluntary contributions of scientists and networks from around the World. The ISMN is hosted by the Vienna University of Technology and provides free access to the data set at http://ismn. geo. tuwien. ac. at/networks. The ISMN currently contains SM data contributions from more than 35 networks and about 2,000 stations located in North America, Asia, Europe, and Australia. While the database contains measurements from as early as 1964, most data sets were initiated during the last decade (see Table 4). A long-time data set of gravimetrically measured SM has been previously presented by Robock et al. (2005), who compiled 45 years (1958–2002) of SM data for the top 1-cm soil layer from over 141 stations in croplands in the Ukraine with 10-day temporal resolution. However, this data set does not represent all the biomes to the same extent, which may provide uncertainties for validation of SM estimates. The latest SM networks in the United States are the COSMOS and GNSS networks, which are described in Sections 3.1 and 3.4. These data have been used for validation of remotely sensed SM products such as SMAP (Akbar & Moghaddam, 2015; Colliander et al., 2017; Montzka, Bogena, et al., 2017), SMOS (Montzka, Bogena, et al., 2017; Van der Schalie et al., 2016), ASCAT (Fascetti et al., 2016), and AMSR-2 (Wu et al., 2016). The USCRN data have been used to validate AMSR-E SM data products (Coopersmith et al., 2015). The ISMN data have been widely used to validate the ESA CCI SM product (Al-Yaari et al., 2016; Chakravorty et al., 2016; Cui et al., 2018; Dorigo et al., 2015; Karthikeyan et al., 2017b). For further information, interested readers are referred to a comprehensive review of Ochsner et al. (2013).

A SM time series may prove to be helpful for evaluation of climate model simulations and identifying trends in the hydrological cycle due to the impact of regional climate change and land use. Some of the stations (e.g., OK Mesonet and ARM SGP Sites) only monitor soil matric potential with matric potential sensors. These matric potentials can be converted to SM estimates via site- and depth-specific soil water retention curves (see section 2). Apart from SM measurements, important atmospheric variables such as precipitation, air temperature, soil temperature, humidity, pressure, and solar radiation are also monitored in some U.S. networks that include SCAN, CRN, and SNOTEL. These auxiliary data assist users with correct interpretations of SM observations. Table 4 provides a detailed overview of the most important ISMNs that are currently measuring SM on an operational basis within and outside the United States. It should be noted that this overview of networks presents a current snapshot with the ISMN continuously expanding.

Not only in the United States but also in Europe and Asia several large-scale SM monitoring networks have been established for research purposes, validation of RS SM products, and as support for natural hazard forecasting. It is widely acknowledged that significant additional efforts are needed to enhance measurement consistency and standardization, data, and metadata. Furthermore, to reach the goal of a fully integrated global SM observation system, it will be important to establish, expand, and improve current SM observations, both in situ and remotely sensed.

6.2. Microwave Satellite SM Data Resources

Microwave RS has been applied for SM retrieval since 1978 (Chen et al., 2012). Recent and currently operating spaceborne sensors that provide SM information include (1) the Advanced Microwave Scanning Radiometer on NASA Earth Observing System Aqua and the GCOM-W1 (AMSR-E and AMSR-2; Jackson et al., 2012; Kachi et al., 2014), (2) the ASCAT on EUMETSAT MetOp-A and MetOp-B (Wagner et al.,

Table 4
Overview of Currently Available In Situ SM Monitoring Networks Contained in the ISMN

Network	Country or state	No. of sites/sensors	Sensor types	Installed depths (cm)	Date	Reference and associated studies	Websites
SCAN (USDA)	United States	232	Hydra Probe Analog; Hydra Probe Digital SDI-12; Hydra Probe Analog; Hydra Probe Digital SDI-12 Thermistor	5, 10, 20, 50, 100	1996 to present	Njoku et al. (2003) and Schaefer et al. (2007)	http://www.wcc.nrcs.usda.gov/
CRN (NOAA)	United States	115	Stevens Hydraprobe II SDI-12	5, 10, 20, 50, 100	2000 to present	Bell et al. (2013)	https://www.ncdc.noaa.gov/crn/
SNOTEL	United States	441	Hydra Probe Analog; Hydra Probe Digital SDI-12	5, 20, 50	1980 to present	Al Bitar et al., 2012	http://www.wcc.nrcs.usda.gov/snow/
COSMOS	United States	109	Cosmic ray Probe	Up to 90	2008 to present	Zreda et al. (2008) and Kohli et al. (2015)	http://cosmos.hwr.arizona.edu/
ARS Watersheds (USDA)	United States	4	Stevens Water; Hydra Probe Analog	5	2002 to present	Jackson et al. (2010)	http://www.ars.usda.gov/main/main.htm
OK Mesonet	United States	103	TDR (Campbell Scientific); Water Matric Potential Sensor 229L	5, 25, 60, 75	1996 to present	Illston et al. (2008)	http://www.mesonet.org/
ARM SGP Sites	United States/Oklahoma, Kansas, Colorado	29	TDR (Campbell Scientific); Water Matric Potential Sensor 229L	2, 5, 15, 25, 35, 50, 60, 85, 125, 175	1993–2015	Schneider et al. (2003)	http://www.arm.gov/
WTM	United States/Texas	53	TDR (Campbell Scientific)	5, 25, 60, 75	1999 to present	Schroeder et al. (2005)	http://www.mesonet.ttu.edu/
AWDN	United States/Nebraska	50	Delta-T Devices; Theta Probe ML2X	10, 25, 50, 100	1997–2010	Wang et al. (2015)	http://www.hprcc.unl.edu/awdn.php
GAEMN	United States/Georgia	81		5, 10, 20	1991 to present	Hoogenboom (1993)	http://www.georgiaweather.net/
SOILSCAPE	United States	136	EC-5	5, 12, 50	2011–2015	Tabatabaeenejad and Moghaddam (2011)	http://soilscape.usc.edu/bootstrap/sites_and_data.html
PBO-H$_2$O or GPS	United States	161	GPS	5	2004 to present	Larson et al. (2008)	http://xenon.colorado.edu/portal/
ICN	United States	19	Neutron Depth Probe (Troxler); Neutron Surface Probe (Troxler)	10, 30, 50, 70, 90, 110, 130, 150, 170, 190, 200	1983–2010	Scott et al. (2010)	http://www.isws.illinois.edu/warm/climnet/soilmoistexp.asp
CTP_SMTMN	China	56	Decagon Devices, EC-TM	5, 10, 20, 40	2010–2013	Zhao et al. (2013)	http://dam.itpcas.ac.cn/rs/?q=data#CTP-SMTMN
Maqu	China	20	ECH20 EC-TM,	5	2008–2010	Su et al. (2011)	http://www.geo.tuwien.ac.at/insitu/data_viewer/ISMN.php

Table 4 (*continued*)

Network	Country or state	No. of sites/sensors	Sensor types	Installed depths (cm)	Date	Reference and associated studies	Websites
CHINA	China	40	Coring device/auger	5, 10, 20, 30, 40, 50, 60, 70, 80, 90, 100	1981–1999	Liu et al. (2011) and Robock et al. (2000)	http://www.geo.tuwien.ac.at/insitu/data_viewer/ISMN.php
NAMHEM	Mongolia	44		10, 20, 30, 40, 50, 60, 70, 80, 90, 100	1964–2002	Robock et al. (2000)	http://www.geo.tuwien.ac.at/insitu/data_viewer/ISMN.php
OzNET or MSMMN	Australia	37	Stevens Water Inc.; Hydra Probe (Stevens);TDR (Campbell Scientific); CS616,	5, 30, 60, 90	2001–2011	Smith et al. (2012)	http://www.oznet.org.au/
AACES	Australia	49	Delta-T Devices; Theta Probe ML2X	5, 6, 25	2010	Peischl et al. (2012)	http://www.moisturemap.monash.edu.au/
SASMAS	Australia	14	CS616; Stevens Hydra Probe	5, 30	2005–2007	Rüdiger et al. (2007)	http://www.eng.newcastle.edu.au/sasmas/SASMAS/sasdata.html

Table 4 (Cont.)

Network	Country or state	No. of sites/sensors	Sensor types	Installed depths (cm)	Date	Reference and associated studies	Websites
TERENO	Germany	5	Hydra Probe II Sdi-12	5, 20, 50	2013–2014	Zacharias et al. (2011)	http://teodoor.icg.kfa-juelich.de/overview-de
TWDEF	United States	36	Acclima TDT	10, 25, 50	2009 to present	L. Lu, et al. (2014)	
UDC-SMOS	Germany	11	IMKO TDR; ECHO EC-5; EC-TE Probes	5, 10, 20, 40	2007–2011	Loew and Mauser (2008)	http://www.geographie.uni-muenchen.de/department/fiona_eng/index.php
MOL-RAO	Germany	2	TRIME-EZ TDR sensor (IMKO GmbH)	8, 15, 30, 45, 60, 90	2003–2014		http://www.dwd.de/DE/forschung/atmosphaeren-beob/lindenberger-saeule/lindenberger-saeule_node.html
Oracle	France	6	Solo 40; TRASE 16; Theta Probe (ML2X)	3, 6	2008–2013		https://bdoh.irstea.fr/ORACLE/
SMOSMANIA	France	21	Theta Probe (ML2X); Theta Probe (ML3); Delta-T Devices)	5, 10, 20, 30	2007–present	Albergel et al. (2008)	http://www.cnrm-game-meteo.fr/spip.php?

Table 4 (*continued*)

Network	Country or state	No. of sites/sensors	Sensor types	Installed depths (cm)	Date	Reference and associated studies	Websites
Umberia	Italy	13	EnviroSCAN probe; EnviroSMART probe; Theta Probe ML2X	5, 15, 25, 35, 45, 55	2002–2014	Brocca, Melone, Moramarco, Wagner, et al. (2010)	http://hydrology.irpi.cnr.it/; http://www.cfumbria.it/ article251&lang=en
Calabria	Italy	5	Theta Probe ML2X	30, 60, 90	2001–2012		http://www.cfd.calabria.it/
HOBE	Denmark	32	Decagon 5TE sensor	5, 25, 55	2009–2014	Bircher et al. (2012)	http://www.ipf.tuwien.ac.at/insitu/
RSMN	Romania	20	5TM sensor	5	2014–present		http://assimo.meteoromania.ro/
REMEDHUS	Spain	24	Hydra Probe (Stevens)	5	2005–present	Martínez-Fernández et al. (2016)	http://campus.usal.es/~hidrus/
FMI-ARC	Finland	27	5TE sensor;Theta Probe ML2X; CS655 reflectometer	2, 5, 10, 20, 40, 60, 80	2007 to present	Bircher et al. (2016)	http://fmiarc.fmi.fi/
WegenerNET	Austria	12	Hydra Probe II; pF-Meter	20, 30	2007 to present	Kabas et al. (2011)	http://wegcenter.uni-graz.at/de/wegenernet/wegenernet-home/

Note. SM = soil moisture; ISMN = International SM Network; AACES: Australian Airborne Calibration Experiments for SMOS; ARS = Agricultural Research Service; AWDN = Automated Weather Data Network; CRN = Climate Reference Network; COSMOS = Cosmic Ray SM Observing System; CTP_SMTMN = Central Tibetan Plateau SM and Temperature Monitoring Network; EC = Electrical Conductivity; FMI-ARC = Finnish Meteorological Institute Arctic Research Center; GAEMN = Georgia Automated Environmental Monitoring Network; HOBE = Hydrological OBservatory; ICN = Illinois Climate Network Data; MOL-RAO = Lindenberg Meteorological Observatory – Richard Assmann Observatory; MSMMN = Murrumbidgee SM Monitoring Network; NAMHEM = National Agency of Meteorology, Hydrology and Environment Monitoring; OK = Oklahoma Mesonet; PBO = Plant Boundary Observatory; RSMN = Romanian SM Network; SASMAS = Scaling and Assimilation of SM and Streamflow; SCAN = Soil Climate Analysis Network; SMOSMANIA = SM Observing System-Meteorological Automatic Network Integrated Application; SNOTEL = SNOwpack TELemetry; SOILSCAPE = SM Sensing Controller and oPtimal Estimator; TERENO = Terrestrial Environmental Observatories; TWDEF = T.W. Daniel Experimental Forest; UDC-SMOS = Upper Danube Catchment-SM and Ocean Salinity; WTM = West Texas Mesonet.

2013), (3) NASA's WindSat Spaceborne Polarimetric Microwave Radiometer on the Naval Research Laboratory's Coriolis satellite (Gaiser et al., 2004), (4) the European SMOS (Kerr et al., 2001); (5) NASA's SMAP (Entekhabi et al., 2010), (6) the JAXA Advanced Land Observation Satellite 2, and (7) the ESA Sentinel-1 (Bartalis et al., 2007), which are selectively described in more detail below and in Table 5. The Scanning Multichannel Microwave Radiometer (SMMR) onboard Nimbus-7 (1978–1987) and the SSM/I satellite data have been interpreted in terms of SM as well (De Jeu, 2003), and though the accuracy may be lower, these data do cover time periods that are otherwise missing. A combination of several initial active and passive satellites is provided by the CCI for global SM. The U.S. and Indian radar mission NISAR (NASA-ISRO SAR Mission) that is currently in the planning stage and projected to be launched in 2021 will operate at the L-band and S-band. However, it is still unclear whether NISAR will generate official SM products. A Tandem-L mission that enables the systematic monitoring of dynamic processes on the Earth surface has been proposed as an innovative interferometric and polarimetric radar mission (Krieger et al., 2007) using a pair of cooperating L-band SAR satellites flying in close formation (Krieger et al., 2009). Moreover, a Copernicus candidate mission has been proposed incorporating optical, thermal, and microwave data from ESA's Sentinels and SMOS with contribution of non-ESA satellites such as ASCAT, Terra-SAR, and RADARSAT-2. The current state of SM RS has been reviewed by Mohanty et al. (2017).

The integration of multiple SM data sources at various spatial and temporal scales is beneficial for numerous applications. An excellent example is NASA's Oak Ridge National Laboratory Distributed Active Archive Center (ORNL DAAC), which provides scientific and other user access to SM data for North America from airborne (Airborne Microwave Observatory of Sub-canopy and Subsurface [AirMOSS]), satellite (SMAP, GRACE) and ground network sources (SCAN, USCRN, COSMOS, SNOTEL, Soil Moisture Sensing Controller and oPtimal Estimator, and FLUXNET) through a single platform called SM Visualizer (http://daac. ornl. gov). The National Snow and Ice Data Center (NSIDC) also manages and distributes such data for users (https://nsidc. org/data).

6.2.1. The Advanced Microwave Scanning Radiometer (AMSR-E/AMSR-2)

The Advanced Microwave Scanning Radiometer for the Earth Observing System (AMSR-E) is a passive multiband sensor onboard of NASA's Earth Observing System Aqua satellite (Figure 19a) that measures geophysical variables related to the Earth's water cycle such as precipitation rate, water vapor, cloud water, sea surface wind/temperature, sea ice concentration, SWE, and SM content. AMSR-E uses the X-band and C-band for SM retrievals. Because of radio frequency interference (RFI) in the C-band (6.9 and 10.7 GHz), especially over the U.S., Middle East, Japan, Italy, and the U.K. (Njoku et al., 2005), the X-band has been extensively used for SM retrieval. The AMSR-E spatial resolution has improved (50 km) when compared to previous missions (e.g., SMMR with 150 km), while sustaining all channels of the previous sensors (i.e., SMMR, SMM/I, and TMI). Providing ~10-year data across several channels, AMSR-E generates new opportunities and very useful insights toward the development of SM retrieval algorithms (e.g., development of SMAP and SMOS algorithms) and long-term monitoring of soil, water, and climate interactions. Several retrieval algorithms have been developed to estimate global SM from AMSR-E data (Du et al., 2016; Jackson et al., 2010; Njoku et al., 2003; Owe et al., 2001). The LPRM developed by VU University Amsterdam in collaboration with NASA (Owe et al., 2008) is one of the more widely applied algorithms for simultaneous SM, vegetation optical depth, and surface temperature retrieval (Cho et al., 2015; Kim et al., 2015; Meesterns et al., 2005).

As a follow-on to AMSR-E, the AMSR-2 (Figure 19b) sensor onboard of Japan's Aerospace Exploration Agency (JAXA) GCOM-W satellite started measuring and releasing brightness temperature (passive) data in multiple frequencies (bands) in January 2012 with a revisit time of 1–2 days and crossing nodes at 1:30 p.m. and 1:30 a.m. local solar time for ascending and descending orbits, respectively. The lower frequencies (6.9 GHz, C-band) provide more accurate SM retrievals for the top ~1–2 cm soil layer (Molero et al., 2017). The underlying concept of AMSR-2 is identical to that of AMSR-E (Kachi et al., 2014). Major improvements of AMSR-2 include (1) a larger reflector system of 2.0-m diameter to provide better spatial resolution, (2) the inclusion of an additional 7.3-GHz dual polarization frequency channel for improvement of RFI mitigation, (3) 12-bit quantization for all channels, and (4) an improved calibration system (Imaoka et al., 2010). Table 5 provides operational details of the AMSR-E and AMSR-2 sensors. AMSR-2 includes several SM products. The LPRM SM product for descending overpass has provided more accurate results than that of ascending orbit (Molero et al., 2017) probably due to the more uniform surface temperature and SM.

Table 5
Overview of Operational Satellite Remote Sensing Instruments and Their Characteristics for SM Retrieval

Property	AMSR-E	AMSR-2	ASCAT	SMOS	SMAP Radiometer	SMAP Radar	Sentinel-1
Sensor type (frequency, GHz)	X/C-band (6.9, 10.65, 18.7, 23.8, 36.5, 89)	X/C-band (6.9, 7.3, 10.6, 18.7, 23.8, 36.5, 89)	C-band (5.3 GHz)	L-band (1.4)	L-band (1.4)	L-band (1.3)	C-band (5.4)
Spatial resolution (km)	6–75 (based on frequency and polarization)	5–60 (based on frequency and polarization)	25	36	36	3	5–40 m
Temporal resolution (days)	1	1	1–2	1–3	1–3 days	1–3 days	3–12
Uncertainty		0.34–1.2 K			1.3 K	0.5 dB	Radiometric 1 dB Stability 0.5 dB
Sponsor	JAXA, NASA's EOS Aqua	JAXA's GCOM-W1 or SHIZUKU	EUMETSAT	ESA/CNES/ CDTI	NASA	NASA	ESA
Data availability[a]	2002–2011	2012 to present	2006 to present	2010 to present	2015 to present	January 2015 to July 2015	2014 to present
Incidence angle (°)	54	55	25–65	0–55	40°	40°	20–47°
Retrieval accuracy	$\geq\pm0.04$ cm³/cm³	$\geq\pm0.04$ cm³/cm³	±0.03–0.07 cm³/cm³	$\pm0.04^{b}$ cm³/cm³	$\pm0.04^{bb}$ cm³/cm³	$\pm0.04^{b}$ cm³/cm³	±0.04–0.08^{c} cm³/cm³
Swath	1,450 km	1,445 km	2 × 550 km	1,000 km	1,000 km	1,000 km	20–400 km
Altitude	705 km	700 km	850 km	758 km	685 km	685 km	700 km
Orbit	Polar	Near polar	Polar	Polar	Near polar	Near polar	Near polar
Need for auxiliary data	Medium	Medium	Low	Low	Low	Low	Medium
Target quantity	SM (cm³/cm³)	SM (cm³/cm³)	Saturation degree (0–1)	SM (cm³/cm³)	SM (cm³/cm³)	SM (cm³/cm³)	SM (cm³/cm³)
Data latency	Irregular updates	~2 hr after imaging, NRT	2 hs after imaging	Less than 3 hr after imaging, NRT	~4 hr after imaging, NRT	Failed	Within few hours after imaging, NRT
Websites	http://www.remss.com/missions/amsre	http://www.remss.com/missions/amsre	http://hsaf.meteoam.it/soil-moisture.php	https://earth.esa.int/web/guest/-/how-to-obtain-data-7329	https://nsidc.org/data/smap/smap-data.html	https://nsidc.org/data/smap/smap-data.html	https://cophub.copernicus.eu
Related studies	Bindlish et al. (2006), Chen et al. (2013), and Njoku H. Lu, et al. (2014), and et al. (2005)	Cho, Choi, and Wagner (2015), and Parinussa et al. (2014)	Albergel et al. (2009) Bartalis et al. (2007), and Naeimi, Bartalis, and Wagner (2009)	Kerr, Waldteufel, Wigneron, et al. (2010), Kerr, Waldteufel, Richaume, et al. (2010), Jackson et al. (2012), and Wigneron et al. (2012)	Chan et al. (2016), Colliander et al. (2017), and Reichle et al. (2017)	Entekhabi et al. (2010) and Kim et al. (2017)	Bauer-Marschallinger et al. (2019) and Greifeneder et al. (2018)

Note. SM = soil moisture; AMSR = Advanced Microwave Scanning Radiometer; ASCAT = Advanced SCATterometer; SMOS = Soil Moisture and Ocean Salinity; SMAP = Soil Moisture Active Passive; JAXA = Japan Aerospace Exploration Agency; NASA = National Aeronautics and Space Administration; EOS = Earth Observing System; GCOM = Global Change Observation System; EUMETSAT = European Organization for the Exploitation of Meteorological Satellite; ESA = European Space Agency; CNES = Centre National d'Etudes Spatiale; CDTI = Centro Para el Desarrollo Tecnological Industrial; GCOM-W = Global Change Observation Mission-Water; NRT = near real time. [a]Planned lifetime is presented in Figure 21. [b]Target accuracy in the top 5 cm for vegetation water content ≤ 5 kg/m². [c]Over grasslands and agricultural areas.
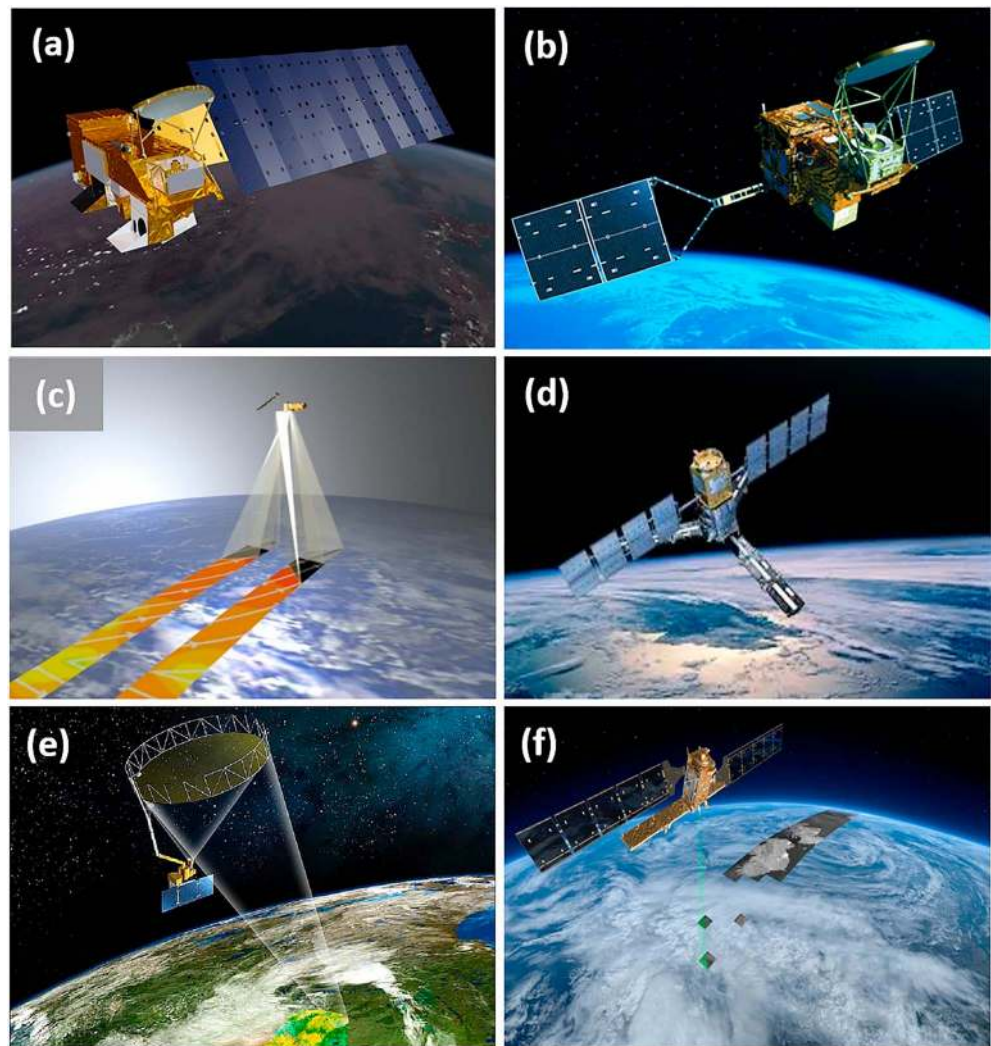
Figure 19. Renderings of the (a) Advanced Microwave Scanning Radiometer for the Earth Observing System, (b) Advanced Microwave Scanning Radiometer 2 (AMSR-2), (c) Advanced Scatterometer (ASCAT), (d) Soil Moisture Ocean Salinity (SMOS), (e) Soil Moisture Active Passive (SMAP), and (f) Sentinel-1 satellites.

6.2.2. The ASCAT

The Active Microwave Instrument Wind Scatterometer onboard of the European Remote Sensing (ERS) satellite is a C-band (5.3 GHz) sensor initially intended for wind monitoring but also widely utilized as the first active sensor for retrieving SM. The ERS-1 SCAT has been monitoring the Earth between 1991 and 2000. The second instrument (ERS-2 SCAT) was launched in 1995 and ceased operation in 2011. The ERS-1/2 SCAT had a spatial resolution of 50 km and a revisit time of 2–7 days. ERS-1/2 SCAT provides a valuable long-term SM data set for climate change applications that is used to create the ESA CCI active SM products. As a successor of ERS-1/2 SCAT, the ASCAT is a C-band scatterometer with no SAR-based resolution enhancement deployed on satellite platforms of the European Organization for the EUMETSAT (Figure 19c). The EUMETSAT MetOp-A satellite was launched in October 2006, and MetOp-B was launched in September 2012. The MetOp-C platform was launched in November 2018. The instrument was initially designed for monitoring wind speed and direction over the oceans, but ASCAT has also been widely used for monitoring SM (Albergel et al., 2009; Draper et al., 2011; Matgen et al., 2012) due to its high-quality calibration, high radiometric accuracy, and multiple-viewing capabilities (Wagner et al., 2013). The ASCAT sensor includes three vertically polarized antennas oriented at 45°, 90°, and 135° angles with respect to the satellite track, resulting in a double swath of about 500 km with a gap of about 360 km. The ASCAT near-surface SM estimates are obtained with a linear change detection retrieval algorithm

developed by Wagner et al. (1999), where estimates are obtained at a distinct incidence angle (taken at 40°). This algorithm yields SM content in terms of relative saturation. The algorithm is part of the WAter Retrieval Package software, which provides the means for deriving long-term SM time series (Naeimi et al., 2009; Naeimi, Scipal, et al., 2009). The basic assumptions of the algorithm include a linear relationship between backscatter (dB) and near-surface SM and stability of backscatter despite seasonal change in vegetation and roughness (Naeimi et al., 2009a & 2009b). Thus, a disadvantage of the change detection algorithm is that the different contributions to the observed total backscatter from the soil, vegetation, and soil-vegetation interaction effects cannot be separated (Wagner et al., 2013). It should be noted that the algorithm calculates only relative changes in SM and not absolute SM. Hence, tie points to convert relative saturation to absolute SM are required.

The MetOp-C, unlike SMOS and SMAP, is an operational platform that generates a real-time operational product that is publicly distributed by EUMETSAT (https://navigator.eumetsat.int/product/EO:EUM: DAT:METOP:SOMO12). This constitutes a much stronger commitment to data continuity than provided by scientific missions such as SMOS and SMAP.

6.2.3. The Soil Moisture Ocean Salinity (SMOS) Mission

The SMOS satellite with the Microwave Imaging Radiometer with Aperture Synthesis (MIRAS) instrument is developed by the Centre d'Etudes Spatiales de la Biosphère with support from ESA and in collaboration with the Centre National d'Etudes Spatiales (CNES) and the Centro Para el Desarrollo Tecnological Industrial (Figure 19d). SMOS is the first satellite dedicated to the global measurement of near-surface SM (top 5 cm) with moderate spatial resolution (Kerr et al., 2001; Kerr et al., 2010). Using an interferometric radiometer, SMOS captures brightness temperature (T_b) at several incidence angles. The radiometer exploits the interferometry principle, where 69 small receivers measure the phase difference of the incident radiation emitted from the Earth's surface. The technique is based on cross correlation of observations from all receiver pair combinations to generate the scene T_b. As the satellite moves along its orbital path, each observed area is imaged at various viewing angles. The microwave signal within the L-band is much more sensitive to changes in SM than it is to atmospheric disturbances or land surface characteristics (i.e., surface roughness, soil texture, topography, and soil bulk density; Kerr et al., 2012). The SMOS mission provides SM estimates generated from T_b (L1) via the SMOS L2 processor (Kerr et al., 2010), which in principle contains the L-MEB model proposed by Wigneron et al. (2007). In general, L-MEB is applied to compute multiangular top-of-the-atmosphere brightness temperatures based on a set of soil (e.g., moisture, temperature, and texture), vegetation (e.g., water content and temperature), and radiative transfer parameters (e.g., single scattering albedo, polarization coupling factor, and surface roughness). The retrieval algorithm as outlined in Kerr et al. (2012) is based on a Bayesian approach, where L-MEB based brightness temperatures are compared with direct observations through minimizing a cost function. SMOS L1 and L2 products have been used to derive higher-level products, L3 and L4. SMOS L3 products include surface SM and vegetation optical depth (VOD), while SMOS L4 products provide root-zone SM (0–100 cm), surface roughness, neural network-based SM from AMSR-E/SMOS synergies, and an agricultural drought index with spatial resolution of 25 km (EASE-2 grid; Al Bitar et al., 2013; Mecklenburg et al., 2016; Parrens et al., 2016; Rodríguez-Fernández et al., 2016). A comprehensive overview of modeling approaches and SM retrieval algorithms has been presented by Wigneron et al. (2017).

The recent diurnal L3 product, SMOS-IC, has been released by the French Institut National de la Recherche Agronomique in collaboration with the Centre d'Etudes Spatiales de la biosphere to provide global estimations of SM (Figure 20, top) and VOD (Fernandez-Moran et al., 2017). The VOD product can be used in support of agricultural applications related to food security (Mecklenburg et al., 2016). SMOS-IC is based on L-MEB, but its algorithm is simpler than the operational SMOS L2 and L3 SM retrieval algorithms. In SMOS-IC pixels are assumed homogeneous (a single value of each input model parameter is used for the whole pixel), while operational SMOS L2 and L3 algorithms correct for pixel heterogeneity. This provides greater independence of SMOS-IC from uncertainties in auxiliary data (e.g., MODIS LAI data and SM information used as auxiliary data in L2/L3 algorithms to estimate T_b in the pixel fractions of heterogeneous pixels) and tends to perform better than previous SMOS products due to considering updated soil roughness and vegetation albedo parameters for calibration of L-MEB SM retrievals based on ISMN SM data (Fernandez-Moran et al., 2017; Parrens et al., 2016). L-band observations have been challenged by unexpected RFI. Despite being a protected band for scientific studies, the SMOS mission has suffered significantly from RFI effects
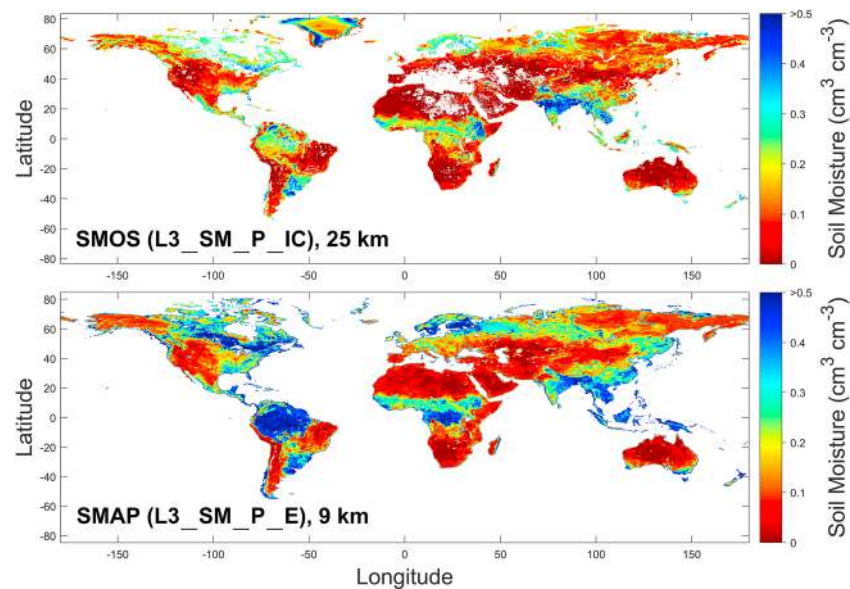
Figure 20. Comparison of SMOS-IC (top) and SMAP L3 (bottom) monthly surface (0–5 cm) soil moisture retrievals for August 2017. SMOS = Soil Moisture Ocean Salinity; SMAP = Soil Moisture Active Passive.

in certain regions (Oliva et al., 2012). The number of RFI sources has been reduced in Europe, North and South America, and China but remains significant in Asia and the Middle East (Soldo et al., 2016). SMOS data are publicly available from ESA (L2 and L3; http://smos-diss.eo.esa.int/) and CATDS (L3 and L4; http://www.catds.fr/Products).

6.2.4. The SMAP Mission

The SMAP satellite is the most recent microwave sensor designed to measure and map SM within the top 5 cm of soil and to discern between frozen and thawed states by applying both active and passive sensors. The major science objectives of SMAP are to understand processes that link the water, energy, and carbon cycles, land surface global water, and energy fluxes and to improve weather and climate predictions (Entekhabi et al., 2010). This was intended to be accomplished with an instrument that combines L-band radar with an L-band radiometer, which share a conically rotating 6-m aperture reflector antenna that scans a 1,000-km-wide swath while the observatory orbits the Earth (Figure 19e and Table 5). The radiometer provides "passive" measurements of microwave emissions from the upper soil layer. It is more sensitive to near-surface SM and less sensitive to the effects of surface roughness and vegetation when compared to the radar. The SMAP mission yields 15 publicly available baseline science data products that include near-surface and root-zone SM (RZSM) estimates. The RZSM estimates are based on the assimilation of SMAP data into land surface models (NASA Catchment land surface model; Reichle et al., 2014). The joint processing of the radar and radiometer data was intended to yield SM at spatial resolutions of 3, 9, and 36 km with 3-day temporal resolution (Entekhabi et al., 2010).

While the SMAP satellite was designed to spend at least 3 years in orbit, the high-resolution SMAP radar failed in July 2015 (three months after launch), leaving only the SMAP radiometer operational to this day. The SMAP target accuracy for SM is 0.04 cm^3/cm^3 (based on unbiased RMSE) and is determined based on threshold VWC less than 5 kg/m^2. There are two types of SMAP level 2/3 passive surface SM products: the standard product is posted on a 36-km Equal-Area Scalable Earth (EASE)-2 grid (L2/3 SM_P), while the optimally interpolated "enhanced" product is posted on a 9-km EASE-2 grid (L2/3 SM_P_E). The actual resolution of the latter is coarser than 9 km (Figure 20, bottom). Both products include SM retrievals for both a.m. and p.m. orbits. These data have a revisit time of 2–3 days at any location and a latency of 12–24 hr from the time of observation. Of particular interest is the SMAP level 4 (L4) model-based SM product obtained from assimilating SMAP level 2 (L2) brightness temperature observations into the NASA catchment land surface model (Reichle et al., 2017). SMAP L4 provides global estimates of both surface (0–5 cm) and RZSM (down to 100 cm) with 9-km spatial and 3-hr temporal resolutions,

interpolated from the coarse-scale (36 km) observations in space and in time (Reichle et al., 2017). The improved SMAP L4 product resolution provides additional information about the spatial variability of SM making it suitable for medium-scale applications. As a replacement for the radar, SMAP has recently released an active/passive SM product at a 3-km posting, which uses C-band backscatter observations from Sentinel-1 to replace the SMAP L-band radar. It is only available for the locations and times where SMAP and Sentinel-1 overlap.

The experience gained from SMOS aided SMAP in the development of better back-end mitigation tools and filters for RFI for both radiometer and radar instruments (Colliander et al., 2017). L-band RFI is a critical threat to future efforts to globally measure SM. It should be noted that to date, SMAP provides the most accurate global SM products (L3 and L4) for various applications (Chan et al., 2016 & 2018; Chen et al., 2018; Colliander et al., 2017; Crow et al., 2017; Koster et al., 2016). Passive SMAP data are publicly available from the National Soil and Ice Data Center (NSIDC) (https://nsidc. org/data/smap/smap-data. html).

6.2.5. The Sentinel-1 Mission

The ESA Sentinel-1 mission (S-1) is a two-satellite polar-orbiting and day-and night-radar imaging system for land and ocean monitoring (Figure 19f). The goal of the mission is to provide data continuity following the retirement of ERS-2 and Envisat (Paloscia et al., 2013). The S-1 yields improved spatial, temporal, and radiometric resolutions when compared to the previous Envisat ASAR GM mode, while working at nearly the same frequency (e.g., 5.4 versus 5.3 GHz; Table 5). Another improvement is the application of cross polarization to correct for seasonal vegetation effects in the copolarized backscatter measurements. In general, due to the better penetration of horizontally polarized (HH) waves through vertically oriented vegetation (grasses, crops), HH polarization is preferred (Brown et al., 2003). While the ESA provides Level-1 georeferenced single looked complex and projected multilook ground range detected products, a dedicated SM product is not available. Several attempts have been made to develop algorithms for retrieving SM from S-1 SAR data (Balenzano et al., 2012; Pierdicca et al., 2014). For example, Paloscia et al. (2013) presented an Artificial Neural Network-based algorithm to retrieve SM from S-1 data and tested their approach based on in situ ground data from several test sites in Italy, Australia, and Spain and obtained mean RMSEs less than 0.046 cm^3/cm^3, which is in line with S-1 target retrieval accuracy (0.05 cm^3/cm^3).

In general, SM retrieval from SAR data is challenging due to the confounding influence of surface roughness and vegetation on the signal. Although numerous approaches utilizing different backscatter models have been developed, SM retrieval from S-1 data remains an enigma, mainly due to significant roughness changes (e.g., due to agricultural practices) and higher complexity of vegetation characterization at finer scales (e.g., wheat versus sugar beet) (Barrett et al., 2009). Due to the loss of the SMAP radar, S-1 is currently the only active sensor with a high spatial but 6-day temporal resolution for near-surface SM estimations. Such temporal resolution is not adequate for applications where 3 days or less is required. Recently, the S-1 radar backscatter measurements (C-band) have been combined with SMAP radiometer brightness temperature (L-band) observations to produce a high resolution SMAP-Sentinel-1 SM product (SPL2SMAP_S) with 3-km EASE-grid providing SM from April 2015 to present and available to the public through NASA DAAC at the NSIDC (https://nsidc. org/data/SPL2SMAP_S/versions/2) (Das et al., 2018b).

6.2.6. The CCI

The CCI is a part of ESA's global monitoring of Essential Climate Variables (program, which includes SM). The CCI aims to provide the most complete and consistent global SM products based on several active and passive microwave remote sensors dating back to 1978. The record is based on three products that differ in the data source: (1) an active-only data set, (2) a passive-only data set, and (3) a merged active-passive data set (Liu et al., 2012; Wagner et al., 2012). The active data set (1991–2014) was generated with the change detection algorithm (Naeimi, Scipal, et al., 2009; Wagner, Lemoine, & Rott, 1999) based on observations from the C-band scatterometer onboard of ERS-1, ERS-2 (AMI SCAT) and METOP-A (ASCAT). The passive data set (1978–2014) was generated by VU University Amsterdam in collaboration with NASA using the LPRM (Owe et al., 2008) based on observations from Nimbus 7 SMMR, DMSP SSM/I, TRMM TMI, and Aqua AMSR-E (Liu et al., 2012). The new 04.2 version of the CCI additionally includes passive AMSR-2 and SMOS SM data in the merged SM product (Chung et al., 2018). It is possible to include SM data from new satellite missions (i.e., SMAP, Aquarius, and Sentinel-1) (Wagner et al., 2012) (Figure 21). This CCI SM merged data set is publically available from https://www.esa-soilmoisture-cci.org. Figure 22 shows an example of the CCI product for global monitoring of SM.
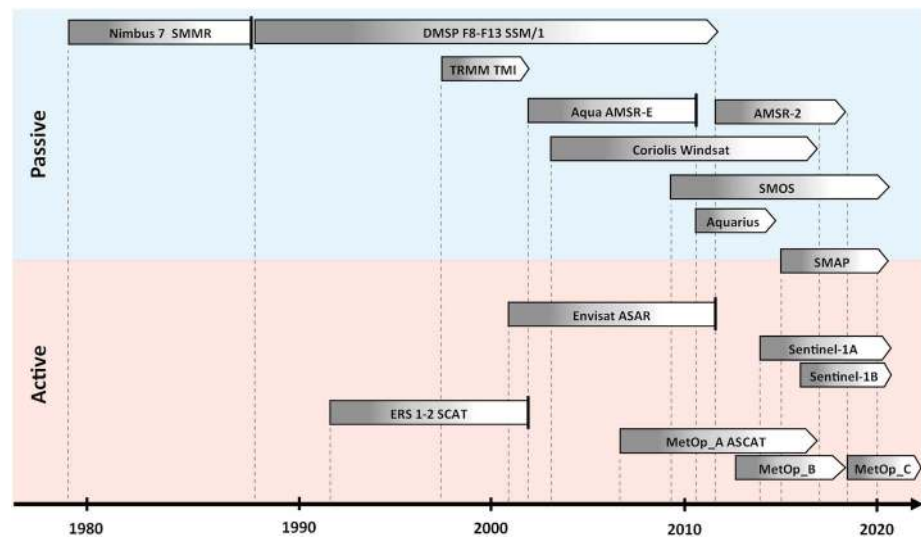
Figure 21. Active and passive microwave remote sensors used for generation of the European Space Agency climate change initiative data sets. Although the SMAP and Aquarius missions have not been included in the latest version of the climate change initiative (Essential Climate Variable SM 04.2), they are already included in this diagram to highlight their potential future inclusions. Envisat Advanced Synthetic Aperture Radar (ASAR) and Sentinel-1 are merely shown for evaluation purposes. While the vertical black solid lines represent the start/end of missions, the arrows indicate that a specific mission has been in orbit beyond the planned mission lifetime (adapted and expanded from Chung et al., 2018). TMI = Tropical Rainfall Measuring Mission [TRMM] Microwave Imager; AMSR-E = Advanced Microwave Scanning Radiometer for the Earth Observing System; AMSR-2 = Advanced Microwave Scanning Radiometer 2; SMOS = Soil Moisture Ocean Salinity; SMAP = Soil Moisture Active Passive; ASCAT = Advanced Scatterometer; SMMR = Scanning Multichannel Microwave Radiometer; ERS 1-2 SCAT = European Remote Sensing Satellites 1-2 Scatterometers.

6.2.7. Evaluation of Microwave Satellite SM Retrievals

SM retrieval from RS observations may be biased by numerous factors, which are mainly related to atmospheric interferences, vegetation properties, and soil roughness. This necessitates comprehensive validation of the resulting SM estimates. Significant efforts have been devoted to the development of novel algorithms providing reliable SM estimates for a variety of land surface conditions (Al-Yaari et al., 2017; Das et al., 2011; Fernandez-Moran et al., 2017; Kerr et al., 2016; McNairn et al., 2015; Montzka et al., 2014; Piles et al., 2009; Rodríguez-Fernández et al., 2015; Schwank et al., 2010; van der Schalie et al., 2018; Vittucci et al., 2016).

Validation of SM retrievals is commonly performed based on data from in situ SM networks. For example, validation of SMAP SM products is performed with a global network of 34 high-quality core validation sites that provide estimates of SM at SMAP grid product scales (Colliander et al., 2017). A comprehensive assessment of SMAP L4 surface and root-zone SM products based on sparse network and core validation sites in the World has been provided by Reichle et al. (2017). Their findings indicate that the SMAP L4 meets its established SM retrieval accuracy requirement (0.04 cm^3/cm^3) with ubRMSE of 0.035–0.038 cm^3/cm^3 and 0.026–0.03 cm^3/cm^3 for surface and root-zone retrievals, respectively (https://nsidc.org/data/smap/technical-references). Table 6 provides an overview of validations of a number of SMAP SM products.

Data provided by the SMOS mission has a target SM retrieval error of less than 0.04 cm^3/cm^3. Experimental validation has been carried out in Europe (Dall'Amico et al., 2012; Dente et al., 2012; Fascetti et al., 2016; Pierdicca et al., 2015; Rötzer et al., 2014; Wigneron et al., 2012), the United States (Al Bitar et al., 2012; Jackson et al., 2012; Wagner et al., 2014), Africa (Fascetti et al., 2016; Louvet et al., 2015; Pierdicca et al., 2015), South America (Niclòs et al., 2016), and Australia (van der Schalie et al., 2015). The validation ranged from local (Jackson et al., 2012; Louvet et al., 2015) to continental scales (Al Bitar et al., 2012; Fascetti et al., 2016). Different validation experiments for SMOS SM products have generally revealed varying retrieval accuracies ranging from 0.030 to 0.140 cm^3/cm^3 depending on soil type, seasonality, and vegetation density (see also Table 6). For example, for rain-fed croplands in Argentina, Niclòs et al. (2016) determined a SM retrieval uncertainty of ±0.07 cm^3/cm^3 for SMOS L2 SM products. Louvet et al. (2015) evaluated SMOS L3
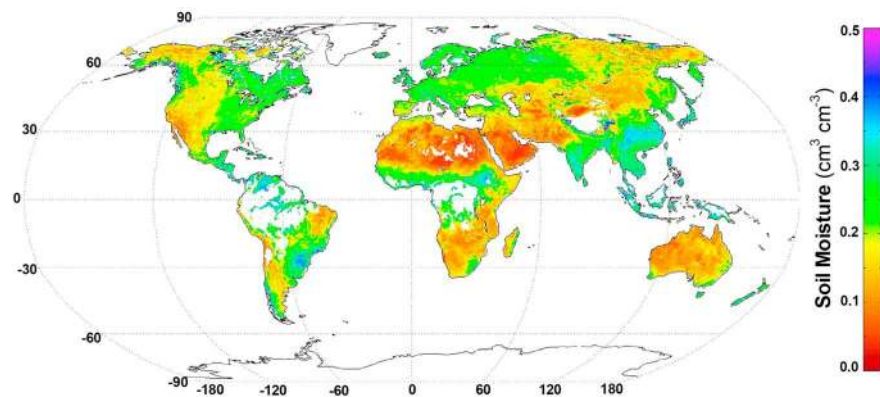
Figure 22. Soil moisture seasonality (climatology) in August derived from the combination of six active and passive sensors over the period from 1979 to 2010 (Source: Technische Universität Wien, http://www.esa-soilmoisture-cci.org/node/93; WACMOS: Water Cycle Multi-mission Observation Strategy).

SM data with ground-based SM measurements at the local and regional scales over West Africa and found an average RMSE of 0.047 cm^3/cm^3. Petropoulos et al. (2015) extensively evaluated SMOS SM operational estimates for some European sites with a variety of climate, environmental, biome, and seasonal conditions against the Carbo-Europe in situ network and found that SMOS performed better for low vegetation cover (with a RMSE from 0.044 to 0.061 cm^3/cm^3) and during the autumn season (with a RMSE of 0.076 cm^3/cm^3). Global comparison of SMOS to other missions like AMSR-2 indicated consistent results for SMOS over all surfaces from very dry (African Sahel, Arizona) to wet (tropical rain forests; Al-Yari et al., 2014; Kerr et al., 2016; Van der Schalie et al., 2016).

Since AMSR-2 is a new passive system, efforts have been devoted to the evaluation of the quality of its SM estimates by utilizing existing in situ observation networks (Cho, Choi, & Wagner, 2015; H. Lu et al., 2014; Parinussa et al., 2014). For example, Kim et al. (2015) evaluated the accuracy of global AMSR-2 SM estimates based on COSMOS networks in the United States, Australia, Europe, and Africa and reported reliable performance. More recently, Wu et al. (2016) evaluated the performance for ascending and descending AMSR-2 SM products during a 3-year period (2012–2015) based on in situ measurements at 598 stations of the ISMN network obtained for various land cover types and ecoregions. Their results revealed the best agreement with in situ measurements for the Great Plains (RMSE 0.051 cm^3/cm^3) and the worst for forested areas (RMSE 0.094 cm^3/cm^3; see also Table 6).

Validation experiments for ASCAT SM estimates indicated reasonable performance for several regions in Europe, with even somewhat better results than provided by the initial SMOS and best AMSR-E SM retrievals. The performance of ASCAT for mountainous regions or desert land was unsatisfactory (Wagner et al., 2013). A comparison between ASCAT and SMOS SM retrievals with in situ ground measurements in Europe and Northern Africa for the period from 2010 to 2013 has shown similar results (with mean RMSE 0.124 cm^3/cm^3; Fascetti et al., 2016). A validation experiment for ASCAT and SMOS SM data for four U.S. watersheds yielded large differences. The ASCAT SM estimates were very noisy and unstable, which may be due to higher sensitivity of the active observations to surface roughness (Leroux et al., 2014). In a similar study, Rötzer et al. (2014) evaluated SMOS and ASCAT SM products based on upscaled in situ measurements at three TERENO test sites in western Germany for the time period from 2010 to 2012. They applied the Water Flow and Balance Simulation (WaSiM) model for upscaling in situ measurements and found that while SMOS provided relatively constant bias, ASCAT bias was variable throughout the year. While ASCAT provides accurate SM estimates for bare and sparsely vegetated soils, estimates for tropical forests and other densely vegetated regions are associated with significant SM retrieval errors (Wagner et al., 2013).

The ASCAT surface SM estimates have been applied to determine SM distributions within the soil profile by means of the Soil Water Index (SWI), an exponential relationship that links surface and subsurface SM via a characteristic time length (Ceballos et al., 2005; De Lange et al., 2008; Wagner et al., 1999). For example, Paulik et al. (2014) evaluated SWI estimates based on in situ measurements at 664 stations (distributed over 23 observation networks) in the United States for a 5-year period and found an average correlation

Table 6
Overview of Different Active and Passive Microwave Remote Sensors Used to Estimate Near-Surface SM, Including RMSE and Coefficient of Determination (R^2)

Sensor	Product	Version/ retrieval algorithm	Spatial scale (km)	Sensor depth (cm)	Land cover	SM networks	No. of sensors	Country	RMSE/ ubRMSE (cm^3/cm^3)	R	References
SMAP	L2_SM_AP		9 and 3	5	Cropland, grassland, savanna, shrubland, forest, baren/ sparse, natural mosaic	U.S. core validation networks, sparse validation networks (SCAN, USCRN, OK mesonet, MAHASRI, SMOSMania, Pampas)	>500	United States, Australia, Spain, Canada, Mongolia, Argentina, Niger, Netherland, Tibet, Benin, Kuwait	0.024–0.081	0.19–0.93	Das et al. (2018)
SMAP	L4_SM SSM L4_SM RZSM	Version 2	9 and 36	4, 5, 7.5, 10, 20, 25, 30, 45, 50, 60	Cropland, grassland, savanna, shrubland, forest, baren/ sparse	U.S. core validation networks/Sparse validation networks (SCAN, USCRN, OK mesonet, OzNet)	43 717	United States, Australia, Spain, Canada, Mongolia, Argentina, Niger, Denmark	0.026–0.071 0.017–0.049	0.62–0.70 0.63–0.92	Reichle et al. (2017a)
SMAP	L2_SM_P	SCA-H SCA-V DCA	36	4, 5, 7.5, 10, 20, 25, 30, 45, 50, 60	Cropland, grassland, shrubland	U.S core validation networks/Sparse validation networks (GPS, COSMOS, SCAN, CRN)	275 482	United States, Canada, Argentina, Spain, Australia	0.021–0.082	0.30–0.95	Chan et al. (2016)
SMAP	L2_SM_P_E	SCA-H SCA-V DCA	9	4, 5, 7.5, 10, 20, 25, 30, 45, 50, 60	Cropland, grassland, shrubland, natural mosaic	U.S. core validation networks Sparse validation network (GPS, COSMOS, SCAN, CRN, OK mesonet, MAHASRI, SMOSMania, Pampas)	>500	United States, Canada, Argentina, Spain, Australia, Denmark, Mongolia, Netherland	0.019–0.087	0.40–0.91	Chan et al. (2018)
SMAP	L3_SM_P L3_SM_A L3_SM_AP		36 9 3	5	Cropland, grassland, shrubland	Sparse validation networks (SCAN & CRN)	268	United States		0.64–0.65 0.27–0.30 0.57–0.60	Pan et al. (2016)
SMAP	L2_SM_P L2_SM_AP L2_SM_A		36 9 3	5	Cropland, grassland, shrubland, forest, savanna, baren/ sparse	Core validation networks (34 sites)	283 (in situ values were upscaled to SMAP size)	United States, Canada, Mexico, Italy, Argentina, Spain, Australia, Finland, Germany, Mongolia, Netherland, Austria, Kenya	0.020–0.082 0.018–0.084 0.014–0.104	0.50–0.98 0.29–0.98 0.08–0.83	Colliander et al. (2017)
SMOS	L2_SM L3_SM NN_SM	v551-v620 v300	40 25	5	Cropland, grassland, shrubland, natural mosaic	US core validation networks/Sparse validation networks (SCAN, SNOTEL, OzNet)	476	United States, Europe, Africa	0.033–0.146 0.031–0.124 0.030–0.143	0.33–0.89 0.37–0.85 0.36–0.89	Kerr et al. (2016)
SMOS	L3_SM	v2.46	25	5	Mixed crops, forest, savana, savanna	Benin, Niger, Mali	120	West Africa	0.032–0.076	0.70–0.77	Louvet et al. (2015)

Table 6 (Cont.)

Table 6 *(continued)*

Sensor	Product	Version/ retrieval algorithm	Spatial scale (km)	Sensor depth (cm)	Land cover	SM networks	No. of sensors	Country	RMSE/ ubRMSE (cm^3/cm^3)	R	References
SMOS	L3_SM	v2.72	25	5	Grassland, shrubland	Walnut Gulch, Little Washita, Murrumbidgee	87	United States (Arizona, Oklahoma), Australia (Yanco)	0.030–0.118		Molero et al. (2016)
SMOS			40	5	Grassland, shrubland, cropland, forest	Core validation networks (Walnut Gulch, Little Washita, little River, Reynolds Creek)	85	United States (Arizona, Oklahoma, Georgia, Idaho)	0.034–0.072	0.14–0.81	Jackson et al. (2012)
SMOS	L2_SM	v620	40	5	Cropland, grassland, shrubland	Sparse validation networks (CRN, SCAN)	127	United States	0.092	0.56	Rodríguez-Fernández et al. (2017)
SMOS	L2_SM L3_SM	v620 v300	25	5	Grassland, shrubland, copland, savanna	Walnut Gulch, Little Washita, AMMA-CATCH		United States, Niger; Benin	0.050–0.075 0.044–0.110	0.63–0.81 0.61–0.80	Al Bitar et al. (2017)
SMOS	L2_SM			5	Cropland, grassland, wetland, forest	Sparse validation networks (CRN, SNOTEL)	18	United States	0.032–0.130	0.28–0.82	Al Bitar et al. (2012)
SMOS	L2_SM	v4.00		5	Cropland, grassland, shrubland	Sparse validation networks (SCAN, CRN, COSMOS, OK Micro- & mesonet)		United States	0.05–0.13	0.40–0.58	Collow et al. (2012)
SMOS	SM_L2	v5.51	40	5	Forest, grassland, shrubland	ISMN networks	88	Europe (Germany, Italy, Denmark, Poland, France)	0.037		Pierdicca et al. (2015)
SMOS	SM_L3		25	8	cropland, forest	OzNet network	49	Australia	0.084–0.106	0.75–0.77	van der Schalie et al. (2015)
SMOS	SM_L2	v5.51	40	5		ISMN networks: TERENO, UDC SMOSMANIA, Hydrol-Net-PERUGIA, SWEX, REMEDHUS, VAS		Europe (France, Germany, Italy, Poland, Spain), North Africa	0.126	0.46	Fascetti et al. (2016)
SMOS	SM_L2	v620	25	5	Forest	SCAN		United States, south America, Africa	0.09–0.204	0.108–0.742	Vittucci et al. (2016)
ASCAT		WARP5	25	10, 20, 40	mixed	Umbria, Vallaccia, Spoleto	210	Italy	0.035–0.042	0.80–0.92	Brocca, Melone, Moramarco, & Morbidelli (2010)
ASCAT		WARP5	25	4, 7, 10, 20, 30,	Grassland, bare soil, cropland	IRPI, UMSUOL, REMEDHUS, Vallcebre, SMOSMANIA, Valescure	>50	Europe (Italy, Spain, France, Luxembourg)	0.085–0.279	0.44–0.92	Brocca et al. (2011)

Table 6 (Cont.)

Table 6 (*continued*)

Sensor Product	Version/retrieval algorithm	Spatial scale (km)	Sensor depth (cm)	Land cover	SM networks	No. of sensors	Country	RMSE/ubRMSE (cm³/cm³)	R	References
ASCAT	WARP 5.5	25	5	Grassland, forest, cropland	TERENO	900	Germany	0.05–0.10	0.48–0.54	Rötzer et al. (2014)
ASCAT	WARP	25	5		SMOSMANIA, SMOSREX	13	France	0.152–0.396	0.26–0.91	Albergel et al. (2009)
ASCAT H07 SM-OBS-1		25	5	Forest and nonforest	ISMN networks: TERENO, UDC SMOSMANIA, HydroI-Net-PERUGIA, SWEX, REMEDHUS, VAS		Europe (France, Germany, Italy, Poland, Spain), North Africa	0.094–0.134	0.39–0.52	Fascetti et al. (2016)
ASCAT L2_SM	v5.0	12.5	4, 5, 7.5, 10, 20, 25, 30, 45, 50, 60	Cropland, grassland, shrubland, natural mosaic	Sparse validation network (GPS, COSMOS, SCAN, CRN, OK mesonet, MAHASRI, SMOS Mania, Pampas)	271	United States, Canada, Argentina, Spain, Australia, Denmark, Mongolia, Netherland		0.60–0.78	Chen et al. (2018)
ASCAT H101-H16 H102-H103 H08		25 12.5 1	5		SMOSMANIA network, Reference plots	7 23	France	0.078–0.091 0.085–0.094 0.074–0.075	0.49–0.50 0.44–0.50 0.55–0.56	El Hajj et al. (2018)
AMSR-2L3	JAXA	25	5	Grassland, bare soil	Tibetan plateau (Naqu and Pali networks)	77	China	0.024–0.113	0.40–0.80	Chen et al. (2017)
AMSR-2L3	DCA JAXA LPRM	25	5	Grassland, forest, cropland	Genhe	10	Mongolia	0.118–0.130 0.138–0.139 0.400–0.597	0.12–0.19 0.28–0.40 0.08–0.39	Cui et al. (2017)
AMSR-E	LSMED	25	5	Cropland, forest, pasture, wetland	Georgia (Little River)	17	United States	0.031–0.081	0.61–0.78	Sahoo et al. (2008)
AMSR-E	VUA-NASA	25	5 8	Grassland	Murrumbidgee and Goulburn River networks	12	Australia	0.013–0.066	0.54–0.94	Draper et al. (2009)
AMSR-E L3	LPRM PRI NASA	25	4, 7, 10, 20, 30,	Grassland, bare soil, cropland	IRPI, UMSUOL, REMEDHUS, Vallcebre, SMOSMANIA, Valescure	>50	Europe (Italy, Spain, France, Luxembourg)		0.45–0.81 0.15–0.71 0.04–0.64	Brocca et al. (2011)
AMSR-E	LSMED	25	5 6	Cropland	Walnut Creek (Iowa SCAN site, SMEX02 network)	34	United States	0.04	0.75	McCabe et al. (2005)

Note. SM = soil moisture; RMSE = root-mean-square error; SMAP = Soil Moisture Active Passive; SCAN = Soil Climate Analysis Network; OK = Oklahoma; SMOSMANIA = Soil Moisture Observing System – Meteorological Automatic Network Integrated Application; SSM = Special Sensor Microwave; RZSM = Root Zone Soil Moisture; SCA = Single Channel Algorithm; GPS = Global Positioning System; COSMOS = Cosmic ray Soil Moisture Observing System; CRN = Climate Reference Network; SMOS = Soil Moisture Ocean Salinity; SNOTEL = SNOwpack TELemetry; ISMN = International Soil Moisture Network; UDC = Upper Danube Catchment; ASCAT = Advanced Scatterometer; WARP = WAter Retrieval Package; SMOSREX = Surface Monitoring Of the Soil Reservoir EXperiment; JAXA = Japan Aerospace Exploration Agency; LPRM = Land Parameter Retrieval Model; NASA = National Aeronautics and Space Administration.

coefficient of 0.54 and RMSEs below 0.079 cm^3/cm^3. A global validation of the ASCAT SWI with in situ data from the ISMN has been provided by Paulik et al. (2012). The ASCAT near-surface SM products have also been assimilated into land surface models to provide profile SM (Dharssi et al., 2011; Draper et al., 2011, 2012; Reichle et al., 2007). An ASCAT root-zone SM profile product, the so-called SM-Data Assimilation System-2, SM-DAS-2 or H14, has been developed by the European Organization for the EUMETSAT based on a near-surface SM index, the H-16 SM-OBS-3 product, and a Simplified Extended Kalman Filter Data Assimilation System (De Rosnay et al., 2011). This product is available for four soil layers from the surface down to 3 m (i.e., 0–7, 7–28, 28–100, and 100–289 cm) with global daily coverage. This product has been evaluated based on in situ measurements and yielded better SM estimates than model or satellite estimates alone (Albergel et al., 2010, 2012). The ASCAT root-zone SM profile retrieval algorithm is now operational at the European Centre for Medium-Range Weather Forecasts (ECMWF). A significant constraint of ASCAT SM data is the irregular temporal coverage.

However, so far only a few validation experiments have been conducted to determine the performance of the S-1 data with regard to SM retrieval. Table 6 provides an overview of the accuracy and performance of validation experiments used to retrieve SM from various microwave satellite remote sensors.

Several studies have been conducted to evaluate CCI products based on in situ measurements and finer spatial resolution remotely sensed SM data. In a comprehensive validation, Dorigo et al. (2015) evaluated historical CCI products based on ground measurements at 596 sites from 28 globally distributed SM networks. They reported RMSE of 0.05 cm^3/cm^{-3} ($R = 0.46$) for absolute values and 0.04 cm^3/cm^{-3} ($R = 0.36$) for SM anomalies. In a similar study, Wang et al. (2015) performed reliability analysis of CCI products for croplands in North China for the period from 1981 to 2010. They obtained an average triple collocation (TC) random error of 0.052 cm^3/cm^3 and an average Spearman correlation coefficient of 0.42. A quality assessment of 5-year CCI data based on estimates from Envisat ASAR (Wide Swath Mode) for various climate, topography, land cover, and soil-type conditions has provided reasonable agreement between the ASAR and CCI data sets, with correlation values larger than 0.55 (Pratola et al., 2015). It has been pointed out that the merged products have a similar or better performance than individual products (Dorigo et al., 2015). Recently, Gruber et al. (2017) proposed a new merging approach based on weighted averaging and error variance estimates obtained from TC analysis for blending multi-platform (active/passive) SM products, which is being used in the new CCI product (version v03.x and higher). An overview of validation results for microwave satellite SM retrievals is given in Table 6.

High spatial variability of SM results in significant differences between the point-scale in situ SM sensors and the coarse-scale satellite-based SM retrievals, which provides a significant challenge for the validation of SM from the current and the upcoming SM satellite missions. Upscaling point-scale SM could help to fill in the scale gaps and provide reliable validation of satellite SM products. An excellent review of the SM upscaling problem and measurement density requirements for ground based SM data has been provided by Crow et al. (2012).

6.3. Airborne Microwave Sensors and Imagery

Over the past few decades, extensive L-band and C-band airborne observations have been conducted with the aim of preparation for L-band and C-band satellite missions. Such microwave instruments are only capable of measuring near-surface SM, which is then assimilated into hydrologic models to determine profile SM (Draper et al., 2012; Montzka et al., 2011; see also section 7.2). There is significant interest in direct, large-scale, profile SM measurements because data assimilation approaches that couple satellite-based near-surface SM and subsurface SM may fail under specific circumstances (Kumar et al., 2009; Walker et al., 2002). The application of lower-frequency (deeper measurement) airborne microwave remote sensors for profile SM quantification has been an area of extensive research in recent years. In this section we focus on lower-frequency airborne activities only. At the lower P-band microwave frequencies, the signal penetrates to deeper soil depths, which allows direct profile SM sensing, which is of significant importance for many agricultural, hydrological, and meteorological applications and which is critical to strategic management of water resources.

6.3.1. The AirMOSS Mission

The NASA AirMOSS mission that consists of a P-band fully polarimetric SAR represents the first attempt to provide high-resolution observations of RZSM and net ecosystem exchange (NEE). The project targets nine regions representative of the major North American climatic biomes for estimating the impact of RZSM on

regional carbon fluxes and integrating the measurement-constrained estimates of regional carbon fluxes to the continental scale of North America (Chapin et al., 2012; Tabatabaeenejad et al., 2013). In contrast to L-band and C-band microwave remote sensors, AirMOSS is designed to provide direct RZSM estimates. For the AirMOSS mission, NASA has adapted its Uninhabited Aerial Vehicle Synthetic Aperture Radar, a pod-based repeat-pass polarimetric SAR that operates within the L-band (~1.2 GHz) and incorporated a P-band (280–440 MHz) SAR, which operates at different frequencies onboard a Gulfstream-3 aircraft. The AirMOSS is capable of penetrating through vegetation extending to soil depths of about 0.5 m. The actual measurement depth depends on SM status, soil type, and vegetation cover (Moghaddam et al., 2000). It should be noted that P-band SAR observations are influenced by Faraday rotation resultant from the anisotropic ionosphere and the action of the geomagnetic field. This distorts P-band data and complicates their direct application for SM retrieval (Qi & Jin, 2007; Rignot et al., 1995).

AirMOSS test flights started in August 2012 and science operations commenced in October 2012. The surveys cover approximately 25×100-km areas that contain FLUXNET sites for ground calibration and span regions ranging from boreal forests in Saskatchewan (Canada) to tropical forests in La Selva (Costa Rica) (Tabatabaeenejad et al., 2015). The flights have provided high spatial resolution (100 m) measurements for nine regions representative for the major North American biomes (Figure 23) at subweekly, seasonal, and annual time scales. Furthermore, AirMOSS data can provide a direct means for validating RZSM algorithms applied for the SMAP L4 SM retrieval (Tabatabaeenejad et al., 2015). A cross comparison between AirMOSS and model-based RZSM estimates generated by the Flux-Penn State Hydrology Model (Flux-PIHM) over the nine biome sites demonstrated comparable levels of accuracy for the two products when evaluated against in situ SM measurements and a significant temporal cross correlation. However, the AirMOSS RZSM retrievals showed higher spatial and temporal variability than the Flux-PIHM estimates (Crow et al., 2018). AirMOSS data are publicly available from NASA at *https://airmoss. jpl. nasa. gov*.

6.3.2. The E-SAR

The Experimental Synthetic Aperture Radar (E-SAR) onboard the German DLR DO228 aircraft is capable of simultaneously capturing data within the X-band, C-band, L-band, and P-band. The measurement modes include single channel operation mode (i.e., one wavelength and polarization at a time), the SAR Interferometry mode (X-band and C-band), and the SAR Polarimetry mode (L-band and P-band). The E-SAR captures an area of $3–5 \times 20$ km with slant range resolution of 2.3 to 4.5 m and azimuth resolution of 0.7 to 2.5 m. The E-SAR has been in operation since 1989 and has been continuously improved and applied to various SM and ice study campaigns such as AgriSAR (Synthetic Aperture Radar in Agriculture, 2006), OPAQUE (Operational discharge and flooding predictions in head catchments, 2007–2008), SARTEO (Synthetic Aperture Radar within TERENO framework, 2008; Bogena et al., 2018), and ICESAR (Synthetic Aperture Radar for Ice, 2007) (Jagdhuber et al., 2015; Parrella et al., 2016). In 2012, the Microwaves and Radar Institute of the German Aerospace Center (DLR) developed an improved E-SAR version, termed F-SAR, based on the same platform and frequencies. Several studies have demonstrated the capability of E-SAR for SM retrieval. Zwieback et al. (2015) showed that SM variations significantly affect E-SAR L-band radar signals (i.e., phase, coherence, and phase triplets). Jagdhuber et al. (2015) coupled full polarimetric L-band E-SAR data with an iterative generalized hybrid decomposition method to retrieve SM for vegetated land surfaces and obtained RMSEs ranging from 0.04 to 0.044 cm^3/cm^3 for different vegetation covers and soil types. The retrieved RZSM from microwave airborne instruments can provide validation of RZSM retrievals from assimilation of near-surface SM into hydrological models, which is discussed in section 7.2.

6.3.3. The Polarimetric L-Band Multibeam Radiometer

The Polarimetric L-band Multibeam Radiometer (PLMR) is a passive microwave remote sensor onboard a small aircraft owned by the Australian Research Council and several Australien universities. It provides brightness temperature data at six different incidence angles ($\pm 7°$, $\pm 21.5°$, and $\pm 38.5°$) to estimate high-resolution SM, salinity, and temperature at low to moderate vegetation conditions. The radiometer includes a thermal imager (FLIR ThermaCam S60, 7.5–13μ) and a dual polarization L-band (1.4 GHz) radiometer with 1- and 50-m resolutions, respectively, at a flight elevation of 150 m above ground. The instrument's accuracy is 0.7 for H- and 2°K for V-polarizations, which translates to a SM accuracy better than 0.01 cm^3/cm^3. It was used to assess the performance of the core algorithm (L-MEB) used for SMOS SM retrieval (Peischl et al., 2014; Yan et al., 2015). For example, Panciera et al. (2009) used PLMR brightness
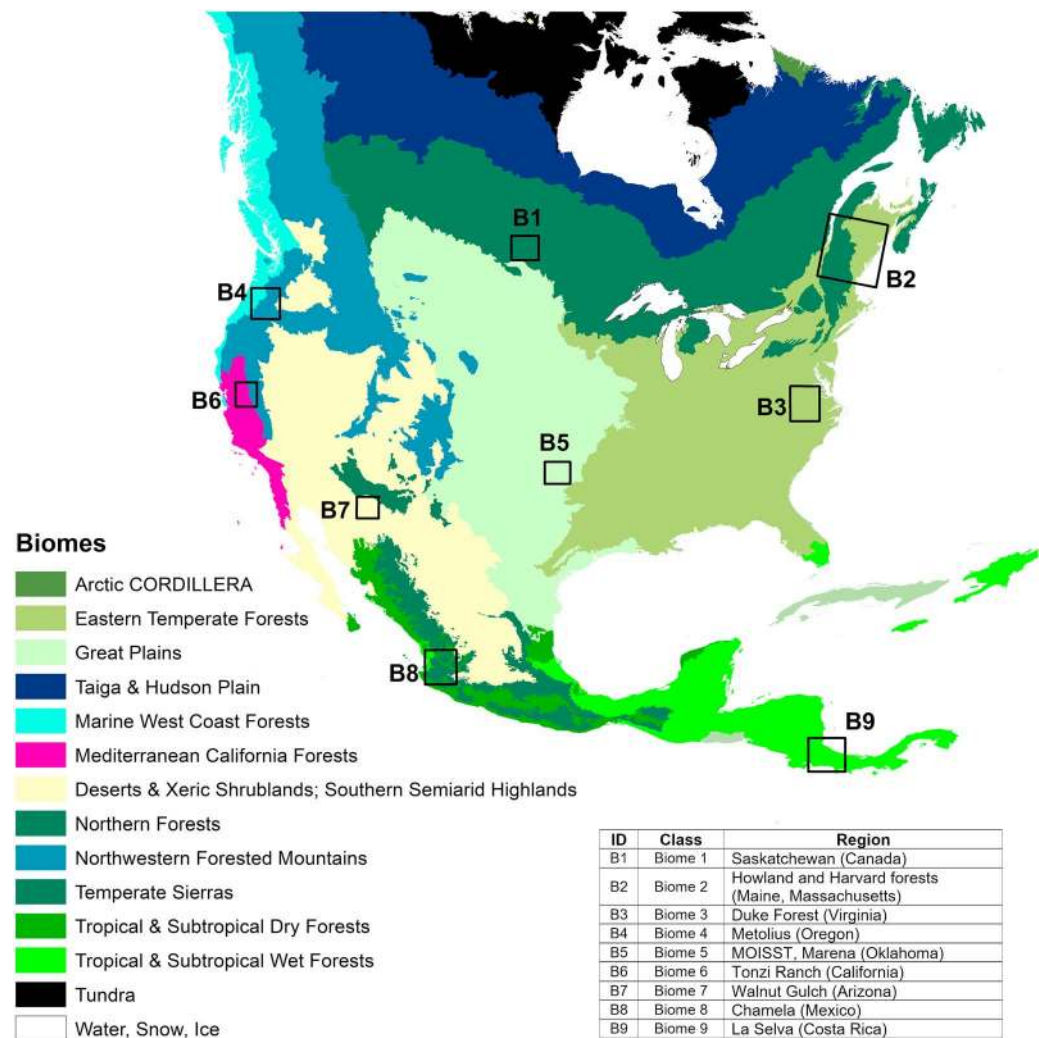
Biomes	
■	Arctic CORDILLERA
■	Eastern Temperate Forests
■	Great Plains
■	Taiga & Hudson Plain
■	Marine West Coast Forests
■	Mediterranean California Forests
■	Deserts & Xeric Shrublands; Southern Semiarid Highlands
■	Northern Forests
■	Northwestern Forested Mountains
■	Temperate Sierras
■	Tropical & Subtropical Dry Forests
■	Tropical & Subtropical Wet Forests
■	Tundra
□	Water, Snow, Ice

ID	Class	Region
B1	Biome 1	Saskatchewan (Canada)
B2	Biome 2	Howland and Harvard forests (Maine, Massachusetts)
B3	Biome 3	Duke Forest (Virginia)
B4	Biome 4	Metolius (Oregon)
B5	Biome 5	MOISST, Marena (Oklahoma)
B6	Biome 6	Tonzi Ranch (California)
B7	Biome 7	Walnut Gulch (Arizona)
B8	Biome 8	Chamela (Mexico)
B9	Biome 9	La Selva (Costa Rica)

Figure 23. The Airborne Microwave Observatory of Sub-canopy and Subsurface study regions in North America.

temperature data from National Airborne Field Experiment conducted in southeastern Australia in 2005 to evaluate the L-MEB algorithm for SM retrieval and showed good accuracy with errors less than 0.048 cm^3/cm^3 for crops and grasslands. It was also used in different studies for detection of land surface SM changes (Ma et al., 2017; Summerell et al., 2009). The PLMR was also used in SMAP experiments in Australia for an algorithm development test-bed for the SMAP mission (Panciera et al., 2014; Wu et al., 2014, 2015).

6.3.4. The Passive Active L-Band Sensor

The Passive Active L-band Sensor (PALS) onboard NASA's P-3, NCAR C-130, and Twin Otter International's aircrafts is a combined dual polarization radiometer and radar operating at 1.41 and 1.26 GHz, respectively. The antenna is a high beam efficiency conical horn with relatively low side lobes pointed at a 38° incidence angle and the spatial resolution 600-m at 1,200-m altitude. It was designed and built as the prototype for the Aquarius and SMAP missions to assess the benefits of combining active and passive microwave sensors for SM and ocean salinity RS (Colliander et al., 2017; Wilson et al., 2001). PALS has been used in varying configurations for four major field experiments between 1999 and 2007 (Colliander et al., 2012). PALS observations have been used to improve the calibration and validation of SMAP SM algorithms (Colliander et al., 2012). For example, McNarin et al. (2015) used PALS in a 6-week Canada-U.S. field campaign in 2012 (SMAPVEX12) to simulate SMAP data. They showed that PALS radar backscatter and radiometer brightness temperature data were able to closely follow dry down and wetting events during SMAPVEX12. Akbar and Moghaddam (2015) used PALS data in Iowa in 2002

(SMEX02) and introduced a combined active-passive approach based on numerical modeling and parameter optimization in support of SMAP SM retrieval and showed retrieval errors of 0.035 cm^3/cm^3 for corn (VWC equal to 5 kg/m^2). Colliander et al. (2015) used PALS data acquired during the SMAP validation experiment in 2012 to evaluate SMOS satellite brightness temperature observations and found differences less than 5 and 6°K for V and H polarizations, respectively. They concluded that PALS estimates are of significant value for the development of SMAP SM retrieval algorithms. Examples for other widely applied microwave airborne systems for SM retrieval include the L-band Electronically Scanned Thinned Array Radiometer (Gao et al., 2004; Guha et al., 2003), the C/X-band Polarimetric Scanning Radiometer (Bindlish et al., 2006; Das & Mohanty, 2008), and the L-band radiometer 2D-DTAR (Rye et al., 2010).

7. Root-Zone SM Estimation

As discussed above, most of the commonly applied RS methods provide only skin and near-surface SM estimates. The increased interest in estimating RZSM based on RS observations has led to close cross-disciplinary collaborations between the RS community and soil physicists and hydrologists with the central goal of linking RZSM to remotely sensed skin and near-surface data. Correlations of surface and RZSM at different depths are influenced by many factors such as soil type, land use, and prevailing hydroclimatological conditions (Mahmood & Hubbard, 2007). Nonetheless, several approaches, reviewed by Kostov and Jackson (1993), indicated that accurate estimation of RZSM based on near-surface SM is possible. Kostov and Jackson (1993) categorized these approaches into four main classes: (1) empirical regression-based models, (2) knowledge-based approaches, (3) microwave brightness temperature inversion techniques, and (4) combinations of remotely sensed data with soil water flow models. They concluded that "Proper integration of remote sensing and modeling is probably the best approach to the problem of profile SM estimation". Soil water flow models commonly applied to this approach are classified as analytical and numerical models as discussed below.

7.1. Analytical Modeling

One approach to link RZSM to surface/near-surface SM is the derivation of a simple analytical equation from an approximate mass balance equation (Albergel et al., 2008; Ceballos et al., 2005; Wagner, Lemoine, & Rott, 1999). An excellent contribution to this class of models is the pioneering work of Wagner, Lemoine, and Rott (1999), who introduced a simple one-parameter model by solving the following approximate mass balance equation:

$$L\frac{\mathrm{d}\theta}{\mathrm{d}t} = C(\theta_{\mathrm{sur}}-\theta) \tag{14}$$

where θ is the volumetric SM content averaged from $z = 0$ to $z = L$ (z denotes soil depth), θ_{sur} is the SM content at the surface ($z = 0$), t is the time, and C is a pseudo diffusivity coefficient that depends on the soil properties. Solving equation (14), Wagner et al. (1999a) obtained the following simple equation to estimate deeper layer (profile) SM, $\theta(t)$, from a time series of remotely retrieved surface/near-surface SM, $\theta_{\mathrm{sur}}(t_i)$, data

$$\theta(t) = \frac{\sum_i \theta_{\mathrm{sur}}(t_i)\exp[-(t-t_i)/T]}{\sum_i \exp[-(t-t_i)/T]} \tag{15}$$

where $T = C/L$ is a "characteristic time length" or recession constant, considered to be a calibration parameter to be determined by fitting model estimations to ground observations.

Although the solution of Wagner, Lemoine, and Rott (1999) relies on some simplifying assumptions (i.e., neglect of transpiration and invariant soil diffusivity), it is useful as a general concept for estimating the profile SM, accounting for the decreasing influence of measurements with increasing time lag. Equation (15) has been tested with both simulated and measured data and yielded good results (Tobin et al., 2017). The model has also been extensively used to improve the description of the RZSM for rainfall-runoff applications (Brocca, Melone, Moramarco, Wagner, et al., 2010; Brocca, Tullo, et al., 2012; Manfreda et al., 2011; Matgen et al., 2012).
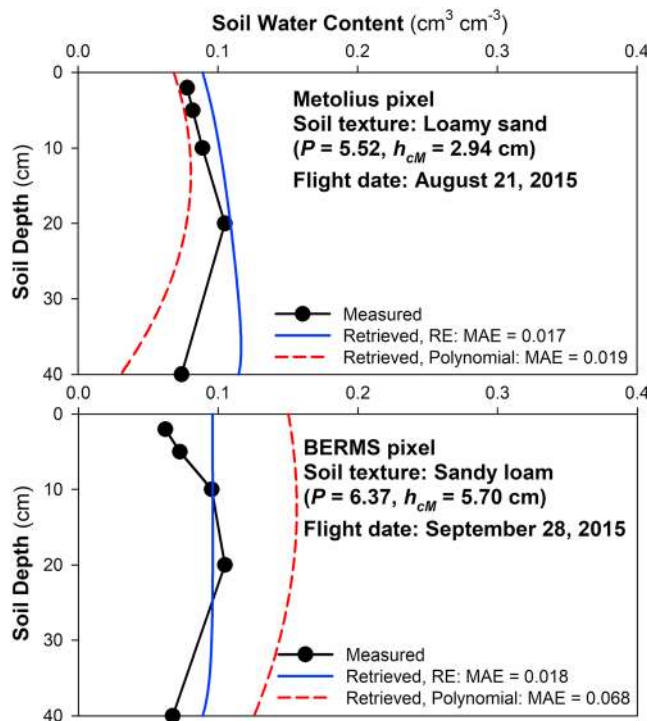
Figure 24. Comparison of the Richards' equation (RE)-based solution for Airborne Microwave Observatory of Sub-canopy and Subsurface soil moisture retrieval with measured soil moisture data and the polynomial algorithm for two flights over the Metolius (Oregon) and BERMS (Saskatchewan) sites in 2015. The MAE denotes the mean absolute error (cm³/cm³).

Another analytical approach for retrieving RZSM is the physically based model of Sadeghi et al. (2017), which builds on the second-order polynomial model of Tabatabaeenejad et al. (2015). Sadeghi, Tabatabaeenejad, et al. (2017) mathematically solved Richards' equation (RE; see equation (17) and section 7.2.1) for unsaturated flow in soil and introduced a more realistic model for retrieving profile SM from AirMOSS P-band radar data. The general form of their equation, neglecting initial and boundary conditions, is

$$\theta = \left[c_1 z + c_2 \exp\left(\frac{z}{h_{cM}}\right) + c_3 \right]^{\frac{1}{P}} \tag{16}$$

where $c1$, $c2$, and $c3$ denote the unknown coefficients that need to be retrieved, P and h_{cM} are soil-dependent parameters related to water retention function parameters (van Genuchten, 1980). The values of these two parameters are available for the 12 soil textural classes of the USDA classification scheme (Carsel & Parrish, 1988; Sadeghi, Tabatabaeenejad, et al., 2017). The AirMOSS retrieved SM profiles, using equation (16), revealed better performance than the original AirMOSS polynomial algorithm by improving the inversion accuracy and providing more accurate SM profiles (Figure 24).

7.2. Numerical Modeling and Data Assimilation

For several years, SM has been estimated with "open loop" strategies, where hydrological land surface models are simply coupled with precipitation and other meteorological data. For example, SM has been provided as volumetric or soil wetness by the National Centers for Environmental Prediction-National Center for Atmospheric Research (NCEP-NCAR; Kalnay et al., 1996), the ECMWF (Simmons & Gibson, 2000), the Japanese 25-year Reanalysis (JRA-25) project, the Global Land Data Assimilation System (GLDAS; Rodell et al., 2004; https://rda.ucar.edu/), the Global Energy and Water Cycle Experiment (GEWEX) Global Soil Wetness Project (GSWP-2; Dirmeyer et al., 2006), and the North American Land Data Assimilation System (NLDAS; Luo, 2003).

Another strategy to provide high-accuracy RZSM is the combination of surface SM measurements with a numerical model. Numerical modeling to estimate RZSM from near-surface SM estimates is commonly accompanied by sequential data assimilation, that is, the combination of observations with previous simulations for estimations used for the next model forecast (Entekhabi et al., 1994; Crow & Wood, 2003; Das & Mohanty, 2006; Han et al., 2013; Montzka et al., 2011; Song, Shi, et al., 2014). Reichle et al. (2004) were among the first to show that the assimilation of SM observations can globally improve model-based RZSM predictions (Reichle et al., 2007; Reichle & Koster, 2005). In geosciences, and especially for estimation of RZSM, sequential data assimilation often forms an inverse problem. Here, near-surface SM (indirect measurements) can be used to update RZSM simulations (previous forecast) to initialize a corrected state for the next prediction (Hoeben & Troch, 2000). With this approach, a dynamically consistent motion picture of the hydrological system can be generated with known error bars (Ghil & Malanotterizzoli, 1991). In this case, accurate precipitation observations serve as the driving force for the hydrological model and have similar significance and largely independent information to contribute to the RZSM algorithm as compared to assimilated near-surface SM measurements (Reichle et al., 2014). The benefit of near-surface SM data assimilation to infer RZSM is the connection to water and energy cycles, for example, evapotranspiration and infiltration estimation (De Lannoy & Reichle, 2016; Lievens et al., 2015).

Various assimilation techniques such as the Ensemble Kalman Filter (Evensen, 1997), the Particle Filter (Gordon et al., 1993; Moradkhani et al., 2005), or variational methods (Lorenc, 2003) including their modifications have been applied to RZSM estimation (Montzka et al., 2012). Sabater et al. (2007) compared different assimilation methods for RZSM retrieval. In addition to the assimilation method, subsurface physical

models also play an important role in the improvement of RZSM estimates. Kumar et al. (2009) found this to be a function of surface-root-zone coupling strength, where the catchment land surface model outperforms the Mosaic, Noah and Community Land Model (CLM) models by describing the deviations from the equilibrium SM profile. The coupling to very deep soils is weaker but still possible using longer assimilation periods with more observations (Walker & Houser, 2001). During extreme hot conditions, the long-term correlations between near-surface and RZSM conditions degrade (Hirschi et al., 2014), and inversion may become misleading. A decoupling occurs during such extended drying periods as a result of a divergence between the drying rates at the soil surface and at deeper locations within the soil profile (Walker et al., 2002). However, Sabater et al. (2007) tested various data assimilation techniques derived from Kalman filter and variational methods and generated satisfactory RZSM results by assimilation of near-surface SM measurements into a model. Reichle et al. (2004) were among the first to show the discrepancy between absolute SM values between the datasets (satellite, model, and in situ) and point out the importance of bias correction and rescaling data before SM retrievals can be assimilated into land surface models. Yilmaz and Crow (2013) evaluated the optimality of three bias correction approaches including CDF matching, least squares regression, and TC to remove systematic differences between modeled and observed values and concluded that TC is the optimal approach. However, TC rescaling only helps for multiplicative biases, whereas CDF matching and least squares regression deal with both additive and multiplicative biases.

There are various examples of near-surface SM assimilation for improved RZSM estimation (e.g., Carrera et al., 2015; Draper et al., 2012; Kumar et al., 2014; Lievens et al., 2017; Pan et al., 2012). Dumedah et al. (2015) used the advanced Evolutionary Data Assimilation procedure to assimilate downscaled (1 km) SMOS surface SM data into the Joint UK Land Environment Simulator to better estimate the RZSM for the western plains of New South Wales in Australia. Assimilation yielded a clear improvement of RZSM retrieval by 34% for the 0- to 30-cm soil depth, 59% for the 30- to 60-cm soil depth, and 63% for the 60- to 90-cm soil depth based on RMSE. Draper et al. (2012) used an ensemble Kalman filter to separately and jointly assimilate ASCAT and AMSR-E into the NASA Catchment land surface model and recommended that joint assimilation of active and passive microwave observations provide maximum accuracy for RZSM estimation. Kolassa et al. (2017) combined active and passive microwave data from ASCAT and AMSR-E in a SM assimilation system and obtained highly accurate SM products. Lievens et al. (2017) demonstrated that joint assimilation of high-resolution Sentinel-1 and SMAP observations can improve the spatiotemporal accuracy of surface and root-zone SM estimates. Koster et al. (2018) indicated that integration of SMAP L2 surface SM data into the Catchment land surface model (the same as SMAP L4 model) along with model calibration can improve simulated SM and streamflow estimates. This has important ramifications for maximizing the effective employment of SMAP data in hydrological simulations. Hain et al. (2012) used dual assimilation of thermal infrared and passive microwave satellite observations of SM into the Noah land surface model and reported improvements for surface and RZSM. In addition to RZSM, satellite-derived SM data have been used for initialization of numerical weather prediction models. In a study by Drusch (2007), the TRMM Microwave Imager (TMI) SM product with 40-km resolution was used in three data assimilation experiments with the Integrated Forecast System (IFS) of the ECMWF over the southern United States to infer RZSM and improve weather parameters and forecast quality. Satellite SM products have been used to correct precipitation estimates with a water balance model via matching of observed and simulated SM. Pellarin et al. (2008) demonstrated that the use of AMSR-E SM measurements can be useful to suppress a significant number of wrongly detected rain events.

Often, the model hydraulic parameterization leads to inadequate SM profile predictions. However, surface SM assimilation for improved RZSM simulation can help to constrain the parameter space (Han et al., 2013; Lee et al., 2014; Montzka et al., 2011). The process of combining observations and model forecasts during data assimilation is typically carried out by weighting each on the basis of their respective errors (Kumar et al., 2012). Therefore, one important issue during near-surface SM data assimilation is the correct estimation of the observation error characteristics (Reichle et al., 2008). Typically, most data assimilation approaches assume random, zero-mean observation errors, but in reality biases are unavoidable and it is difficult to attribute the bias to the model or the observations. Assimilating biased observations would lead to biased model states (including RZSM) and model parameters. Therefore, several bias removal techniques have been developed (Kumar et al., 2012). These techniques correct for both additive and multiplicative

biases. In contrast to dynamically bias-aware data assimilation systems (Chen et al., 2014; De Lannoy et al., 2007; Montzka et al., 2013; Ryu et al., 2009), typically a priori bias mitigation is performed. Kumar et al. (2012) compared the attribution of the bias to the model and a priori calibration of respective model parameters with the attribution to the observations and a priori SM climatology matching. They found similar assimilation skills for near surface and RZSM, where the spatial variability of skill scores is reduced by a priori parameter optimization. A priori bias mitigation strategies include cumulative distribution function matching (Reichle & Koster, 2004) and least squares regression rescaling (Crow & Zhan, 2007), or TC (Stoffelen, 1998). Applications of near-surface SM assimilation are discussed in Lievens et al. (2015), Parrens et al. (2014), Rains et al. (2017), and Xu et al. (2015).

7.2.1. Soil Water Flow Governing Equation

Estimating RZSM from surface/near-surface SM is commonly accomplished through a land surface or hydrological model. Land surface models applied to the RZSM simulations commonly consider a limited number of soil layers along the soil profile and calculate SM for each layer using a water balance equation (Crow & Wood, 2003; Sabater et al., 2007). More sophisticated hydrological models solve the SM profile on a much finer grid where water flow is modeled based on Richards' (1931) equation (Das & Mohanty, 2006; Entekhabi et al., 1994; Han et al., 2012a; Heathman et al., 2003; Montzka et al., 2011). RE combines the Buckingham-Darcy equation (Buckingham, 1907), $q = -K(\nabla h - 1)$, and the continuity principle (conservation of mass), $\partial\theta/\partial t = -\nabla q$. Modified to account for root water uptake, the one-dimensional (1-D) form of RE is written as

$$\frac{\partial\theta}{\partial t} = \frac{\partial}{\partial z}\left(K\frac{\partial h}{\partial z} - K\right) - S(z) \tag{17}$$

where q is the water flux density [LT^{-1}], K is the unsaturated hydraulic conductivity [LT^{-1}], h is the pressure head [L], θ is the volumetric SM content [L^{3}L^{-3}], t is time [T], z is soil depth [L] assumed positive downward from the soil surface, and S is the sink term [L^{3}L^{-3}T^{-1}] (i.e., root water uptake).

7.2.2. Soil Hydraulic Functions

In an unsaturated soil, h and K are functions of θ which are referred to as SHPs or "soil hydraulic functions" (SHFs) and assumed to be invariant for a given soil. Provided that $K(\theta)$ and $h(\theta)$ for any given soil component are known, solving RE subject to specific initial and boundary conditions would result in an estimate of the SM profile, $\theta(z)$, at any time of interest, t.

Various mathematical relationships exist for SHFs, $h(\theta)$ and $K(\theta)$. The most widely used unimodal SHFs are relationships introduced by Gardner (1958), Brooks and Corey (1964), van Genuchten (1980), Russo (1988), and Kosugi (1994, 1996) (Sadeghi et al., 2016; Tuller & Or, 2005a). The retention curves (see section 2) are empirical relationships, and the conductivity models are derived from substitution of the retention curve into a bundle of cylindrical capillaries (BCC) model. These empirical SHFs are commonly parametrized via nonlinear regression analysis of measured h-θ and K-θ data for a soil of interest.

Several studies conducted within the past few decades have provided evidence that in addition to capillary forces, adsorptive surface forces significantly impact the matric potential, especially in fine-textured soils with high specific surface areas (Lebeau & Konrad, 2010; Peters & Durner, 2008; Tuller et al., 1999; Tuller & Or, 2005b).

Direct measurements of SHPs mostly rely on inversion of Darcy's law for steady state conditions or an approximate analytical or numerical solution of RE for transient conditions. Therefore, these methods are limited to the so-called "Darcy scale," where the RE originates, such as the sample scale (Kool et al., 1985; Peters & Durner, 2008) or column scale (Sadeghi et al., 2014; Shao & Horton, 1998) in laboratory analyses and at the point scale (Simunek & van Genuchten, 1996) and block/plot scale (Hillel et al., 1972) in field experiments. Hence, these methods are not optimal for large-scale modeling of soil water flow, for example, at the satellite footprint scale. To tackle this problem, effective SHPs at the footprint scale have been recently investigated using RS techniques (Babaeian et al., 2016).

Most of the existing methods for RS-based estimation of SHPs rely on inverse modeling of RE or its extended forms in which footprint scale effective SHPs are solved such that model simulations best fit remotely sensed data. Camillo et al. (1986) were among the first to estimate soil hydraulic parameters (Brooks-Corey parameters) by inversion of an extended form of RE accounting for nonisothermal soil water flow and heat

transfer to fit microwave-based surface SM and soil temperature. They conducted a plot-scale experiment, where passive microwave data were acquired with a dual-polarized L-band radiometer mounted on a boom truck. Later, Ines and Mohanty (2008a, 2008b, 2009) developed Genetic-Algorithm-based inverse modeling and data assimilation methods for estimating footprint-scale effective values of the van Genuchten (1980) soil hydraulic parameters, incorporating time series data of airborne and satellite (e.g., AMSR-E) RS-based near-surface SM data. In a synthetic study, Montzka et al. (2011) explored the potential of using near-surface SM retrieved from different satellites to estimate SHPs (van Genuchten parameters) and SM profiles using the 1-D RE and a particle filtering data assimilation method. The inverse modeling approaches for estimation of SHPs using RS data have been thoroughly reviewed by Mohanty (2013).

Besides inverse modeling approaches, there exist a few studies on the potential of direct estimation of SHPs using RS data. Hollenbec et al. (1996) indicated that soil hydraulic heterogeneity could be identified by detection of relative changes in passive microwave RS observations. They concluded that the variogram of relative change indicates existence of an effective correlation length much larger than that commonly observed in ground-based soil surveys, and their findings encourage the use of passive microwave RS for assessing soil hydraulic characteristics that are valid at a scale appropriate for hydrometeorological models. Mattikalli et al. (1998) observed that temporal changes of airborne passive microwave (L-band) brightness temperature (a function of SM) held statistically significant negative lognormal relationships with saturated hydraulic conductivity (K_s). They showed that regression-based models could accurately relate the brightness temperature variations to K_s across large regions.

Limited literature exists on predicting SHPs based on hyperspectral optical imaging (Babaeian et al., 2015a). Such methods are mainly based on regression models between SHPs or parameters as target variables and various features of soil absorbance and reflectance spectra as explanatory variables. These regression-based predictive models were termed "spectrotransfer functions" or "spectral transfer functions", STFs, and spectral pedotransfer functions (analogous to "PTFs"; Babaeian, Homaee, Vereecken, et al., 2015; Santra et al., 2009). Studies of Santra et al. (2009), Babaeian, Homaee, Montzka, et al. (2015), and Babaeian, Homaee, Vereecken, et al. (2015)) are among a few in this category, relating soil reflectance at various optical wavelengths (400–2,500 nm) to K_s and van Genuchten hydraulic parameters. Although the STFs were developed using laboratory spectroscopy (i.e., a spectroradiometer), they are potentially promising for airborne and spaceborne hyperspectral remote sensors for SHPs estimation (see section 5.1.2). Recently, Babaeian et al. (2016) used coarse-scale STFs and Spectral Pedotransfer Functions (SPTFs) to provide coarse-scale estimates of the van Genuchten-Mualem hydraulic parameters. They evaluated the effective values of the hydraulic parameters and showed that the coarse-scale spectral transfer functions coupled with vadose zone flow modeling can be applied to predict profile SM dynamics at larger scales.

7.2.3. Scale Mismatch

Since the RE has been originally developed for the Darcy scale, which ranges from the representative elementary volume (REV) to the sample or column scale, application of RE to the RS footprint scale, i.e., from a few meters to hundreds of kilometers, may lead to physically unrealistic results. When solving RE in order to simulate $\theta(z,t)$, h should be translated as θ. As mentioned above, this is accomplished through the application of the soil water retention curve, which is valid for hydrostatic conditions (i.e., no flow). This means that a "local equilibrium" between water content and water potential is assumed when solving RE (Vogel & Ippisch, 2008). The equilibrium (stationary) condition is not always guaranteed, for example, when solving the RE numerically in a coarsely discretized domain. Therefore, allocation of more computational resources to solve the RE for finer spatial grids is often required not only to avoid numerical errors but also to satisfy the local equilibrium assumption (Roth, 2008). Failure to satisfy this essential requirement is not only due to the numerical discretization issue but also may occur at the scale of the REV. Roth (2008) argued that "violation of the stationary assumption at the scale of the REV leads to a fundamental failure of the Richards' equation that cannot be amended." This condition is observed, for example, with infiltration instabilities that lead to localized flow processes.

Several studies addressed the much debated question: "Do the underlying physics in the RE formulation apply at large scales of practical interest?" (Or et al., 2015). Several authors (Or et al., 2015; Roth, 2008; Vogel & Ippisch, 2008) argued that, due to the underlying assumption of local equilibrium, there exists an upper limit of spatial discretization (δ) above which the solution is expected to be biased. By equating

diffusive and convective water flows, Vogel and Ippisch (2008) analytically derived an upper limit for δ. Their solution showed δ ranges from a few centimeters to a few meters depending on the SHPs (smaller δ for coarser soils) and the total water potential gradient (smaller δ for larger gradients). For large-scale hydrologic applications, Or et al. (2015) also indicated that the spatial extent of lateral flow interactions under most natural capillary gradients rarely exceed a few meters. Despite this fact, the RE has been widely applied at the footprint scale as discussed above. For such applications the spatial discretization of the numerical solution of the RE is limited to the remote sensor's spatial resolution (e.g., from 10 m for optical Sentinel-2 to about 40 km for microwave SMOS and SMAP). This scale mismatch should be considered as an unavoidable source of error in numerical models linking surface SM and RZSM (Entekhabi et al., 1994; Han et al., 2012a; Heathman et al., 2003).

Due to inherent spatial variability of soil properties, application of the RE at large scales is accompanied with upscaling SHPs from point to footprint scale. Two general approaches for upscaling SHPs are commonly applied: (1) forward upscaling and (2) inverse upscaling (i.e., inverse modeling; Vereecken et al., 2007). Forward upscaling methods directly calculate large-scale properties from small-scale properties. Various theories exist for forward upscaling of SHPs such as simple averaging (Zhu & Mohanty, 2006), percolation theory (Hunt & Idriss, 2009; Samouelian et al., 2007), homogenization theory (Neuweiler & Cirpka, 2005; Neuweiler & Vogel, 2007), hybrid mixture theory (Hassanizadeh & Gray, 1979), similar/dissimilar media scaling theory (Miller & Miller, 1956; Sadeghi et al., 2012; Warrick et al., 1977), stochastic methods (Yeh et al., 1985; Zhang & Lu, 2002), and renormalization methods (King & Neuweiler, 2002; Saucier, 1992). Forward upscaling requires detailed information of SHPs at small scales, and hence, is not appropriate for RS applications. As discussed above, a common approach to incorporate RS data for effective SHP estimation is inverse modeling, where SHFs are parametrized to match the RE solution with RS-based observations at large scales. This strategy may alleviate the scale mismatch issue discussed above, as it basically calibrates RE so that it fits large scale observations. However, calibration of RE in hydrological models with insufficiently fine discretization will likely result in parameter values that are physically unrealistic (Downer & Ogden, 2004). Here the effective parameters also appear to be dependent on the type of boundary condition (Vereecken et al., 2007). In other words, the parameters may not work under boundary conditions different from those applied during calibration.

8. Spatial and Temporal Variability of SM

The high variability of SM in space and time is well documented (Crow et al., 2012; Famiglietti et al., 2008; Vereecken et al., 2014) and to a certain extent the cause for the large variability of SM estimates obtained with the various sensing methods discussed above. The surface soil layer generally exhibits the largest SM variability, due to the interaction of environmental (soil properties, topography, and vegetation), meteorological (precipitation and temperature), and human factors, which decrease with soil depth. The magnitude of the variabilities depends on the extent of scale (see section 2.2) as it first increases with increasing extent and then when reaching a threshold remains constant (Brocca, Tullo, et al., 2012). The relationship between mean SM and the standard deviation of SM has been considered as an important aspect when analyzing the spatial variability of SM (Brocca, Melone, Moramarco, & Morbidelli 2010; Famiglietti et al., 2008). Figure 25 depicts an example of this relationship for surface SM (0–5 cm) from SMAP L4 data (April 2015 to May 2017) from the Tonzi Ranch site in California for an area about 2,000 km^2. In particular, a convex upward relationship can be identified between mean and standard deviation of surface SM (Brocca, Melone, Moramarco, & Morbidelli, 2010; Western et al., 2004) when the data set covers the whole range from dry to wet conditions. Crow et al. (2012) reviewed different techniques for spatial upscaling of SM and discussed the upscaling problem and measurement density requirements for ground SM networks. While this relationship describes spatial SM variability, it does not provide information about temporal variability. Thus, the question is how can both spatial and temporal variabilities be quantified and made comparable between different data sets?

In contrast to methods only describing variability in the spatial domain, for example, geostatistics (Haining et al., 2010), or only in the temporal domain, for example, time series analysis (Fu, 2011; Sprott, 2003), there exist several methods that simultaneously analyze both space and time domains. Especially for SM, the combined analysis of spatial and temporal patterns of observations is important to understand their origin. Several methods have been proposed for analysis of the spatiotemporal SM variability, including
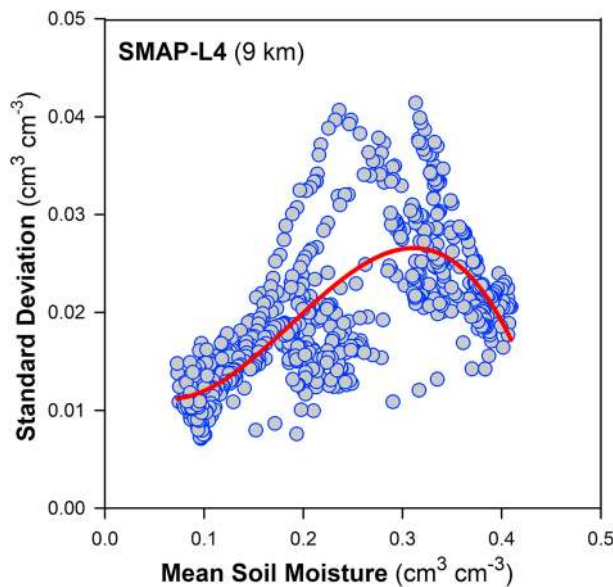
Figure 25. Relationship between mean surface soil moisture and standard deviation for SMAP L4 data for the 2,000-km^2 Tonzi Ranch site in California. The red line represents a fitted third-order polynomial function. SMAP = Soil Moisture Active Passive.

Temporal Stability Analysis (TSA; Martinez-Fernandez & Ceballos, 2005), TC (Crow et al., 2015; Gruber et al., 2017), and Empirical Orthogonal Functions (EOFs; Yoo & Kim, 2004). In this section we discuss EOF and TSA as new methods available for understanding spatiotemporal variability of SM.

8.1. EOFs

EOF analysis, which is also known as principal component analysis (PCA), decomposes the observed variability of a data set into a set of orthogonal spatial patterns and a set of multivariate time series called expansion coefficients (Korres et al., 2010). With this separation, EOFs can be used to identify the dominant processes and essential parameters controlling spatiotemporal SM patterns (Korres et al., 2010). A temporal sequence of spatial variables is expressed as a result of the superposition of two or more temporally stable spatial structures. The spatial distribution of the variable at a specific point in time is then defined as a weighted average of those patterns, where the weights vary with time. The first EOF loadings (also called the eigenvectors) typically contain the dominant fractions of the spatiotemporal variability, whereas the last EOF loadings contain the residual variance classified as observation uncertainty or more generally as noise. Therefore, the approach can be used to efficiently extract information from observed data and to describe hydrological behavior in heterogeneous systems in a quantitative way (Hohenbrink & Lischeid, 2015). For more details see Hannachi et al. (2007).

Typical applications for SM datasets mainly include an analysis of the origins of spatiotemporal patterns. Korres et al. (2010) related patterns of field-scale SM measurements to soil properties and topography. They applied EOF analysis and indicated that soil properties and topography control the spatiotemporal patterns of SM. Perry and Niemann (2008) analyzed the TARRAWARRA data set (Western & Grayson, 1998) and found a primary pattern association with soil water lateral redistribution. The second factor that was found to impact SM distribution patterns was solar radiation, which differentially insolated the surface due to topography. Moreover, they decomposed the data set into EOFs, interpolated the EOFs using a standard interpolation method, and used the interpolated EOFs to reconstruct the fine-scale SM patterns in time. This method outperformed the standard interpolation methods. Kim and Barros (2002) and Jawson and Niemann (2007) explained the relationship between the spatial structure of estimated SM and that of ancillary data including topography, soil texture, and vegetation cover with an EOF analysis. Joshi and Mohanty (2010) quantified the contribution of soil texture to SM variability from the watershed to regional scales, as microwave remotely sensed SM is retrieved with dielectric mixing models such as that from Wang and Schmugge (1980) that, in part, is based on the dominant soil texture within the measurement footprint.

In addition to topography and soil properties, Qiu et al. (2014) also analyzed the role of precipitation on SM variability at different spatial scales. They were able to quantify the influence of rainfall variability on SM being small at watershed scales and larger at regional and national scales (e.g., China). This is because large-scale SM distribution is more closely related to atmospheric forcing processes. Nied et al. (2013) reduced the dimensionality of their SM data set to identify the main driving patterns of flood initiation. The EOF analysis of Fang et al. (2015) of simulated and observed SM revealed that introduction of heterogeneity in soil porosity effectively improved estimates of SM patterns. In the same region, Koch et al. (2016) and Graf et al. (2014) conducted an EOF analysis on SM data and clustered the resulting loadings to separate wet and dry periods. This classification was further used to assess the seasonality of the SM patterns.

Fan and Dool (2004) showed the dominance of El Niño–Southern Oscillation in the first EOF of global long-term SM simulations. Bauer-Marschallinger et al. (2013) performed a similar study for Australia. Schubert et al. (2004) found the causes of long-term drought in the U.S. Great Plains in the El Niño–Southern Oscillation and pan-Pacific sea surface temperature anomalies. Wang et al. (2015) found correlations of

the Palmer Drought Severity Index in China with the Northern Hemisphere polar vortex, the Arctic Oscillation, and the North Atlantic Oscillation. Tatli and Turkes (2011) analyzed different drought indices with and without SM information in an EOF analysis to identify the most suitable index for drought characterization in Turkey. EOFs are also used in downscaling approaches; for example, Busch et al. (2012) developed a topography-related downscaling algorithm, where the associated expansion coefficients are estimated on the basis of the spatial average SM.

8.2. TSA of Spatial Structures

In contrast to EOFs, TSA assumes that there exists a single spatial pattern that manifests itself at all times as spatial distributions of soil vegetation atmosphere transfer variables. TSA is considered to be a valuable tool for identifying a small number of representative sampling points to estimate the grid mean SM. It temporally averages the relative differences of the observations at a specific location to the spatial mean of all observations at a specific point in time (Vachaud et al., 1985). Each observation point is then ranked from dry to wet locations, which describes the spatial pattern. Currently, the use of the mean relative difference is the most common way to characterize the temporal stability (Vanderlinden et al., 2012). TSA of SM has been reported for various spatial scales (Brocca, Melone, Moramarco, & Morbidelli, 2010; Mohanty & Skaggs, 2001) from subfield (Abdu et al., 2017; Pachepsky et al., 2005) to regional (Brocca, Tullo, et al., 2012, Cho & Choi, 2014; Martínez-Fernández & Ceballos, 2003) to global scales (Rötzer et al., 2015). The applications of TSA are versatile, because the description of relative spatial SM patterns can be used for multiple purposes. For example, the site rankings can also be used to reduce the number of observation points in an area of interest by keeping the majority of the information about the spatiotemporal variability. So-called "catchment average SM monitoring" sites were proposed for such locations at the watershed scale, which are able to represent the spatial mean SM (Western et al., 1998). Applications of the monitoring site reduction or representative areal mean estimation can be found in Martinez et al. (2008), Schneider et al. (2008), Thierfelder et al. (2003), Zhao et al. (2013), and Zucco et al. (2014). This concept has interesting applications for upscaling and downscaling approaches for satellite RS SM validation (Dumedah et al., 2013; Molero et al., 2018; Vanderlinden et al., 2012). Rötzer et al. (2014) used the TSA method to validate remotely sensed SM products from SMOS and ASCAT in a relative way, focusing on the spatial patterns of SM. Also, Bhatti et al. (2013) and Cosh et al. (2006) used TSA for satellite SM validation. Zhang et al. (2016) analyzed the SM regimes under different land covers using TSA. It was determined that vegetation is able to introduce patterns in the spatial distribution of SM (Wang et al., 2015). Lin (2006) reported that the high spatial variability of SM in a catchment is largely a result of soil type and landform controls rather than a random process. In other regions temporally stable SM patterns can be directly attributed to relatively high clay contents (Gao et al., 2011). Ran et al. (2017) examined the capability of TSA for irrigated agricultural landscapes and indicated that irrigation practices reduce the accuracy of the representative sampling error at the 1 and 5 km scales. They introduced a stratified TSA that mitigates systematic and random errors by combining previous information through stratification, which is important for validation of remotely sensed SM. Several SM TSA results focus on SHPs (Cosh et al., 2008; Lin et al., 2016). But in hilly areas the contribution of topography to spatial structures in SM increases (Brocca et al., 2009). The higher the mountains, the larger is the effect of snow distribution on SM patterns (Williams et al., 2009). At larger scales, meteorological factors increase their impact (Cho & Choi, 2014). In addition to SM, matric potential has also been studied with more direct insights on the detailed soil characteristics and controls of spatial variability and temporal stability (Yu et al., 2015).

8.3. TC Analysis

TC analysis was initially developed for ocean wind studies (Stofflen, 1998), but it is also used in land surface hydrology (Chen et al., 2017; Yilmaz & Crow, 2014). TC relies on a linear error model to reduce the error from an approximated linear relationship between different measurements of a geophysical variable. The metrics that are typically used to assess the error of each data set are the variance of its errors and the correlation with the true SM (Chen et al., 2016; Gruber et al., 2016). TC has been applied in the context of calibration, validation, bias correction, and error characterization to allow comparisons of diverse data records from measurement and estimation techniques such as in situ SM and RS/modeled SM. In a study by Chen et al. (2017), TC analysis was used for real validation of the SMAP L2 SM product at five core

validation sites in the United States and it was found that TC can solve the impact of random representativeness errors in the point-scale data against footprint-scale SM estimates and provide an unbiased estimation of the satellite versus ground correlation metric. TC and other error estimation methods only provide an estimation of the total observation error variance that is the summation of the autocorrelated and the white observation error. This can lead to inaccurate results in SM data analysis at time scales that are shorter than the autocorrelation length of the errors. Some advances have been made in TC analysis. Dong and Crow (2017) proposed a more generalized TC algorithm, which decomposes total errors provided by TC into its autocorrelated and white error components, helpful for the ESA CCI SM data set and additionally for hydrology and climatology studies that require decomposed error information. Recently, Molero et al. (2018) evaluated the spatiotemporal representativeness degree of in situ SM within the satellite footprint in Little Washita (U.S.) and Yanco (Australia) at timescales from 0.5 to 128 days. They proposed a new approach called Wavelet-based Correlation (WCor) and concluded that in contrast to the TC method, which performs well at the week and month scales, WCor provides consistent results at all time scales and is a robust method for sparse SM networks. An overview of implementations of SM TC analysis has been presented in Gruber et al. (2016).

9. Application of SM Information and Outlook

There are numerous Earth and environmental sciences disciplines and applications benefitting from detailed SM information (Figure 26). For example, knowledge of the SM status and its spatial and temporal variability is key for forecasting weather and climate, modeling hydrological processes, predicting and monitoring of extreme natural events (e.g., droughts, fires, and dust storms), managing water resources, agricultural plant production and productivity, and for sustaining ecosystem services (Vereecken et al., 2016). A brief discussion of SM information applications follows.

9.1. Weather Forecasting and Hydrological Modeling

The SM status governs water and energy exchange processes between the land surface and the atmosphere. When soils are moist, the major portion of the net radiation is utilized for evapotranspiration (i.e., latent heat flux), which leads to uplift of water vapor and cloud formation when the air temperature falls below the dew point temperature. In dry soils, on the other hand, more energy is invested in sensitive heat exchange, which reduces the atmospheric vapor pressure and cloud cover. Knowledge of the spatial and temporal SM variability aids in constraining the lower boundary conditions in atmospheric simulations. SM information can be applied for accuracy improvement of rainfall estimations via a bottom-up approach (Koster et al., 2016Koster et al., 2018). Pellarin et al. (2008) was among the first to estimate precipitation occurrence from AMSR-E surface SM observations in West Africa. Brocca et al. (2014) assumed that if soil is considered as a natural rain gauge, then rainfall can be successfully estimated from SM observations (i.e., ground based or satellite based) with the SM2RAIN model that inverts the soil water balance equation. SM data have been extensively used for validation of numerical weather prediction models (Cui et al., 2009; Drusch, 2007). Specifically, the impact of SM on high temperature weather and heatwave events has been well documented (Fischer et al., 2007; Lau & Kim, 2012; Zeng et al., 2014). For instance, Fischer et al. (2007) indicated that during a heatwave, the SM is extremely low, which greatly increases the surface temperature and substantially reduces the latent heat flux. This confirms the key role of SM as a lower boundary in the partitioning of net radiation into latent and sensible heat fluxes and the evolution of the heatwave (Miralles et al., 2014). Incorrect estimation of SM leads to erroneous simulations of the surface layer evolution and hence precipitation and cloud cover forecasts could consequently be affected. Collow et al. (2014) examined the impact of SM on precipitation, temperature, and humidity and pointed out that accurate initialization of SM in numerical weather forecasting models could improve temperature, humidity, and precipitation forecasts for the U. S. Great Plains.

As already discussed, SM is a key state variable and of crucial importance for hydrological modeling. Ground and satellite SM products have been connected to hydrological models for prediction of hydrological fluxes. However, the effective application of SM information for such modeling efforts is still in an infancy state. Vereecken et al. (2015) discussed the value of SM information from a global hydrological observatory network for identifying soil hydrological processes. Recently, Sadeghi et al. (2019) proposed an analytical model based on RE for estimation of the net water flux (precipitation minus evapotranspiration) from near-surface
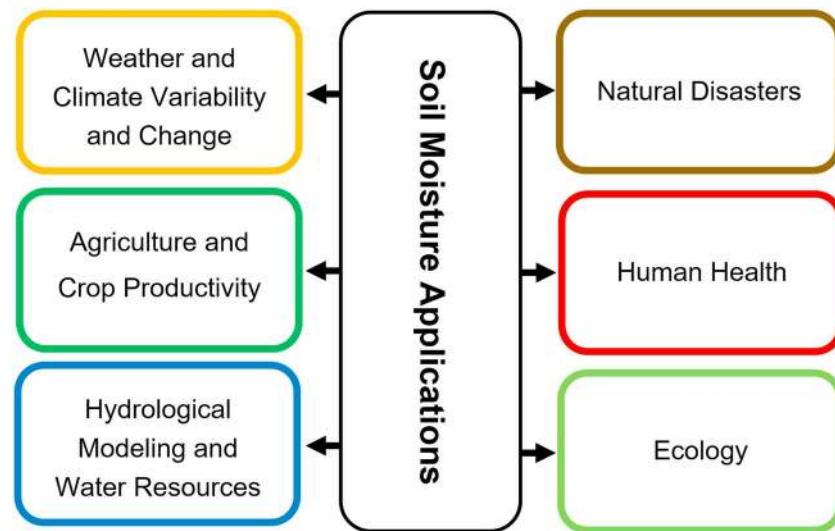
Figure 26. Importance of SM information for various disciplines and applications.

SM observations for different soil and vegetation conditions. Recent applications of SM data for hydrological modeling have focused on joint assimilation of remotely sensed SM products and streamflow data into distributed hydrologic models to provide more accurate estimations of SM (Lievens et al., 2016 & 2017; Verhoest et al., 2015). Yan and Moradkhani (2016) used a particle filter Markov chain Monte Carlo method to assimilate synthetic ASCAT SM retrievals and synthetic streamflow data into a fully distributed Sacramento SM Accounting model for the Salt River Watershed in Arizona. They revealed that solely assimilating outlet streamflow leads to biased SM estimates, whereas joint assimilation of streamflow and SM products provides better predictions of surface SM. Lievens et al. (2015) coupled SMOS L3 SM data in the Variable Infiltration Capacity land surface model using Ensemble Kalman Filter data assimilation to improve modeled SM and streamflow prediction accuracies with high spatial resolution in Australia. They showed that assimilation with SMOS SM reduces modeled SM RMSE from 0.058 to 0.046 cm^3/cm^3 and enhances correlation from 0.56 to 0.71, which demonstrates the merit of SMOS data assimilation for streamflow predictions at large scale. Crow et al. (2017) validated the claim of improvement of operational hydrologic forecasting through RS SM products and concluded that SMAP L4, which is the product of L-band microwave radiometry and a data assimilation technique, provides a SM product with the highest hydrologic forecasting skill observed to date for forecasting streamflow response to future rainfall events. More recently, Crow et al. (2018) used SMAP L4 surface and root-zone SM in combination with remotely sensed precipitation and streamflow observations and explored the relationship between prestorm SM and rainfall infiltration in the south central United States. They found that land surface models generally underestimate the correlation strength between prestorm SM and storm runoff.

Mahanama et al. (2008) examined the contribution of SM to streamflow initialization during subseasonal and seasonal periods and pointed out that accurate SM data can contribute between 10% and 60% of the total streamflow prediction accuracy that can potentially be obtained for perfect predictions of meteorological forcing. Soil profile moisture measurements (10, 20, and 40 cm) along with rainfall data as inputs of a generalized regression neural network model significantly improved runoff prediction accuracy for the Tiber River in Italy (Tayfur et al., 2014).

Data from WSMN or spatiotemporal information of SM are increasingly being used to validate hydrological models (Fang et al., 2015; Koch et al., 2016; Wang et al., 2015) and to improve our understanding of hydrological processes. Koch et al. (2016) compared the performances of the Hydro-Geosphere (HGS) model, the European Hydrological System Model (MIKE SHE), and the ParFlow-CLM model for prediction of SM status, discharge, and cumulative water balance components. All three models performed well-predicting discharge and the water balance components but diverged in their predictions of SM status. A comprehensive review of hydrological applications of radar SM retrievals is also provided by Kornelsen and Coulibaly (2013).

9.2. Agriculture and Crop Productivity

Information about the SM status is crucial for agricultural applications to, for example, identify field traffic-ability for heavy farm machinery or to make informed irrigation management decisions. Global scale SM data assimilation can improve the representation of agricultural drought (Bolten & Crow et al., 2012). While various factors, such as temperature stress and nutrient availability, impact the growth and persistence of plants, much of the initial focus has been on those crop systems that are water controlled (Laio et al., 2001; Ridolfi et al., 2000; Rodriguez-Iturbe et al., 1999). The dynamics of SM has a significant impact on plant stress and the adaptability of various plant species to particular climate and soil conditions. Monitoring the amount of moisture retained in soil is critical for a healthy rhizosphere growth environment and aids with crop yield forecasts and irrigation planning. Early assessment of SM reserves and monitoring the change in plant available soil water, for example, with RS techniques, assist crop growers with risk reduction strategies. McNairn et al. (2012) argued that the Canadian RADARSAT-2 satellite can provide accurate estimates of field scale SM, which has been further advanced with the launch of the ESA Sentinel satellites as part of the Copernicus program. Continuous information of SM status can be used in crop growth models in combination with data assimilation approaches to provide growers with crop water demand estimates for precision irrigation management (Ines et al., 2013). Han et al. (2016) showed that the assimilation of continuous SM data from cosmic ray neutron observations into the CLM can be used for real-time irrigation scheduling for citrus trees. Recently, Andreasen et al. (2017) demonstrated the potential of using mobile cosmic ray neutron detection to support precision farming. Louvet et al. (2015) used SMOS L3 SM data in conjunction with the TRMM satellite-based precipitation product (TMPA) with 3-hr time resolution in West Africa and produced a NRT SM product with good accuracy (RMSE 0.030–0.044 cm^3/cm^3) for potential applications in agriculture and for drought detection. Escorihuela et al. (2018) showed that the use of SMOS SM in synergy with Sentinel-1 SM provides high spatial resolution SM maps with high accuracy (RMSE less than 0.040 cm^3/cm^3) applicable for the national and global desert early warning systems.

9.3. Natural Disasters

SM is a key variable for operational flood forecasts (Komma et al., 2008; Silvestro & Rebora, 2014; Wanders et al., 2014), characterization of landslide occurrence (Baum et al., 2010; Krzeminska et al., 2012) and for monitoring drought conditions (Chakrabarti et al., 2014; Scaini et al., 2015).

9.3.1. Landslides and SM

The ability to predict the spatial and temporal occurrence of rainfall-triggered shallow landslides is of crucial importance for prevention of human life and property losses. SM data are applied in conjunction with precipitation forcing as inputs for landslide models to obtain real-time assessment and forecasting of landslide occurrence (Posner & Georgakakos, 2015; Ray & Jacobs, 2007). SM plays a critical role for slope stability, that is, as SM increases, slope stability decreases. Landslides commonly occur when SM is high. As soil saturation increases the pore water pressure increases and once the pressure exceeds the cohesive soil strengths, landslides are triggered. Coe et al. (2003) demonstrated that there is a positive correlation between SM content and landslide velocity, with velocities being highest during high SM conditions.

Remotely sensed SM data have been used to forecast landslides. For example, Brocca, Ponziani, et al. (2012) used the SWI provided by the ASCAT satellite in conjunction with the antecedent precipitation index (API) to improve the accuracy of landslide forecasting models in central Italy. Ray et al. (2010) used AMSR-E SM products as input information for a dynamic physically based slope stability model to generate landslide susceptibility maps. SM observations have been also used in landslide prediction models. Recently, Segoni et al. (2018) demonstrated that SM threshold values can be defined to better predict landslides and improve the performance of regional scale landslide early warning systems in Italy.

9.3.2. Floods and SM

Measurement and mapping of SM can potentially improve flood forecasting because initial SM conditions impact timing of flood initiation and peak runoff during storm events. The initial water content in conjunction with the infiltration capacity determines how much precipitation water can be added to the soil porous system before surface runoff (i.e., overland flow) and potential flooding occur. Silvestro and Rebora (2014) pointed out that the initial SM conditions substantially influence flood forecasting. They argued that the variability of flood forecasts is not constant and depends on the type and characteristics of the event and
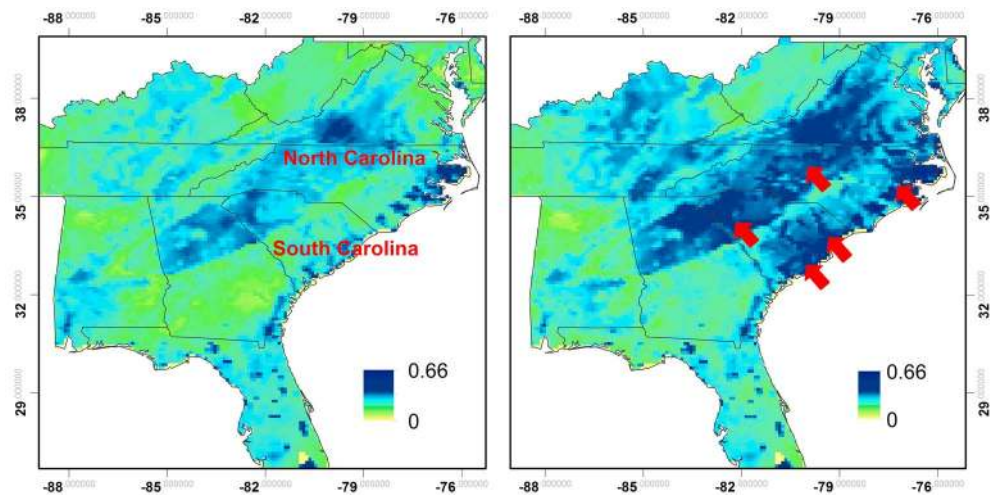
Figure 27. Surface soil moisture in North and South Carolina retrieved from the Soil Moisture Active Passive level-4 product on 2 September 2015 (before flooding, left) and on 5 October 2015 (after flooding, right). Large parts of North and South Carolina (red arrows) appear dark blue, representing the impact of heavy localized rains and flooding. Regions in darker blue indicate areas with saturated soil conditions and possibly standing water. Large-scale flooding was experienced all over South Carolina from 1 to 5 October 2015.

the initial SM conditions. Laiolo et al. (2016) used SM and LST to update the state variables of a physically based, distributed, and continuous hydrological model. They investigated the impact of SM and LST on the hydrological cycle and showed a general reduction of model discharge prediction errors by as much as 10%. Pauwels et al. (2001) assimilated European Remote Sensing Satellite ERS-1 and ERS-2 surface SM data into the TOPMODEL based Land-Atmosphere Transfer Scheme, which led to 20–50% reduction of discharge prediction errors for the Zwalm catchment in Belgium. Han et al. (2012b) demonstrated the potential for improved streamflow predictions through assimilation of in situ near-surface SM with the Soil Water Assessment Tools model. The assimilation significantly reduced RMSE values for streamflow predictions. Recently, high spatial and moderate temporal resolution SM from the ESA Sentinel-1 satellite has been assimilated into hydrological models for improving continuous streamflow simulations and enhancing flash flood predictions for civil protection applications in Italy (Cenci et al., 2017).

Remotely sensed SM observations have improved NRT flood forecasts for large catchments. Tekeli and Fouli (2017) argued that incorporating antecedent SM information with a CDF based threshold value derived from AMSR-E products can significantly reduce false flood warnings in Saudi Arabia. Wanders et al. (2014) evaluated the added value of assimilated remotely sensed SM for the European Flood Awareness System and its potential to improve the timing and height prediction of the flood peak and low flows. They found that when remotely sensed SM data were used, the timing errors of the flood predictions significantly decreased, especially for shorter lead times. In addition, imminent floods can be forecasted more precisely. Such capabilities can improve the response time of government agencies to provide emergency and disaster relief. An excellent example is the major flood events throughout North and South Carolina on 5 October 2015, where SM data from SMAP were able to clearly show areas of potential flooding and the extent of flooding prior to the event (see Figure 27).

9.3.3. Drought and SM

Another increasingly important application of remotely sensed SM information is to monitor global drought conditions. There are four main drought categories that include meteorological, agricultural or agro-ecological, hydrological, and socioeconomic droughts (Dracup et al., 1980; Wilhite & Glantz, 1985). Meteorological drought is defined based on the number of days with precipitation below a specific threshold. Hydrological drought is commonly associated with effects of precipitation shortfalls on surface or subsurface water resources. The frequency and severity of hydrological drought are often defined for the watershed or basin scales. The definition of agricultural drought is based on soil water deficiency and its effect on crop production, that is, when evapotranspirative losses exceed the plant available SM content. Finally, socioeconomic drought occurs when the overall water demand exceeds supply.

SM is a direct determinant of agricultural drought conditions that are commonly preceded by meteorological drought and succeeded by hydrological drought. Despite the obvious importance of SM, classical drought monitoring indices such as the Palmer Drought Severity Index neglect SM. Several in situ SM-based drought indicators have been recommended for agricultural drought monitoring, including the SM index (Sridhar et al., 2008), soil water deficit (Torres-Ruiz et al., 2013), and plant available water (PAW; McPherson et al., 2007). These indices identify drought conditions based on water deficit and plant available soil water. A major benefit of SM-based drought indices when compared to precipitation-based indices is that SM not only characterizes drought events but also responds to both precipitation and evapotranspiration processes. Detailed discussions about SM drought indices are provided in Ochsner et al. (2013) and Torres et al. (2013).

More recently, several studies have attempted to improve potential applicability of SM indices for drought monitoring. For example, Cammalleri et al. (2016) proposed a novel Drought Severity Index for detecting main drought events and estimating both the extent and magnitude of drought. The index is based on a multiplicative combination of the observed soil water deficit intensity and on the rarity of the event compared with that of the site history (frequency of drought), in order to obtain a single measure of the severity of a specific soil water status in terms of drought. The DSI varies between 0 (no drought) and 1 (extreme drought), where the values between 0 and 1 can represent slight, moderate, and severe drought conditions. The applicability of the DSI has been evaluated for vegetated lands in Europe for the time period from 1995 to 2012, yielding better results for a broad range of conditions than commonly applied drought indices (Cammalleri et al., 2016).

Sohrabi et al. (2015) proposed a new SM drought index (SODI) that considers temporal variations in precipitation, temperature, potential evapotranspiration, run-off and SM to determine onset, continuation, and cessation of droughts. The SODI is based on available water capacity and SM deviation from estimated field capacity (θ_{FC}). This time-dependent drought index combines advantages of other drought indices by characterizing soil water retention processes and determining dry and wet conditions in subsequent time steps. The SODI yielded better results for quantifying severe droughts associated with climate variability than precipitation-based indices. The advantage of SODI is that the index is, in fact, a time-dependent and continuous index that characterizes SM dynamics during time transitions from the current time step to the next.

Although SM is a key indicator for agricultural drought assessment, less attention has been paid to the application of in situ SM networks for systematic drought monitoring. This may be due to the fact that these networks commonly measure absolute values of SM and do not provide SM in terms of PAW. Within this context, the Oklahoma Mesonet (McPherson et al., 2007) is an exception, providing average daily PAW maps at three different soil depths (i.e., 10, 40 and 80 cm), which are publicly available from www.mesonet.org. It should be noted that the Mesonet does not directly measure SM; instead, a heat pulse measurement is used to infer soil matric potential, which is related to SM using water retention calibration data. Recently, Ford et al. (2015) used the in situ SM data from 45 Mesonet stations for early drought warning in Oklahoma and concluded that Mesonet observations are an important source of information for early warning of flash drought events in the Southern Great Plains of the United States.

SM-based drought indices have been also developed based on remotely sensed information (Babaeian et al., 2018; Scaini et al., 2015) and land surface models (Mo & Lettenmaier, 2014). Because the number of ground SM stations and networks is limited (see section 6.1), remotely sensed SM information has great potential for continuous SM and drought monitoring. Chakrabarti et al. (2014) demonstrated that assimilation of downscaled (km) SMOS SM estimates into the decision support system for the agro-technology transfer (DSSAT) crop growth model can be used to analyze the impact of agricultural drought on crop yields. Recently, Babaeian et al. (2018) analyzed optical satellite SM retrievals for a range of climate, land cover and soil conditions for potential monitoring of agricultural drought in the United States. They compared the OPTRAM-based Soil Water Deficit Index with the widely applied Crop Moisture Index (CMI) and saw similar patterns between these two indices and concluded that OPTRAM-based Soil Water Deficit Index can potentially be applied for agricultural drought monitoring. However, to date there are no operational agricultural drought monitoring systems that rely on remotely sensed SM. Recently, a new SMOS L3 SM-based drought index product has been introduced by Al Bitar et al. (2013) for global monitoring of drought and is available from ftp://ftp.ifremer.fr/Land_products.
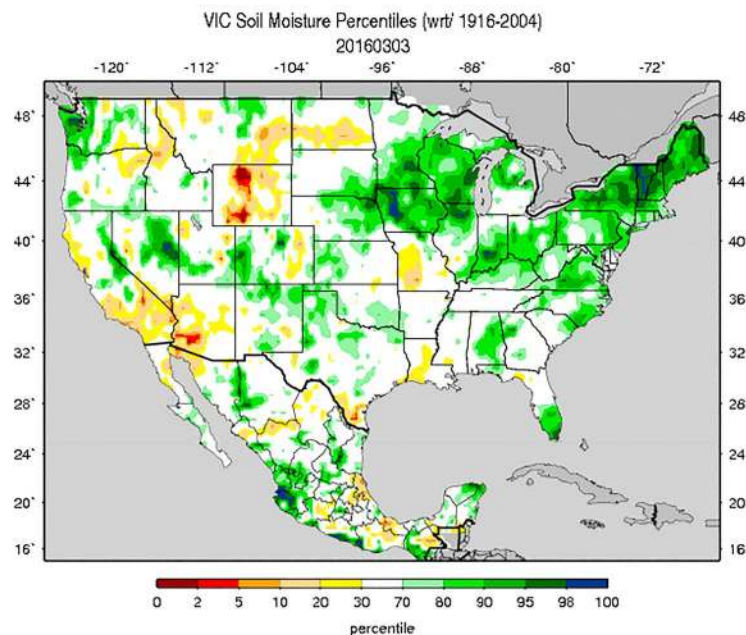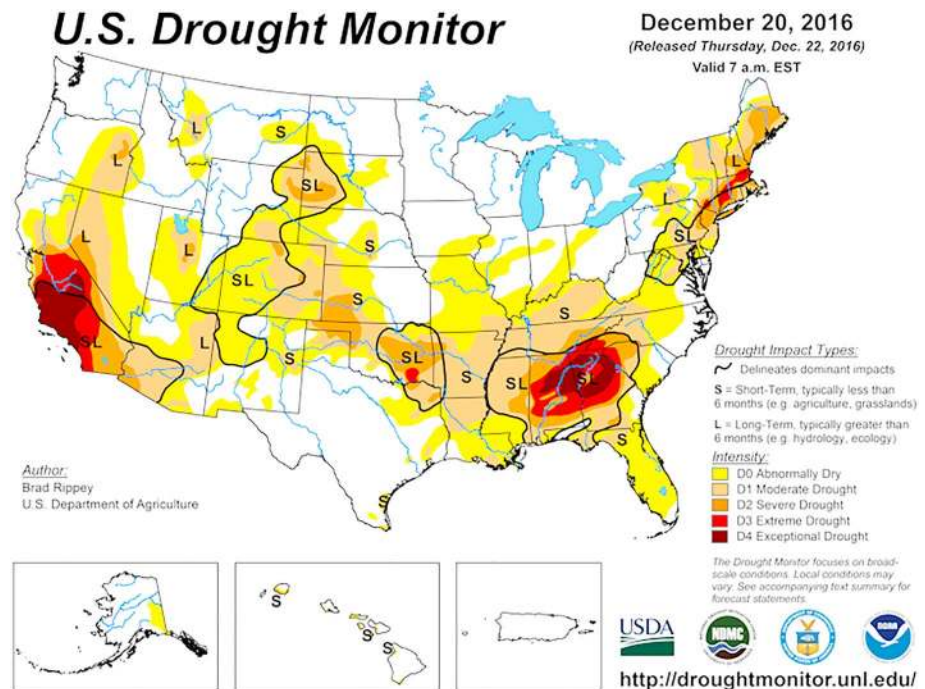
Figure 28. U.S. Drought Monitor map for 20 December 2016 (top) and the soil moisture percentile with respect to the 1916–2004 climatological period (bottom) estimated with the Community Land Model for 22 December 2016. (http://droughtmonitor.unl.edu; http://www.hydro.washington.edu/forecast/monitor).

Real-time drought monitoring systems are crucial for early warning and adaptive management of negative environmental drought impacts. A real-time monitoring system, the U.S. Drought Monitor (USDM), has been established by the National Drought Mitigation Center and is accessible via www.droughtmonitor. unl.edu (Figure 28, top). The USDM depicts drought integrated across all time scales and differentiates between agricultural and hydrological impacts. It is based on measurements of climatic, hydrologic, and soil conditions as well as reported impacts and observations from more than 350 contributors around the United States. There is a substantial correspondence between the USDM map and SM percentile map obtained from

the CLM, which simulates surface water for the continental United States (Figure 28, bottom). SMAP SM is a potential input data source used by the U.S. Drought Monitor (Eswar et al., 2018).

10. Summary

State-of-the-art SM measurement, monitoring, and modeling capabilities were reviewed with the aim of extending the use of increasingly available RS data and to identify critical future research needs and directions. The latest ground, proximal, and satellite RS techniques; databases; and modeling approaches that have been developed in recent years to characterize surface, near-surface and root-zone SM for a wide range of spatial and temporal resolutions have been discussed. The main conclusions, challenges, and opportunities can be summarized as follows:

1. SM networks and spatiotemporal SM data are increasingly applied to validate satellite RS observations. Information from these networks is also utilized to characterize spatial SM dynamics, validate hydrological models, identify trends in the hydrological cycle, identify needs yet to be developed, and improve our understanding of hydrological processes. The problem with validation tests of coarse-scale SM products are mainly due to disconnects between the sensing depth of ground and remote sensors and the scaling disparity (support or measurement volume) between in situ measurements and satellite sensor resolution. Antecedent and precise calibration of in situ sensors is crucial for reliable validation of remotely sensed SM estimates. Validation methods for these tests need to be further refined and standardized with due accounting for these scale mismatches that affect reliable validation. Along with the advancement of more reliable sensors and data acquisition systems, the number of in situ SM networks continues to increase. Because most of these networks have evolved without international standardization, they present challenges to the validation of satellite-based SM estimation and are not always representative of the larger surrounding area.

2. The utilization of RS data within the optical and thermal bands with shallow measurement depth for surface and near-surface SM retrieval is sometimes restricted by atmospheric conditions (clouds and water vapor), causing uncertainty in relating soil reflectance/temperature to SM. On the other hand, most of the methods that use spectral/thermal data are, in principal, empirical models, which suffer from the associated limitations of site specificity. Advances are needed for deriving physically based models for SM retrieval from high spatial/temporal resolution optical/thermal RS data.

3. The applicability of RS techniques reviewed in this paper is dependent on the scale (spatial and temporal) of interest and availability of data; hence, no single method can be suggested as a universal solution. While the combined use of active and passive microwave products may improve the resulting SM retrieval accuracy, it certainly improves the spatial resolution. Proximal RS methods and their combinations can potentially be used for mapping and monitoring SM variability at intermediate scales as well as for validating microwave RS SM products using field surveys. Improving, testing, and integrating new monitoring techniques able to provide SM measurements at intermediate scales like COSMOS, GPS, and EMI are potential new topics for future research. Because of the loss of the SMAP radar, there is a need for planning of a follow-on mission for providing SM with higher spatiotemporal resolution.SM spatial variability affects the accuracy of SM estimations from satellite remote sensors. Modeling and simulating SM spatial variability are important to improve validation of coarse-scale SM products. SM variability is associated not only with soil properties but also with the distribution and intensity of rainfall across the land surface and the heterogeneity of the vegetation cover. Within this context, SM data may be used for estimating rainfall by considering the soil as a natural rain gauge. SM estimates can also be integrated into hydrological models to estimate total water losses and gains, accounting for factors such as runoff, drainage, and ground-water recharge.

4. SM is a key indicator for agricultural drought assessment, but little attention has been paid to the application of in situ networks and RS products for systematic drought monitoring. This may be due to the fact that these networks and products only measure absolute values of SM and do not provide SM in terms of PAW, which is a real representation of plant water stress. In this context, integration of remotely sensed SM products with SHPs provides unique opportunities to determine PAW and enhance drought monitoring. Integration of remotely sensed SM products and soil profile data (PAW) will provide invaluable information for better characterizing and monitoring of agricultural drought. Information about root-zone SM is critical for crop producers as it aids with irrigation and drought management in dryland

agricultural. An increase in spatial and temporal resolution of SM satellite data can be expected in future, which will provide new opportunities for precision management of individual fields. This will be beneficial where installation of SM sensors and UAV observations are not feasible.

5. It is necessary to improve SM retrieval accuracy over densely vegetated regions through development of new algorithms that precisely incorporate vegetation optical depth.

6. A remaining grand RS challenge is the accurate estimation of root-zone SM from the SM content within the first few centimeters of the soil profile. The most commonly applied technique for retrieving root-zone SM from satellite RS is assimilation of near-surface SM measurements into, for example, land surface or crop growth models. Further information such as groundwater table depth, highly spatially resolved soil data, and remotely sensed crop information should be considered for constraining root-zone SM estimates. In addition, improved descriptions of subsurface processes that control the status of root-zone SM are necessary to remove model prediction biases and to further decrease estimation uncertainty.

Symbols and Notation

θ_v	Volumetric soil moisture content
θ_m	Gravimetric soil moisture content
θ_s	Saturated water content
S_e	Relative saturation
θ_{FC}	Water content at field capacity
θ_{PWP}	Water content at permanent wilting point
ψ_m	Matric potential
AirMOSS	Airborne Microwave Observatory of Sub-canopy and Subsurface
AMSR-E	Advanced Microwave Scanning Radiometer for the Earth Observing System
AMSR-2	Advanced Microwave Scanning Radiometer 2
ASCAT	Advanced Scatterometer
CCI	Climate Change Initiative
CLM	Community Land Model
ComRAD	Combined radar/radiometer ground-based L-band simulator
COSMOS	Cosmic ray Soil Moisture Observing System
CRNP	Cosmic Ray Neutron Probe
CyGNSS	Cyclone Global Navigation Satellite System
EC_a	Apparent Electrical Conductivity
ECMWF	European Centre for Medium-Range Weather Forecasts
ELBARA	ETH L-Band Radiometer
EM	Electromagnetic
EMI	Electromagnetic Induction
EOF	Empirical Orthogonal Functions
ESA	European Space Agency
E-SAR	Experimental Synthetic Aperture Radar
FVC	Fractional Vegetation Cover
GCOM-W	Global Change Observation Mission-Water
GNSS	Global Navigation Satellite System
GPR	Ground Penetrating Radar
GPS	Global Positioning System
HPP	Heat Pulse Probe
ISMN	International Soil Moisture Network
JAXA	Japan Aerospace Exploration Agency
JULES	Joint UK Land Environment Simulator
L-MEB	L-band Microwave Emission of the Biosphere
LPRM	Land Parameter Retrieval Model
LST	Land Surface Temperature
MLR	Multiple Linear Regression

NASA	National Aeronautics and Space Administration
NDVI	Normalized Difference Vegetation Index
NIR	Near-Infrared
NP	Neutron Probe
NRT	Near Real Time
NSIDC	U.S. National Snow and Ice Data Center
OK	Oklahoma
PALS	Passive Active L-band Sensor
PAW	Plant Available Water
PLMR	Polarimetric L-band Multibeam Radiometer
PTF	Pedotransfer Function
RE	Richards' equation
REV	Representative Elementary Volume
RFI	Radio Frequency Interference
RS	Remote Sensing
RZSM	Root Zone Soil Moisture
SAR	Synthetic Aperture Radars
SCA	Single Channel Algorithm
SCAN	Soil Climate Analysis Network
SHFs	Soil Hydraulic Functions
SHPs	Soil Hydraulic Properties
STFs	Spectrotransfer Functions
SM	Soil Moisture
SMAP	Soil Moisture Active Passive
SMOS	Soil Moisture Ocean Salinity
SMOSMANIA	Soil Moisture Observing System – Meteorological Automatic Network Integrated Application
SNOTEL	SNOwpack TELemetry
SODI	Soil Moisture Drought Index
SSM/I	Special Sensor Microwave Imager
SWE	Snow Water Equivalent
SWI	Soil Water Index
SWIR	Shortwave Infrared
TC	Triple Collocation
TDR	Time Domain Reflectometry
TSA	Temporal Stability Analysis
USDM	U.S. Drought Monitor
VWC	Vegetation Water Content
WDI	Water Deficit Index
WSMN	Wireless Soil Moisture Network

Glossary

Brightness Temperature	The brightness temperature is a measurement of the radiance of the microwave radiation traveling upward from the top of the atmosphere to the satellite, expressed in units of the temperature of an equivalent black body.
Buckingham-Darcy Equation	The equation of motion for flow under partially saturated soil conditions. Similar to Darcy's law, except that hydraulic conductivity is not a constant, but a function of the matric potential.
Continuity Principle (Equation)	The continuity equation states mathematically that mass can neither be created or destroyed.

Cosmic Rays	High-energy radiation mainly originating outside the Solar System. Any stable particles such photons (gamma rays), electrons, protons, nuclei, or neutrinos. Upon impact with the Earth's atmosphere, cosmic rays can produce showers of secondary particles that sometimes reach the surface. The most common type of cosmic rays detected on Earth are protons.
Data Assimilation	The combining of diverse data, possibly sampled at different times and intervals and different locations, into a unified and consistent description of a physical system, such as the state of the atmosphere.
Dielectric Permittivity (Dielectric Constant)	The degree to which a medium resists the flow of electric charge, defined as the ratio of the electric displacement to the electric field strength.
Diffuse Reflectance Spectroscopy	Spectroscopic method that relies on a focused projection of a spectrometer beam onto a sample of interest, where it is reflected, scattered and transmitted through the sample material. The back reflected, diffusely scattered light (some of which is absorbed by the sample) is then collected by the accessory and directed to the detector optics.
Electromagnetic Induction (EMI) Survey	An electrical exploration method in which electric current is introduced into the ground via electromagnetic induction and in which the magnetic field associated with the current is determined
Electromagnetic Radiation	A traveling wave motion resulting from changing electric or magnetic fields. Electromagnetic radiation ranges from x-rays (and gamma rays) of short wavelength, through the ultraviolet, visible, and infrared regions, to radar and radio waves of relatively long wavelength.
Field Capacity	The content of soil water, on a mass or volume basis, remaining in a soil after full saturation due to irrigation or precipitation after internal redistribution due to gravity-driven flow (free drainage). For practical purposes the water content at field capacity is often assumed to coincide with a matric potential of -330 cm.
Fresnel Reflectance Equations	The Fresnel equations (or Fresnel coefficients) describe the reflection and transmission of light (or electromagnetic radiation in general) when incident on an interface between different optical media.
Gamma Radiation	Penetrating electromagnetic radiation arising from the radioactive decay of atomic nuclei. The wavelength is generally in the range 1×10^{-10} to 2×10^{-13} meters.
Gravimetric Water Content	Ratio of the mass of water within bulk soil to the mass of oven dry (105°C) soil.
Ground Penetrating Radar (GPR)	A GPR maps the form of contrasting electrical properties (dielectric permittivity and conductivity) of the subsurface and records information on the amplitude (strength), phase (structure) and time (speed) of electromagnetic energy reflected from subsurface features.
Hydraulic Conductivity	The proportionality factor in Darcy's law, as applied to viscous flow of water in soil, that represents the ability of soil to conduct water and is equivalent to the flux of water per unit gradient of hydraulic potential.
Matric Potential	Potential energy of soil water due to capillary and adsorptive surface forces that hold water within the soil matrix.
Neural Network	A network of neurons that are connected through synapses or weights. Each neuron performs a simple calculation that is a function of the activations of the neurons that are connected to it. Through feedback mechanisms and/or the nonlinear output response of neurons, the network as a whole is capable of performing extremely complicated tasks, including universal computation and universal approximation.
Optical Depth	Natural logarithm of the ratio of incident to transmitted radiant power through a material

Pedotransfer Functions (PTF)	Predictive functions of distinct soil properties using data from soil surveys.
Permanent Wilting Point	Below the permanent wilting point that is defined as the water content at -15000 cm matric potential, water is so tightly bound within the soil matrix that plants are no longer able to recover their turgidity and irreversibly wilt. This is only an approximation, as the permanent wilting point depends on plant physiology.
Plant Available Water	The amount of water released between in situ field capacity and the permanent wilting point.
Poiseuille's Law	States that the velocity of flow of a liquid through a circular tube varies directly with the pressure and the fourth power of the diameter of the tube and inversely with the length of the tube and the coefficient of viscosity of the liquid. Valid for steady, well-developed laminar flow.
Radar (Radio Detection and Ranging)	A method, system or technique, including equipment components, for using beamed, reflected, and timed electromagnetic radiation to detect, locate, and (or) track objects, to measure altitude and to acquire a terrain image. The radio detection instrument consists of a transmitter that sends out high-frequency radio waves and a receiver that picks them up after they have been reflected by an object.
Radiative Transfer	Physical phenomenon of energy transfer in the form of electromagnetic radiation. The propagation of radiation through a medium is affected by absorption, emission, and scattering processes. The radiative transfer equation describes these interactions mathematically.
Radio Frequency	Alternating (AC) electric current or radio waves, oscillating in the frequency range from around 20 kHz to around 300 GHz, roughly between the upper limit of audio frequencies and the lower limit of infrared frequencies.
Radiometer	An instrument for quantitatively measuring the intensity of electromagnetic radiation in some band of wavelengths in any part of the electromagnetic spectrum. Usually used with a modifier, such as an infrared radiometer or a microwave radiometer.
Representative Elementary Volume (REV)	Smallest volume over which a measurement can be made that will yield a value representative of the whole.
Richards' Equation	Most commonly used partial differential equation to represent transient flow through unsaturated porous media.
Soil Bulk Density	The mass of oven dry (105°C) soil per unit bulk volume. The value is expressed as kilogram per cubic meter.
Soil Thermal Conductivity	The proportionality factor in Fourier's law that represents the ability of soil to conduct heat and is equivalent to the thermal flux per unit temperature gradient.
Soil Thermal Diffusivity	The ratio of the thermal conductivity to the volumetric heat capacity.
Soil Water Characteristic	The relationship between the soil-water content (by mass or volume) and the matric potential. Also called the water retention curve or isotherm, and the water release curve.
Swath	The width of an imaged scene in the range dimension, measured in either ground range or slant range on the swath.
Volumetric Heat Capacity	The heat required to raise the temperature of 1 cm^3 of soil by 1°C. The change in heat content of unit volume of soil per unit change in soil temperature.
Volumetric Water Content	The soil-water content expressed as the volume of water per unit bulk volume of soil.
Young-Laplace Equation	Nonlinear partial differential equation that describes the capillary pressure difference sustained across the interface between two static fluids, such as water and air, due to the phenomenon of surface tension.

References

Abdu, H., Robinson, D. A., Boettinger, J., & Jones, S. B. (2017). Electromagnetic induction mapping at varied soil moisture reveals field-scale soil textural patterns and gravel lenses. *Frontiers of Agricultural Science and Engineering*, *4*(2), 135–145. https://doi.org/10.15302/J-FASE-2017143

Akbar, R., & Moghaddam, M. (2015). A combined active passive soil moisture estimation algorithm with adaptive regularization in support of SMAP. *IEEE Transactions on Geoscience and Remote Sensing*, *53*(6), 3312–3324. https://doi.org/10.1109/TGRS.2014.2373972

Akyildiz, I. F., & Stuntebeck, E. P. (2006). Wireless underground sensor networks: Research challenges. *Ad Hoc Networks*, *4*(6), 669–686. https://doi.org/10.1016/j.adhoc.2006.04.003

Al Bitar A., Kerr, Y. H., Merlin, O., Cabot, F., & Wigneron, J.P. (2013). Global drought index from SMOS soil moisture. Geoscience and Remote Sensing Symposium (IGARSS). IEEE International Geoscience and Remote Sensing Symposium, IGARSS 2013.

Al Bitar, A., Leroux, D., Kerr, Y. H., Merlin, O., Richaume, P., Sahoo, A., & Wood, E. F. (2012). Evaluation of SMOS soil moisture products over continental US using the SCAN/SNOTEL network. *IEEE Transactions on Geoscience and Remote Sensing*, *50*(5), 1572–1586. https://doi.org/10.1109/TGRS.2012.2186581

Al Bitar, A., Mialon, A., Kerr, Y. H., Cabot, F., Richaume, P., Jacquette, E., et al. (2017). The global SMOS Level 3 daily soil moisture and brightness temperature maps. *Earth System Science Data*, *9*(1), 293–315. https://doi.org/10.5194/essd-9-293-2017

Al Nakshabandi, G., & Kohnke, H. (1965). Thermal conductivity and diffusivity of soils as related to moisture tension and other physical properties. *Agricultural Meteorology*, *2*(4), 271–279. https://doi.org/10.1016/0002-1571(65)90013-0

Albergel, C., Calvet, J. C., De Rosnay, P., Balsamo, P., Wagner, W., Hasenauer, S., et al. (2010). Cross-evaluation of modelled and remotely sensed surface soil moisture with in situ data in Southwestern France. *Hydrology and Earth System Sciences*, *14*(11), 2177–2191. https://doi.org/10.5194/hess-14-2177-2010

Albergel, C., De Rosnay, P., Gruhier, C., Mun Ozsabater, J., Hasenauer, S., Isaksen, S., et al. (2012). Evaluation of remotely sensed and modelled soil moisture products using global ground based in situ observations. *Remote Sensing of Environment*, *118*, 215–226. https://doi.org/10.1016/j.rse.2011.11.017

Albergel, C., Rüdiger, C., Carrer, D., Calvet, J.-C., Fritz, N., Naeimi, V., et al. (2009). An evaluation of ASCAT surface soil moisture products with in-situ observations in Southwestern France. *Hydrology and Earth System Sciences*, *13*(2), 115–124. https://doi.org/10.5194/hess-13-115-2009

Albergel, C., Rudiger, C., Pellarin, T., et al. (2008). From near-surface to root-zone soil moisture using an exponential filter: an assessment of the method based on in-situ observations and model simulations. *Hydrology and Earth System Sciences*, *12*(6), 1323–1337. https://doi.org/10.5194/hess-12-1323-2008

Allred, B. J., Ehsani, M. R., & Saraswat, D. (2005). The impact of temperature and shallow hydrologic conditions on the magnitude and spatial pattern consistency of electromagnetic induction measured soil electrical conductivity. *Transctions of the ASAE*, *48*(6), 2123–2135. https://doi.org/10.13031/2013.20098

Al-Yaari, A., Wigneron, J. P., Kerr, Y., De Jeu, R., Rodríguez-Fernández, N., Van Der Schalie, R., et al. (2016). Testing regression equations to derive long-term global soil moisture datasets from passive microwave observations. *Remote Sensing of Environment*, *180*, 453–464. https://doi.org/10.1016/j.rse.2015.11.022

Al-Yaari, A., Wigneron, J. P., Kerr, Y., Rodríguez-Fernández, N., O'Neill, P. E., Jackson, T. J., et al. (2017). Evaluating soil moisture retrievals from ESA's SMOS and NASA's SMAP brightness temperature datasets. *Remote Sensing of Environment*, *193*, 257–273. https://doi.org/10.1016/j.rse.2017.03.010

Amani, M., Parsian, S., MirMazloumi, S. M., & Aieneh, O. (2016). Two new soil moisture indices based on the NIR-red triangle space of Landsat-8 data. *International Journal of Applied Earth Observation and Geoinformation*, *50*, 176–186. https://doi.org/10.1016/j.jag.2016.03.018

Andreasen, M., Jensen, K. H., Desilets, D., Franz, T. E., Zreda, M., Bogena, H. R., & Looms, M. C. (2017). Status and perspectives on the cosmic-ray neutron method for soil moisture estimation and other environmental science applications. *Vadose Zone Journal*, *16*(8). https://doi.org/10.2136/vzj2017.04.0086

Angstrom, A. (1925). The Albedo of various surfaces of ground. *Geografiska Annaler*, *7*, 323–342.

Anne, N. J. P., Abd-Elrahman, A. H., Lewis, D. B., & Hewitt, N. A. (2014). Modeling soil parameters using hyperspectral image reflectance in subtropical coastal wetlands. *International Journal of Applied Earth Observation and Geoinformation*, *33*, 47–56. https://doi.org/10.1016/j.jag.2014.04.007

Ardekani, M. R. M. (2013). Off-and on-ground GPR techniques for field-scale soil moisture mapping. *Geoderma*, *200-201*, 55–66. https://doi.org/10.1016/j.geoderma.2013.02.010

Baatz, R., Bogena, H. R., Hendricks Franssen, H. J., Huisman, J. A., Montzka, C., & Vereecken, H. (2015). An empirical vegetation correction for soil water content quantification using cosmic ray probes. *Water Resources Research*, *51*, 2030–2046. https://doi.org/10.1002/2014WR016443

Baatz, R., Bogena, H. R., Hendricks Franssen, H. J., Huisman, J. A., Qu, W., Montzka, C., & Vereecken, H. (2014). Calibration of a catchment scale cosmic-ray probe network: A comparison of three parameterization methods. *Journal of Hydrology*, *516*, 231–244. https://doi.org/10.1016/j.jhydrol.2014.02.026

Babaeian, E., Homaee, M., Montzka, C., Vereecken, H., & Norouzi, A. A. (2015). Towards retrieving soil hydraulic properties by hyperspectral remote sensing. *Vadose Zone Journal*, *14*(3). https://doi.org/10.2136/vzj2014.07.0080

Babaeian, E., Homaee, M., Montzka, C., Vereecken, H., Norouzi, A. A., & van Genuchten, M. T. (2016). Soil moisture prediction of bare soil profiles using diffuse spectral reflectance information and vadose zone flow modeling. *Remote Sensing of Environment*, *187*, 218–229. https://doi.org/10.1016/j.rse.2016.10.029

Babaeian, E., Homaee, M., Vereecken, H., Montzka, C., Norouzi, A. A., & van Genuchten, M. T. (2015). A comparative study of multiple approaches for predicting the soil-water retention curve: Hyperspectral Information vs. basic soil properties. *Soil Science Society of America Journal*, *79*(4), 1043–1058. https://doi.org/10.2136/sssaj2014.09.0355

Babaeian, E., Sadeghi, M., Franz, T. E., Jones, S., & Tuller, M. (2018). Mapping soil moisture with the OPtical TRApezoid Model (OPTRAM) based on long-term MODIS observations. *Remote Sensing of Environment*, *211*, 425–440. https://doi.org/10.1016/j.rse.2018.04.029

Baghdadi, N., Cresson, R., El Hajj, M., Ludwig, R., & La Jeunesse, I. (2012). Estimation of soil parameters over bare agriculture areas from C-band polarimetric SAR data using neural networks. *Hydrology and Earth System Sciences*, *16*, 1607–1621. https://doi.org/10.5194/hess-16-1607-2012

Balcom, B. J., Barrita, J. C., Choi, C., Beyea, S. D., Goodyear, D. J., & Bremner, T. W. (2003). Single-point magnetic resonance imaging (MRI) of cement based materials. *Materials and Structure*, *36*(3), 166–182. https://doi.org/10.1007/BF02479555

Balenzano, A., Mattia, F., Satalino, G., Pauwels, V., & Snoeij, P. (2012). SMOSAR algorithm for soil moisture retrieval using Sentinel-1 data. Paper presented at IEEE International Geoscience and Remote Sensing Symposium, Munich, Germany. https://doi.org/10.1109/IGARSS.2012.6351332.

Barrett, B. W., Dwyer, E., & Whelan, P. (2009). Soil moisture retrieval from active spaceborne microwave observations: An evaluation of current techniques. *Remote Sensing*, *1*(3), 210–242. https://doi.org/10.3390/rs1030210

Barrie, P. (2000). Characterization of porous media using NMR methods. *Annual Reports on NMR spectroscopy.*, *41*, 265–316.

Bartalis, Z., Wagner, W., Naeimi, V., Hasenauer, S., Scipal, K., Bonekamp, H., et al. (2018). Initial soil moisture retrievals from the METOP-A Advanced Scatterometer (ASCAT). *Geophysical Research Letters*, *34*, L20401. https://doi.org/10.1029/2007GL091088

Bauer-Marschallinger, B., Dorigo, W. A., Wagner, W., & van Dijk, A. I. J. M. (2013). How oceanic oscillation drives soil Moisture variations over Mainland Australia: An analysis of 32 years of satellite observations. *Journal of Climate*, *26*, 10159–10173. https://doi.org/10.1175/JCLI-D-13-00149.1

Bauer-Marschallinger, B., Freeman, V., Cao, S., Paulik, C., Schaufle, S., Stachl, T., et al. (2019). Toward global soil moisture monitoring with Sentinel-1: Harnessing assets and overcoming obstacles. *IEEE Transactions on Geoscience and Remote Sensing*, *57*(1), 520–539. https://doi.org/10.1109/TGRS.2018.2858004

Baum, R. L., Godt, J. W., & Savage, W. Z. (2010). Estimating the timing and location of shallow rainfall-induced landslides using a model for transient, unsaturated infiltration. *Journal of Geophysical Research*, *115*, F03013. https://doi.org/10.1029/2009JF001321

Bell, J. E., Palecki, M. A., Baker, C. B., Collins, W. G., Lawrimore, J. H., Leeper, R. D., et al. (2013). U.S. climate reference network soil moisture and temperature observations. *Journal of Hydrometeorology*, *14*(3), 977–988. https://doi.org/10.1175/JHM-D-12-0146.1

Ben-Dor, E., & Banin, A. (1995). Near infrared analysis as a rapid method to simultaneously evaluate several soil properties. *Soil Science Society of America Journal*, *59*, 364–372. https://doi.org/10.2136/sssaj1995.03615995005900020014x

Ben-Dor, E., Patkin, K., Banin, A., & Karnieli, A. (2002). Mapping of several soil properties using DAIS-7915 hyperspectral scanner data—A case study over clayey soils in Israel. *International Journal of Remote Sensing*, *23*(6), 1043–1062. https://doi.org/10.1080/01431160010006962

Bhatti, H. A., Rientjes, T., Verhoef, W., & Yaseen, M. (2013). Assessing temporal stability for coarse scale satellite moisture validation in the Maqu Area, Tibet. *Sensors*, *13*, 10725–10748. https://doi.org/10.3390/s130810725

Bindlish, R., Jackson, T., Sun, R., Cosh, M., Yueh, S., & Dinardo, S. (2009). Combined passive and active microwave observations of soil moisture during CLASIC. *IEEE Geoscience and Remote Sensing Letters*, *6*(4), 644–648. https://doi.org/10.1109/LGRS.2009.2028441

Bindlish, R., Jackson, T. J., Gasiewski, A. J., Klein, M., & Njoku, E. G. (2006). Soil moisture mapping and AMSR-E validation using the PSR in SMEX02. *Remote Sensing of Environment*, *103*(2), 127–139. https://doi.org/10.1016/j.rse.2005.02.003

Binley, A., Cassiani, G., Middleton, R., & Winship, P. (2002). Vadose zone flow model parameterization using cross-borehole radar and resistivity imaging. *Journal of Hydrology*, *267*(3–4), 147–159. https://doi.org/10.1016/S0022-1694(02)00146-4

Binley, A., Winship, P., Middleton, R., Pokar, M., & West, J. (2001). High-resolution characterization of vadose zone dynamics using cross-borehole radar. *Water Resources Research*, *37*(11), 2639–2652. https://doi.org/10.1029/2000WR000089

Bircher, S., Andreasen, M., Vuollet, J., Vehviläinen, J., Rautiainen, K., Jonard, F., et al. (2016). Soil moisture sensor calibration for organic soil surface layers. *Geoscientific Instrumentation. Methods and Data Systems Discussions.*, *5*, 447–493. https://doi.org/10.5194/gi-5-109-2016

Bircher, S., Skou, N., Jensen, K. H., Walker, J. P., & Rasmussen, L. (2012). A soil moisture and temperature network for SMOS validation in Western Denmark. *Hydrology and Earth System Sciences*, *16*(5), 1445–1463. https://doi.org/10.5194/hess-16-1445-2012

Blonquist, J. M., Jones, S. B., & Robinson, D. A. (2005). Standardizing characterization of electromagnetic water content sensors: Part 2. Evaluation of seven sensing systems. *Vadose Zone Journal*, *4*(4), 1059–1069. https://doi.org/10.2136/vzj2004.0141

Blume, T., Zehe, E., & Bronstert, A. (2009). Use of soil moisture dynamics and patterns at different spatio-temporal scales for the investigation of subsurface flow processes. *Hydrology and Earth System Sciences*, *13*(7), 1215–1233. https://doi.org/10.5194/hess-13-1215-2009

Bogena, H. R., Herbst, M., Huisman, J. A., Rosenbaum, U., Weuthen, A., & Vereecken, H. (2010). Potential of wireless sensor networks for measuring soil water content variability. *Vadose Zone Journal*, *9*(4), 1002–1013. https://doi.org/10.2136/vzj2009.0173

Bogena, H. R., Huisman, J. A., Baatz, R., Hendricks Franssen, H. J., & Vereecken, H. (2013). Accuracy of the cosmic-ray soil water content probe in humid forest ecosystems: The worst case scenario. *Water Resources Research*, *49*, 5778–5791. https://doi.org/10.1002/wrcr.20463

Bogena, H. R., Huisman, J. A., Güntner, A., Hübner, C., Kusche, J., Jonard, F., et al. (2015). Emerging methods for noninvasive sensing of soil moisture dynamics from field to catchment scale: a review. *Wiley Interdisciplinary Reviews Water*, *2*(6), 635–647. https://doi.org/10.1002/wat2.1097

Bogena, H. R., Huisman, J. A., Meier, H., Rosenbaum, U., & Weuthen, A. (2009). Hybrid wireless underground sensor networks: Quantification of signal attenuation in soil. *Vadose Zone Journal*, *8*(3), 755–761. https://doi.org/10.2136/vzj2008.0138

Bogena, H. R., Huisman, J. A., Oberdörster, C., & Vereecken, H. (2007). Evaluation of a low-cost soil water content sensor for wireless network applications. *Journal of Hydrology*, *344*(1-2), 32–42. https://doi.org/10.1016/j.jhydrol.2007.06.032

Bogena, H. R., Montzka, C., Huisman, J. A., Graf, A., Schmidt, M., Stockinger, M., et al. (2018). The TERENO-Rur hydrological observatory: A multi-scale multi-compartment research platform for the advancement of hydrological science. *Vadose Zone Journal*, *17*(1). https://doi.org/10.2136/vzj2018.03.0055

Bogrekci, I., & Lee, W. S. (2006). Effects of soil moisture content on absorbance spectra of sandy soils in sensing phosphorus concentration using UV-VIS-NIR spectroscopy. *Transactions of the ASABE*, *49*(4), 1175–1180. https://doi.org/10.13031/2013.21717

Brevik, E. C., & Fenton, T. E. (2002). Influence of soil water content, clay, temperature, and carbonate minerals on electrical conductivity readings taken with an EM-38. *Soil Horizons*, *43*(1), 9–13. https://doi.org/10.2136/sh2002.1.0009

Bristow, K. L., Campbell, G. S., & Calissendorff, K. (1993). Test of a heat-pulse probe for measuring changes in soil water content. *Soil Science Society of America Journal*, *57*(4), 930–934. https://doi.org/10.2136/sssaj1993.03615995005700040008x

Bristow, K. L., Kluitenberg, G. J., & Horton, R. (1994). Measurement of soil thermal properties with a dual-probe heat-pulse technique. *Soil Science Society of America Journal*, *58*, 1288–1294. https://doi.org/10.2136/sssaj1994.03615995005800050002x

Brocca, L., Ciabatta, L., Massari, C., Moramarco, T., Hahn, S., Hasenauer, S., et al. (2014). Soil as a natural rain gauge: Estimating global rainfall from satellite soil moisture data. *Journal of Geophysical Research: Atmospheres*, *119*, 5128–5141. https://doi.org/10.1002/2014JD021489

Brocca, L., Hasenauer, S., Lacava, T., Melone, F., Moramarco, T., Wagner, W., et al. (2011). Soil moisture estimation through ASCAT and AMSR-E sensors: An intercomparison and validation study across Europe. *Remote Sensing of Environment*, *145*, 3390–3408.

Brocca, L., Melone, F., Moramarco, T., & Morbidelli, R. (2009). Soil moisture temporal stability over experimental areas in Central Italy. *Geoderma*, *148*, 364–374. https://doi.org/10.1016/j.geoderma.2008.11.004

Brocca, L., Melone, F., Moramarco, T., & Morbidelli, R. (2010). Spatial-temporal variability of soil moisture and its estimation across scales. *Water Resources Research*, *46*, W02516. https://doi.org/10.1029/2009WR008016

Brocca, L., Melone, F., Moramarco, T., Wagner, W., & Hasenauer, S. (2010). ASCAT soil wetness index validation through in situ and modeled soil moisture data in central Italy. *Remote Sensing of Environment*, *114*(11), 2745–2755. https://doi.org/10.1016/j.rse.2010.06.009

Brocca, L., Tullo, T., Melone, F., Moramarco, T., & Morbidelli, R. (2012). Catchment scale soil moisture spatial-temporal variability. *Journal of Hydrology*, *422*, 63–75. https://doi.org/10.1016/j.jhydrol.2011.12.039

Brocca, L., Ponziani, F., Moramarco, T., Melone, F., Berni, N., & Wagner, W. (2012). Improving landslide forecasting using ASCAT-derived soil moisture data: A case study of the Torgiovannetto landslide in Central Italy. *Remote Sensing*, *4*(5), 1232–1244. https://doi.org/10.3390/rs4051232

Brooks, R. H., & Corey, A. T. (1964). *Hydraulic properties of porous media*. Hydrology Papers: Colorado State University, Fort Collins.

Brown, S. C. M., Quegan, S., Morrison, K., Bennett, J. C., & Cookmartin, G. (2003). High-resolution measurements of scattering in wheat canopies- implications for crop parameter retrieval. *IEEE Transactions on Geoscience and Remote Sensing*, *41*, 1602–1610. https://doi.org/10.1109/TGRS.2003.814132

Brummer, E., & Mardock, E. S. (1945). A neutron method for measuring saturation in laboratory flow measurements. *Transactions of the AIME*, *165*(1). https://doi.org/10.2118/946133-G

Brunfeldt, D. R., & Ulaby, F. T. (1984). Measured microwave emission and scattering in vegetation canopies. *IEEE Transactions on Geoscience and Remote Sensing*, *6*, 520–524. https://doi.org/10.1109/TGRS.1984.6499163

Bryant, R., Thoma, D., Moran, S., Holifield, C., Goodrich, D., Keefer, T., et al. (2003). Evaluation of hyperspectral, infrared temperature and radar measurements for monitoring surface soil moisture. Paper presented at the First Interagency Conference on Research in the Watersheds, 27-30.

Buckingham, E. (1907). Studies on the movement of soil moisture. Bull., USDA, Bureau of Soils. 38. Washington D.C.

Busch, F. A., Niemann, J. D., & Coleman, M. (2012). Evaluation of an empirical orthogonal function-based method to downscale soil moisture patterns based on topographic attributes. *Hydrological Processes*, *26*, 2696–2709. https://doi.org/10.1002/hyp.8363

Calamita, G., Perrone, A., Brocca, L., Onorati, B., & Manfreda, S. (2015). Field test of a multi-frequency electromagnetic induction sensor for soil moisture monitoring in southern Italy test sites. *Journal of Hydrology*, *529*, 316–329. https://doi.org/10.1016/j.jhydrol.2015.07.023

Camillo, P. J., O'Neill, P. E., & Gurney, R. J. (1986). Estimating soil hydraulic parameters using passive microwave data. *IEEE Transactions on Geoscience and Remote Sensing*, *6*, 930–936. https://doi.org/10.1109/TGRS.1986.289708

Cammalleri, C., Micale, F., & Vogt, J. (2016). A novel soil moisture-based drought severity index (DSI) combining water deficit magnitude and frequency. *Hydrological Processes*, *30*(2), 289–301. https://doi.org/10.1002/hyp.10578

Campbell, G. S. (1985). *Soil Physics with Basic-Transport Models for Soil-Plant Systems*. New York: Elsevier. ISBN: 9780080869827.

Campbell, G. S., Calissendorff, C., & Williams, J. H. (1991). Probe for measuring soil specific heat using a heat-pulse method. *Soil Science Society of America Journal*, *55*(1), 291–293. https://doi.org/10.2136/sssaj1991.03615995005500010052x

Carlson, T. (2007). An overview of the triangle method for estimating surface evapotranspiration and soil moisture from satellite imagery. *Sensors*, *7*(8), 1612–1629. https://doi.org/10.3390/s7081612

Carlson, T. N. (2013). Triangle models and misconceptions. *International Journal of Remote Sensing Application*, *3*(3), 155–158.

Carlson, T. N., Gillies, R. R., & Perry, E. M. (1994). A method to make use of thermal infrared temperature and NDVI measurements to infer soil water content and fractional vegetation cover. *Remote Sensing Reviews*, *52*, 45–59. https://doi.org/10.1080/02757259409532220

Carrera, M. L., Belair, S., & Bilodeau, B. (2015). The Canadian land data assimilation system (CaLDAS): Description and synthetic evaluation study. *Journal of Hydrometeorology*, *16*(3), 1293–1314. https://doi.org/10.1175/JHM-D-14-0089.1

Carroll, T. R. (1981). Airborne soil moisture measurement using natural terrestrial Gamma radiation. *Soil Science*, *132*(5), 358–366.

Carroll, Z. L., & Oliver, M. A. (2005). Exploring the spatial relations between soil physical properties and apparent electrical conductivity. *Geoderma*, *128*(3), 354–374. https://doi.org/10.1016/j.geoderma.2005.03.008

Carsel, R. F., & Parrish, R. S. (1988). Developing joint probability distributions of soil water retention characteristics. *Water Resources Research*, *24*(5), 755–769. https://doi.org/10.1029/WR024i005p00755

Castaldi, F., Palombo, A., Pascucci, S., Pignatti, S., Santini, F., & Casa, R. (2015). Reducing the influence of soil moisture on the estimation of clay from hyperspectral data: A case study using simulated PRISMA data. *Remote Sensing*, *7*(11), 15561–15582. https://doi.org/10.3390/rs71115561

Ceballos, A., Scipal, K., Wagner, W., & Martinez-Fernandez, J. (2005). Validation of ERS scatterometer-derived soil moisture data in the central part of the Duero Basin (Spain). *Hydrological Processes*, *19*(8), 1549–1566. https://doi.org/10.1002/hyp.5585

Cenci, L., Pulvirenti, L., Boni, G., Chini, M., Matgen, P., Gabellani, S., et al. (2017). An evaluation of the potential of Sentinel 1 for improving flash flood predictions via soil moisture–data assimilation. *Advances in Geosciences*, *44*, 89–100. https://doi.org/10.5194/adgeo-44-89-2017

Chakrabarti, S., Bongiovanni, T., Judge, J., Zotarelli, L., & Bayer, C. (2014). Assimilation of SMOS soil moisture for quantifying drought impacts on crop yield in agricultural regions. *IEEE Journal of Selected Topics in Applied Earth Observations and Remote Sensing*, *7*(9), 3867–3879. https://doi.org/10.1109/JSTARS.2014.2315999

Chakravorty, A., Chahar, B. R., Sharma, O. P., & Dhanya, C. T. (2016). A regional scale performance evaluation of SMOS and ESA-CCI soil moisture products over India with simulated soil moisture from MERRA-Land. *Remote Sensing of Environment*, *186*, 514–527. https://doi.org/10.1016/j.rse.2016.09.011

Chan, S. K., Bindlish, R., O'Neill, P., Jackson, T., Njoku, E., Dunbar, S., et al. (2018). Development and assessment of the SMAP enhanced passive soil moisture product. *Remote Sensing of Environment*, *204*, 931–941. https://doi.org/10.1016/j.rse.2017.08.025

Chan, S. K., Bindlish, R., O'Neill, P. E., Njoku, E., Jackson, T., Colliander, A., et al. (2016). Assessment of the SMAP passive soil moisture product. *IEEE Transactions on Geoscience and Remote Sensing*, *54*(8), 4994–5007. https://doi.org/10.1109/TGRS.2016.2561938

Chang, C. W., Laird, D. A., Mausbach, M. J., & Hurburgh, C. R. (2001). Near-infrared reflectance spectroscopy–Principal components regression analyses of soil properties. *Soil Science Society of America Journal*, *65*(2). https://doi.org/10.2136/sssaj2001.652480x

Chapin, E., Chau, A., Chen, J., Heavey, B., Hensley, S., Lou, Y., et al. (2012). *AirMOSS: An airborne P-band SAR to measure root-zone soil moisture*, (pp. 693–698). Atlanta, GA: Paper presented at IEEE Radar Conference.

Chauhan, N. S., Miller, S., & Ardanuy, P. (2003). Spaceborne soil moisture estimation at high resolution: A microwave-optical/IR synergistic approach. *International Journal of Remote Sensing*, *24*(22), 4599–4622. https://doi.org/10.1080/0143116031000156837

Chen, F., Crow, W. T., Bindlish, R., Colliander, A., Burgin, M. S., Asanuma, J., & Aida, K. (2018). Global-scale evaluation of SMAP, SMOS and ASCAT soil moisture products using triple collocation. *Remote Sensing of Environment*, *214*, 1–13. https://doi.org/10.1016/j.rse.2018.05.008

Chen, F., Crow, W. T., Colliander, A., Cosh, M. H., Jackson, T. J., Bindlish, R., et al. (2017). Application of triple collocation in ground-based validation of soil moisture active/passive (SMAP) level 2 data products. *IEEE Journal of Selected Topics in Applied Earth Observations and Remote Sensing*, *10*(2), 489–502. https://doi.org/10.1109/JSTARS.2016.2569998

Chen, F., Crow, W. T., & Ryu, D. (2014). Dual forcing and state correction via soil moisture assimilation for improved rainfall-runoff modeling. *Journal of Hydrometeorology*, *15*(5), 1832–1848. https://doi.org/10.1175/JHM-D-14-0002.1

Chen, X. Z., Chen, S. S., Zhong, R. F., Su, Y. X., Liao, J. S., Li, D., et al. (2012). A semi-empirical inversion model for assessing surface soil moisture using AMSR-E brightness temperatures. *Journal of Hydrology*, *456*, 1–11. https://doi.org/10.1016/j.jhydrol.2012.05.022

Chen, Y., Yang, K., Qin, J., Zhao, L., Tang, W., & Han, M. (2013). Evaluation of AMSR-E retrievals and GLDAS simulations against observations of a soil moisture network on the central Tibetan Plateau. *Journal of Geophysical Research: Atmospheres*, *118*, 4466–4475. https://doi.org/10.1002/jgrd.50301

Chen, Y. Y., Yang, K., Qin, J., Cui, Q., Lu, H., La, Z., et al. (2017). Evaluation of SMAP, SMOS, and AMSR2 soil moisture retrievals against observations from two networks on the Tibetan Plateau. *Journal of Geophysical Research: Atmospheres*, *122*, 5780–5792. https://doi.org/10.1002/2016JD026388

Chew, C., Reager, J. T., & Small, E. (2018). CYGNSS data map flood inundation during the 2017 Atlantic hurricane season. *Scientific Reports*, *8*, 1–8. https://doi.org/10.1038/s41598-018-27673-x

Chew, C. C., Small, E. E., Larson, K. M., & Zavorotny, V. U. (2014). Effects of near-surface soil moisture on GPS SNR data: development of a retrieval algorithm for soil moisture. *IEEE Transaction of Geoscience and Remote Sensing*, *52*(1), 537–543. https://doi.org/10.1109/TGRS.2013.2242332

Cho, E., & Choi, M. (2014). Regional scale spatio-temporal variability of soil moisture and its relationship with meteorological factors over the Korean peninsula. *Journal of Hydrology*, *516*, 317–329. https://doi.org/10.1016/j.jhydrol.2013.12.053

Cho, E., Choi, M., & Wagner, W. (2015). An assessment of remotely sensed surface and root zone soil moisture through active and passive sensors in northeast Asia. *Remote Sensing of Environment*, *160*, 166–179. https://doi.org/10.1016/j.rse.2015.01.013

Cho, E., Moon, H., & Choi, M. (2015). First assessment of the advanced microwave scanning radiometer 2 (AMSR2) soil moisture contents in Northeast Asia. *Journal of the Meteorological Society of Japan*, *93*(1), 117–129. https://doi.org/10.2151/jmsj.2015-008

Chung, D., Dorigo, W., de Jeu, R.A.M., Hahn, S., Melzer, T., Parinussa, R.M., Paulik, C. et al. (2018). Algorithm theoretical baseline document (ATBD) D2.1 version 04.2. ESA climate change initiative phase II, Soil Moisture

Claps, P., & Laguardia, G. (2004). Assessing spatial variability of soil water content through Thermal Inertia and NDVI. *Remote Sensing*, 378–387. https://doi.org/10.1117/12.510984

Clark, R. N. (1999). *Spectroscopy of rocks and minerals, and principles of spectroscopy*. New York: John Wiley and Sons.

Coe, J. A., Ellis, W. L., Godt, J. W., Savage, W. Z., Savage, J. E., Michael, J. A., et al. (2003). Seasonal movement of the Slumgullion landslide determined from Global Positioning System surveys and field instrumentation, July 1998–March 2002. *Engineering Geology*, *68*(1-2), 67–101. https://doi.org/10.1016/S0013-7952(02)00199-0

Colliander, A., Chan, S., Kim, S. B., Das, N., Yueh, S., Cosh, M., et al. (2012). Long term analysis of PALS soil moisture campaign measurements for global soil moisture algorithm development. *Remote Sensing of Environment*, *121*, 309–322. https://doi.org/10.1016/j.rse.2012.02.002

Colliander, A., Jackson, T., McNairn, H., Chazanoff, S., Dinardo, S., Latham, B., et al. (2015). Comparison of airborne passive and active L-band system (PALS) brightness temperature measurements to SMOS observations during the SMAP validation experiment 2012 (SMAPVEX12). *IEEE Geoscience and Remote Sensing Letters*, *12*(4), 801–805. https://doi.org/10.1109/LGRS.2014.2362889

Colliander, A., Jackson, T. J., Bindlish, R., Chan, S., Das, N., Kim, S. B., et al. (2017). Validation of SMAP surface soil moisture products with core validation sites. *Remote Sensing of Environment*, *191*, 215–231. https://doi.org/10.1016/j.rse.2017.01.021

Collow, T. W., Robock, A., Basara, J. B., & Illston, B. G. (2012). Evaluation of SMOS retrievals of soil moisture over the central United States with currently available in-situ observations. *Journal of Geophysical Research*, *117*, D09113. https://doi.org/10.1029/2011JD017095

Collow, T. W., Robock, A., & Wu, W. (2014). Influences of soil moisture and vegetation on convective precipitation forecasts over the United States Great Plains. *Journal of Geophysical Research: Atmospeheres*, *119*, 9338–9358. https://doi.org/10.1002/2014JD021454

Coopersmith, E. J., Bell, J. E., & Cosh, M. H. (2015). Extending the soil moisture data record of the US Climate Reference Network (USCRN) and Soil Climate Analysis Network (SCAN). *Advances in Water Resources*, *79*, 80–90. https://doi.org/10.1016/j.advwatres.2015.02.006

Coopersmith, E. J., Cosh, M. H., Bindlish, R., & Bell, J. (2015). Comparing AMSR-E soil moisture estimates to the extended record of the U.S. Climate Reference Network (USCRN). *Advances in Water Resources*, *85*, 79–85. https://doi.org/10.1016/j.advwatres.2015.09.003

Corwin, D. L., & Lesch, S. M. (2003). Application of soil electrical conductivity to precision agriculture: Theory, principles, and guidelines. *Agronomy Journal*, *95*, 455–471.

Cosh, M. H., Jackson, T. J., Moran, S., & Bindlish, R. (2008). Temporal persistence and stability of surface soil moisture in a semi-arid watershed. *Remote Sensing of Environment*, *112*, 304–313. https://doi.org/10.1016/j.rse.2007.07.001

Cosh, M. H., Jackson, T. J., Starks, P., & Heathman, G. (2006). Temporal stability of surface soil moisture in the Little Washita River watershed and its applications in satellite soil moisture product validation. *Journal of Hydrology*, *323*, 168–177. https://doi.org/10.1016/j.jhydrol.2005.08.020

Crapolicchio, R., & Lecomte, P. (2004). The ERS-2 scatterometer mission: Events and long-loop instrument and data performances assessment. In: Proceedings of the ENVISAT & ERS Symposium, 6–10.

Crow, W. T., Berg, A. A., Cosh, M. H., Loew, A., Mohanty, B. P., Panciera, R., et al. (2012). Upscaling sparse ground-based soil moisture observations for the validation of coarse-resolution satellite soil moisture products. *Reviews of Geophysics*, *50*, 2011RG000372, L19406. https://doi.org/10.1029/2011RG000372

Crow, W. T., Chen, F., Reichle, R. H., & Liu, Q. (2017). L-band microwave remote sensing and land data assimilation improve the representation of prestorm soil moisture conditions for hydrologic frecasting. *Geophysical Research Letters*, *44*, 5495–5503. https://doi.org/10.1002/2017GL073642

Crow, W. T., Chen, F., Reichle, R. H., Xia, Y., & Liu, Q. (2018). Exploiting soil moisture, precipitation, and streamflow observations to evaluate soil moisture/runoff coupling in land surface models. *Geophysical Research Letters*, *45*, 4869–4878. https://doi.org/10.1029/2018GL077193

Crow, W. T., Lei, F. N., Hain, C., Anderson, M. C., Scott, R. L., Billesbach, D., & Arkebauer, T. (2015). Robust estimates of soil moisture and latent heat flux coupling strength obtained from triple collocation. *Geophysical Research Letters*, *42*, 8415–8423. https://doi.org/10.1002/2015GL065929

Crow, W. T., Milak, S., Moghaddam, M., Tabatabaeenejad, A., Jaruwatanadilok, S., Yu, X., et al. (2018). Spatial and temporal variability of root zone soil moisture acquired from hydrologic modeling and AirMOSS P-band radar. *IEEE Journal of Selected Topics in Applied Earth Observations and Remote Sensing.*, *11*(12), 4578–4590. https://doi.org/10.1109/JSTARS.2018.2865251

Crow, W. T., & Wood, E. F. (2003). The assimilation of remotely sensed soil brightness temperature imagery into a land surface model using Ensemble Kalman filtering: A case study based on ESTAR measurements during SGP97. *Advances in Water Resources*, *26*, 137–149. https://doi.org/10.1016/S0309-1708(02)00088-X

Crow, W. T., & Zhan, X. W. (2007). Continental-scale evaluation of remotely sensed soil moisture products. *IEEE Geoscience and Remote Sensing Letters*, *4*(3), 451–455. https://doi.org/10.1109/LGRS.2007.896533

Cui, C., Xu, J., Zeng, J., Chen, K.-S., Bai, X., Lu, H., et al. (2018). Soil moisture mapping from satellites: An inter-comparison of SMAP, SMOS, FY3B, AMSR2, and ESA CCI over two dense network regions at different spatial scales. *Remote Sensing*, *10*(1), 33. https://doi.org/10.3390/rs10010033

Cui, H. Z., Jiang, L. M., Du, J. Y., Zhao, S. J., Wang, G. X., Lu, Z., & Wang, J. (2017). Evaluation and analysis of AMSR-2, SMOS, and SMAP soil moisture products in the Genhe area of China. *Journal of Geophysical Research: Atmospheres*, *122*, 8650–8666. https://doi.org/10.1002/2017JD026800

Cui, X. F., Parker, D. J., & Morse, A. P. (2009). The drying out of soil moisture following rainfall in a numerical weather prediction model and implications for malaria prediction in West Africa. *Weather and Forecasting*, *24*(6), 1549–1557. https://doi.org/10.1175/2009WAF2222240.1

Dall'Amico, J. T., Schlenz, F., Loew, A., & Mauser, W. (2012). First results of SMOS soil moisture validation in the upper Danube catchment. *IEEE Transactions on Geoscience and Remote Sensing*, *50*, 1507–1516. https://doi.org/10.1109/TGRS.2011.2171496

Das, N. N., Entekhabi, D., Dunbar, R. S., Colliander, A., Chen, F., Crow, W., et al. (2018). The SMAP mission combined active-passive soil moisture product at 9 km and 3 km spatial resolutions. *Remote Sensing of Environment*, *211*, 204–217. https://doi.org/10.1016/j.rse.2018.04.011

Das, N. N., Entekhabi, D., Kim, S., Jagdhuber, T., Dunbar, S., Yueh, S., et al. (2018). High resolution enhanced product based on SMAP active-passive approach using Sentinel-1A and 1B SAR data. *The International Archives of the Photogrammetry, Remote Sensing and Spatial Information Sciences.*, *XLII-5*, 203–205. https://doi.org/10.5194/isprs-archives-XLII-5-203-2018

Das, N. N., Entekhabi, D., & Njoku, E. G. (2011). An algorithm for merging SMAP radiometer and radar data for high-resolution soil-moisture retrieval. *IEEE Transactions on Geoscience and Remote Sensing*, *49*(5), 1504–1512. https://doi.org/10.1109/TGRS.2010.2089526

Das, N. N., & Mohanty, B. P. (2006). Root zone soil moisture assessment using remote sensing and vadose zone modeling. *Vadose Zone Journal*, *5*(1), 296–307. https://doi.org/10.2136/vzj2005.0033

Das, N. N., & Mohanty, B. P. (2008). Temporal dynamics of PSR-based soil moisture across spatial scales in an agricultural landscape during SMEX02: A wavelet approach. *Remote Sensing of Environment.*, *112*(2), 522–534. https://doi.org/10.1016/j.rse.2007.05.007

Das, N. N., Mohanty, B. P., Cosh, M. H., & Jackson, T. J. (2008). Modeling and assimilation of root zone soil moisture using remote sensing observations in Walnut Gulch watershed during SMEX04. *Remote Sensing of Environment*, *112*(2), 415–429. https://doi.org/10.1016/j.rse.2006.10.027

De Jeu, R. A. M. (2003), Retrieval of land surface parameters using passive microwave remote sensing, Ph.D. dissertation, Dept. of Geo-Environ. Sci., Vrije Univ. Amsterdam, Netherlands.

De Jong, E., Ballantyne, A. K., Cameron, D. R., & Read, D. W. L. (1979). Measurement of apparent electrical conductivity of soils by an electromagnetic induction probe. *Soil Science Society of America Journal*, *43*, 810–812. https://doi.org/10.2136/sssaj1979.03615995004300040040x

De Lange, R., Beck, R., van de Giesen, N., Friesen, J., de Wit, A., & Wagner, W. (2008). Scatterometer-derived soil moisture calibrated for soil texture with a one-dimensional water-flow model. *IEEE Transactions on Geoscience and Remote Sensing*, *46*(12), 4041–4049. https://doi.org/10.1109/TGRS.2008.2000796

De Lannoy, G., & Reichle, R. (2016). Global assimilation of multi-angle and multi-polarization SMOS brightness temperature observations into the GEOS-5 catchment land surface model for soil moisture estimation. *Journal of Hydrometeorology*, *17*(2), 669–691. https://doi.org/10.1175/JHM-D-15-0037.1

De Lannoy, G. J. M., Reichle, R. H., Houser, P. R., Pauwels, V. R. N., & Verhoest, N. E. C. (2007). Correcting for forecast bias in soil moisture assimilation with the ensemble Kalman filter. *Water Resources Research*, *43*, W09410. https://doi.org/10.1029/2006WR005449

De Rosnay, P., Drusch, M., Balsamo, G., Isaksen, L., & Albergel, C. (2011). Extended Kalman Filter soil moisture analysis in the IFS, n127. 12–16. ECMWF Spring Newsletter.

De Vries, D. A. (1958). Simultaneous transfer of heat and moisture in porous media, Eos. *Transactions American Geophysical Union*, *39*(5), 909–916. https://doi.org/10.1029/TR039i005p00909

De Vries, D. A. (1963). The physics of plant environments. In L. T. Evans (Ed.), *Environmental control of plant growth*, (pp. 5–22). New York, London: Academic Press.

Dente, L., Ferrazzoli, P., Su, Z., van der Velde, R., & Guerriero, L. (2014). Combined use of active and passive microwave satellite data to constrain a discrete scattering model. *Remote Sensing of Environment*, *155*, 222–238. https://doi.org/10.1016/j.rse.2014.08.031

Dente, L., Su, Z., & Wen, J. (2012). Validation of SMOS soil moisture products over the Maqu and Twente regions. *Sensors*, *12*, 9965–9986. https://doi.org/10.3390/s120809965

Desilets, D., Zreda, M., & Ferré, T. P. A. (2010). Nature's neutron probe: Land surface hydrology at an elusive scale with cosmic rays. *Water Resources Research*, *46*, W11505. https://doi.org/10.1029/2009WR008726

Dharssi, I., Bovis, K. J., Macpherson, B., & Jones, C. P. (2011). Operational assimilation of ASCAT surface soil wetness at the Met Office. *Hydrology and Earth System Sciences*, *15*, 2729–2746. https://doi.org/10.5194/hess-15-2729-2011

Dirmeyer, P. A., Gao, X., Zhao, M., Guo, Z., Oki, T., & Hanasaki, N. (2006). GSWP-2: Multimodel analysis and implications for our perception of the land surface. *Bulletin of the American Meteorological Society*, *87*, 1381–1397. https://doi.org/10.1175/BAMS-87-10-1381

Djamai, N., Magagi, R., Goita, K., Hosseini, M., Cosh, M., Berg, A., & Toth, B. (2015). Evaluation of SMOS soil moisture products over the CanEx-SM10 area. *Journal of Hydrology*, *520*, 254–267. https://doi.org/10.1016/j.jhydrol.2014.11.026

Dobriyal, P., Qureshi, A., Badola, R., & Hussain, S. A. (2012). A review of the methods available for estimating soil moisture and its implications for water resource management. *Journal of Hydrology*, *458-459*, 110–117. https://doi.org/10.1016/j.jhydrol.2012.06.021

Dobson, M. C., Ulaby, F. T., Hallikainen, M. T., & El-Rayes, M. A. (1985). Microwave dielectric behavior of wet soil. Part II: Dielectric mixing models. *IEEE Transactions on Geoscience and Remote Sensing*, *23*(1), 35–46. https://doi.org/10.1109/TGRS.1985.289498

Dong, J., Ochsner, T. E., Zreda, M., Cosh, M. H., & Zou, C. B. (2014). Calibration and validation of the COSMOS rover for surface soil moisture measurement. *Vadose Zone Journal*, *13*(4). https://doi.org/10.2136/vzj201308148

Dong, J. Z., & Crow, W. T. (2017). An improved triple collocation analysis algorithm for decomposing autocorrelated and white soil moisture retrieval errors. *Journal of Geophysical Research: Atmospheres*, *122*, 13081–13094. https://doi.org/10.1002/2017JD027387

Doolittle, J. A., & Brevik, E. C. (2014). The use of electromagnetic induction techniques in soils studies. *Geoderma*, *223*, 33–45. https://doi.org/10.1016/j.geoderma.2014.01.027

Dorigo, W. A., Gruber, A., de Jeu, R. A. M., Wagner, W., Stacke, T., Loew, A., et al. (2015). Evaluation of the ESA CCI soil moisture product using ground-based observations. *Remote Sensing of Environment*, *162*, 380–395. https://doi.org/10.1016/j.rse.2014.07.023

Dorigo, W. A., Wagner, W., Hohensinn, R., Hahn, S., Paulik, C., Xaver, A., et al. (2011). The international soil moisture network: A data hosting facility for global in situ soil moisture measurements. *Hydrology and Earth System Sciences*, *15*(5), 1675–1698. https://doi.org/10.5194/hess-15-1675-2011

Downer, C. W., & Ogden, F. L. (2004). Appropriate vertical discretization of Richards' equation for two-dimensional watershed-scale modelling. *Hydrological Processes*, *18*(1), 1–22. https://doi.org/10.1002/hyp.1306

Dracup, J. A., Lee, K. S., & Paulson, E. G. (1980). On the definition of droughts. *Water Resources Research*, *16*(2), 297–302.

Draper, C., Mahfouf, J. F., Calvet, J. C., Martin, E., & Wagner, W. (2011). Assimilation of ASCAT near-surface soil moisture into the SIM hydrological model over France. *Hydrology and Earth System Sciences*, *15*(12), 3829–3841. https://doi.org/10.5194/hess-15-3829-2011

Draper, C. S., Reichle, R. H., De Lannoy, G. J. M., & Liu, Q. (2012). Assimilation of passive and active microwave soil moisture retrievals. *Geophysical Research Letters*, *39*, L04401. https://doi.org/10.1029/2011GL050655

Draper, C. S., Walker, J. P., Steinle, P. J., de Jeu, R. A. M., & Holmes, T. R. H. (2009). An evaluation of AMSR-E derived soil moisture over Australia. *Remote Sensing of Environment*, *113*(4), 703–710. https://doi.org/10.1016/j.rse.2008.11.011

Drusch, M. (2007). Initializing numerical weather prediction models with satellite-derived surface soil moisture: Data assimilation experiments with ECMWF's Integrated Forecast System and the TMI soil moisture data set. *Journal of Geophysical Research*, *112*, W02013. https://doi.org/10.1029/2006JD007478

Drusch, M., Scipal, K., De Rosnay, P., Balsamo, G., Andersson, E., Bougeault, P., & Viterbo, P. (2009). Towards a Kalman Filter based soil moisture analysis system for the operational ECMWF Integrated Forecast System. *Geophysical Research Letters*, *36*, L10401. https://doi.org/10.1029/2009GL037716

Dumedah, G., Walker, J. P., & Merlin, O. (2015). Root-zone soil moisture estimation from assimilation of downscaled soil moisture and ocean salinity data. *Advances in Water Resources*, *84*, 14–22. https://doi.org/10.1016/j.advwatres.2015.07.021

Dumedah, G., Walker, J. P., & Mililli, B. (2013). *Examining the impact of scale variations on soil moisture downscaling using temporal persistence*, Paper presented at 20th *International Congress on Modelling and Simulation*, (). Australia: Adelaide.

Edzes, H. T., van Dusschoten, D., & Van As, H. (1998). Quantitative T2 imaging of plant tissues by means of multi-echo MRI microscopy. *Magnetic Resonance Imaging*, *16*(2), 185–196. https://doi.org/10.1016/S0730-725X(97)00274-9

El Hajj, M., Baghdadi, N., Zribi, M., Rodriguez-Fernandez, N., Wigneron, J. P., Al-Yaari, A., et al. (2018). Evaluation of SMOS, SMAP, ASCAT and Sentinel-1 soil moisture products at sites in southwestern France. *Remote Sensing*, *10*(4), 569. https://doi.org/10.3390/rs10040569

Elfouhaily, T. M., & Guérin, C. A. (2004). A critical survey of approximate scattering wave theories from random rough surfaces. *Waves in Random Media*, *14*(4), R1–R40. https://doi.org/10.1088/0959-7174/14/4/R01

Entekhabi, D., Nakamura, H., & Njoku, E. G. (1994). Solving the inverse problem for soil moisture and temperature profiles by sequential assimilation of multifrequency remotely sensed observations. *IEEE Transactions on Geoscience and Remote Sensing*, *32*(2), 438–448. https://doi.org/10.1109/36.295058

Entekhabi, D., Njoku, E. G., O'Neill, P. E., Kellogg, K. H., Crow, W. T., Edelstein, W. N., et al. (2010). The soil moisture active passive (SMAP) mission. *Proceedings of the IEEE*, *98*(5), 704–716. https://doi.org/10.1109/JPROC.2010.2043918

Entin, J. K., Robock, A., Vinnikov, K. Y., Hollinger, S. E., Liu, S., & Namkhai, A. (2000). Temporal and spatial scales of observed soil moisture variations in the extratropics. *Journal of Geophysical Research*, *105*, 11865–11877. https://doi.org/10.1029/2000JD900051

Eswar, R., Das, N. N., Poulsen, C., Behrangi, A., Swigart, J., Svoboda, M., et al. (2018). SMAP soil moisture change as an indicator of drought conditions. *Remote Sensing*, *10*(5), 788. https://doi.org/10.3390/rs10050788

Evan, J. G., Ward, H. C., Blake, J. R., Hewitt, E. J., Morrison, R., Fry, M., et al. (2016). Soil water content in Sothern England derived from a cosmic-ray soil moisture observing system: COSMOS-UK. *Hydrological Process*, *30*, 4987–4999. https://doi.org/10.1002/hyp.10929

Evensen, G. (1997). Advanced data assimilation for strongly nonlinear dynamics. *Monthly Weather Review*, *125*(6), 1342–1354. https://doi.org/10.1175/1520-0493(1997)125<1342:ADAFSN>2.0.CO;2

Famiglietti, J. S., Devereaux, J. A., Laymon, C. A., Tsegaye, T., Houser, P. R., Jackson, T. J., et al. (1999). Ground-based investigation of soil moisture variability within remote sensing footprints during the Southern Great Plains 1997 (SGP97) hydrology experiment. *Water Resources Research*, *35*(6), 1839–1851. https://doi.org/10.1029/1999WR900047

Famiglietti, J. S., Ryu, D. R., Berg, A. A., Rodell, M., & Jackson, T. J. (2008). Field observations of soil moisture variability across scales. *Water Resources Research*, *44*, W01423. https://doi.org/10.1029/2006WR005804

Fan, Y., & Dool, H. (2004). Climate Prediction Center global monthly soil moisture data set at 0.5° resolution for 1948 to present. *Journal of Geophysical Research*, *109*, D10102. https://doi.org/10.1029/2003JD004345

Fang, B., Lakshmi, V., Bindlish, R., & Jackson, T. J. (2018). Downscaling of SMAP soil moisture using land surface temperature and vegetation data. *Vadose Zone Jornal*, *17*(1). https://doi.org/10.2136/vzj2017.11.0198

Fang, Z. F., Bogena, H., Kollet, S., Koch, J., & Vereecken, H. (2015). Spatio-temporal validation of long-term 3D hydrological simulations of a forested catchment using empirical orthogonal functions and wavelet coherence analysis. *Journal of Hydrology*, *529*, 1754–1767. https://doi.org/10.1016/j.jhydrol.2015.08.011

Fares, A., Safeeq, M., Awal, R., Fares, S., & Dogan, A. (2016). Temperature and probe-to-probe variability effects on the performance of capacitance soil moisture sensors in an oxisol. *Vadose Zone Journal*, *15*(3). https://doi.org/10.2136/vzj2015.07.0098

Fascetti, F., Pierdicca, N., Pulvirenti, L., Crapolicchio, R., & Munoz-Sabater, J. (2016). A comparison of ASCAT and SMOS soil moisture retrievals over Europe and Northern Africa from 2010 to 2013. *International Journal of Applied Earth Observation and Geoinformation*, *45*, 135–142. https://doi.org/10.1016/j.jag.2015.09.008

Fernandez-Moran, R., Al-Yaari, A., Mialon, A., Mahmoodi, A., Al Bitar, A., De Lannoy, G., et al. (2017). SMOS-IC: An alternative SMOS soil moisture and vegetation optical depth product. *Remote Sensing*, *9*(5), 457. https://doi.org/10.3390/rs9050457

Fischer, E. M., Seneviratne, S. I., Lüthi, D., & Schär, C. (2007). Contribution of land-atmosphere coupling to recent European summer heat waves. *Geophysical Research Letters*, *34*, L06702. https://doi.org/10.1029/2006GL029068

Ford, T. W., Rapp, A. D., & Quiring, S. M. (2015). Does afternoon precipitation occur preferentially over dry or wet soils in Oklahoma? *Journal of Hydrometeorology*, *16*(2), 874–888. https://doi.org/10.1175/JHM-D-14-0005.1

Franz, T. E., Zreda, M., Ferre, T. P. A., Rosolem, R., Zweck, C., Stillman, S., et al. (2012). Measurement depth of the cosmic ray soil moisture probe affected by hydrogen from various sources. *Water Resources Research*, *48*, W08515. https://doi.org/10.1029/2012WR011871

Franz, T. E., Zreda, M., Rosolem, R., & Ferre, T. P. A. (2012). Field validation of a cosmic-ray neutron sensor using a distributed sensor network. *Vadose Zone Journal*, *11*(4). https://doi.org/10.2136/vzj2012.0046

Fu, T. C. (2011). A review on time series data mining. *Engineering Applications of Artificial Intelligence*, *24*(1), 164–181. https://doi.org/10.1016/j.engappai.2010.09.007

Gaiser, P. W., St Germain, K. M., Twarog, E. M., Poe, G. A., Purdy, W., Richardson, D., et al. (2004). The WindSat spaceborne polarimetric microwave radiometer: Sensor description and early orbit performance. *IEEE Transactions on Geoscience and Remote Sensing*, *42*(11), 2347–2361. https://doi.org/10.1109/TGRS.2004.836867

Galeazzi, C., Sacchetti, A., Cisbani, A., & Babini, G. (2008). The PRISMA program. Proceedings of IGARSS 2008. Paper presented at IEEE International Geoscience and Remote Sensing Symposium. Boston, MA, USA, July 6-11.

Gao, H. L., Wood, E. F., Drusch, M., Crow, W., & Jackson, T. J. (2004). Using a microwave emission model to estimate soil moisture from ESTAR observations during SGP99. *Journal of Hydrometeorology*, *5*(1), 49–63. https://doi.org/10.1175/1525-7541(2004)005<0049:UAMEMT>2.0.CO;2

Gao, X. D., Wu, P. T., Zhao, X. N., Shi, Y. G., & Wang, J. W. (2011). Estimating spatial mean soil water contents of sloping jujube orchards using temporal stability. *Agricultural Water Management*, *102*, 66–73. https://doi.org/10.1016/j.agwat.2011.10.007

Gao, Z., Xu, X., Wang, J., Yang, H., Huang, W., & Feng, H. (2013). A method of estimating soil moisture based on the linear decomposition of mixture pixels. *Mathematical and Computer Modelling*, *58*(3-4), 606–613. https://doi.org/10.1016/j.mcm.2011.10.054

Gardner, W. R. (1958). Some steady state solutions of the unsaturated moisture flow equation with application to evaporation from a water table. *Soil Science*, *85*(4), 228–232. https://doi.org/10.1097/00010694-195804000-00006

Global Climate Observing System. (2010). Implementation plan for the global observing system for climate in support of the UNFCCC. (Technical Report WMO/TD No. 1244, 23pp). https://www.wmo.int/pages/prog/gcos/Publications/gcos-92_GIP_ES.pdf.

van Genuchten, M. T. (1980). A closed-form equation for predicting the hydraulic conductivity of unsaturated soils. *Soil Science Society of America Journal*, *44*, 892–898. https://doi.org/10.2136/sssaj1980.03615995004400050002x

Gherboudj, I., Magagi, R., Berg, A. A., & Toth, B. (2011). Soil moisture retrieval over agricultural fields from multi-polarized and multi-angular RADARSAT-2 SAR data. *Remote Sensing of Environment*, *115*(1), 33–43. https://doi.org/10.1016/j.rse.2010.07.011

Ghil, M., & Malanotterizzoli, P. (1991). Data assimilation in meteorology and oceanography. *Advances in Geophysics*, *33*, 141–266. https://doi.org/10.1016/S0065-2687(08)60442-2

Ghose, R., & Slob, E. C. (2006). Quantitative integration of seismic and GPR reflections to derive unique estimates for water saturation and porosity in subsoil. *Geophysical Research Letters*, *33*, L05404. https://doi.org/10.1029/2005GL025376

Gillies, R. R., Kustas, W. P., & Humes, K. S. (1997). A verification of the triangle method for obtaining surface soil water content and energy fluxes from remote measurements of the Normalized Difference Vegetation Index (NDVI) and surface. *International journal of remote sensing*, *18*(15), 3145–3166. https://doi.org/10.1080/014311697217026

Gordon, N. J., Salmond, D. J., & Smith, A. F. M. (1993). Novel approach to nonlinear non-Gaussian Bayesian state estimation. *IEE Proceedings-F Radar and Signal Processing*, *140*(2), 107–113.

Graf, A., Bogena, H. R., Drue, C., Hardelauf, H., Putz, T., Heinemann, G., & Vereecken, H. (2014). Spatiotemporal relations between water budget components and soil water content in a forested tributary catchment. *Water Resources Research*, *50*, 4837–4857. https://doi.org/10.1002/2013wr014516

Graham, C. B., & Lin, H. S. (2011). Controls and frequency of preferential flow occurrence: A 175-event analysis. *Vadose Zone Journal*, *10*(3), 816–831. https://doi.org/10.2136/vzj2010.0119

Grayson, R. B., & Western, A. W. (1998). Towards areal estimation of soil water content from point measurements: Time and space stability of mean response. *Journal of Hydrology*, *207*, 68–82. https://doi.org/10.1016/S0022-1694(98)00096-1

Greifeneder, F., Khamala, E., Sendabo, D., Wagner, W., Zebisch, M., Farah, H., & Notarnicola, C. (2018). Detection of soil moisture anomalies based on Sentinel-1. *Physics and Chemistry of the Earth, Parts A/B/C*. https://doi.org/10.1016/j.pce.2018.11.009

Grote, K., Hubbard, S. S., & Rubin, Y. (2003). Field-scale estimation of volumetric water content using GPR ground wave techniques. *Water Resources Research*, *39*(11), 1321. https://doi.org/10.1029/2003WR002045

Gruber, A., Dorigo, W. A., Crow, W., & Wagner, W. (2017). Triple Collocation-Based Merging of Satellite Soil Moisture Retrievals. *IEEE Transactions on Geoscience and Remote Sensing*, *55*(12), 6780–6792. https://doi.org/10.1109/TGRS.2017.2734070

Gruber, A., Su, C.-H., Zwieback, S., Crow, W. T., Dorigo, W. A., & Wagner, W. (2016). Recent advances in (soil moisture) triple collocation analysis. *International Journal of Applied Earth Observation and Geoinformation*, *45*, 200–211. https://doi.org/10.1016/j.jag.2015.09.002

Guha, A., Jacobs, J. M., Jackson, T. J., Cosh, M. H., Hsu, E. C., & Judge, J. (2003). Soil moisture mapping using ESTAR under dry conditions from the Southern Great Plains Experiment (SGP99). *IEEE Transactions on Geoscience and Remote Sensing*, *41*(10), 2392–2397. https://doi.org/10.1109/TGRS.2003.817187

Guillot, G., Trokiner, A., Darrasse, L., & Saint-Jalmes, H. (1989). Drying of a porous rock monitored by NMR imaging. *Journal of Physics D: Applied Physics*, *22*(11), 1646–1649. https://doi.org/10.1088/0022-3727/22/11/013

Hain, C. R., Crow, W. T., Anderson, M. C., & Mecikalski, J. R. (2012). An ensemble Kalman filter dual assimilation of thermal infrared and microwave satellite observations of soil moisture into the Noah land surface model. *Water Resources Research*, *48*, W11517. https://doi.org/10.1029/2011WR011268

Haining, R. P., Kerry, R., & Oliver, M. A. (2010). Geography, spatial data analysis, and geostatistics: an overview. *Geogrraphical Analysis*, *42*, 7–31. https://doi.org/10.1111/j.1538-4632.2009.00780.x

Han, E., Merwade, V., & Heathman, G. (2012a). Application of data assimilation with the root zone water quality model for soil moisture profile estimation in the upper Cedar Creek, Indiana. *Hydrological Processes*, *26*, 1707–1719. https://doi.org/10.1002/hyp.8292

Han, E., Merwade, V., & Heathman, G. C. (2012b). Implementation of surface soil moisture data assimilation with watershed scale distributed hydrological model. *Journal of hydrology*, *416*, 98–117. https://doi.org/10.1016/j.jhydrol.2011.11.039

Han, X., Franssen, H. J. H., Bello, M. A. J., Rosolem, R., Bogena, H., Alzamora, F. M., et al. (2016). Simultaneous soil moisture and properties estimation for a drip irrigated field by assimilating cosmic-ray neutron intensity. *Journal of Hydrology*, *539*, 611–624. https://doi.org/10.1016/j.jhydrol.2016.05.050

Han, X. J., Franssen, H. J. H., Li, X., Zhang, Y. L., Montzka, C., & Vereecken, H. (2013). Joint assimilation of surface temperature and L-Band microwave brightness temperature in land data assimilation. *Vadose Zone Journal*, *12*(3). https://doi.org/10.2136/vzj2012.0072

Hannachi, A., Jolliffe, I. T., & Stephenson, D. B. (2007). Empirical orthogonal functions and related techniques in atmospheric science: A review. *International Journal of Climatology*, *27*, 1119–1152. https://doi.org/10.1002/joc.1499

Harvey, O. R., & Morgan, C. L. S. (2009). Predicting regional-scale soil variability using single calibrated apparent soil electrical conductivity model. *Soil Science Society of America Journal*, *73*, 164–169. https://doi.org/10.2136/sssaj2008.007

Hasan, S., Montzka, C., Rüdiger, C., Ali, M., Bogena, H. R., & Vereecken, H. (2014). Soil moisture retrieval from airborne L-band passive microwave using high resolution multispectral data. *ISPRS Journal of Photogrammetry and Remote Sensing*, *91*, 59–71. https://doi.org/10.1016/j.isprsjprs.2014.02.005

Hassan-Esfahani, L., Torres-Rua, A., Jensen, A., & McKee, M. (2015). Assessment of surface soil moisture using high-resolution multi-spectral imagery and artificial neural networks. *Remote Sensing*, *7*(3), 2627–2646. https://doi.org/10.3390/rs70302627

Hassanizadeh, S. M., & Gray, W. G. (1979). General conservation equations for multiphase systems. 1. Averaging procedure. *Advances in Water Resources*, *2*, 131–144. https://doi.org/10.1016/0309-1708(79)90025-3

Haubrock, S., Chabrillat, S., Lemmnitz, C., & Kaufmann, H. (2008). Surface soil moisture quantification models from reflectance data under field conditions. *International Journal of Remote Sensing*, *29*, 3–29. https://doi.org/10.1080/01431160701294695

Haubrock, S. N., Chabrillat, S., Kuhnert, M., Hostert, P., & Kaufmann, H. (2008). Surface soil moisture quantification and validation based on hyperspectral data and field measurements. *Journal of Applied Remote Sensing*, *2*(1), 023552. https://doi.org/10.1117/1.3059191

Heathman, G. C., Starks, P. J., Ahuja, L. R., & Jackson, T. J. (2003). Assimilation of surface soil moisture to estimate profile soil water content. *Journal of Hydrology*, *279*, 1–17. https://doi.org/10.1016/S0022-1694(03)00088-X

Heilman, J. L., Kanemasu, E. T., Rosenberg, N. J., & Blad, B. L. (1976). Thermal scanner measurement of canopy temperatures to estimate evapotranspiration. *Remote Sensing of Environment*, *5*, 137–145. https://doi.org/10.1016/0034-4257(76)90044-4

Hillel, D., Krentos, V. D., & Stylianou, Y. (1972). Procedure and test of an internal drainage method for measuring soil hydraulic characteristics in situ. *Soil Science*, *114*(5), 395–400. https://doi.org/10.1097/00010694-197211000-00011

Hirschi, M., Mueller, B., Dorigo, W., & Seneviratne, S. I. (2014). Using remotely sensed soil moisture for land-atmosphere coupling diagnostics: The role of surface vs. root-zone soil moisture variability. *Remote Sensing of Environment*, *154*, 246–252. https://doi.org/10.1016/j.rse.2014.08.030

Hoeben, R., & Troch, P. A. (2000). Assimilation of active microwave observation data for soil moisture profile estimation. *Water Resources Research*, *36*(10), 2805–2819. https://doi.org/10.1029/2000WR900100

Hohenbrink, T. L., & Lischeid, G. (2015). Does textural heterogeneity matter? Quantifying transformation of hydrological signals in soils. *Journal of Hydrology*, *523*, 725–738. https://doi.org/10.1016/j.jhydrol.2015.02.009

Hollmann, R., Merchant, C. J., Saunders, R., Downy, C., Buchwitz, M., Cazenave, A., et al. (2013). The ESA climate change initiative: Satellite data records for essential climate variables. *Bulletin of the American Meteorological Society*, *94*(10), 1541–1552. https://doi.org/10.1175/BAMS-D-11-00254.1

Holmes, J. W. (1955). Calibration and field use of the neutron scattering method of measuring soil water content. *Australian Journal of Applied Science*, *7*, 45–58.

Hoogenboom, G. (1993). The Georgia automated environmental monitoring network. Paper presented at Geordia Water Resources Conference, Georgia, USA.

Hopmans, J. W., Šimunek, J., & Bristow, K. L. (2002). Indirect estimation of soil thermal properties and water flux using heat pulse probe measurements: Geometry and dispersion effects. *Water Resources Research*, *38*(1), 1006. https://doi.org/10.1029/2000WR000071

Huan-Jun, L., Yuan-Zhi, Z., Xin-Le, Z., Bai, Z., Kai-Shan, S., Zong-Ming, W., & Na, T. (2009). Quantitative analysis of moisture effect on black soil reflectance. *Pedosphere*, *19*(4), 532–540. https://doi.org/10.1016/S1002-0160(09)60146-6

Huisman, J. A., Hubbard, S. S., Redman, J. D., & Annan, A. P. (2003). Measuring soil water content with ground penetrating radar: A review. *Vadose Zone Journal*, *2*(4), 476–491. https://doi.org/10.2113/2.4.476

Huisman, J. A., Snepvangers, J., Bouten, W., & Heuvelink, G. B. M. (2002). Mapping spatial variation in surface soil water content: Comparison of ground-penetrating radar and time domain reflectometry. *Journal of Hydrology*, *269*(3–4), 194–207. https://doi.org/10.1016/S0022-1694(02)00239-1

Huisman, J. A., Snepvangers, J. J. J. C., Bouten, W., & Heuvelink, G. B. M. (2003). Monitoring temporal development of spatial soil water content variation: comparison of ground-penetrating radar and time domain reflectometry. *Vadose Zone Journal*, *2*(4), 519–529. https://doi.org/10.2136/vzj2003.5190

Huisman, J. A., Sperl, C., Bouten, W., & Verstraten, J. M. (2001). Soil water content measurements at different scales: accuracy of time domain reflectometry and ground penetrating radar. *Journal of Hydrology*, *245*, 48–58. https://doi.org/10.1016/S0022-1694(01)00336-5

Hummel, J. W., Sudduth, K. A., & Hollinger, S. E. (2001). Soil moisture and organic matter prediction of surface and subsurface soils using an NIR soil sensor. *Computers and Electronics in Agriculture*, *32*(2), 149–165. https://doi.org/10.1016/S0168-1699(01)00163-6

Hunt, A. G., & Idriss, B. (2009). Percolation-based effective conductivity calculations for bimodal distributions of local conductances. *Philosophical Magazine*, *89*, 22–24. https://doi.org/10.1080/14786430802660431

Hupet, F., Trought, M. C. T., Greven, M., Green, S. R., & Clothier, B. E. (2005). Data requirements for identifying macroscopic water stress parameters: A study on grapevines. *Water Resources Reseacrh*, *41*, W06008. https://doi.org/10.1029/2004WR003609

Huth, N. I., & Poulton, P. L. (2007). An electromagnetic induction method for monitoring variation in soil moisture in agroforestry systems. *Soil Research*, *45*(1), 63–72. https://doi.org/10.1071/SR06093

Illston, B. G., Basara, J. B., Fiebrich, C. A., Crawford, K. C., Hunt, E., Fisher, D. K., et al. (2008). Mesoscale monitoring of soil moisture across a statewide network. *Journal of Atmospheric and Oceanic Technology*, *25*(2), 167–182. https://doi.org/10.1175/2007JTECHA993.1

Imaoka, K., Kachi, M., Fujii, H., Murakami, H., Hori, M., Ono, A., et al. (2010). Global change observation mission (GCOM) for monitoring carbon, water cycles, and climate change. *Proceedings of the IEEE*, *98*(5), 717–734. https://doi.org/10.1109/JPROC.2009.2036869

Ines, A. V. M., & Mohanty, B. P. (2008a). Near-surface soil moisture assimilation for quantifying effective soil hydraulic properties under different hydroclimatic conditions. *Vadose Zone Journal*, *7*(1), 39–52. https://doi.org/10.2136/vzj2007.0048

Ines, A. V. M., & Mohanty, B. P. (2008b). Near-surface soil moisture assimilation to quantify effective soil hydraulic properties using genetic algorithm. 1. Conceptual modeling. *Water Resources Research*, *44*, W06422. https://doi.org/10.1029/2007WR005990

Ines, A. V. M., & Mohanty, B. P. (2009). Near-surface soil moisture assimilation to quantify effective soil hydraulic properties using genetic algorithm. 2. With airborne remote sensing during SGP97 and SMEX02. *Water Resources Research*, *45*, W01408. https://doi.org/10.1029/2008WR007022

Jackson, R. D. (1982). Soil moisture inferences from thermal-infrared measurements of vegetation temperatures. *IEEE Transactions on Geoscience and Remote Sensing*, *20*(3), 282–286. https://doi.org/10.1109/TGRS.1982.350444

Jackson, T. J., Bindlish, R., Cosh, M. H., Zhao, T., Starks, P. J., Bosch, D. D., et al. (2012). Validation of Soil Moisture and Ocean Salinity (SMOS) soil moisture over watershed networks in the U.S. *IEEE Transactions on Geoscience and Remote Sensing*, *50*(5), 1530–1543. https://doi.org/10.1109/TGRS.2011.2168533

Jackson, T. J., Cosh, M. H., Bindlish, R., Starks, P. J., Bosch, D. D., Seyfried, M., et al. (2010). Validation of advanced microwave scanning radiometer soil moisture products. *IEEE Transactions on Geoscience and Remote Sensing*, *48*(12), 4256–4272. https://doi.org/10.1109/TGRS.2010.2051035

Jackson, T. J., & Schmugge, T. J. (1995). Surface soil moisture measurement with microwave radiometery. *Acta Astronautica*, *36*(7), 477–482. https://doi.org/10.1016/0094-5765(94)00288-W

Jagdhuber, T., Hajnsek, I., Bronstert, A., & Papathanassiou, K. P. (2013). Soil moisture estimation under low vegetation cover using a multi-angular polarimetric decomposition. *IEEE Transactions on Geoscience and Remote Sensing*, *51*(4), 2201–2215. https://doi.org/10.1109/TGRS.2012.2209433

Jagdhuber, T., Hajnsek, I., & Papathanassiou, P. K. (2015). An iterative generalized hybrid decomposition for soil moisture retrieval under vegetation cover using fully polarimetric SAR. *IEEE Journal of Selected Topics in Applied Earth Observations and Remote Sensing*, *8*(8), 3911–3922. https://doi.org/10.1109/JSTARS.2014.2371468

Jagdhuber, T., Stockamp, J., Hajnsek, I., & Ludwig, R. (2014). Identification of soil freezing and thawing states using SAR polarimetry at C-band. *Remote Sensing*, *6*(3), 2008–2023. https://doi.org/10.3390/rs6032008

Jawson, S. D., & Niemann, J. D. (2007). Spatial patterns from EOF analysis of soil moisture at a large scale and their dependence on soil, land-use, and topographic properties. *Advances in Water Resources*, *30*, 366–381. https://doi.org/10.1016/j.advwatres.2006.05.006

Jaynes, D. B., Novak, J. M., Moorman, T. B., & Cambardella, C. A. (1994). Estimating herbicide partition coefficients from electromagnetic induction measurements. *Journal of Environmental Quality*, *24*, 36–41.

Jonard, F., Weihermüller, L., Jadoon, K. Z., Schwank, M., Vereecken, H., & Lambot, S. (2011). Mapping field-scale soil moisture with L-band radiometer and ground-penetrating radar over bare soil. *IEEE Transactions on Geoscience and Remote Sensing*, *49*, 2863–2875. https://doi.org/10.1109/TGRS.2011.2114890

Jones, S. B., Blonquist, J. M., Robinson, D. A., Rasmussen, V. P., & Or, D. (2005). Standardizing characterization of electromagnetic water content sensors. *Vadose Zone Journal*, *4*(4), 1048–1058. https://doi.org/10.2136/vzj2004.0140

Jones, S. B., Wraith, J. M., & Or, D. (2002). Time domain reflectometry (TDR) measurement principles and Applications. *Hydrological Processes*, *16*, 141–153. https://doi.org/10.1002/hyp.513

Joshi, C., & Mohanty, B. P. (2010). Physical controls of near-surface soil moisture across varying spatial scales in an agricultural landscape during SMEX02. *Water Resources Research*, *46*, W12503. https://doi.org/10.1029/2010WR009152

Kabas, T., Leuprecht, A., Bichler, C., & Kirchengast, G. (2011). WegenerNet climate station network region Feldbach, Austria: Network structure, processing system, and example results. *Advances in Science and Research*, *6*(1), 49–54. https://doi.org/10.5194/asr-6-49-2011

Kabat, P., & Beekma, J. (1994). Water in the unsaturated zone. In H. P. Ritzema (Ed.), *Drainage principles and applications. ILRI publication 16*, (2nd ed.pp. 383–434). Wageningen, The Netherlands: International Institute for Land Reclamation and Improvement.

Kachanoski, R. G., Wesenbeeck, I. V., & Jong, E. D. (1990). Field scale patterns of soil water storage from non-contacting measurements of bulk electrical conductivity. *Canadian Journal of Soil Science*, *70*(3), 537–542.

Kachi, M., Hori, M., Maeda, T., & Imaoka, K. (2014). *Status of validation of AMSR2 on board the GCOM-W1 satellite, Geoscience and Remote Sensing Symposium (IGARSS)*, (). Quebec, Canada: Paper presented at IEEE International Symposium.

Kalnay, E., Kanamitsu, M., Kistler, R., Collins, W., Deaven, D., Gandin, L., et al. (1996). The NCEP/NCAR 40-year reanalysis project. *Bulletin of the American Meteorological Society*, *77*, 437–471. https://doi.org/10.1175/1520-0477(1996)077<0437:TNYRP>2.0.CO;2

Kamai, T., Tuli, A., Kluitenberg, G. J., & Hopmans, J. W. (2008). Soil water flux density measurements near 1 cm/day using an improved heat pulse probe design. *Water Resources Research*, *44*, W00D14. https://doi.org/10.1029/2008WR007036

Karthikeyan, L., Pan, M., Wanders, N., Kumar, D. N., & Wood, E. F. (2017a). Four decades of microwave satellite soil moisture observations: Part 1. A review of retrieval algorithms. *Advances in Water Resources*, *109*, 106–120. https://doi.org/10.1016/j.advwatres.2017.09.006

Karthikeyan, L., Pan, M., Wanders, N., Kumar, D. N., & Wood, E. F. (2017b). Four decades of microwave satellite soil moisture observations: Part 2. Product validation and inter-satellite comparisons. *Advances in Water Resources*, *109*, 236–252. https://doi.org/10.1016/j.advwatres.2017.09.010

Katzberg, S., Torres, O., Grant, M., & Masters, D. (2006). Utilizing calibrated GPS reflected signals to estimate oil reflectivity and dielectric constant: Results from SMEX02. *Remote Sensing of Environment*, *100*(1), 17–28. https://doi.org/10.1016/j.rse.2005.09.015

Kelleners, T. J., Robinson, D. A., Shouse, P. J., Ayars, J. E., & Skaggs, T. H. (2005). Frequency dependence of the complex permittivity and its impact on dielectric sensor calibration in soils. *Soil Science Society of America Journal*, *69*(1), 67–76. https://doi.org/10.2136/sssaj2005.0067

Kerr, Y. H. (2007). Soil moisture from space: Where are we? *Hydrogeology Journal*, *15*(1), 117–120. https://doi.org/10.1007/s10040-006-0095-3

Kerr, Y. H., Al-Yaari, A., Rodríguez-Fernández, N., Parrens, M., Molero, B., Leroux, D., et al. (2016). Overview of SMOS performance in terms of global soil moisture monitoring after six years in operation. *Remote Sensing of Environment.*, *180*, 40, https://doi.org/10.1016/j.rse.2016.02.042–63.

Kerr, Y. H., Waldteufel, P., Richaume, P., Davenport, I., Ferrazzoli, P., & Wigneron, J. -P. (2010). SMOS level 2 processor soil moisture ATBD. (Report prepared by CBSA, UoR, TV and INRA). https://earth.esa.int/documents/10174/1854519/SMOS_L2_SM_ATBD.

Kerr, Y. H., Waldteufel, P., Richaume, P., Wigneron, J. P., Ferrazzoli, P., Mahmoodi, A., et al. (2012). The SMOS soil moisture retrieval algorithm. *IEEE Transactions on Geoscience and Remote Sensing*, *50*(5), 1384–1403. https://doi.org/10.1109/TGRS.2012.2184548

Kerr, Y. H., Waldteufel, P., Wigneron, J.-P., Delwart, S., Cabot, F., Boutin, J., et al. (2010). The SMOS mission: new tool for monitoring key elements of the global water cycle. *Proceedings of the IEEE*, *98*(5), 666–687. https://doi.org/10.1109/JPROC.2010.2043032

Kerr, Y. H., Waldteufel, P., Wigneron, J. P., Martinuzzi, J., Font, J., & Berger, M. (2001). Soil moisture retrieval from space: The Soil Moisture and Ocean Salinity (SMOS) mission. *IEEE Transactions on Geoscience and Remote Sensing*, *39*(8), 1729–1735. https://doi.org/10.1109/36.942551

Khanna, S., Palacios-Orueta, A., Whiting, M. L., Ustin, S. L., Riaño, D., & Litago, J. (2007). Development of angle indexes for soil moisture estimation, dry matter detection and land-cover discrimination. *Remote Sensing of Environment*, *109*(2), 154–165. https://doi.org/10.1016/j.rse.2006.12.018

Kim, H., & Lakshmi, V. (2018). Use of Cyclone Global Navigation Satellite System (CyGNSS) Observations for Estimation of Soil Moisture. *Geophysical Research Letters*, *45*(16), 8272–8282. https://doi.org/10.1029/2018GL078923

Kim, G., & Barros, A. P. (2002). Space-time characterization of soil moisture from passive microwave remotely sensed imagery and ancillary data. *Remote Sensing of Environment*, *81*(2-3), 393–403. https://doi.org/10.1016/S0034-4257(02)00014-7

Kim, S., Liu, Y. Y., Johnson, F. M., Parinussa, R. M., & Sharma, A. (2015). A global comparison of alternate AMSR2 soil moisture products: Why do they differ? *Remote Sensing of Environment*, *161*, 43–62. https://doi.org/10.1016/j.rse.2015.02.002

Kim, S. B., van Zyl, J. J., Johnson, J. T., Moghaddam, M., Tsang, L., Colliander, A., et al. (2017). Surface soil moisture retrieval using the L-Band synthetic aperture radar onboard the Soil Moisture Active–Passive satellite and evaluation at core validation sites. *IEEE Transactions on Geoscience and Remote Sensing*, *55*(4), 1897–1914. https://doi.org/10.1109/TGRS.2016.2631126

King, P. R., & Neuweiler, I. (2002). Probability upscaling. *Computers Geoscience*, *6*(1), 101–114. https://doi.org/10.1023/A:1016533230647

Kiseleva, O., Hübner, C., Brandelik, A., Kalthoff, N., Kohler, M., Königer, F., & Kottmeier, C. (2014). A new approach to investigate soil moisture dynamics by radio waves. Paper presented at TERENO International Conference, Tucson, Arizona.

Klotzsche, A., Jonard, F., Looms, M. C., van der Kruk, J., & Huisman, J. A. (2018). Measuring soil water content with ground penetrating radar: A decade of progress. *Vadose Zone Journal*, *17*(1). https://doi.org/10.2136/vzj2018.03.0052

Kluitenberg, G. J., Ham, J. M., & Bristow, K. L. (1993). Error analysis of the heat pulse method for measuring soil volumetric heat capacity. *Soil Science Society of America Journal*, *57*(6), 1444–1451. https://doi.org/10.2136/sssaj1993.03615995005700060008x

Knight, J. H., & Kluitenberg, G. J. (2004). Simplified computational approach for dual-probe heat-pulse method. *Soil Science Society of America Journal*, *68*(2), 447–449. https://doi.org/10.2136/sssaj2004.4470

Koch, J., Cornelissen, T., Fang, Z., Bogena, H., Diekkrüger, B., Kollet, S., & Stisen, S. (2016). Inter-comparison of three distributed hydrological models with respect to seasonal variability of soil moisture patterns at a small forested catchment. *Journal of Hydrology*, *533*, 234–249. https://doi.org/10.1016/j.jhydrol.2015.12.002

Kohli, M., Schron, M., Zreda, M., Schmidt, U., Dietrich, P., & Zacharias, S. (2015). Footprint characteristics revised for field-scale soil moisture monitoring with cosmic-ray neutrons. *Water Resources Research*, *51*, 5772–5790. https://doi.org/10.1002/2015WR017169

Koike, T., Nakamura, Y., Kaihotsu, I., Davaa, G., Matsuura, N., Tamagawa, K., & Fujii, H. (2004). Development of an advanced microwave scanning radiometer (AMSR-E) algorithm of soil moisture and vegetation water content. *Annual Journal of Hydraulic Engineers*, *48*(2), 217–222. https://doi.org/10.2208/prohe.48.217

Kolassa, J., Reichle, R. H., & Draper, C. S. (2017). Merging active and passive microwave observations in soil moisture data assimilation. *Remote Sensing of Environment*, *191*, 117–130. https://doi.org/10.1016/j.rse.2017.01.015

Komma, J., Blöschl, G., & Reszler, C. (2008). Soil moisture updating by Ensemble Kalman Filtering in real-time flood forecasting. *Journal of Hydrology*, *357*(3-4), 228–242. https://doi.org/10.1016/j.jhydrol.2008.05.020

Kool, J. B., Parker, J. C., & van Genuchten, M. T. (1985). Determining soil hydraulic properties from one-step outflow experiments by parameter estimation: I. *Theory and numerical studies. Soil Science Society of America Journal*, *49*(6), 1348–1354. https://doi.org/10.2136/sssaj1985.03615995004900060004x

Kornelsen, K., & Coulibaly, P. (2014). Comparison of interpolation, statistical, and data-driven methods for imputation of missing values in a distributed soil moisture dataset. *Journal of Hydrological Engineering*, *19*(1), 26–43. https://doi.org/10.1061/(ASCE)HE.1943-5584.0000767

Kornelsen, K. C., & Coulibaly, P. (2013). Advances in soil moisture retrieval from synthetic aperture radar and hydrological applications. *Journal of Hydrology*, *476*, 460–489. https://doi.org/10.1016/j.jhydrol.2012.10.044

Korres, W., Koyama, C. N., Fiener, P., & Schneider, K. (2010). Analysis of surface soil moisture patterns in agricultural landscapes using Empirical Orthogonal Functions. *Hydrology and Earth System Sciences*, *14*(5), 751–764. https://doi.org/10.5194/hess-14-751-2010

Koster, R. D., Brocca, L., Crow, W. T., Burkin, M. S., & De Lannoy, G. J. M. (2016). Precipitation estimation using L-band and C-band soil moisture retrievals. *Water Resources Research*, *52*, 7213–7225. https://doi.org/10.1002/2016WR019024

Koster, R. D., Crow, W. T., Reichle, R. H., & Mahanama, S. P. (2018). Estimating basin-scale water budgets with SMAP soil moisture data. *Water Resources Research*, *54*(7), 4228–4244. https://doi.org/10.1029/2018WR022669

Koster, R. D., Dirmeyer, P. A., Guo, Z., Bonan, G., Chan, E., Cox, P., et al., & GLACE Team (2004). Regions of strong coupling between soil moisture and precipitation. *Science*, *305*(5687), 1138–1140. https://doi.org/10.1126/science.1100217

Koster, R. D., Liu, Q., Mahanama, S. P. P., & Reichle, R. H. (2018). Improved hydrological simulation using SMAP data: Relative impacts of model calibration and data assimilation. *Journal of Hydrometeorology*, *19*(4), 727–741. https://doi.org/10.1175/JHM-D-17-0228.1

Kostov, K. G., & Jackson, T. J. (1993). Estimating profile soil moisture from surface layer measurements: A review. *Proceedings of SPIE*, *1941*, 125–136. https://doi.org/10.1117/12.154681

Kosugi, K. (1994). Three-parameter lognormal distribution model for soil water retention. *Water Resources Research*, *30*(4), 891–901. https://doi.org/10.1029/93WR02931

Kosugi, K. (1996). Lognormal distribution model for unsaturated soil hydraulic properties. *Water Resources Research*, *32*(9), 2697–2703. https://doi.org/10.1029/96WR01776

Koyama, C. N., Liu, H., Takahashi, K., Shimada, M., Watanabe, M., Khuut, T., & Sato, M. (2017). In-Situ Measurement of Soil Permittivity at Various Depths for the Calibration and Validation of Low-Frequency SAR Soil Moisture Models by Using GPR. *Remote Sensing*, *9*, 580. https://doi.org/10.3390/rs9060580

Krieger, G., Hajnsek, I., Papathanassiou, K., Eineder, M., Younis, M., De Zan, F., et al. (2009). The tandem-L mission proposal: monitoring Earth's dynamics with high resolution SAR interferometry. Paper presented at IEEE Radar Conference, Pasadena, CA.

Krieger, G., Moreira, A., Fiedler, H., Hajnsek, I., Werner, M., Younis, M., & Zink, M. (2007). TanDEM-X: A satellite formation for high-resolution SAR interferometry. *IEEE Transactions on Geoscience and Remote Sensing*, *45*(11), 3317–3341. https://doi.org/10.1109/TGRS.2007.900693

Krzeminska, D. M., Steele-Dunne, S. C., Bogaard, T. A., Rutten, M. M., Sailhac, P., & Geraud, Y. (2012). High-resolution temperature observations to monitor soil thermal properties as a proxy for soil moisture condition in clay-shale landslide. *Hydrological Processes*, *26*(14), 2143–2156. https://doi.org/10.1002/hyp.7980

Kubelka, P., & Munk, F. (1931). Ein Beitrag zur Optik der Farbanstriche. *Zeitschrift für Technische Physik*, *12*, 593–601.

Kumar, S. V., Harrison, K. W., Peters-Lidard, C. D., Santanello, J. A. Jr., & Kirschbaum, D. (2014). Assessing the impact of L-Band observations on drought and flood risk estimation: A decision-theoretic approach in an OSSE Environment. *Journal of Hydrometeorology*, *15*(6), 2140–2156. https://doi.org/10.1175/JHM-D-13-0204.1

Kumar, S. V., Reichle, R. H., Harrison, K. W., Peters-Lidard, C. D., Yatheendradas, S., & Santanello, J. A. (2012). A comparison of methods for a priori bias correction in soil moisture data assimilation. *Water Resources Research*, *48*, W03515. https://doi.org/10.1029/2010WR010261

Kumar, S. V., Reichle, R. H., Koster, R. D., Crow, W. T., & Peters-Lidard, C. D. (2009). Role of subsurface physics in the assimilation of surface soil moisture observations. *Journal of Hydrometeorology*, *10*(6), 1534–1547. https://doi.org/10.1175/2009JHM1134.1

Kuorilehto, M., Kohvakka, M., Suhonen, J., Hämäläinen, P., Hännikäinen, M., & Hamalainen, T. D. (2008). *Ultra-low energy wireless sensor networks in practice: Theory, realization and deployment*. John Wiley and Sons.

Kurum, M., Lang, R. H., O'Neill, P. E., Joseph, A. T., Jackson, T. J., & Cosh, M. H. (2011). A first-order radiative transfer model for microwave radiometry of forest canopies at L-band. *IEEE Transactions on Geoscience and Remote Sensing*, *49*(9), 3167–3179. https://doi.org/10.1109/TGRS.2010.2091139

Kweon, S.-K., & Oh, Y. (2014). Estimation of soil moisture and surface roughness from single-polarized radar data for bare soil surface and comparison with dual- and quad-polarization cases. *IEEE Transactions on Geoscience and Remote Sensing*, *52*(7), 4056–4064. https://doi.org/10.1109/TGRS.2013.2279183

Laio, F., Porporato, A., Ridolfi, L., & Rodriguez-Iturbe, I. (2001). Plants in water-controlled ecosystems: Active role in hydrologic processes and response to water stress. *Advances in Water Resources*, *24*(7), 707–723. https://doi.org/10.1016/S0309-1708(01)00005-7

Laiolo, P., Gabellani, S., Campo, L., Silvestro, F., Delogu, F., Rudari, R., et al. (2016). Impact of different satellite soil moisture products on the predictions of a continuous distributed hydrological model. *International Journal of Applied Earth Observation and Geoinformation*, *48*, 131–145. https://doi.org/10.1016/j.jag.2015.06.002

Lambot, S., Slob, E. C., van den Bosch, I., Stockbroeckx, B., & Vanclooster, M. (2004). Modeling of ground-penetrating radar for accurate characterization of subsurface electric properties. *I IEEE Transactions on Geoscience and Remote Sensing*, *42*(11), 2555–2568. https://doi.org/10.1109/TGRS.2004.834800

Lambot, S., Weihermüller, L., Huisman, J. A., Vereecken, H., Vanclooster, M., & Slob, E. C. (2006). Analysis of air-launched ground-penetrating radar techniques to measure the soil surface water content. *Water Resources Research*, *42*, W11420. https://doi.org/10.1029/2006WR00

Larson, K. M., Braun, J. J., Small, E. E., Zavorotny, V. U., Gutmann, E. D., & Bilich, A. L. (2010). GPS multipath and its relation to near-surface soil moisture content. *IEEE Journal of Selected Topic in Applied Earth Observation and Remote Sensing*, *3*(1), 91–99. https://doi.org/10.1109/JSTARS.2009.2033612

Larson, K. M., Small, E. E., Gutmann, E., Bilich, A., Braun, J., & Zavorotny, V. (2008). Use of GPS receivers as a soil moisture network for water cycle studies. *Geophysical Research Letters*, *35*, L24405. https://doi.org/10.1029/2008GL036013

Lau, W. K. M., & Kim, K. M. (2012). The 2010 Pakistan flood and Russian heat wave: Teleconnection of hydrometeorological extremes. *Journal of Hydrometeorology*, *13*(1), 392–403. https://doi.org/10.1175/JHM-D-11-016.1

Le Hégarat-Mascle, S., Zribi, M., Alem, F., Weisse, A., & Loumagne, C. (2002). Soil moisture estimation from ERS/SAR data: Toward an operational methodology. *IEEE Transactions on Geoscience and Remote Sensing*, *40*(12), 2647–2658. https://doi.org/10.1109/TGRS.2002.806994

Lebeau, M., & Konrad, J.-M. (2010). A new capillary and thin film flow model for predicting the hydraulic conductivity of unsaturated porous media. *Water Resources Research*, *46*, W12554. https://doi.org/10.1029/2010WR009092

Lee, J. H., Pellarin, T., & Kerr, Y. H. (2014). Inversion of soil hydraulic properties from the DEnKF analysis of SMOS soil moisture over West Africa. *Agricultural and Forest Meteorology*, *188*, 76–88. https://doi.org/10.1016/j.agrformet.2013.12.009

Lei, S. J., Bian, Z. F., Daniels, J. L., & Dong-lie Liu, D. L. (2014). Improved spatial resolution in soil moisture retrieval at arid mining area using apparent thermal inertia. *Transactions of Nonferrous Metals Society of China*, *24*(6), 1866–1873. https://doi.org/10.1016/S1003-6326(14)63265-9

Lesaignoux, A., Fabre, S., & Briottet, X. (2013). Influence of soil moisture content on spectral reflectance of bare soils in the 0.4–14 μm domain. *International Journal of Remote Sensing*, *34*(7), 2268–2285. https://doi.org/10.1080/01431161.2012.743693

Li, B., & Rodell, M. (2013). Spatial variability and its scale dependency of observed and modeled soil moisture over different climate regions. *Hydrology and Earth System Sciences*, *17*, 1177–1188. https://doi.org/10.5194/hess-17-1177-2013

Li, H., Robock, A., & Wild, M. (2007). Evaluation of Intergovernmental Panel on Climate Change Fourth Assessment soil moisture simulations for the second half of the twentieth century. *Journal of Geophysical Research*, *112*, D06106. https://doi.org/10.1029/2006JD007455

Lievens, H., De Lannoy, G. J. M., Al Bitar, A., Drusch, M., Dumedah, G., Hendricks, H.-J., et al. (2016). Assimilation of SMOS soil moisture and brightness temperature products into a land surface model. *Remote Sensing of Environment*, *180*, 292–304. https://doi.org/10.1016/j.rse.2015.10.033

Lievens, H., Martens, B., Verhoest, N. E. C., Hahn, S., Reichle, R. H., & Miralles, D. G. (2017). Assimilation of global radar backscatter and radiometer brightness temperature observations to improve soil moisture and land evaporation estimates. *Remote Sensing of Environment*, *189*, 194–210. https://doi.org/10.1016/j.rse.2016.06.025

Lievens, H., Reichle, R. H., Liu, Q., De Lannoy, G. J. M., Dunbar, R. S., Kim, S. B., et al. (2017). Joint Sentinel-1 and SMAP data assimilation to improve soil moisture estimates. *Geophysical Research Letters*, *44*, 6145–6153. https://doi.org/10.1002/2017GL073904

Lievens, H., Tomer, S. K., Al Bitar, A., De Lannoy, G. J. M., Drusch, M., Dumedah, G., et al. (2015). SMOS soil moisture assimilation for improved hydrologic simulation in the Murray Darling Basin, Australia. *Remote Sensing of Environment*, *168*, 146–162. https://doi.org/10.1016/j.rse.2015.06.025

Lin, G., Wang, T., & Zheng, X. (2016). Assessing effects of soil hydraulic properties on the temporal stability of absolute soil moisture content and soil moisture anomaly under different climatic conditions. *Environmental Earth Scineces*, *75*(2), 1–14. https://doi.org/10.1007/s12665-015-4968-4

Lin, H. (2006). Temporal Stability of Soil moisture spatial pattern and subsurface preferential flow pathways in the Shale hills catchment. *Vadose Zone Journal*, *5*(1), 317–340. https://doi.org/10.2136/vzj2005.0058

Liu, W., Baret, F., Gu, X., Tong, Q., Zheng, L., & Zhang, B. (2002). Relating soil surface moisture to reflectance. *Remote Sensing of Environment*, *81*, 238–246.

Liu, Y. Y., Dorigo, W. A., Parinussa, R. M., de Jeu, R. A. M., Wagner, W., McCabe, M. F., et al. (2012). Trend-preserving blending of passive and active microwave soil moisture retrievals. *Remote Sensing of Environment*, *123*, 280–297. https://doi.org/10.1016/j.rse.2012.03.014

Liu, Y. Y., Parinussa, R. M., Dorigo, W. A., De Jeu, R. A. M., Wagner, W., van Dijk, A. I. J. M., et al. (2011). Developing an improved soil moisture dataset by blending passive and active microwave satellite-based retrievals. *Hydrology and Earth System Science*, *15*(2), 425–436. https://doi.org/10.5194/hess-15-425-2011

Lobell, D. B., & Asner, G. P. (2002). Moisture effects on soil reflectance. *Soil Science Society of America Journal*, *66*(3), 722–727. https://doi.org/10.2136/sssaj2002.7220

Loew, A., & Mauser, W. (2008). On the disaggregation of passive microwave soil moisture data using a priori knowledge of temporally persistent soil moisture fields. *IEEE Transactions on Geoscience and Remote Sensing*, *46*(3), 819–834. https://doi.org/10.1109/TGRS.2007.914800

Loijens, H. S. (1980). Determination of soil water content from terrestrial gamma radiation measurements. *Water Resources Research*, *16*(3), 565–573. https://doi.org/10.1029/WR016i003p00565

Looms, M. C., Jensen, K. H., Binley, A., & Nielsen, L. (2008). Monitoring unsaturated flow and transport using cross-borehole geophysical methods. *Vadose Zone Journal*, *7*(1), 227–237. https://doi.org/10.2136/vzj2006.0129

Lopez, L. R., Behrens, T., Schmidt, K., Stevens, A., Alexandre, J., Dematte, M., & Scholten, T. (2013). The spectrum-based learner: A new local approach for modeling soil vis–NIR spectra of complex datasets. *Geoderma*, *195-196*, 268–279. https://doi.org/10.1016/j.geoderma.2012.12.014

Lorenc, A. C. (2003). Modelling of error covariances by 4D-Var data assimilation. *Quarterly Journal of the Royal Meteorological Society*, *129*(595), 3167–3182. https://doi.org/10.1256/qj.02.131

Louvet, S., Pellarin, T., Al Bitar, A., Cappelaere, B., Galle, S., Grippa, M., et al. (2015). SMOS soil moisture product evaluation over West-Africa from local to regional scale. *Remote Sensing of Environment*, *156*, 383–394. https://doi.org/10.1016/j.rse.2014.10.005

Lu, L., Franz, T., Robinson, D. A., & Jones, S. B. (2014). Measured and modeled soil moisture compared with cosmic-ray neutron probe estimates in a mixed forest. *Vadose Zone Journal*, *13*, 12. https://doi.org/10.2136/vzj2014.06.0077

Lu, H., Koike, T., & Yang, K. (2014). Improvement of AMSR2 soil moisture algorithm with considering temperature profile effects in dry soil: A case study in Heihe basin. Paper presented at IEEE Geoscience and Remote Sensing Symposium, Quebec, Canada.

Lu, Y., Liu, X., Heitman, J., Horton, R., & Ren, T. (2016). Determining soil bulk density with thermo-time domain reflectometry: A thermal conductivity-based approach. *Soil Science Society of America Journal*, *80*(1), 48–54. https://doi.org/10.2136/sssaj2015.08.0315

Lu, Y., Lu, S., Horton, R., & Ren, T. (2014). An empirical model for estimating soil thermal conductivity from texture, water content, and bulk density. *Soil Science Society of America Journal*, *78*(6), 1859–1868. https://doi.org/10.2136/sssaj2014.05.0218

Luo, L. (2003). Validation of the North American Land Data Assimilation System (NLDAS) retrospective forcing over the southern Great Plains. *Journal of Geophysical Research*, *108*(D22), 8843. https://doi.org/10.1029/2002JD003246

Ma, C., Li, X., & Wang, S. (2017). Soil moisture estimation based on probabilistic inversion over heterogeneous vegetated fields using airborne PLMR brightness temperature. *Hydrology and Earth System Science*, 1–21. https://doi.org/10.5194/hess-2017-34

Magagi, R., Berg, A. A., Goita, K., Belair, S., Jackson, T. J., Toth, B., et al. (2013). Canadian experiment for soil moisture in 2010 (CanEx-SM10): Overview and preliminary results. *IEEE Transactions on Geoscience and Remote Sensing*, *51*(1), 347–363. https://doi.org/10.1109/TGRS.2012.2198920

Mahanama, S. P., Koster, R. D., Reichle, R. H., & Zubair, L. (2008). The role of soil moisture initialization in subseasonal and seasonal streamflow prediction—A case study in Sri Lanka. *Advances in Water Resources*, *31*(10), 1333–1343. https://doi.org/10.1016/j.advwatres.2008.06.004

Mahmood, R., & Hubbard, K. G. (2007). Relationship between soil moisture of near surface and multiple depths of the root zone under heterogeneous land uses and varying hydroclimatic conditions. *Hydrological Processes*, *21*, 3449–3462.

Mallick, K., Bhattacharya, B. K., & Patel, N. K. (2009). Estimating volumetric surface moisture content for cropped soils using a soil wetness index based on surface temperature and NDVI. *Agricultural and Forest Meteorology*, *149*(8), 1327–1342. https://doi.org/10.1016/j.agrformet.2009.03.004

Manfreda, S., Lacava, T., Onorati, B., Pergola, N., Di Leo, M., Margiotta, M. R., & Tramutoli, V. (2011). On the use of AMSU-based products for the description of soil water content at basin scale. *Hydrology and Earth System Sciences*, *15*(9), 2839–2852. https://doi.org/10.5194/hess-15-2839-2011

Mao, Y. Y., Williamson, M., & Wechsler, R. H. (2015). The dependence of subhalo abundance on halo concentration. *The Astrophysical Journal*, *810*(1), 21. https://doi.org/10.1088/0004-637X/810/1/21

Martinez, C., Hancock, G. R., Kalma, J. D., & Wells, T. (2008). Spatio-temporal distribution of near-surface and root zone soil moisture at the catchment scale. *Hydrological Processes*, *22*(14), 2699–2714. https://doi.org/10.1002/hyp.6869

Martinez, G., Vanderlinden, K., Ordóñez, R., & Muriel, J. L. (2009). Can apparent electrical conductivity improve the spatial characterization of soil organic carbon? *Vadose Zone Journal*, *8*(3), 586–593. https://doi.org/10.2136/vzj2008.0123

Martinez-Fernandez, J., & Ceballos, A. (2005). Mean soil moisture estimation using temporal stability analysis. *Journal of Hydrology*, *312*(1-4), 28–38. https://doi.org/10.1016/j.jhydrol.2005.02.007

Martinez-Fernandez, J., Gonzalez-Zamora, A., Sanchez, N., Gumuzzio, A., & Herrero-Jimenez, C. M. (2016). Satellite soil moisture for agricultural drought monitoring: Assessment of the SMOS derived Soil Water Deficit Index. *Remote Sensing of Environment*, *177*, 277–286. https://doi.org/10.1016/j.rse.2016.02.064

Matgen, P., Heitz, S., Hasenauer, S., Hissler, C., Brocca, L., Hoffmann, L., et al. (2012). On the potential of METOP ASCAT-derived soil wetness indices as a new aperture for hydrological monitoring and prediction: A field evaluation over Luxembourg. *Hydrological Processes*, *26*(15), 2346–2359. https://doi.org/10.1002/hyp.8316

Mattikalli, N. M., Engman, E. T., Jackson, T. J., & Ahuja, L. R. (1998). Microwave remote sensing of temporal variations of brightness temperature and near-surface soil water content during a watershed-scale field experiment, and its application to the estimation of soil physical properties. *Water Resources Research*, *34*(9), 2289–2299. https://doi.org/10.1029/98WR00553

McCabe, M. F., Gao, H., & Wood, E. F. (2005). Evaluation of AMSR-E-derived soil moisture retrievals using ground-based and PSR airborne data during SMEX02. *Journal of Hydrometeorology*, *6*(6), 864–877. https://doi.org/10.1175/JHM463.1

McNairn, H., Jackson, T. J., Wiseman, G., Belair, S., Berg, A., Bullock, P., et al. (2015). The soil moisture active passive validation experiment 2012 (SMAPVEX12): Prelaunch calibration and validation of the SMAP soil moisture algorithms. *IEEE Transactions on Geoscience and Remote Sensing*, *53*(5), 2784–2801. https://doi.org/10.1109/TGRS.2014.2364913

McNairn, H., Merzouki, A., Pacheco, A., & Fitzmaurice, J. (2012). Monitoring soil moisture to support risk reduction for the agriculture sector using RADARSAT-2. *IEEE Journal of Selected Topics in Applied Earth Observations and Remote Sensing*, *5*(3), 824–834. https://doi.org/10.1109/JSTARS.2012.2192416

McNeill, J. D. (1980). Electromagnetic terrain conductivity measurement at low induction numbers. In *Technical Note TN-6*. Geonics Limited, Mississauga, Ontario: Canada pp. 1–15.

McPherson, R. A., Fiebrich, C. A., Crawford, K. C., Kilby, J. R., Grimsley, D. L., Martinez, J. E., et al. (2007). Statewide monitoring of the mesoscale environment: A technical update on the Oklahoma Mesonet. *Journal of Atmospheric and Oceanic Technology*, *24*(3), 301–321. https://doi.org/10.1175/JTECH1976.1

Mecklenburg, S., Drusch, M., Kaleschke, L., Rodriguez-Fernandez, N., Reul, N., Kerr, Y., et al. (2016). ESA's soil moisture and ocean salinity mission: From science to operational applications. *Remote Sensing of Environment.*, *180*, 3–18. https://doi.org/10.1016/j.rse.2015.12.025

Merlin, O., Escorihuela, M. J., Mayoral, M. A., Hagolle, O., Al Bitar, A., & Kerr, Y. (2013). Self-calibrated evaporation-based disaggregation of SMOS soil moisture: An evaluation study at 3 km and 100 m resolution in Catalunya, Spain. *Remote Sensing of Environment*, *130*, 25–38. https://doi.org/10.1016/j.rse.2012.11.008

Merlin, O., Rudiger, C., Al Bitar, A., Richaume, P., Walker, J. P., & Kerr, Y. H. (2012). Disaggregation of SMOS soil moisture in southeastern Australia. *IEEE Transactions on Geoscience and Remote Sensing*, *50*(5), 1556–1571. https://doi.org/10.1109/TGRS.2011.2175000

Merlin, O., Walker, J., Chehbouni, A., & Kerr, Y. (2008). Towards deterministic downscaling of SMOS soil moisture using MODIS derived soil evaporative efficiency. *Remote Sensing of Environment*, *112*(10), 3935–3946. https://doi.org/10.1016/j.rse.2008.06.012

Merz, S., Pohlmeier, A., Balcom, B. J., Enjilela, R., & Vereecken, H. (2016). Drying of a natural soil under evaporative conditions: A comparison of different magnetic resonance methods. *Applied Magnetic Resonance*, *47*(2), 121–138. https://doi.org/10.1007/s00723-015-0736-6

Merz, S., Pohlmeier, A., Vanderborght, J., van Dusschoten, D., & Vereecken, H. (2014). Moisture profiles of the upper soil layer during evaporation monitored by NMR. *Water Resources Research*, *50*, 5184–5195. https://doi.org/10.1002/2013WR014809

Michel, S., Lefevre-Fonollosa M.-J., & Hosford S. (2010). HYPXIM: A hyperspectral satellite defined for science, security and defense users. Paper presented at 2010 Workshop Hyperspectral. Frascati, Italy.

Miernecki, M., Wigneron, J.-P., Lopez-Baeza, E., Kerr, Y., De Jeu, R., De Lannoy, G. J. M., et al. (2014). Comparison of SMOS and SMAP soil moisture retrieval approaches using tower-based radiometer data over a vineyard field. *Remote Sensing of Environment*, *154*, 89–101.

Miller, E. E., & Miller, R. D. (1956). Physical theory for capillary flow phenomena. *Journal of Applied Physics*, *27*, 324–332. https://doi.org/10.1063/1.1722370

Minet, J., Bogaert, P., Vanclooster, M., & Lambot, S. (2012). Validation of ground penetrating radar full-waveform inversion for field scale soil moisture mapping. *Journal of Hydrology*, *424*, 112–123. https://doi.org/10.1016/j.jhydrol.2011.12.034

Miralles, D. G., Crow, W. T., & Cosh, M. H. (2010). Estimating spatial sampling errors in coarse-scale soil moisture estimates derived from point-scale observations. *Journal of Hydrometeorology*, *11*(6), 1423–1429. https://doi.org/10.1175/2010JHM1285.1

Mironov, V. L., Kosolapova, L. G., & Fomin, S. V. (2009). Physically and mineralogically based spectroscopic dielectric model for moist soils. *IEEE Transactions on Geoscience and Remote Sensing*, *47*(7), 2059–2070. https://doi.org/10.1109/TGRS.2008.2011631

Mittelbach, H., & Seneviratne, S. I. (2012). A new perspective on the spatio-temporal variability of soil moisture: Temporal dynamics versus time-invariant contributions. *Hydrology and Earth System Sciences*, *16*(7), 2169–2179. https://doi.org/10.5194/hess-16-2169-2012

Mladenova, I. E., Jackson, T. J., Njoku, E., Bindlish, R., Chan, S., Cosh, M. H., et al. (2014). Remote monitoring of soil moisture using passive microwave-based techniques—Theoretical basis and overview of selected algorithms for AMSR-E. *Remote Sensing of Environment*, *144*, 197–213. https://doi.org/10.1016/j.rse.2014.01.013

Mo, K. C., & Lettenmaier, D. P. (2014). Objective drought classification using multiple land surface models. *Journal of Hydrometeorology*, *15*(3), 990–1010. https://doi.org/10.1175/JHM-D-13-071.1

Mo, T., Choudhury, B. J., Schmugge, T. J., Wang, J. R., & Jackson, T. J. (1982). A model for microwave emission from vegetation-covered fields. *Journal of Geophysical Research*, *87*(C13), 11229–11237. https://doi.org/10.1029/JC087iC13p11229

Moghadas, D., Andr'e, F., Slob, E. C., Vereecken, H., & Lambot, S. (2010). Joint full-waveform analysis of off-ground zero-offset ground penetrating radar and electromagnetic induction synthetic data for estimating soil electrical properties. *Geophysical Journal International*, *182*, 1267–1278. https://doi.org/10.1111/j.1365-246X.2010.04706.x

Moghaddam, M., Saatchi, S. S., & Cuenca, R. H. (2000). Estimating sub-canopy soil moisture with radar. *Journal of Geophysical Research*, *105*(D11), 14899–14911.

Mohanty, B. P. (2013). Soil hydraulic property estimation using remote sensing: A review. *Vadose Zone Journal*, *12*(4), 1–9. https://doi.org/10.2136/vzj2013.06.0100

Mohanty, B. P., Cosh, M. H., Lakshmi, V., & Montzka, C. (2017). Soil moisture remote sensing: State-of-the-science. *Vadose Zone Journal*, *16*(1). https://doi.org/10.2136/vzj2016.10.0105.2017

Mohanty, B. P., & Skaggs, T. H. (2001). Spatio-temporal evolution and time-stable characteristics of soil moisture within remote sensing footprints with varying soil, slope, and vegetation. *Advances in Water Resources*, *24*(9-10), 1051–1067. https://doi.org/10.1016/S0309-1708(01)00034-3

Molero, B., Merlin, O., Malbéteau, Y., al Bitar, A., Cabot, F., Stefan, V., et al. (2016). SMOS disaggregated soil moisture product at 1 km resolution: Processor overview and first validation results. *Remote Sensing of Environment*, *180*, 361–376. https://doi.org/10.1016/j.rse.2016.02.045

Montzka, C., Bogena, H., Jagdhuber, T., Hajnsek, I., Horn, R., Reigber, A., et al. (2014). Active and passive L-band microwave remote sensing for soil moisture—A test-bed for SMAP fusion algorithms. Paper presented at IEEE Geoscience and Remote Sensing Symposium, Quebec, Canada.

Montzka, C., Bogena, H. R., Zreda, M., Monerris, A., Morrison, R., Muddu, S., & Vereecken, H. (2017). Validation of spaceborne and modelled surface soil moisture products with cosmic-ray neutron probes. *Remote Sensing*, *9*(2), 103. https://doi.org/10.3390/rs9020103

Montzka, C., Grant, J. P., Moradkhani, H., Franssen, H. J. H., Weihermuller, L., Drusch, M., & Vereecken, H. (2013). Estimation of radiative transfer parameters from L-Band passive microwave brightness temperatures using advanced data assimilation. *Vadose Zone Journal*, *12*(3). https://doi.org/10.2136/vzj2012.0040

Montzka, C., Herbst, M., Weihermüller, L., Verhoef, A., & Vereecken, H. (2017). A global data set of soil hydraulic properties and sub-grid variability of soil water retention and hydraulic conductivity curves. *Earth System Science Data*, *9*, 529–543. https://doi.org/10.5194/essd-9-529-2017

Montzka, C., Jagdhuber, T., Horn, R., Bogena, H. R., Hajnsek, I., Reigber, A., & Vereecken, H. (2016). Investigation of SMAP fusion algorithms with airborne active and passive L-band microwave remote sensing. *IEEE Transactions on Geoscience and Remote Sensing*, *54*(7), 3878–3889. https://doi.org/10.1109/TGRS.2016.2529659

Montzka, C., Moradkhani, H., Weihermüller, L., Hendricks Franssen, H.-J., Canty, M., & Vereecken, H. (2011). Hydraulic parameter estimation by remotely-sensed top soil moisture observations with the particle filter. *Journal of Hydrology*, *399*(3-4), 410–421. https://doi.org/10.1016/j.jhydrol.2011.01.020

Montzka, C., Pauwels, V. R. N., Han, X., Hendricks Franssen, H.-J., & Vereecken, H. (2012). Multiscale and multivariate data assimilation in terrestrial systems: A review. *Sensors*, *12*, 6291–16333. https://doi.org/10.3390/s121216291

Montzka, C., Rötzer, K., Bogena, H. R., Sanchez, N., & Vereecken, H. (2018). A new soil moisture downscaling approach for SMAP, SMOS, and ASCAT by predicting sub-grid variability. *Remote Sensing*, *10*(3), 427. https://doi.org/10.3390/rs10030427

Moradkhani, H., Hsu, K. L., Gupta, H., & Sorooshian, S. (2005). Uncertainty assessment of hydrologic model states and parameters: Sequential data assimilation using the particle filter. *Water Resources Research*, *41*, W05012. https://doi.org/10.1029/2004WR003604

Moran, M. S., Clarke, T. R., Inoue, Y., & Vidal, A. (1994). Estimating crop water deficit using the relation between surface-air temperature and spectral vegetation index. *Remote sensing of environment*, *49*(3), 246–263. https://doi.org/10.1016/0034-4257(94)90020-5

Mori, Y., Hopmans, J. W., Mortensen, A. P., & Kluitenberg, G. J. (2003). Multi-functional heat pulse probe for the simultaneous measurement of soil water content, solute concentration, and heat transport parameters. *Vadose Zone Journal*, *2*(4), 561–571. https://doi.org/10.2113/2.4.561

Muller, E., & Decamps, H. (2000). Modeling soil moisture-reflectance. *Remote Sensing of Environment*, *76*, 173–180. https://doi.org/10.1016/S0034-4257(00)00198-X

Naeimi, V., Bartalis, Z., & Wagner, W. (2009). ASCAT soil moisture: an assessment of the data quality and consistency with the ERS scatterometer heritage. *Journal of Hydrometeorology*, *10*, 555–563. https://doi.org/10.1175/2008JHM1051.1

Naeimi, V., Scipal, K., Bartalis, Z., Hasenauer, S., & Wagner, W. (2009). An improved soil moisture retrieval algorithm for ERS and METOP scatterometer observations. *IEEE Transactions on Geoscience and Remote Sensing*, *47*, 1999–2013. https://doi.org/10.1109/TGRS.2008.2011617

Narayan, U., Lakshmi, V., & Jackson, T. J. (2006). High-resolution change estimation of soil moisture using L-band radiometer and radar observations made during the SMEX02 experiments. *IEEE Transactions on Geoscience and Remote Sensing*, *44*(6), 1545–1554. https://doi.org/10.1109/TGRS.2006.871199

Neema, D. L., Shah, A., & Patel, A. N. (1987). A statistical optical model for light reflection and penetration through sand. *International Journal of Remote Sensing*, *8*(8), 1209–1217. https://doi.org/10.1080/01431168708954765

Neuweiler, I., & Cirpka, O. A. (2005). Homogenization of Richards equation in permeability fields with different connectivities. *Water Resources Research*, *41*, W02009. https://doi.org/10.1029/2004WR003329

Neuweiler, I., & Vogel, H. J. (2007). Upscaling for unsaturated flow for non-Gaussian heterogeneous porous media. *Water Resources Research*, *43*, W03443. https://doi.org/10.1029/2005WR004771

Niclòs, R., Rivas, R., García-Santos, V., Doña, C., Valor, E., Holzman, M., et al. (2016). SMOS Level-2 soil moisture product evaluation in rain-fed croplands of the Pampean region of Argentina. *IEEE Transactions on Geoscience and Remote Sensing*, *54*(1), 499–512. https://doi.org/10.1109/TGRS.2015.2460332

Nied, M., Hundecha, Y., & Merz, B. (2013). Flood-initiating catchment conditions: A spatio-temporal analysis of large-scale soil moisture patterns in the Elbe River basin. *Hydrology and Earth System Sciences*, *17*, 1401–1414. https://doi.org/10.5194/hess-17-1401-2013

Njoku, E., & Entekhabi, D. (1996). Passive microwave remote sensing of soil moisture. *Journal of Hydrology*, *184*, 101–129. https://doi.org/10.1016/0022-1694(95)02970-2

Njoku, E. G., Ashcroft, P., Chan, T. K., & Li, L. (2005). Global survey and statistics of radio-frequency interference in AMSR-E land observations. *IEEE Transactions on Geoscience and Remote Sensing*, *43*(5), 938–947. https://doi.org/10.1109/TGRS.2004.837507

Njoku, E. G., Jackson, T. J., Lakshmi, V., Chan, T. K., & Nghiem, S. V. (2003). Soil moisture retrieval from AMSR-E. *IEEE Transations on Geoscience and Remote Sensing*, *41*, 215–229. https://doi.org/10.1109/TGRS.2002.808243

Njoku, E. G., Wilson, W. J., Yueh, S. H., Dinardo, S. J., Li, F. K., Jackson, T. J., et al. (2002). Observations of soil moisture using a passive and active low-frequency microwave airborne sensor during SGP99. *IEEE Transactions on Geoscience and Remote Sensing*, *40*(12), 2659–2673. https://doi.org/10.1109/TGRS.2002.807008

O'Neill, P. E., Joseph, A., Nelson, R., Cosh, M. H., Jackson, T. J., Lang, R. H., et al. (2007). ComRAD active/passive microwave measurement of tree canopies. Proceeding in IEEE International Geoscience and Remote Sensing Symposium, 1420–1423. https://doi.org/10.1109/IGARSS.2007.4423073.

Ochsner, T. E., Cosh, M. H., Cuenca, R. H., Dorigo, W. A., Draper, C. S., Hagimoto, Y., et al. (2013). State of the art in large-scale soil moisture monitoring. *Soil Science Society of America Journal*, *77*(6), 1888–1919. https://doi.org/10.2136/sssaj2013.03.0093

Ochsner, T. E., Horton, R., & Ren, T. (2003). Use of the dual-probe heat-pulse technique to monitor soil water content in the vadose zone. *Vadose Zone Journal*, *2*, 572–579. https://doi.org/10.2113/2.4.572

Oh, Y. (2006). Robust inversion technique for retrieving soil moisture from multi-polarized backscatter of bare surface. *Electronics letters*, *42*(7), 414–415. https://doi.org/10.1049/el:20064083

Oh, Y., Sarabandi, K., & Ulaby, F. T. (2002). Semi-empirical model of the ensemble-averaged differential Mueller matrix for microwave backscattering from bare soil surfaces. *IEEE Transactions on Geoscience and Remote Sensing*, *40*(6), 1348–1355. https://doi.org/10.1109/TGRS.2002.800232

Oliva, R., Daganzo, E., Kerr, Y. H., Mecklenburg, S., Nieto, S., Richaume, P., & Gruhier, C. (2012). SMOS radio frequency interference scenario: Status and actions taken to improve the RFI environment in the 1400-1427 MHz passive band. *IEEE Transactions on Geoscience and Remote Sensing*, *50*(5). https://doi.org/10.1109/TGRS.2012.2182775

Oltra-Carrio, R., Baup, F., Fabre, S., Fieuzal, R., & Briottet, X. (2015). Improvement of soil moisture retrieval from hyperspectral VNIR-SWIR data using clay content information: From laboratory to field experiments. *Remote Sensing*, *7*(3), 3184–3205. https://doi.org/10.3390/rs70303184

Or, D., Lehmann, P., & Assouline, S. (2015). Natural length scales define the range of applicability of the Richards equation for capillary flows. *Water Resources Research*, *51*, 7130–7144. https://doi.org/10.1002/2015WR017034

Owe, M., de Jeu, R., & Holmes, T. (2008). Multi-sensor historical climatology of satellite-derived global land surface moisture. *Journal of Geophysical Research*, *113*, F01002. https://doi.org/10.1029/2007JF000769

Owe, M., de Jeu, R. A. M., & Walker, J. (2001). A methodology for surface soil moisture and vegetation optical depth retrieval using the microwave polarization difference index. *IEEE Transactions on Geoscience and Remote Sensing*, *39*, 1643–1694. https://doi.org/10.1109/36.942542

Pachepsky, Y. A., Guber, A. K., & Jacques, D. (2005). Temporal persistance in vertical distribution of soil moisture contents. *Soil Science Society of America Journal*, *69*, 347–352. https://doi.org/10.2136/sssaj2005.0347

Paetzold, R. F., Matzkanin, G. A., & De Los Santos, A. (1985). Surface soil water content measurement using pulsed nuclear magnetic resonance techniques. *Soil Science Society of America Journal*, *49*(3), 537–540. https://doi.org/10.2136/sssaj1985.03615995004900030001x

Paloscia, S., Pettinato, S., Santi, E., Notarnicola, C., Pasolli, L., & Reppucci, A. (2013). Soil moisture mapping using Sentinel-1 images: Algorithm and preliminary validation. *Remote Sensing of Environment*, *134*, 234–248. https://doi.org/10.1016/j.rse.2013.02.027

Pan, M., Cai, X. T., Chaney, N. W., Entekhabi, D., & Wood, E. F. (2016). An initial assessment of SMAP soil moisture retrievals using high-resolution model simulations and in situ observations. *Geophysical Research Letters*, *43*, 9662–9668. https://doi.org/10.1002/2016GL069964

Pan, M., Sahoo, A. K., Wood, E. F., Al Bitar, A., Leroux, D., & Kerr, Y. H. (2012). An initial assessment of SMOS derived soil moisture over the continental United States. *IEEE Journal of Selected Topics in Applied Earth Observations and Remote Sensing*, *5*(5), 1448–1457. https://doi.org/10.1109/JSTARS.2012.2194477

Panciera, R., Walker, J. P., Jackson, T. J., Gray, D. A., Tanase, M. A., Ryu, D., et al. (2014). The soil moisture active passive experiments (SMAPEx): Toward soil moisture retrieval from the SMAP mission. *IEEE Transactions on Geoscience and Remote Sensing*, *52*(1), 490–507. https://doi.org/10.1109/TGRS.2013.2241774

Panciera, R., Walker, J. P., Kalma, J. D., Kim, E. J., Saleh, K., & Wigneron, J. P. (2009). Evaluation of the SMOS L-MEB passive microwave soil moisture retrieval algorithm. *Remote Sensing of Environment*, *113*(2), 435–444. https://doi.org/10.1016/j.rse.2008.10.010

Parinussa, R. M., Holmes, T. R., Wanders, N., Dorigo, W. A., & de Jeu, R. A. (2014). A preliminary study towards consistent soil noisture from AMSR2. *Journal of Hydrometeorology*, *16*(2), 932–947. https://doi.org/10.1175/JHM-D-13-0200.1

Parrella, G., Hajnsek, I., & Papathanassiou, K. P. (2016). Polarimetric decomposition of L-band PolSAR backscattering over the Austfonna ice cap. *IEEE Transactions on Geoscience and Remote Sensing*, *54*(3), 1267–1281. https://doi.org/10.1109/TGRS.2015.2477168

Parrens, M., Mahfouf, J. F., Barbu, A. L., & Calvet, J. C. (2014). Assimilation of surface soil moisture into a multilayer soil model: design and evaluation at local scale. *Hydrology and Earth System Sciences*, *18*(2), 673–689. https://doi.org/10.5194/hess-18-673-2014

Parrens, M., Wigneron, J.-P., Richaume, P., Mialon, A., Al Bitar, A., Fernandez-Moran, R., et al. (2016). Global-scale surface roughness effects at L-band as estimated from SMOS observations. *Remote Sensing of Environment*, *181*, 122–136. https://doi.org/10.1016/j.rse.2016.04.006

Paulik, C., Naeimi, V., Dorigo, W., & Kidd, R. (2012). A global validation of the ASCAT Soil Water Index (SWI) with in situ data from the International Soil Moisture Network. *International Journal of Applied Earth Observation and Geoformation*, *30*(1), 10189. https://doi.org/10.1016/j.jag.2014.01.007

Paulik, C., Wouter, D., Wolgang, W., & Richard, W. (2014). Validation of the ASCAT Soil Water Index using in situ data from the International Soil Moisture Network. *International Journal of Applied Earth Observations and Geoinformation*, *30*, 1–8. https://doi.org/10.1016/j.jag.2014.01.007

Pauwels, V. R., Hoeben, R., Verhoest, N. E., & De Troch, F. P. (2001). The importance of the spatial patterns of remotely sensed soil moisture in the improvement of discharge predictions for small-scale basins through data assimilation. *Journal of Hydrology*, *251*(1), 88–102. https://doi.org/10.1016/S0022-1694(01)00440-1

Peck, E., Carroll, T., & Vandermark, S. (1980). Operational aerial snow surveying in the United States. *IEEE Transactions on Geoscience and Remote Sensing*, *6*, 930–936. https://doi.org/10.1109/TGRS.1986.289708

Peck, E. L., Bissell, V. C., Jones, E. B., & Burge, D. L. (1971). Evaluation of snow water equivalent by airborne measurement of passive terrestrial gamma radiation. *Water Resources Research*, *7*(5), 1151–1159. https://doi.org/10.1029/WR007i005p01151

Peischl, S., Walker, J. P., Rüdiger, C., Ye, N., Kerr, Y. H., Kim, E., et al. (2012). The AACES field experiments: SMOS calibration and validation across the Murrumbidgee River catchment. *Hydrology and Earth System Sciences*, *16*(6), 1697–1708. https://doi.org/10.5194/hess-16-1697-2012

Peischl, S., Walker, J. P., Ye, N., Ryu, D., & Kerr, Y. (2014). Sensitivity of multi-parameter soil moisture retrievals to incidence angle configuration. *Remote Sensing of Environment*, *143*, 64–72. https://doi.org/10.1016/j.rse.2013.11.019

Pellarin, T., Ali, A., Chopin, F., Jobard, I., & Berges, J. C. (2008). Using spaceborne surface soil moisture to constrain satellite precipitation estimates over West Africa. *Geophysical Research Letters*, *35*, L02813. https://doi.org/10.1029/2007GL032243

Pellenq, J., Kalma, J., Boulet, G., Saulnier, G. M., Wooldridge, S., Kerr, Y. H., & Chehbouni, A. (2003). A disaggregation scheme for soil moisture based on topography and soil depth. *Journal of Hydrology*, *276*(1), 112–127. https://doi.org/10.1016/S0022-1694(03)00066-0

Peng, J., Loew, A., Merlin, O., & Verhoest, N. E. C. (2016). A review of spatial downscaling of satellite remotely sensed soil moisture. *Reviews of Geophysics*, *55*, 341–366. https://doi.org/10.1002/2016RG000543

Peng, J., Shen, H., & Wu, J. S. (2013). Soil moisture retrieving using hyperspectral data with the application of wavelet analysis. *Environmental Earth Science*, *69*(1), 279–288. https://doi.org/10.1007/s12665-012-1955-x

Peplinski, N. R., Ulaby, F. T., & Dobson, M. C. (1995). Dielectric properties of soils in the 0.3-1.3-GHz range. *IEEE Transactions on Geoscience and Remote Sensing*, *33*(3), 803–807. https://doi.org/10.1109/36.387598

Perry, M. A., & Niemann, J. D. (2008). Generation of soil moisture patterns at the catchment scale by EOF interpolation. *Hydrology and Earth System Science*, *12*, 39–53. https://doi.org/10.5194/hess-12-39-2008

Peters, A., & Durner, W. (2008). A simple model for describing hydraulic conductivity in unsaturated porous media accounting for film and capillary flow. *Water Resources Research*, *44*, W11417. https://doi.org/10.1029/2008WR007136

Petropoulos, G. P., Griffiths, H. M., Dorigo, W., Xaver, A., & Gruber, A. (2013). Surface soil moisture estimation: Significance, controls and conventional measurement techniques. In G. P. Petropoulos (Ed.), *Remote sensing of energy fluxes and soil moisture content* (Chapter 2, pp. 29–48). Taylor and Francis.

Petropoulos, G. P., Ireland, G., & Barrett, B. (2015). Surface soil moisture retrievals from remote sensing: Current status, products and future trends. *Physics and Chemistry of the Earth*, *83–84*, 36–56. https://doi.org/10.1016/j.pce.2015.02.009

Philpot, W. D. (2010). Spectral reflectance of wetted soils. Paper presented at Art, Science and Applications of Reflectance Spectroscopy (ASARS) Conference. Boulder CO. https://doi.org/10.13140/2.1.2306.0169.

Pierdicca, N., Fascetti, F., Pulvirenti, L., Crapolicchio, R., & Muñoz-Sabater, J. (2015). Analysis of ASCAT, SMOS, in-situ and land model soil moisture as a regionalized variable over Europe and North Africa. *Remote Sensing of Environment*, *170*, 280–289. https://doi.org/10.1016/j.rse.2015.09.005

Pierdicca, N., Pulvirenti, L., & Pace, G. (2014). A prototype software package to retrieve soil moisture from sentinel-1 data by using a Bayesian multitemporal algorithm. *IEEE Journal of Selected Topic in Applied Earth Observations and Remote Sensing*, *7*, 153–166. https://doi.org/10.1109/JSTARS.2013.2257698

Piles, M., Camps, A., Vall-Llossera, M., Corbella, I., Panciera, R., Rudiger, C., et al. (2011). Downscaling SMOS-derived soil moisture using MODIS visible/infrared data. *IEEE Transactions on Geoscience and Remote Sensing*, *49*(9), 3156–3166. https://doi.org/10.1109/TGRS.2011.2120615

Piles, M., Entekhabi, D., & Camps, A. (2009). A change detection algorithm for retrieving high-resolution soil moisture from SMAP radar and radiometer observations. *IEEE Transactions on Geoscience and Remote Sensing*, *47*, 4125–4131. https://doi.org/10.1109/Tgrs.2009.2022088

Piles, M., Sánchez, N., Vall-llossera, M., Camps, A., Martínez-Fernández, J., Martinez, J., & Gonzalez-Gambau, V. (2014). A downscaling approach for SMOS land observations: Evaluation of high-resolution soil moisture maps over the Iberian Peninsula. *IEEE Journal of Selected Topics in Applied Earth Observations and Remote Sensing*, *7*(9), 3845–3857. https://doi.org/10.1109/JSTARS.2014.2325398

Posner, A. J., & Georgakakos, K. P. (2015). Soil moisture and precipitation thresholds for real-time landslide prediction in El Salvador. *Landslides*, *12*(6), 1179–1196. https://doi.org/10.1007/s10346-015-0618-x

Pratola, C., Barrett, B., Gruber, A., & Dwyer, E. (2015). Quality assessment of the CCI ECV soil moisture product using ENVISAT ASAR wide swath data over Spain, Ireland and Finland. *Remote Sensing*, *7*, 15388–15423. https://doi.org/10.3390/rs71115388

Price, J. C. (1980). The potential of remotely sensed thermal infrared data to infer surface soil-moisture and evaporation. *Water Resources Research*, *16*(4), 787–795. https://doi.org/10.1029/WR016i004p00787

Prigent, C., Aires, F., Rossow, W. B., & Robock, A. (2005). Sensitivity of satellite microwave and infrared observations to soil moisture at a global scale: Relationship of satellite observations to in situ soil moisture measurements. *Journal of Geophysical Research*, *110*, D07110. https://doi.org/10.1029/2004JD005087

Profeti, G., & Macintosh, H. (1997). Flood management through Landsat TM and ERS SAR data: A case study. *Hydrological Processes*, *11*, 1397–1408. https://doi.org/10.1002/(SICI)1099-1085(199708)11:10<1397::AID-HYP530>3.0.CO;2-Y

Qi, R. Y., & Jin, Y. Q. (2007). Analysis of the effects of Faraday rotation on spaceborne polarimetric SAR observations at P-band. *IEEE Transactions on Geoscience and Remote Sensing*, *45*(5), 1115–1122. https://doi.org/10.1109/TGRS.2007.892583

Qiu, J. X., Mo, X. G., Liu, S. X., & Lin, Z. H. (2014). Exploring spatiotemporal patterns and physical controls of soil moisture at various spatial scales. *Theoretical and Applied Climatology*, *118*, 159–171. https://doi.org/10.1007/s00704-013-1050-6

Qu, W., Bogena, H. R., Huisman, J. A., Martinez, G., Pachepsky, Y. A., & Vereecken, H. (2014). Effects of soil hydraulic properties on the spatial variability of soil water content: Evidence from sensor network data and inverse modeling. *Vadose Zone Journal*, *13*(12), 1–12. https://doi.org/10.2136/vzj2014.07.0099

Qu, W., Bogena, H. R., Huisman, J. A., Vanderborght, J., Schuh, M., Priesack, E., & Vereecken, E. (2015). Predicting subgrid variability of soil water content from basic soil information. *Geophysical Research Letters*, *42*, 789–796. https://doi.org/10.1002/2014GL062496

Rahimzadeh-Bajgiran, P., Berg, A. A., Champagne, C., & Omasa, K. (2013). Estimation of soil moisture using optical/thermal infrared remote sensing in the Canadian Prairies. *ISPRS Journal of Photogrammetry and Remote Sensing*, *83*, 94–103. https://doi.org/10.1016/j.isprsjprs.2013.06.004

Rahman, M. M., Moran, M. S., Thoma, D. P., Bryant, R., Collins, C. D. H., Jackson, T., et al. (2008). Mapping surface roughness and soil moisture using multi-angle radar imagery without ancillary data. *Remote Sensing of Environment*, *112*(2), 391–402. https://doi.org/10.1016/j.rse.2006.10.026

Rains, D., Han, X., Lievens, X., Montzka, C., & Verhoest, N. E. C. (2017). SMOS brightness temperature assimilation into the Community Land Model. *Hydrology and Earth System Science*, *21*, 5929–5951. https://doi.org/10.5194/hess-2017-188

Ran, Y. H., Li, X., Jin, R., Kang, J., & Cosh, M. H. (2017). Strengths and weaknesses of temporal stability analysis for monitoring and estimating grid-mean soil moisture in a high-intensity irrigated agricultural landscape. *Water Resources Research*, *53*, 283–301. https://doi.org/10.1002/2015WR018182

Ray, R. L., & Jacobs, J. M. (2007). Relationships among remotely sensed soil moisture, precipitation and landslide events. *Natural Hazards*, *43*(2), 211–222. https://doi.org/10.1007/s11069-006-9095-9

Ray, R. L., Jacobs, J. M., & Cosh, M. H. (2010). Landslide susceptibility mapping using downscaled AMSR-E soil moisture: A case study from Cleveland Corral, California, US. *Remote Sensing of Environment*, *114*(11), 2624–2636. https://doi.org/10.1016/j.rse.2010.05.033

Reedy, R. C., & Scanlon, B. R. (2003). Soil water content monitoring using electromagnetic induction. *Journal of Geotechnical and Geoenvironmental Engineering*, *129*(11), 1028–1039. https://doi.org/10.1061/(ASCE)1090-0241(2003)129:11(1028)

Reichle, R. H., & Koster, R. D. (2004). Bias reduction in short records of satellite soil moisture. *Geophysical Research Letters*, *31*, L19501. https://doi.org/10.1029/2004GL020938

Reichle, R. H., De Lannoy, G. J. M., Forman, B. A., Draper, C. S., & Liu, Q. (2014). Connecting satellite observations with water cycle variables through land data assimilation: Examples using the NASA GEOS-5 LDAS. *Surveys in Geophysics*, *35*(3), 577–606. https://doi.org/10.1007/s10712-013-9220-8

Reichle, R. H., De Lannoy, G. J. M., Liu, Q., Ardizzone, J. V., Colliander, A., Conaty, A., et al. (2017). Assessment of the SMAP level-4 surface and root-zone soil moisture product using in situ measurements. *Journal of Hydrometeorology*, *18*(10), 2621–2645. https://doi.org/10.1175/JHM-D-17-0063.1

Reichle, R. H., & Koster, R. D. (2005). Global assimilation of satellite surface soil moisture retrievals into the NASA catchment land surface model. *Geophysical Research Letters*, *32*, F01002. https://doi.org/10.1029/2004GL021700

Reichle, R. H., Koster, R. D., Dong, J. R., & Berg, A. A. (2004). Global soil moisture from satellite observations, land surface models, and ground data: Implications for data assimilation. *Journal of Hydrometeorology*, *5*(3), 430–442. https://doi.org/10.1175/1525-7541(2004)005<0430:GSMFSO>2.0.CO;2

Reichle, R. H., Koster, R. D., Liu, P., Mahanama, S. P. P., Njoku, E. G., & Owe, M. (2007). Comparison and assimilation of global soil moisture retrievals from the Advanced Microwave Scanning Radiometer for the Earth Observing System (AMSR-E) and the Scanning Multichannel Microwave Radiometer (SMMR). *Journal of Geophysical Research*, *112*, D09108. https://doi.org/10.1029/2006JD008033

Reichle, R. H., Lucchesi, R. A., Ardizzone, J. V., Kim, G. K., & Weiss, B. H. (2014). Soil Moisture Active Passive (SMAP) mission level 4 surface and root zone soil moisture (L4_SM) product specification document. Greenbelt, MD.

Ren, T., Kluitenberg, G. J., & Horton, R. (2000). Determining soil water flux and pore water velocity by a heat pulse technique. *Soil Science Society of America Journal*, *64*(2), 552–560. https://doi.org/10.2136/sssaj2000.642552x

Richards, L. A. (1931). Capillary conduction of liquids through porous mediums. *Physics*, *1*, 318–333. https://doi.org/10.1063/1.1745010

Ridolfi, L., D'Odorico, P., Porporato, A., & Rodriguez-Iturbe, I. (2000). Impact of climate variability on the vegetation water stress. *Journal of Geophysical Research*, *105*(D14), 18013–18025.

Rignot, E. J., Zimmermann, R., & Vanzyl, J. J. (1995). Spaceborne applications of P-band imaging radars for measuring forest biomass. *IEEE Transactions on Geoscience and Remote Sensing*, *33*(5), 1162–1169. https://doi.org/10.1109/36.469480

Ritsema, C. J., Kuipers, H., Kleiboer, L., Van Den Elsen, E., Oostindie, K., Wesseling, J. G., et al. (2009). A new wireless underground network system for continuous monitoring of soil water contents. *Water Resources Research*, *45*, W00D36. https://doi.org/10.1029/2008WR007071

Robinson, D. A., Abdu, H., & Jones, S. (2012). Imaging of hill-slope soil moisture wetting patterns in a semi-arid oak savanna catchment using time-lapse electromagnetic induction. *Journal of Hydrology*, 416–417. https://doi.org/10.1016/j.jhydrol.2011.11.034

Robinson, D. A., Binley, A., Crook, N., Day-Lewis, F. D., Ferré, T. P. A., Grauch, V. J. S., et al. (2008). Advancing process-based watershed hydrological research using near-surface geophysics: A vision for, and review of, electrical and magnetic geophysical methods. *Hydrological Processes*, *22*(18), 3604–3635. https://doi.org/10.1002/hyp.6963

Robinson, D. A., Campbell, C. S., Hopmans, J. W., Hornbuckle, B. K., Jones, S. B., Knight, R., et al. (2008). Soil moisture measurement for ecological and hydrological watershed-scale observatories: A Review. *Vadose Zone Journal*, *7*(1), 358–389. https://doi.org/10.2136/vzj2007.0143

Robinson, D. A., Jones, S. B., Wraith, J. M., Or, D., & Friedman, S. P. (2003). A review of advances in dielectric and electrical conductivity measurement in soils using time domain reflectometry. *Vadose Zone Journal*, *2*(4), 444–475. https://doi.org/10.2113/2.4.444

Robock, A., & Li, H. (2006). Solar dimming and CO_2 effects on soil moisture trends. *Geophysical Research Letters*, *33*, L20708. https://doi.org/10.1029/2006GL027585

Robock, A., Mu, M., Vinnikov, K., Trofimova, I. V., & Adamenko, T. I. (2005). Forty-five years of observed soil moisture in the Ukraine: No summer desiccation (yet). *Journal of Geophysical Research*, *32*, L03401. https://doi.org/10.1029/2004GL021914

Robock, A., Vinnikov, K. Y., Srinivasan, G., & Entin, J. K. (2000). The global soil moisture data bank. *Bulletin of the American Meteorological Society*, *81*(6), 1281–1299. https://doi.org/10.1175/1520-0477(2000)081<1281:TGSMDB>2.3.CO;2

Rodell, M., Houser, P. R., Jambor, U., Gottschalck, J., Mitchell, K., Meng, C.-J., et al. (2004). The global land data assimilation system. *Hydrological Sciences Bulletin*, *25*, 51–62.

Rodriguez-Alvarez, N., Bosch-Lluis, X., Camps, A., Vall-Ilossera, M., Valencia, E., Marchan-Hernandez, J. F., & Ramos-Perez, I. (2009). Soil moisture retrieval using GNSS-R techniques: Experimental results over a bare soil field. *IEEE Transaction of Geoscience and Remote Sensing*, *47*, 3616–3624. https://doi.org/10.1109/TGRS.2009.2030672

Rodriguez-Alvarez, N., Camps, A., Vall-Ilossera, M., Bosch-Lluis, X., Monerris, A., Ramos-Perez, I., et al. (2010). Land geophysical parameters retrieval using the interference pattern GNSS-R technique. *IEEE Transaction of Geoscience and Remote Sensing*, *49*(1), 71–84. https://doi.org/10.1109/TGRS.2010.2049023

Rodríguez-Fernández, N. J., Aires, F., Richaume, P., Kerr, Y. H., Prigent, C., Kolassa, J., et al. (2015). Soil moisture retrieval using neural networks: Application to SMOS. *IEEE Transactions on, Geoscience and Remote Sensing*, *53*(11), 5991–6007. https://doi.org/10.1109/TGRS.2015.2430845

Rodríguez-Fernández, N. J., Kerr, Y. H., van der Schalie, R., Al-Yaari, A., & Wigneron, J. –P., de Jeu, R., et al. (2016). Long term global surface soil moisture fields using an SMOS-trained neural network applied to AMSR-E data. *Remote Sensing*, *8*(11), 1–27. https://doi.org/10.3390/rs8110959

Rodríguez-Fernández, N. J., Sabater, J. M., Richaume, P., de Rosnay, P., Kerr, Y. H., Albergel, C., et al. (2017). SMOS near-real-time soil moisture product: Processor overview and first validation results. *Hydrology and Earth System Sciences*, *21*(10), 5201–5216. https://doi.org/10.5194/hess-21-5201-2017

Rodriguez-Iturbe, I., D'odorico, P., Porporato, A., & Ridolfi, L. (1999). On the spatial and temporal links between vegetation, climate, and soil moisture. *Water Resources Research*, *35*(12), 3709–3722.

Romshoo, S. A. (2004). Geostatistical analysis of soil moisture measurements and remotely sensed data at different spatial scales. *Environmental Geology*, *45*(3), 339–349. https://doi.org/10.1007/s00254-003-0891-1

Rosenbaum, U., Bogena, H. R., Herbst, M., Huisman, J. A., Peterson, T. J., Weuthen, A., et al. (2012). Seasonal and event dynamics of spatial soil moisture patterns at the small catchment scale. *Water Resources Research*, *48*, W10544. https://doi.org/10.1029/2011WR011518

Roth, K. (2008). Scaling of water flow through porous media and soils. *European Journal of Soil Science*, *59*, 125–130. https://doi.org/10.1111/j.1365-2389.2007.00986.x

Roth, K., Schulin, R., Fluhler, H., & Attinger, W. (1990). Calculation of time domain reflectometry for water content measurement using a composite dielectric approach. *Water Resources Research.*, *26*, 2267–2273. https://doi.org/10.1029/WR026i010p02267

Rötzer, K., Montzka, C., Bogena, H., Wagner, W., Kerr, Y. H., Kidd, R., & Vereecken, H. (2014). Catchment scale validation of SMOS and ASCAT soil moisture products using hydrological modeling and temporal stability analysis. *Journal of Hydrology*, *519*, 934–946. https://doi.org/10.1016/j.jhydrol.2014.07.065

Rötzer, K., Montzka, C., & Vereecken, H. (2015). Spatio-temporal variability of global soil moisture products. *Journal of Hydrology*, *522*, 187–202. https://doi.org/10.1016/j.jhydrol.2014.12.038

Rötzer, K., Montzka, K., Entekhabi, D., Konings, A. G., McColl, K. A., Piles, M., & Vereecken, H. (2017). Relationship between vegetation microwave optical depth and cross-polarized backscatter from multiyear Aquarius observations. *IEEE Journal of Selected Topics in Applied Earth Observations and Remote Sensing*, *10*(10), 4493–4503. https://doi.org/10.1109/JSTARS.2017.2716638

Rüdiger, C., Hancock, G., Hemakumara, H. M., Jacobs, B., Kalma, J. D., Martinez, C., et al. (2007). Goulburn River experimental catchment data set. *Water Resources Research*, *43*, W10601. https://doi.org/10.1029/2006WR005837

Rudolph, S., van der Kruk, J., von Hebel, C., Ali, M., Herbst, M., Montzka, C., et al. (2015). Linking satellite derived LAI patterns with subsoil heterogeneity using large-scale ground-based electromagnetic induction measurements. *Geoderma*, *241-242*, 262–271. https://doi.org/10.1016/j.geoderma.2014.11.015

Russo, D. (1988). Determining soil hydraulic properties by parameter estimation: On the selection of a model for the hydraulic properties. *Water Resources Research*, *24*(3), 453–459. https://doi.org/10.1029/WR024i003p00453

Ryu, D., Crow, W. T., Zhan, X. W., & Jackson, T. J. (2009). Correcting unintended perturbation biases in hydrologic data assimilation. *Journal of Hydrometeorology*, *10*(3), 734–750. https://doi.org/10.1175/2008JHM1038.1

Sabater, J. M., Jarlan, L., Calvet, J. C., Bouyssel, F., & De Rosnay, P. (2007). From near-surface to root-zone soil moisture using different assimilation techniques. *Journal of Hydrometeorology*, *8*(2), 194–206. https://doi.org/10.1175/JHM571.1

Sadeghi, M., Babaeian, E., Arthur, E., Jones, S. B., & Tuller, M. (2018). Soil physical properties and processes. In M. Kutz (Ed.), *Handbook of environmental engineering*, (pp. 137–207). Hoboken, NJ: Wiley. ISBN-10: 1118712943

Sadeghi, M., Babaeian, E., Tuller, M., & Jones, S. B. (2017). The optical trapezoid model: A novel approach to remote sensing of soil moisture applied to Sentinel-2 and Landsat-8 observations. *Remote Sensing of Environment*, *198*(1), 52–68. https://doi.org/10.1016/j.rse.2017.05.041

Sadeghi, M., Ghahraman, B., Warrick, A. W., Tuller, M., & Jones, S. B. (2016). A critical evaluation of the Miller and Miller similar media theory for application to natural soils. *Water Resources Research*, *52*, 3829–3846. https://doi.org/10.1002/2015WR017929

Sadeghi, M., Ghahraman, B., Ziaei, A. N., Davary, K., & Reichardt, K. (2012). Invariant solutions of Richards' equation for water movement in dissimilar soils. *Soil Science Society of America Journal*, *76*, 1–9. https://doi.org/10.2136/sssaj2011.0275

Sadeghi, M., Jones, B. S., & Philpot, W. D. (2015). A linear physically-based model for remote sensing of soil moisture using shortwave infrared bands. *Remote Sensing of Environment*, *164*, 66–76. https://doi.org/10.1016/j.rse.2015.04.007

Sadeghi, M., Sheng, W., Babaeian, E., Tuller, M., & Jones, S. B. (2018). High-resolution shortwave infrared imaging of water infiltration into dry soil. *Vadose Zone Journal*, *16*(13). https://doi.org/10.2136/vzj2017090167

Sadeghi, M., Tabatabaeenejad, A., Tuller, M., Moghaddam, M., & Jones, S. B. (2017). Advancing NASA's AirMOSS P-Band radar root zone soil moisture retrieval algorithm via incorporation of Richards' equation. *Remote Sensing*, *9*(1), 1–17. https://doi.org/10.3390/rs9010017

Sadeghi, M., Tuller, M., Gohardoust, M. R., & Jones, S. B. (2014). Column-scale unsaturated hydraulic conductivity estimates in coarse textured homogeneous and layered soils derived under steady-state evaporation from a water table. *Journal of Hydrology*, *519*, 1238–1248. https://doi.org/10.1016/j.jhydrol.2014.09.004

Sadeghi, M., Tuller, M., Warrick, A. W., Babaeian, E., Parajuli, K., Gohardoust, M. R., & Jones, S. B. (2019). An analytical model for estimation of land surface net water flux from near-surface soil moisture observations. *Journal of Hydrology*, *570*, 26–37. https://doi.org/10.1016/j.jhydrol.2018.12.038

Sahoo, A. K., Houser, P. R., Ferguson, C., Wood, E. F., Dirmeyer, P. A., & Kafatos, M. (2008). Evaluation of AMSR-E soil moisture results using the in-situ data over the Little River Experimental Watershed, Georgia. *Remote Sensing of Environment*, *112*(6), 3142–3152. https://doi.org/10.1016/j.rse.2008.03.007

Samouelian, A., Vogel, H. J., & Ippisch, O. (2007). Upscaling hydraulic conductivity based on the topology of the sub-scale structure. *Advances in Water Resources*, *30*, 1179–1189. https://doi.org/10.1016/j.advwatres.2006.10.011

Sánchez, N., Alonso-Arroyo, A., Martínez-Fernández, J., Piles, M., González- Zamora, A., Camps, A., & Vall-llosera, M. (2015). On the synergy of airborne GNSS-R and Landsat 8 for soil moisture estimation. *Remote Sensing*, *7*, 9954–9974. https://doi.org/10.3390/rs70809954

Sandholt, I., Rasmussen, K., & Andersen, J. (2002). A simple interpretation of the surface temperature/vegetation index space for assessment of surface moisture status. *Remote Sensing of environment*, *79*(2), 213–224. https://doi.org/10.1016/S0034-4257(01)00274-7

Santi, E., Pierdicca, S., Pettinato, S., & Fontanelli, G. (2016). Application of artificial neural networks for the soil moisture retrieval from active and passive microwave spaceborne sensors. *International Journal of Applied Earth Observation and Geoinformation*, *48*, 61–73. https://doi.org/10.1016/j.jag.2015.08.002

Santra, P., Sahoo, R. N., Das, B. S., Samal, R. N., Pattanaik, A. K., & Gupta, V. K. (2009). Estimation of soil hydraulic properties using proximal spectral reflectance in visible, near-infrared, and shortwave-infrared (VIS-NIR-SWIR) region. *Geoderma*, *152*, 338–349. https://doi.org/10.1016/j.geoderma.2009.07.001

Saucier, A. (1992). Effective permeability of multifractal porous media. *Physica A: Statistical Mechanics and its Applications*, *183*, 381–397. https://doi.org/10.1016/0378-4371(92)90290-7

Scaini, A., Sánchez, N., Vicente-Serrano, S. M., & Martínez-Fernández, J. (2015). SMOS-derived soil moisture anomalies and drought indices: A comparative analysis using in situ measurements. *Hydrological Processes*, *29*(3), 373–383. https://doi.org/10.1002/hyp.10150

Schaefer, G. L., Cosh, M. H., & Jackson, T. J. (2007). The USDA natural resources conservation service soil climate analysis network (SCAN). *Journal of Atmospheric and Oceanic Technology*, *24*, 2073–2077. https://doi.org/10.1175/2007JTECHA930.1

Schieldge, J. P., Kahle, A. B., & Alley, R. E. (1982). A numerical-simulation of soil-temperature and moisture variations for a bare field. *Soil Science*, *133*(4), 197–207. https://doi.org/10.1097/00010694-198204000-00001

Schneider, J. M., Fisher, D. K., Elliott, R. L., Brown, G. O., & Bahrmann, C. P. (2003). Spatiotemporal variations in soil water: First results from the ARM SGP CART network. *Journal of Hydrometeorology*, *4*, 106–120. https://doi.org/10.1175/1525-7541(2003)004<0106:SVISWF>2.0.CO;2

Schneider, K., Huisman, J. A., Breuer, L., Zhao, Y., & Frede, H. G. (2008). Temporal stability of soil moisture in various semi-arid steppe ecosystems and its application in remote sensing. *Journal of Hydrology*, *359*, 16–29. https://doi.org/10.1016/j.jhydrol.2008.06.016

Schnur, M. T., Xie, H., & Wang, X. (2010). Estimating root zone soil moisture at distant sites using MODIS NDVI and EVI in a semi-arid region of southwestern USA. *Ecological Informatics*, *5*, 400–409. https://doi.org/10.1016/j.ecoinf.2010.05.001

Schroeder, J. L., Burgett, W. S., Haynie, K. B., Sonmez, I., Skwira, G. D., Doggett, A. L., & Lipe, J. W. (2005). The West Texas mesonet: A technical overview. *Journal of Atmospheric and Oceanic Technology*, *22*(2), 211–222. https://doi.org/10.1175/JTECH-1690.1

Schröter, I., Paasche, H., Dietrich, P., & Wollschläger, U. (2015). Estimation of catchment-scale soil moisture patterns based on terrain data and sparse TDR measurements using a fuzzy C-means clustering approach. *Vadose Zone Journal*, *14*(11). https://doi.org/10.2136/vzj2015.01.0008

Schubert, S. D., Suarez, M. J., Pegion, P. J., Koster, R. D., & Bacmeister, J. T. (2004). Causes of long-term drought in the US Great Plains. *Journal of Climate*, *17*, 485–503. https://doi.org/10.1175/1520-0442(2004)017<0485:COLDIT>2.0.CO;2

Schwank, M., Volksch, I., Wigneron, J. P., Kerr, Y. H., Mialon, A., de Rosnay, P., & Matzler, C. (2010). Comparison of two bare-soil reflectivity models and validation with L-band radiometer measurements. *IEEE Transactions on Geoscience and Remote Sensing*, *48*(1), 325–337. https://doi.org/10.1109/TGRS.2009.2026894

Schwank, M., Wiesmann, A., Werner, C., Mätzler, C., Weber, D., Murk, A., et al. (2010). ELBARA II, an L-band radiometer system for soil moisture research. *Sensors*, *10*(1), 584–612. https://doi.org/10.3390/s100100584

Scott, R. W., Krug, E. C., Burch, S. L., Mitdarfer, C. R., & Nelson, P. F. (2010). *Investigations of soil moisture under sod in east-central Illinois, Rep. Invest. 119*, (). Champaign: Illinois State Water Survey.

Segoni, S., Rosi, A., Lagomarsino, D., Fanti, R., & Casagli, N. (2018). Brief communication: Using averaged soil moisture estimates to improve the performances of a regional-scale landslide early warning system. *Natural Hazards and Earth System Sciences*, *18*, 807–812. https://doi.org/10.5194/nhess-18-807-2018

Seneviratne, S. I., Corti, T., Davin, E. L., Hirschi, M., Jaeger, E. B., Lehner, I., et al. (2010). Investigating soil moisture–climate interactions in a changing climate: A review. *Earth Science Reviews*, *99*(3-4), 125–161. https://doi.org/10.1016/j.earscirev.2010.02.004

Serbin, G., & Or, D. (2003). Near-surface soil water content measurements using Horn antenna radar. *Vadose Zone Journal*, *2*(4), 500–510. https://doi.org/10.2136/vzj2003.0500

Seyfried, M. S., & Murdock, M. D. (2004). Measurement of soil water content with a 50-MHz soil dielectric sensor. *Soil Science Society of America Journal*, *68*(2), 394–403. https://doi.org/10.2136/sssaj2004.3940

Shafian, S., & Maas, S. J. (2015). Index of soil moisture using raw Landsat image digital count data in Texas high plains. *Remote Sensing*, *7*(3), 2352–2372. https://doi.org/10.3390/rs70302352

Shanahan, P. W., Binley, A., Whalley, W. R., & Watts, C. W. (2015). The use of electromagnetic induction to monitor changes in soil moisture profiles beneath different wheat genotypes. *Soil Science Society of America Journal*, *79*(2), 459–466. https://doi.org/10.2136/sssaj2014.09.0360

Shao, M., & Horton, R. (1998). Integral method for estimating soil hydraulic properties. *Soil Science Society of America Journal*, *62*, 585–592. https://doi.org/10.2136/sssaj1998.03615995006200030005x

Sheets, K. R., & Hendrickx, J. M. H. (1995). Noninvasive soil water content measurement using electromagnetic induction. *Water Resources Research*, *31*(10), 2401–2409. https://doi.org/10.1029/95WR01949

Sheng, W., Zhou, R., Sadeghi, M., Babaeian, E., Robinson, D. A., Tuller, M., & Jones, S. B. (2017). A TDR array probe for monitoring near-surface soil moisture distribution. *Vadose Zone Journal*, *16*(4). https://doi.org/10.2136/vzj2016.11.0112

Sihvola, A. (1999). *Electromagnetic mixing formulas and applications. The Institute on of Engineering and Technology*. London, UK.

Silvestro, F., & Rebora, N. (2014). Impact of precipitation forecast uncertainties and initial soil moisture conditions on a probabilistic flood forecasting chain. *Journal of Hydrology*, *519*, 1052–1067. https://doi.org/10.1016/j.jhydrol.2014.07.042

Simmons, A. J., & Gibson, J. K. (2000). The ERA-40 project plan. ERA-40 Project Report Series, 1, 63 pp.

Simunek, J., & van Genuchten, M. T. (1996). Estimating unsaturated soil hydraulic properties from tension disc infiltrometer data by numerical inversion. *Water Resources Research*, *32*, 2683–2696.

Slavich, P. G., & Yang, J. (1990). Estimation of field scale leaching rates from chloride mass balance and electromagnetic induction measurements. *Irrigation Science*, *11*, 7–14. https://doi.org/10.1007/BF00189989

Smith, A. B., Walker, J. P., Western, A. W., Young, R. I., Ellett, K. M., Pipunic, R. C., et al. (2012). The Murrumbidgee soil moisture monitoring network data set. *Water Resources Research*, *48*, W07701. https://doi.org/10.1029/2012WR011976

Sobrino, J. A., Franch, B., Mattar, C., Jimenez-Munoz, J. C., & Corbari, C. (2012). A method to estimate soil moisture from airborne hyperspectral scanner (AHS) and ASTER data: Application to SEN2FLEX and SEN3EXP campaigns. *Remote Sensing of Environment*, *117*, 415–428. https://doi.org/10.1016/j.rse.2011.10.018

Sohrabi, M. M., Ryu, J. H., Abatzoglou, J., & Tracy, J. (2015). Development of soil moisture drought index to characterize droughts. *Journal of Hydrologic Engineering*, *20*(11). https://doi.org/104015025.084-0699/04015025(15)

Soldo, Y., Khazaal, A., Cabot, F., & Kerr, Y. H. (2016). An RFI index to quantify the contamination of SMOS data by radio-frequency interference. *IEEE Journal of Selected Topics in Applied Earth Observations and Remote Sensing*, *9*(4), 1577–1589. https://doi.org/10.1109/JSTARS.2015.2425542

Song, X., Ma, J., Li, X., Leng, P., Zhou, F., & Li, S. (2014). First results of estimating surface soil moisture in the vegetated areas using ASAR and Hyperion data: The Chinese Heihe River Basin Case Study. *Remote Sensing*, *6*(12), 12055–12069. https://doi.org/10.3390/rs61212055

Song, X., Shi, L., Ye, M., Yang, J., & Navon, I. M. (2014). Numerical comparison of iterative ensemble Kalman filters for unsaturated flow inverse modeling. *Vadose Zone Journal*, *13*(2). https://doi.org/10.2136/vzj2013.05.0083

Sprott, J. C. (2003). *Chaos and Time Series Analysis*. Oxford: Oxford University Press.

Sridhar, V., Hubbard, K. G., You, J., & Hunt, E. D. (2008). Development of the soil moisture index to quantify agricultural drought and its user friendliness in severity-area-duration assessment. *Journal of Hydrometeorology*, *9*(4), 660–676. https://doi.org/10.1175/2007JHM892.1

Srivastava, H. S., Patel, P., Manchanda, M. L., & Adiga, S. (2003). Use of multi-incidence angle RADARSAT-1 SAR data to incorporate the effect of surface roughness in soil moisture estimation. *IEEE Transactions on Geoscience and Remote Sensing*, *41*(7), 1638–1640. https://doi.org/10.1109/TGRS.2003.813356

Srivastava, N., Mansimov, E., & Salakhutdinov, R. (2015). *Unsupervised learning of video representations using LSTMs*. Canada: University of Toronto.

Srivastava, P. K., Han, D., Rico-Ramirez, M. A., Al-Shrafany, D., & Islam, T. (2013). Data fusion techniques for improving soil moisture deficit using SMOS satellite and WRF-NOAH land surface model. *Water Resources Management*, *27*, 5069–5087. https://doi.org/10.1007/s11269-013-0452-7

Srivastava, P. K., O'Neill, P., Cosh, M., Kurum, M., Lang, R., & Joseph, A. (2015). Evaluation of dielectric mixing models for passive microwave soil moisture retrieval using data from ComRAD ground-based SMAP simulator. *IEEE Journal of Selected Topics in Applied Earth Observations and Remote Sensing*, *8*(9), 4345–4354. https://doi.org/10.1109/JSTARS.2014.2372031

Stisen, S., Sandholt, I., Nørgaard, A., Fensholt, R., & Jensen, K. H. (2008). Combining the triangle method with thermal inertia to estimate regional evapotranspiration-applied to MSG-SEVIRI data in the Senegal River basin. *Remote Sensing of Environment*, *112*(3), 1242–1255. https://doi.org/10.1016/j.rse.2007.08.013

Stockinger, M. P., Bogena, H. R., Lücke, A., Diekkrüger, B., Weiler, M., & Vereecken, H. (2014). Seasonal soil moisture patterns: Controlling transit time distributions in a forested headwater catchment. *Water Resources Research*, *50*, 5270–5289. https://doi.org/10.1002/2013WR014815

Stoffelen, A. (1998). Toward the true near-surface wind speed: Error modeling and calibration using triple collocation. *Journal of Geophysical Research*, *103*(C4), 7755–7766.

Stuffler, T., Kaufmann, C., Hofer, S., Förster, K. P., Schreier, G., Müller, A., et al. (2006). The EnMAP hyperspectral imager: An advanced optical payload for future applications in Earth observation programs. Paper presented at 57th IAC (International Astronautical Congress), Valencia, Spain.

Su, Z., Wen, J., Dente, L., Velde, R., Wang, L., Ma, Y., et al. (2011). The Tibetan Plateau observatory of plateau scale soil moisture and soil temperature (Tibet-Obs) for quantifying uncertainties in coarse resolution satellite and model products. *Hydrology and Earth System Sciences*, *15*(7), 2303–2316. https://doi.org/10.5194/hess-15-2303-2011

Sudduth, K., Kitchen, N. R., Chung, S.-O., & Drummond, S. T. (2010). Site-specific compaction, soil physical property, and crop yield relationships for claypan soils. Paper presented at Annual International Meeting of American Society of Agricultural and Biological Engineers, Pittsburgh, PA.

Sugathan, N., Biju, V., & Renuka, G. (2014). Influence of soil moisture content on surface albedo and soil thermal parameters at a tropical station. *Journal of Earth System Sciences*, *125*(5), 1115–1128. https://doi.org/10.1007/s12040-014-0452-x

Summerell, G., Shoemark, V., Grant, S., & Walker, J. P. (2009). Using passive microwave response to soil moisture change for soil mapping: A case study for the Livingstone Creek Catchment. *IEEE Geoscience and Remote Sensing Letters*, *6*(4), 649–652. https://doi.org/10.1109/TGRS.2014.2350988

Sun, H. (2016). Two-stage trapezoid: A new interpretation of the land surface temperature and fractional vegetation coverage space. *IEEE Journal of Selected Topics in Applied Earth Observations and Remote Sensing*, *9*(1), 336–346. https://doi.org/10.1109/JSTARS.2015.2500605

Tabatabaeenejad, A., Burgin, M., Duan, X., & Moghaddam, M. (2013). *Airborne microware observatory of subcanopy and subsurface radar retrieval of root zone soil moisture: Preliminary results. Paper presented at IEEE Radar*. Ottawa, ON: Conf. https://doi.org/10.1109/RADAR.2013.6586082

Tabatabaeenejad, A., Burgin, M., Duan, X., & Moghaddam, M. (2015). P-band radar retrieval of subsurface soil moisture profile as a second-order polynomial: First AirMOSS results. *IEEE Transactions on Geoscience and Remote Sensing*, *53*(2), 645–658. https://doi.org/10.1109/TGRS.2014.2326839

Tabatabaeenejad, A., & Moghaddam, M. (2011). Radar retrieval of surface and deep soil moisture and effect of moisture profile on inversion accuracy. *IEEE Geoscience and Remote Sensing Letters*, *8*(3), 478–482. https://doi.org/10.1109/LGRS.2010.2087741

Tatli, H., & Turkes, M. (2011). Empirical orthogonal function analysis of the palmer drought indices. *Agricultural and Forest Meteorology*, *151*, 981–991. https://doi.org/10.1016/j.agrformet.2011.03.004

Tayfur, G., Zucco, G., Brocca, L., & Moramarco, T. (2014). Coupling soil moisture and precipitation observations for predicting hourly runoff at small catchment scale. *Journal of Hydrology*, *510*, 363–371. https://doi.org/10.1016/j.jhydrol.2013.12.045

Tekeli, A. E., & Fouli, H. (2017). Reducing false flood warnings of TRMM rain rates thresholds over Riyadh city, Saudi Arabia by utilizing AMSR-E soil moisture information. *Water Resources Management*, *31*, 1243–1256. https://doi.org/10.1007/s11269-017-1573-1

Teuling, A. J., Uijlenhoet, R., Hupet, F., van Loon, E. E., & Troch, P. A. (2006). Estimating spatial mean root-zone soil moisture from point-scale observations. *Hydrology and Earth System Sciences*, *10*(5), 755–767. https://doi.org/10.5194/hess-10-755-2006

Thierfelder, T. K., Grayson, R. B., von Rosen, D., & Western, A. W. (2003). Inferring the location of catchment characteristic soil moisture monitoring sites. *Covariance structures in the temporal domain. Journal of Hydrology*, *280*, 13–32. https://doi.org/10.1016/s0022-1694(03)00077-5

Tian, J., & Philpot, W. D. (2015). Relationship between surface soil water content, evaporation rate, and water absorption band depths in SWIR reflectance spectra. *Remote Sensing of Environment*, *169*, 280–289. https://doi.org/10.1016/j.rse.2015.08.007

Topp, G. C., Davis, J. L., & Annan, A. P. (1980). Electromagnetic determination of soil water content: measurements in coaxial transmission lines. *Water Resources Research*, *16*, 574–582.

Torres, G. M., Lollato, R. P., & Ochsner, T. E. (2013). Comparison of drought probability assessments based on atmospheric water deficit and soil water deficit. *Agronomy Journal*, *105*(2), 428–436. https://doi.org/10.2134/agronj2012.0295

Torres-Ruiz, J. M., Diaz-Espejo, A., Morales-Sillero, A., Martín-Palomo, M. J., Mayr, S., Beikircher, B., & Fernández, J. E. (2013). Shoot hydraulic characteristics, plant water status and stomatal response in olive trees under different soil water conditions. *Plant and Soil*, *373*(1-2), 77–87. https://doi.org/10.1007/s11104-013-1774-1

Toure, A., Thomson, K. P., Edwards, G., Brown, R. J., & Brisco, B. G. (1994). Adaptation of the MIMICS backscattering model to the agricultural context-wheat and canola at L- and C-bands. *IEEE Transactions on Geoscience and Remote Sensing*, *32*(1), 47–61. https://doi.org/10.1109/36.285188

Triantafilis, J., Lesch, S. M., La Lau, K., & Buchanan, S. M. (2009). Field level digital soil mapping of cation exchange capacity using electromagnetic induction and a hierarchical spatial regression model. *Soil Research*, *47*(7), 651–663. https://doi.org/10.1071/SR08240

Tromp-van Meerveld, H. J., & McDonnell, J. J. (2009). Assessment of multi-frequency electromagnetic induction for determining soil moisture patterns at the hillslope scale. *Journal of Hydrology*, *368*, 56–67. https://doi.org/10.1016/j.jhydrol.2009.01.037

Tuller, M., & Islam, M. R. (2005). Field methods for monitoring solute transport. In J. Álvarez-Benedí, & R. Muñoz-Carpena (Eds.), *Soil-water-solute process characterization: An integrated approach*, (pp. 309–355). Boca Raton, FL: CRC Press.

Tuller, M., & Or, D. (2005a). Water retention and characteristic curve. *Encyclopedia of Soils in the Environment*, *4*(1), 278–289.

Tuller, M., & Or, D. (2005b). Water films and scaling of soil characteristic curves at low water contents. *Water Resources Research*, *41*, W09403. https://doi.org/10.1029/2005WR004142

Tuller, M., Or, D., & Dudley, L. M. (1999). Adsorption and capillary condensation in porous media: Liquid retention and interfacial configurations in angular pores. *Water Resources Research*, *35*(7), 1949–1964. https://doi.org/10.1029/1999WR900098

Twomey, S. A., Bohren, C. F., & Mergenthaler, J. L. (1986). Reflectance and albedo differences between wet and dry surfaces. *Applied Optics*, *25*, 431–437. https://doi.org/10.1364/AO.25.000431

Ulaby, F. T., Moore, R. K., & Fung, A. K. (1982). Microwave remote sensing: active and passive. Radar remote sensing and surface scattering and emission theory. In *Microwave remote sensing: active and passive*, (Vol. 2). Addison-Wesley pp 628.

Ulaby, F. T., Moore, R. K., & Fung, A. K. (1986). *Microwave remote sensing: Active and passive from theory to applications*, (Vol. 3, pp. 1826–1827). Addison Wesley.

Ulaby, F. T., Razani, M., & Dobson, M. C. (1983). Effects of vegetation cover on the microwave radiometric sensitivity to soil moisture. *IEEE Transactions on Geoscience and Remote Sensing*, (1), 51–61. https://doi.org/10.1109/TGRS.1983.350530

Underwood, N., van Vavel, C. H. M., & Swanson, R. W. (1954). A portable slow neutron flux meter for measuring soil moisture. *Soil Science*, *77*, 339–340.

Vachaud, G., Desilans, A. P., Balabanis, P., & Vauclin, M. (1985). Temporal stability of spatially measured soil-water probability density-function. *Soil Science Society of America Journal*, *49*, 822–828. https://doi.org/10.2136/sssaj1985.03615995004900040006x

Vachaud, G., Royer, J. M., & Cooper, J. D. (1977). Comparison of methods of calibration of a neutron probe by gravimetry or neutron-capture model. *Journal of Hydrology*, *34*(3), 343–356. https://doi.org/10.1016/0022-1694(77)90141-X

Valente, A., Morais, R., Tuli, A., Hopmans, J. W., & Kluitenberg, G. J. (2006). Multi-functional probe for small-scale simultaneous measurements of soil thermal properties, water content, and electrical conductivity. *Sensors and Actuators A: Physical*, *132*(1), 70–77. https://doi.org/10.1016/j.sna.2006.05.010

van der Kruk, J. (2006). Properties of surface waveguides derived from inversion of fundamental and higher mode dispersive GPR data. *IEEE Transactions on Geoscience and Remote Sensing*, *44*(10), 2908–2915. https://doi.org/10.1109/TGRS.2006.877286

van der Schalie, R., de Jeu, R., Rodríguez-Fernández, N., Al-Yaari, A., Kerr, Y., Wigneron, J. P., et al. (2018). The effect of three different data fusion approaches on the quality of soil moisture retrievals from multiple passive microwave sensors. *Remote Sensing*, *10*(1), 107. https://doi.org/10.3390/rs10010107

van der Schalie, R., Parinussa, R., Renzullo, L., van Dijk, A., Su, C.-H., & de Jeu, R. (2015). SMOS soil moisture retrievals using the land parameter retrieval model: Evaluation over the Murrumbidgee Catchment, southeast Australia. *Remote Sensing of Environment*, *163*, 70–79. https://doi.org/10.1016/j.rse.2015.03.006

Van der Kruk, J., Jacob, R. W., & Vereecken, H. (2010). Properties of precipitation-induced multilayer surface waveguides derived from inversion of dispersive TE and TM GPR data. *Geophysics*, *75*(4), WA263–WA273.

Van der Schalie, R., Kerr, Y. H., Wigneron, J. P., Rodríguez-Fernández, N. J., Al-Yaari, A., & de Jeu, R. A. M. (2016). Global SMOS soil moisture retrievals from the land parameter retrieval model. *International Journal of Applied Earth Observation and Geoinformation*, *45*, 125–134. https://doi.org/10.1016/j.jag.2015.08.005

Van Meirvenne, M., Islam, M. M., DeSmedt, P., Meerschman, E., Van DeVijver, E., & Saey, T. (2013). Key variables for the identification of soil management classes in the Aeolian landscapes of north-west Europe. *Geoderma*, *199*, 99–105. https://doi.org/10.1016/j.geoderma.2012.07.017

Vanderlinden, K., Vereecken, H., Hardelauf, H., Herbst, M., Martinez, G., Cosh, M. H., & Pachepsky, Y. A. (2012). Temporal stability of soil water contents: A review of data and analyses. *Vadose Zone Journal*, *11*(4). https://doi.org/10.2136/Vzj2011.0178

Vaz, C. M. P., Jones, S., Meding, M., & Tuller, M. (2013). Evaluation of standard calibration functions for eight electromagnetic soil moisture sensors. *Vadose Zone Journal*, *12*(2). https://doi.org/10.2136/vzj2012.0160

Vereecken, H., Huisman, J. A., Hendricks Franssen, H. J., Brüggemann, N., Bogena, H. R., Kollet, S., et al. (2015). Soil hydrology: Recent methodological advances, challenges, and perspectives. *Water Resources Research*, *51*, 2616–2633. https://doi.org/10.1002/2014WR016852

Vereecken, H., Huisman, J. A., Pachepsky, Y., Montzka, C., van der Kruk, J., Bogena, H., et al. (2014). On the spatio-temporal dynamics of soil moisture at the field scale. *Journal of Hydrology*, *516*, 76–96. https://doi.org/10.1016/j.jhydrol.2013.11.061

Vereecken, H., Kasteel, R., Vanderborght, J., & Harter, T. (2007). Upscaling hydraulic properties and soil water flow processes in heterogeneous soils: A review. *Vadose Zone Journal*, *6*, 1–28. https://doi.org/10.2136/vzj2006.0055

Vereecken, H., Schnepf, A., Hopmans, J. W., Javaux, M., Or, D., Roose, T., et al. (2016). Modeling soil processes: Review, key challenges, and new perspectives. *Vadose Zone Journal*, *15*(5). https://doi.org/10.2136/vzj2015.09.013

Verhoest, N. E., Lievens, H., Wagner, W., Álvarez-Mozos, J., Moran, M. S., & Mattia, F. (2008). On the soil roughness parameterization problem in soil moisture retrieval of bare surfaces from synthetic aperture radar. *Sensors*, *8*(7), 4213–4248. https://doi.org/10.3390/s8074213

Verhoest, N. E. C., van den Berg, M. J., Martens, B., Lievens, H., Wood, E. F., Pan, M., et al. (2015). Copula-based downscaling of coarse-scale soil moisture observations with implicit bias correction. *IEEE Transactions on Geoscience and Remote Sensing*, *53*(6), 3507–3521. https://doi.org/10.1109/TGRS.2014.2378913

Verstraeten, W. W., Veroustraete, F., van der Sande, C. J., Grootaers, I., & Feyen, J. (2006). Soil moisture retrieval using thermal inertia, determined with visible and thermal spaceborne data, validated for European forests. *Remote Sensing of Environment*, *101*(3), 299–314. https://doi.org/10.1016/j.rse.2005.12.016

Vey, S., Güntner, A., Wickert, J., Blume, T., & Ramatschi, M. (2016). Long-term soil moisture dynamics derived from GNSS interferometric reflectometry: A case study for Sutherland, South Africa. *GPS Solutions*, *20*(4), 641–654. https://doi.org/10.1007/s10291-015-0474-0

Vincente-Serrano, S., Pons-Fernandez, X., & Cuadrat-Prats, J. (2004). Mapping soil moisture in the central Ebro river valley (northeast Spain) with Landsat and NOAA satellite imagery: A comparison with meteorological data. *International Journal of Remote Sensing*, *25*(20), 4325–4350.

Vinnikov, K. Y., Robock, A., Qiu, S., Entin, J. K., Owe, M., Choudhury, B. J., et al. (1999). Satellite remote sensing of soil moisture in Illinois, United States. *Journal of Geophysical Research*, *104*(D4), 4145–4168.

Viscarra Rossel, R. A., Walvoort, D. J. J., McBratney, A. B., Janik, L. J., & Skjemstad, J. O. (2006). Visible, near infrared, mid infrared or combined diffuse reflectance spectroscopy for simultaneous assessment of various soil properties. *Geoderma*, *131*, 59–75. https://doi.org/10.1016/j.geoderma.2005.03.007

Vittucci, C., Ferrazzoli, P., Kerr, Y. H., Richaume, P., Guerriero, L., Rahmoune, R., & Vaglio Laurin, G. (2016). SMOS retrieval over forests: Exploitation of optical depth and tests of soil moisture estimates. *Remote Sensing of Environment*, *180*, 115–127. https://doi.org/10.1016/j.rse.2016.03.004

Vogel, H. J., & Ippisch, O. (2008). Estimation of a critical spatial discretization limit for solving the Richards' equation at large scales. *Vadose Zone Journal*, *7*(1), 112–114. https://doi.org/10.2136/vzj2006.0182

Wagner, W., Bloschl, G., Pampaloni, P., Calvet, J. C., Bizzarri, B., Wigneron, J. P., & Kerr, Y. (2007). Operational readiness of microwave remote sensing of soil moisture for hydrologic applications. *Nordic Hydrology*, *38*(1), 1–20. https://doi.org/10.2166/nh.2007.029

Wagner, W., Brocca, L., Naeimi, V., Reichle, R., Draper, C., de Jeu, R., et al. (2014). Clarifications on the comparison between SMOS, VUA, ASCAT, and ECMWF soil moisture products over four watersheds in US. *IEEE Transactions on Geoscience and Remote Sensing*, *52*(3), 1901–1906. https://doi.org/10.1109/TGRS.2013.2282172

Wagner, W., Dorigo, W., de Jeu, R., Fernandez, D., Benveniste, J., Haas, E., & Ertl, M. (2012). Fusion of active and passive microwave observations to create an essential climate variable data record on soil moisture. ISPRS annals of the photogrammetry. *Remote Sensing and Spatial Information Sciences*, *7*, 315–321. https://doi.org/10.5194/isprsannals-I-7-315-2012

Wagner, W., Hahn, S., Kidd, R., Melzer, T., Bartalis, Z., Hasenauer, S., et al. (2013). The ASCAT soil moisture product: A review of its specifications, validation results, and emerging applications. *Meteorologische Zeitschrift*, *22*, 5–33. https://doi.org/10.1127/0941-2948/2013/0399

Wagner, W., Lemoine, G., & Rott, H. (1999). A method for estimating soil moisture from ERS scatterometer and soil data. *Remote Sensing of Environment*, *70*, 191–207. https://doi.org/10.1016/S0034-4257(99)00036-X

Wagner, W., Noll, J., Borgeaud, M., & Rott, H. (1999). Monitoring soil moisture over the Canadian prairies with the ERS Scatterometer. *IEEE Transactions on Geoscience and Remote Sensing*, *37*, 206–216. https://doi.org/10.1109/36.739155

Walker, J. P., & Houser, P. R. (2001). A methodology for initializing soil moisture in a global climate model: Assimilation of near-surface soil moisture observations. *Journal of Geophysical Research*, *106*(D11), 11761–11774.

Walker, J. P., Willgoose, G. R., & Kalma, J. D. (2002). Three-dimensional soil moisture profile retrieval by assimilation of near-surface measurements: Simplified Kalman filter covariance forecasting and field application. *Water Resources Research*, *38*(12), 1301. https://doi.org/10.1029/2002WR001545

Wan, Z., Zhang, Y., Zhang, Q., & Li, Z. L. (2004). Quality assessment and validation of the MODIS global land surface temperature. *International Journal of Remote Sensing*, *25*(1), 261–274. https://doi.org/10.1080/0143116031000116417

Wanders, N., Karssenberg, D., Roo, A. D., De Jong, S. M., & Bierkens, M. F. P. (2014). The suitability of remotely sensed soil moisture for improving operational flood forecasting. *Hydrology and Earth System Sciences*, *18*(6), 2343–2357. https://doi.org/10.5194/hess-18-2343-2014

Wang, H. J., Chen, Y. N., Pan, Y. P., & Li, W. H. (2015). Spatial and temporal variability of drought in the arid region of China and its relationships to teleconnection indices. *Journal of Hydrology*, *523*, 283–296. https://doi.org/10.1016/j.jhydrol.2015.01.055

Wang, P., Li, X., Gong, J., & Song, C. (2001). Vegetation temperature condition index and its application for drought monitoring. *IEEE International Geoscience and Remote Sensing Symposium*. https://doi.org/10.1109/IGARSS.2001.976083

Wang, S., Mo, X., Liu, S., Lin, Z., & Hu, S. (2015). Validation and trend analysis of ECV soil moisture data on cropland in North China Plain during 1981–2010. *International Journal of Applied Earth Observation and Geoformation*, *48*, 110–121. https://doi.org/10.1016/j.jag.2015.10.010

Wang, T., & Franz, T. E. (2015). Field observations of regional controls of soil hydraulic properties on soil moisture spatial variability in different climate zones. *Vadose Zone Journal*, *14*(8). https://doi.org/10.2136/vzj2015.02.0032

Wang, W., Huang, D., Wang, X. G., Liu, Y. R., & Zhou, F. (2011). Estimation of soil moisture using trapezoidal relationship between remotely sensed land surface temperature and vegetation index. *Hydrology and Earth System Science*, *15*, 1699–1712. https://doi.org/10.5194/hess-15-1699-2011

Wang, Z., Lu, Y., Kojima, Y., Lu, S., Zhang, M., Chen, Y., & Horton, R. (2016). Tangent line/second-order bounded mean oscillation waveform analysis for short TDR probe. *Vadose Zone Journal*, *15*(1). https://doi.org/10.2136/vzj2015.04.0054

Warrick, A. W., Mullen, G. J., & Nielsen, D. R. (1977). Scaling of field measured hydraulic properties using a similar media concept. *Water Resources Research*, *13*, 355–362. https://doi.org/10.1029/WR013i002p00355

Weidong, L., Baret, F., Xingfa, G., Qingxi, T., Lanfen, Z., & Bing, Z. (2002). Relating soil moisture to reflectance. *Remote Sensing of Environment*, *81*, 238–246. https://doi.org/10.1016/S0034-4257(01)00347-9

Weihermüller, L., Huisman, J. A., Lambot, S., Herbst, M., & Vereecken, H. (2007). Mapping the spatial variation of soil water content at the field scale with different ground penetrating radar techniques. *Journal of Hydrology*, *340*(3), 205–216. https://doi.org/10.1016/j.jhydrol.2007.04.013

Western, A. W., & Bloschl, G. (1999). On the spatial scaling of soil moisture. *Journal of Hydrology*, *217*(3–4), 203–224. https://doi.org/10.1016/S0022-1694(98)00232-7

Western, A. W., Bloschl, G., & Grayson, R. B. (1998). Geostatistical characterisation of soil moisture patterns in the Tarrawarra a catchment. *Journal of Hydrology*, *205*, 20–37. https://doi.org/10.1016/S0022-1694(97)00142-X

Western, A. W., & Grayson, R. B. (1998). The Tarrawarra data set: Soil moisture patterns, soil characteristics, and hydrological flux measurements. *Water Resources Research*, *34*, 2765–2768.

Western, A. W., Grayson, R. B., & Green, T. R. (1999). The Tarrawarra project: High resolution spatial measurement, modelling and analysis of soil moisture and hydrological response. *Hydrological Processes*, *13*(5), 633–652.

Western, A. W., Zhou, S.-L., Grayson, R. B., McMahon, T. A., Blöschl, G., & Wilson, D. J. (2004). Spatial correlation of soil moisture in small catchments and its relationship to dominant spatial hydrological processes. *Journal of Hydrology*, *286*, 113–134. https://doi.org/10.1016/j.jhydrol.2003.09.014

White, M. L., Shaw, J. N., Raper, R. L., Rodekohr, D., & Wood, C. W. (2012). A multivariate approach for high-resolution soil survey development. *Soil Science*, *177*(5), 345–354.

Wiekenkamp, I., Huisman, J. A., Bogena, H. R., Lin, H. S., & Vereecken, H. (2016). Spatial and temporal occurrence of preferential flow in a forested headwater catchment. *Journal of Hydrology*, *534*, 139–149. https://doi.org/10.1016/j.jhydrol.2015.12.050

Wigneron, J. P., Kerr, Y., Waldteufel, P., Saleh, K., Escorihuela, M. J., Richaume, P., et al. (2007). L-Band microwave emission of the biosphere (L-MEB) model: Description and calibration against experimental data sets over crop fields. *Remote Sensing of Environment*, *107*(4), 639–655. https://doi.org/10.1016/j.rse.2006.10.014

Wigneron, J.-P., Schwank, M., Baeza, E. L., Kerr, Y., Novello, N., Millan, C., et al. (2012). First evaluation of the simultaneous SMOS and ELBARA-II observations in the Mediterranean region. *Remote Sensing of Environment*, *124*, 26–37. https://doi.org/10.1016/j.rse.2012.04.014

Wilheit, T. T. (1978). Radiative transfer in a plane stratified dielectric. *IEEE Transactions on Geoscience Electronics.*, *16*(2), 138–143. https://doi.org/10.1109/TGE.1978.294577

Wilhite, D. A., & Glantz, M. H. (1985). Understanding: The drought phenomenon: The role of definitions. *Water International.*, *10*(3), 111–120. https://doi.org/10.1080/02508068508686328

Williams, B., Walker, J., & Anderson, J. (2006). Spatial variability of regolith leaching and salinity in relation to whole farm planning. *Australian Journal of Experimental Agriculture*, *46*, 1271–1277.

Williams, C. J., McNamara, J. P., & Chandler, D. G. (2009). Controls on the temporal and spatial variability of soil moisture in a mountainous landscape: The signature of snow and complex terrain. *Hydrology and Earth System Sciences*, *13*, 1325–1336. https://doi.org/10.5194/hess-13-1325-2009

Wilson, W. J., Yueh, S. H., Dinardo, S. J., Chazanoff, S. L., Kitiyakara, A., Li, F. K., et al. (2001). Passive active L- and S-band (PALS) microwave sensor for ocean salinity and soil moisture measurements. *IEEE Transactions on Geoscience and Remote Sensing*, *39*(5), 1039–1048. https://doi.org/10.1109/36.921422

Wraith, J., & Or, D. (1999). Temperature effects on soil bulk dielectric permittivity measured by time domain reflectometry: Experimental evidence and hypothesis development. *Water Resources Research*, *35*(2), 361–369. https://doi.org/10.1029/1998WR900006

Wu, Q., Liu, H., Wang, L., & Deng, C. (2016). Evaluation of AMSR-2 soil moisture products over the contiguous United States using in situ data from the International Soil Moisture Network. *International Journal of Applied Earth Observation and Geoinformation*, *45*, 187–199. https://doi.org/10.1016/j.jag.2015.10.011

Wu, X. L., Walker, J. P., Das, N. N., Panciera, R., & Rudiger, C. (2014). Evaluation of the SMAP brightness temperature downscaling algorithm using active-passive microwave observations. *Remote Sensing of Environment*, *155*, 210–221. https://doi.org/10.1016/j.rse.2014.08.021

Wu, X. L., Walker, J. P., Rudiger, C., Panciera, R., & Gray, D. A. (2015). Simulation of the SMAP data stream from SMAPEx field campaigns in Australia. *IEEE Transactions on Geoscience and Remote Sensing*, *53*(4), 1921–1934. https://doi.org/10.1109/TGRS.2014.2350988

Xu, X. Y., Tolson, B. A., Li, J., Staebler, R. M., Seglenieks, F., Haghnegandar, A., & Davison, B. (2015). Assimilation of SMOS soil moisture over the Great Lakes basin. *Remote Sensing of Environment*, *169*, 163–175. https://doi.org/10.1016/j.rse.2015.08.017

Yan, H., & Moradkhani, H. (2016). Combined assimilation of streamflow and satellite soil moisture with the particle filter and geostatistical modeling. *Advances in Water Resources*, *94*, 364–375. https://doi.org/10.1016/j.advwatres.2016.06.002

Yan, S., Jiang, L. M., Chai, L. N., Yang, J. T., & Kou, X. K. (2015). Calibration of the L-MEB model for croplands in HiWATER using PLMR observation (dagger). *Remote Sensing*, *7*(8), 10878–10897. https://doi.org/10.3390/rs70810878

Yang, C., Sakai, M., & Jones, S. B. (2013). Inverse method for simultaneous determination of soil water flux density and thermal properties with a penta-needle heat pulse probe. *Water Resources Research*, *49*, 5851–5864. https://doi.org/10.1002/wrcr.20459

Yang, Y. T., Guan, H. D., Long, L., Liu, B., Qin, G. H., Qin, J., & Batelaan, O. (2015). Estimation of surface soil moisture from thermal infrared remote sensing using an improved trapezoid method. *Remote Sensing*, *7*(7), 8250–8270. https://doi.org/10.3390/rs70708250

Yeh, T. C. J., Gelhar, L. W., & Gutjahr, A. L. (1985). Stochastic analysis of unsaturated flow in heterogeneous soils. 1. Statistically isotropic media. *Water Resources Research*, *21*, 447–456. https://doi.org/10.1029/WR021i004p00447

Yilmaz, M. T., & Crow, W. T. (2013). The optimality of potential rescaling approaches in land data assimilation. *Journal of Hydrometeorology*, *14*(2), 650–660. https://doi.org/10.1175/JHM-D-12-052.1

Yilmaz, M. T., & Crow, W. T. (2014). Evaluation of assumptions in soil moisture triple collocation analysis. *Journal of Hydrometeorology*, *15*(3), 1293–1302. https://doi.org/10.1175/JHM-D-13-0158.1

Yoo, C., & Kim, S. (2004). EOF analysis of surface soil moisture field variability. *Advances in Water Resources*, *27*(8), 831–842. https://doi.org/10.1016/j.advwatres.2004.04.003

Yu, H., Yang, P., & Lin, H. (2015). Spatiotemporal patterns of soil matric potential in the Shale hills critical zone observatory. *Vadose Zone Journal*, *14*. https://doi.org/10.2136/vzj2014.11.0167

Zacharias, S., Bogena, H., Samaniego, L., Mauder, M., Fuß, R., Pütz, T., et al. (2011). A network of terrestrial environmental observatories in Germany. *Vadose Zone Journal*, *10*(3), 955–973. https://doi.org/10.2136/vzj2010.0139

Zeng, X. M., Wang, B., Zhang, Y., Song, S., Huang, X., Zheng, Y., et al. (2014). Sensitivity of high-temperature weather to initial soil moisture: A case study using the WRF model. *Atmospheric Chemistry and Physics*, *14*(18), 9623–9639. https://doi.org/10.5194/acp-14-9623-2014

Zhan, X., Houser, P. R., Walker, J. P., & Crow, W. T. (2006). A method for retrieving high-resolution surface soil moisture from hydros L-band radiometer and radar observations. *IEEE Transactions on Geoscience and Remote Sensing*, *44*(6), 1534–1544. https://doi.org/10.1109/TGRS.2005.863319

Zhang, D., & Lu, Z. (2002). Stochastic analysis of flow in a heterogeneous unsaturated–saturated system. *Water Resources Research*, *38*(2), 1018. https://doi.org/10.1029/2001WR000515

Zhang, D., Tang, R., Tang, B. H., Wu, H., & Li, Z. L. (2015). A simple method for soil moisture determination from LST–VI feature space using nonlinear interpolation based on thermal infrared remotely sensed data. *IEEE Journal of Selected Topics in Applied Earth Observations and Remote Sensing*, *8*(2), 638–648. https://doi.org/10.1109/JSTARS.2014.2371135

Zhang, F., Zhang, L. W., Shi, J. J., & Huang, J. F. (2014). Soil moisture monitoring based on land surface temperature-vegetation index space derived from MODIS data. *Pedosphere*, *24*(4), 450–460. https://doi.org/10.1016/S1002-0160(14)60031-X

Zhang, N., Hong, Y., Qin, Q., & Liu, L. (2013). VSDI: A visible and shortwave infrared drought index for monitoring soil and vegetation moisture based on optical remote sensing. *International Journal of Remote sensing*, *34*(13), 4585–4609. https://doi.org/10.1080/01431161.2013.779046

Zhang, S., Calvet, J.-C., Darrozes, J., Roussel, N., Frappart, F., & Bouhours, G. (2018). Deriving surface soil moisture from reflected GNSS signal observations from a grassland site in southwestern France. *Hydrology and Earth System Sciences*, *22*, 1931–1946. https://doi.org/10.5194/hess-22-1931-2018

Zhang, S., Roussel, N., Boniface, K., Ha, M. C., Frappart, F., Darrozes, J., et al. (2017). Use of reflected GNSS SNR data to retrieve either soil moisture or vegetation height from a wheat crop. *Hydrological and Earth System Science*, *21*, 4767–4784. https://doi.org/10.5194/hess-21-4767-2017

Zhang, Y., & Wegehenkel, M. (2006). Integration of MODIS data into a simple model for the spatial distributed simulation of soil water content and evapotranspiration. *Remote Sensing if Environment*, *104*(4), 393–408. https://doi.org/10.1016/j.rse.2006.05.011

Zhang, Y., Xiao, Q., & Huang, M. (2016). Temporal stability analysis identifies soil water relations under different land use types in an oasis agroforestry ecosystem. *Geoderma*, *271*, 150–160. https://doi.org/10.1016/j.geoderma.2016.02.023

Zhao, L., Yang, K., Qin, J., Chen, Y., Tang, W., Montzka, C., et al. (2013). Spatiotemporal analysis of soil moisture observations within a Tibetan mesoscale area and its implication to regional soil moisture measurements. *Journal of Hydrology*, *482*, 92–104. https://doi.org/10.1016/j.jhydrol.2012.12.033

Zhao, W., & Li, Z. L. (2013). Sensitivity study of soil moisture on the temporal evolution of surface temperature over bare surfaces. *International Journal of Remote Sensing*, *34*(9-10), 3314–3331. https://doi.org/10.1080/01431161.2012.716532

Zhu, J., & Mohanty, B. P. (2006). Effective scaling factor for transient infiltration in heterogeneous soils. *Journal of Hydrology*, *319*(1-4), 96–108. https://doi.org/10.1016/j.jhydrol.2005.07.004

ZigBee Alliance. (2010). ZigBee Alliance. Available at www.zigbee.org/ (verified 31 May 2010). Zigbee Alliance, San Ramon, CA.

Zreda, M., Desilets, D., Ferre, T. P. A., & Scott, R. L. (2008). Measuring soil moisture content non-invasively at intermediate spatial scale using cosmic-ray neutrons. *Geographical Research Letters*, *35*, L21402. https://doi.org/10.1029/2008GL035655

Zreda, M., Shuttleworth, W. J., Zeng, X., Zweck, C., Desilets, D., Franz, T., & Rosolem, R. (2012). COSMOS: The COsmic-ray Soil Moisture Observing System. *Hydrology and Earth System Sciences*, *16*, 4079–4099. https://doi.org/10.5194/hess-16-4079-2012

Zucco, G., Brocca, L., Moramarco, T., & Morbidelli, R. (2014). Influence of land use on soil moisture spatial-temporal variability and monitoring. *Journal of Hydrology*, *516*, 193–199. https://doi.org/10.1016/j.jhydrol.2014.01.043

Zwieback, S., Hensley, S., & Hajnsek, I. (2015). Assessment of soil moisture effects on L-band radar interferometry. *Remote Sensing of Environment*, *164*, 77–89. https://doi.org/10.1016/j.rse.2015.04.012